Mechanism of Arsenic release in ecosystems of Southeast Asia delta : Mekong Deltas Vietnam

Thi Hai Van Phan

Communauté
UNIVERSITÉ Grenoble Alpes

THÈSE

Pour obtenir le grade de

DOCTEUR DE LA COMMUNAUTÉ UNIVERSITÉ GRENOBLE ALPES

Spécialité : **Science de la Terre, de l'Univers et de l'Environnement**

Arrêté ministériel : 7 août 2006

Présentée par

Thi Hai Van PHAN

Thèse dirigée par **Prof. Laurent CHARLET** et
codirigée par **Prof. Rizlan BERNIER-LATMANI**

préparée au sein du **l'Institut des Sciences de la Terre**
dans **l'École Doctorale Terre - Univers - Environnement**

L'arsenic dans les écosystèmes du sud-est asiatique : Mekong Delta Vietnam

Thèse soutenue publiquement le **05 Janvier 2017,**
devant le jury composé de :

M. Douglas KENT
PR. U.S Geological Survey (USGS) (Rapporteur)
M. Guillaume MORIN
DR. Université Pierre et Marie Curie (Rapporteur)
M. Laurent CHARLET
PR. Université Grenoble Alpes – ISTERRE, Grenoble (Directeur)
Mme Rizlan BERNIER-LATMANI
PR. École Polytechnique Fédérale de Lausanne (Co-Directeur)
M. Georges VACHAUD
DR. Université Grenoble Alpes – LTHE, Grenoble (Examinateur)
Mme Célestine DELBART
DR. Université de Tours (Examinateur)

Contents

Acknowledgements

During the period of this thesis, I have had the opportunity to spend time in three different institutions: the Université Grenoble-Alpes (UGA), France, Ecole Polytechnique Fédérale de Lausanne (EPFL), Switzerland and Ho Chi Minh City University of Technology (HCMUT), Vietnam. In each university, I have got a lot experiences from people who have been generous to me with their time, knowledge and guidance. They have shared and helped me with the innumerable challenges both to research and to living in new countries. Without their support, encouragement, it was not possible to complete my doctoral study at UGA. I would like to give special thanks all those who contributed directly or indirectly to the development of this thesis.

First of all, I would like to express my greatest thanks to my main director, Prof. Laurent Charlet for hosting me and sharing with me his creativity, knowledge and enthusiasm for environmental research. He provided me with the opportunity to work in a multi-disciplinary field at the geochemistry and geophysics. He has always been ready to discuss for scientific subjects. I also have heart-full appreciation for my co-advisor Prof. Rizlan Bernier-Latmani at Environmental Microbiology Laboratory group in EPFL. I thank for motivating me to pursue doctoral study, ensuring all-time access to her laboratory, logistic supports during field campaigns and spending time for academic discussions.

I would like to give special thanks for my teacher, Prof. Jean Gagnon at PAVAL laboratory, chemistry and life sciences, UGA. I feel really fortunate meeting him at Coup de Pouce Étudiants – Grenoble. He helped me not only in English and French studying but also in academic subjects. I have also enjoyed those non-scientific discussions with him, which has enriched me as human beings.

I also thank all of everyone (past and present) in the Geochemie 4D groups and ISTerre. Particularly, I would like to warmly acknowledge the supports of Fabrizio Bardelli. Without his analytical supports, it was not possible to finish my study on time. He also ensured unlimited access for any scientific discussions and was always ready to help me revise articles. I am very much thankful to Alejandro Fernandez-Martinez, Delphine Tisserand, Antoine Gehin, Ekaterina Markelova, Timothée Bonnet, Bin Ma, Stéphane Garambois, Géraldine Sarret, Nathaniel Findling and Sarah Bureau for their discussions and analytical supports. I am also thankful to all of my colleagues and friends both in

Geochemie 4D group and ISTerre for creating a nice and homely working environment and keeping me mentally fresh.

In Lausanne, to everyone in the EML group, I would like to acknowledge the analytical support and scientific discussions from Manon Frutschi, Yuheng Wang, Maria Pilar Asta, Alexandre Bagnoud, Leia Falquet and Matthew Reid.

I also thank Francesco D'Acapito and Giovanni Lepore for the assistance during XAS measurements at the LISA beamline at the ESRF (BM08), and Giuliana Aquilanti for the assistance at the XAFS beamline at the Elettra synchrotron. I would like to acknowledge to my colleagues Nguyen Phuoc Dan, Dinh Quoc Tuc and Vo Le Phu at HCMUT for collecting sediments and fieldworks in Vietnam. I am thankful to Lorenzo Spadini and Marie-Christine Morel in LTHE for their analytical supports.

For the thesis jury, I thank to Prof. Douglas Kent and Dr. Guillaume Morin for agreeing to review this manuscript and act as the external examiners during my thesis committee.

I would like to give a big thank-you sincerely to all my family, my friends, and my colleagues from Vietnam for their mental support and encouragement during this very challenging and interesting experience. Additionally, I cannot forget to address a deep gratitude to my husband and daughter who always support me. Without their unconditional love and cooperation it was impossible to accomplish this research.

Last but not least, I am grateful for the financial support provided to me by the UGA and for the acceptance me as a PhD student by the Graduate School Earth-Universe-Environment of the UGA. This study has been conducted under the framework of CARE-RESCIF initiatives.

Résumé

L'arsenic est un métalloïde toxique et cancérigène qui a reçu une attention considérable dans les régions deltaïques de l'Asie du Sud-Est au cours des deux dernières décennies. Certains habitants du Bangladesh, de l'Inde, du Cambodge et du Vietnam ont été signalés comme souffrant de lésions cutanées et arsenicose résultant d'un empoisonnement chronique par l'arsenic. Il est en général convenu que la dissolution réductrice de minerais de fer sédimentaires, provoquée par des bactéries réductrices en présence de matière organique naturelle, est un processus important qui conduit à la libération d'arsenic dans l'aquifère. Les sédiments deltaïques du delta du Mékong au Vietnam sont connus pour contenir des concentrations élevées d'arsenic qui fluctuent en fonction des conditions redox. Ils sont également soumis à une oscillation régulière des conditions d'oxydoréduction due aux inondations saisonnières (Fig. S.1). Ce travail de thèse s'intéresse plus particulièrement à l'impact de ces oscillations sur la mobilité de l'arsenic.

Figure S.1. Inondation dans la plaine alluviale du delta du Mékong dans un district de An Giang, Vietnam (Photographe : Nguyen Ky Nam (2011) / Source : *http://www.ERCT.com*)

Comprendre les facteurs qui influent la mobilité de l'arsenic et sa toxicité dans l'eau contenue dans les sédiments sous l'influence des cycles d'oxydoréduction du soufre et du fer est un défi. En outre, la biogéochimie de l'arsenic est également d'un intérêt particulier en raison de la sensibilité des changements de spéciation entre les phases aqueuses et solides au sein d'une gamme de E_h et de condition de pH trouvées dans de nombreux environnements. Pendant les périodes d'inondation, le sol et le sous-sol deviennent saturés d'eau et la diffusion dans le sol de l'oxygène provenant de l'atmosphère est limitée. Par conséquent, la matière organique du delta alluvial et la surface du sol pourraient être mises en œuvre dans le système sédiment-aquifère Cela peut conduire à stimuler les communautés bactériennes anaérobies présentes dans le sol. En fonction des conditions redox oscillantes, le soufre peut également avoir un effet significatif sur la spéciation et la concentration puisque les niveaux d'arsenic sont contrôlés par le taux de réduction microbienne du sulfate, la solubilité de phases de sulfite contenant de l'arsenic, et / ou les procédés d'adsorption du souffre de minéraux Dans la phase solide, le FeAsS (arsénopyrite), As_2S_3 (orpiment), AsS (realgar) ou thiol-arsénite lié à la matière organique peuvent se former et l'élimination de l'arsenic par adsorption sur le FeS (mackinawite) et le partitionnement en FeS_2 ont été rapportés (Fig. S.2). Par conséquent, la spéciation et la concentration du souffre pourraient être étroitement liées à la phase aqueuse. Le sulfate (SO_4^{2-}), souvent présent dans les eaux souterraines du delta du Mékong, peut provenir à la fois de l'oxydation de la pyrite et de la dissolution du gypse ($CaSO_4$) car l'aquifère dans cette région est formé au niveau du plateau Moc Hoa. Une transformation importante de SO_4^{2-} des sédiments deltaïques résulte de la réduction bactérienne. La réduction microbienne ou chimique du sulfate en sulfite peut précipiter le fer sous forme de FeS et FeS_2 ou former des composés organiques du soufre ou du soufre élémentaire ($S_{8(s)}$). En fonction du pH, des valeurs de E_h et du rapport SO_4^{2-} / Fe(III), les bactéries peuvent favoriser le SO_4^{2-} plus que le Fe comme accepteur terminal d'électrons. En outre, le sulfure peut être ré-oxydé en des espèces intermédiaires telles que S^0, $S_2O_3^{2-}$, SO_3^{2-} qui sont connues pour être microbiologiquement disproportionnées, réduisant ainsi la concentration en sulfure. Cette microbienne de transformation redox provoque des changements dans les équilibres chimiques, puis dans la minéralogie, le processus de sorption et la spéciation aqueuse, et par conséquent tout ce qui influence la mobilisation de l'arsenic. Une grande partie du travail a déjà été effectuée au cours des dernières années pour établir un mécanisme de libération et d'adsorption de l'arsenic dans des conditions réductrices. Cependant, une attention relativement limitée a été consacrée à l'étude des effets

cumulatifs du cycle périodique d'oxydoréduction sur la minéralogie du sol, de l'action de la communauté microbienne, de la matière organique et de l'influence du soufre ainsi que de la contribution de l'arsenic et de sa mobilité. La simulation du cycle redox représente un aspect important dans notre compréhension de l'influence d'une variété d'environnement naturel et artificiel, y compris les plaines inondables, les rizières et les aquifères peu profonds.

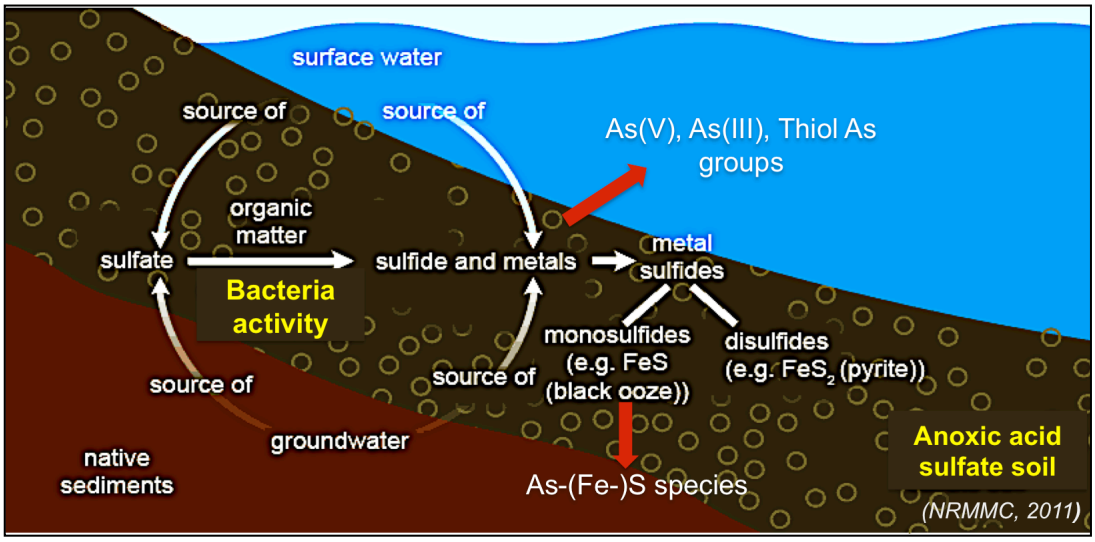

Figure S.2. Schéma du processus microbien de réduction de sulfate dans un sol acide anoxique sulfaté (non à l'échelle) (modifié à partir de l'orientation nationale pour la gestion des sols acides sulfatés dans les eaux intérieures Écosystèmes aquatiques - Protection de l'environnement et du patrimoine et du Conseil ministériel de la gestion des ressources naturelles, 2011)

Une étude des propriétés géophysiques et chimiques du sol et des eaux souterraines dans le district de An Phu, situé à proximité du delta du Mékong, a été menée sur le terrain depuis 2014. Le site d'étude est situé le long de la frontière cambodgienne où le terrain est plus élevé de 2,0 à 4,0 m au-dessus du niveau de la mer. Chaque année, le débordement du Mékong inonde une grande surface pour une longue période. Les inondations saisonnières dans le delta du Mékong commencent habituellement durant les mois de juin ou juillet et se terminent durant les mois novembre ou décembre. Des inondations jusqu'à 3,5 ou 4,5 m d'eau sont considérées comme normales dans la majorité de la région de An Phu. Nous avons constaté que les niveaux élevés d'arsenic dans les puits sont le risque le plus important pour la santé humaine dans cette région (Fig. S.3). Environ 200 000 personnes vivent dans le district de An Phu et on estime que 12,7 millions de Vietnamiens vivent dans le delta du Mékong dont les concentrations en arsenic dans les eaux souterraines sont supérieures à 100 ppb. Bien qu'aucun problème de santé tels que des lésions cutanées et

une arsenicose n'a été observés suite à l'exposition à l'arsenic, une mise en garde précoce est importante.

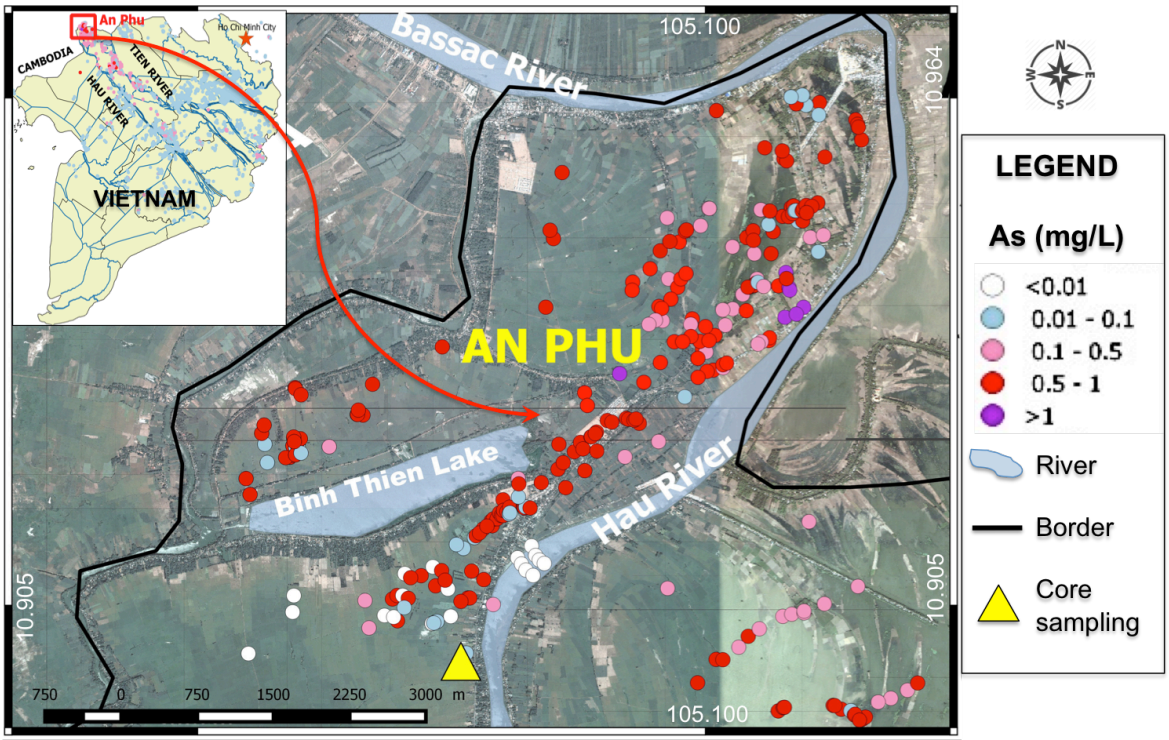

Figure S.3. Localisation de la zone d'étude et distribution de l'arsenic dans le delta du Mékong et de la région de An Phu (modifiés par Erban et al., 2013 et mis à jour des données sur l'arsenic en Janvier 2014 et Avril 2015)

Des relevés géophysiques d'électromagnétisme inductif (EM) ont été largement utilisés en hydrologie pour cartographier la percolation de l'eau dans les formations proches de la surface, pour estimer l'étendue et la structure interne des aquifères peu profonds, et pour déterminer l'étendue de la contamination des eaux souterraines. Dans le cadre de cette thèse, l'approche a été de déterminer une relation entre la géochimie de l'arsenic dans les eaux souterraines et les propriétés géophysiques du sol à l'aide d'un simple dispositif EM 31. Cette approche n'a pas été appliquée auparavant à l'étude de l'arsenic dans le delta du Mékong. La comparaison entre les concentrations d'arsenic mesurées dans les eaux souterraines pompées dans 40 puits peu profonds (< 40 m de profondeur) et la conductivité électrique mesurée à la surface a été réalisée (Fig. S.4).

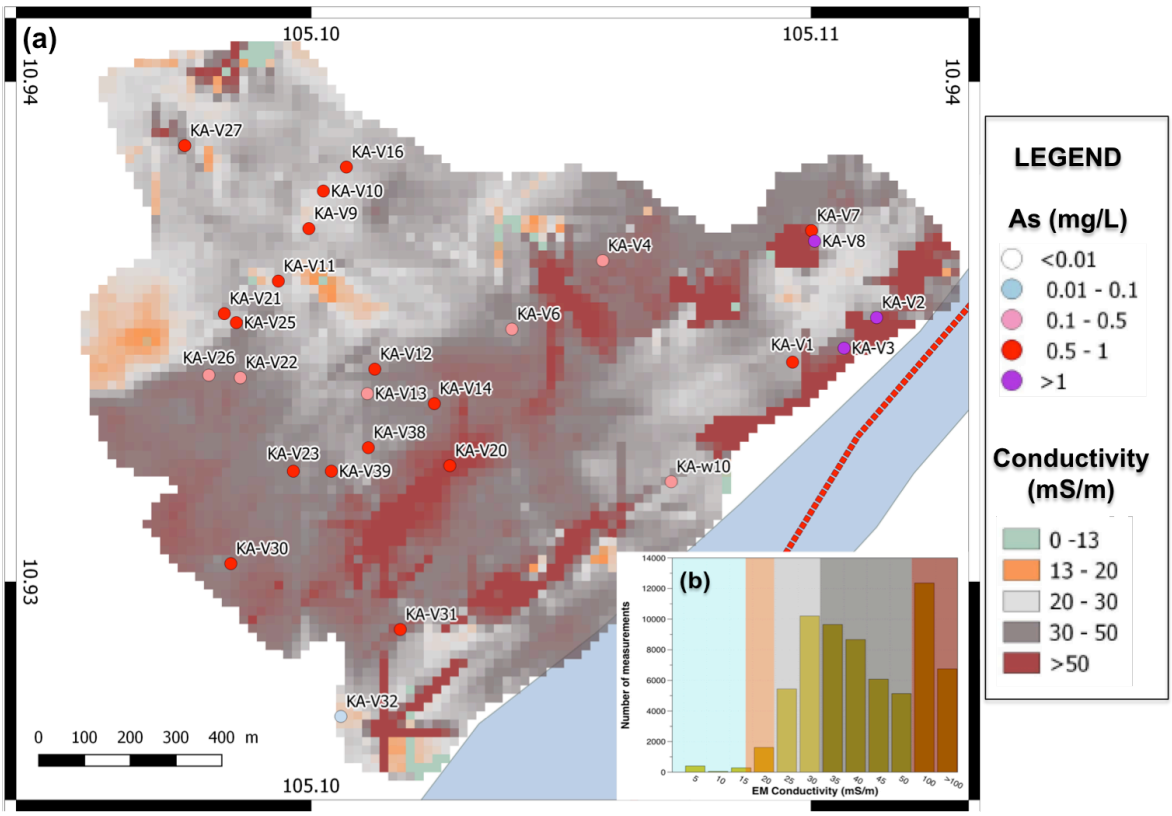

Figure S.4. (a) Carte des mesures de conductivité électrique à l'aide de dispositif EM31 et (b) Histogramme des valeurs de conductivité EM mesurées sur le site de l'étude.

A partir des résultats d'analyse des eaux souterraines, des sédiments et des données géophysiques, nous montrons que la perméabilité et la teneur en argile du sol dérivée grâce à la mesure EM de conductivité sont corrélés positivement et significativement (R^2 = 0,83, n = 27) avec la distribution de la concentration en arsenic dans l'aquifère peu profond (Fig. S.5). Cela souligne que la recharge des eaux souterraines à travers les argiles du sol et du sous-sol peut améliorer les conditions de réduction dans l'aquifère. Les résultats suggèrent également le rôle important du HCO_3^-, de Fe / Mn (hydr)oxyde et de minéraux argileux dans la mobilisation de l'arsenic qui présente une menace majeure pour la santé des populations locales de cette province.

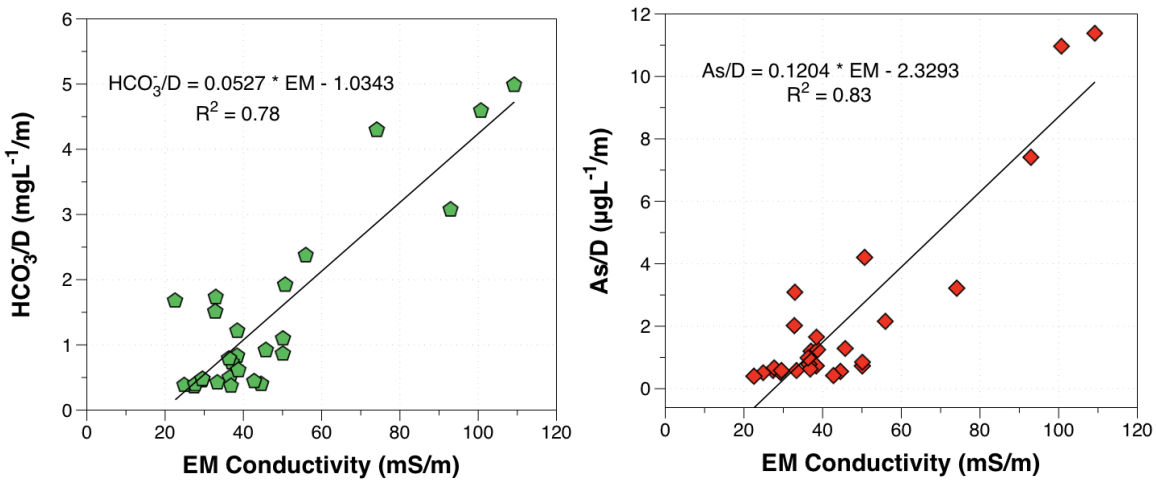

Figure S.5. Comparaison du rapport de (a) HCO_3^- et (b) As et de la distance entre la rivière et les puits en fonction des données de conductivité EM

Des expériences en laboratoire ont été effectuées sur des échantillons de sol en utilisant un système de bioréacteur pour déterminer l'impact du changement redox saisonnier causé par les inondations sur les sédiments du delta du Mékong (Fig. S.6). Des expériences ont été menées dans des conditions biotiques avec deux réacteurs contenant des sédiments aqueux et de l'arsenic avec des concentrations en sulfate différentes. Des cycles de réduction et d'oxydation ont été obtenus grâce à une combinaison de gaz (N_2 / CO_2 et air comprimé). De plus, afin de stimuler le métabolisme de la communauté microbienne présente dans le milieu, du carbone organique dissous (cellobiose) a été introduit dans le réacteur. Une caractérisation exhaustive de paramètres de la phase aqueuse, comme E_h, pH, DOC, types de S, Fe et arsenic a été effectuée en utilisant des méthodes d'analyse appropriées. En outre, la caractérisation de la phase solide a été réalisée par diffraction de rayons X. L'ARN ribosomal 16S a été extrait à partir d'échantillons de boues et amplifié par PCR. Le séquençage de l'ADN est effectué pour déterminer les changements dans la composition de la population microbienne et en utilisant une sonde spécifique pour détecter la présence de bactéries sulfo-réductrices pendant les cycles expérimentaux.

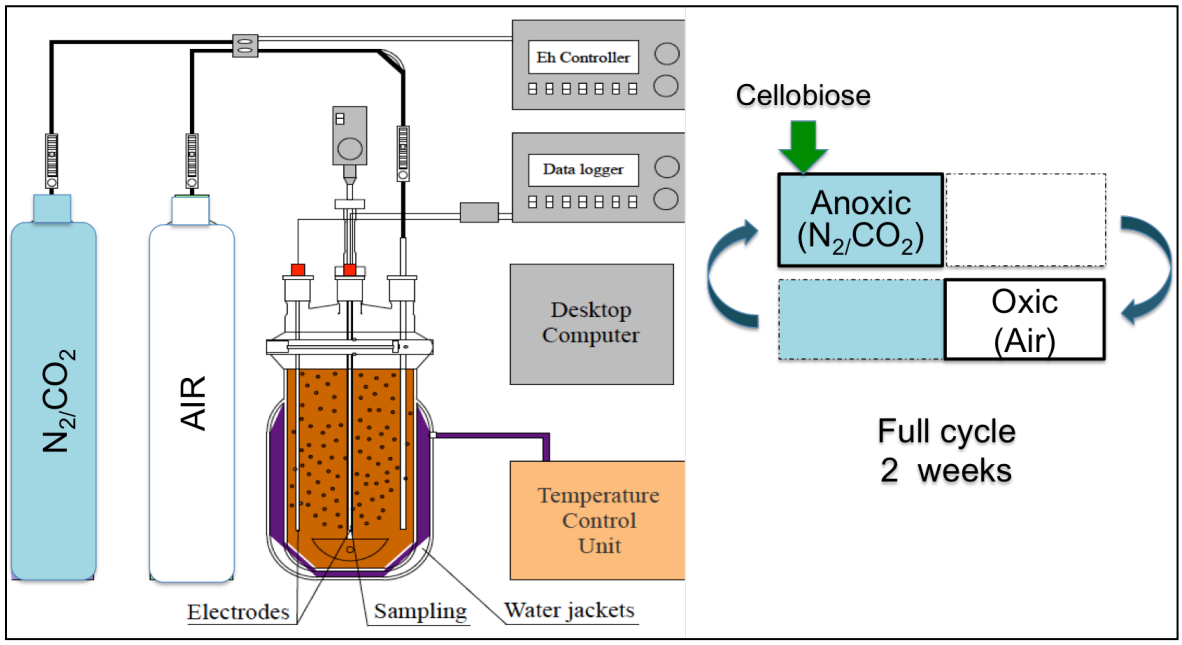

Figure S.6. Schéma du système de bioréacteur permettant des cycles redox, ainsi que les conditions utilisées pour les demi-cycles anoxiques et oxiques (2 semaines pour un cycle complet) au cours des expériences décrites dans le chapitre 3 et 4 pendant lesquelles E_h est contrôlée par une alternance d'air et de gaz de N_2 / CO_2.

Ces expériences ont permis de vérifier la mobilité de l'arsenic tout au long des demi-cycles anoxiques et oxiques séquentielles, en plus des changements dans la chimie de la phase aqueuse, dans la minéralogie, dans la spéciation de la phase solide et dans la population bactérienne naturelle. Les résultats ont montré que la concentration en arsenic total dans les sédiments peut être libérée dans la solution lors d'événements périodiques de réduction en raison de la dissolution réductrice de composés d'(hydr)oxydes de fer comportant de l'arsenic. Une conséquence inattendue fut que les cycles consécutifs de réduction des sédiments et de l'oxydation conduit à la séquestration de l'arsenic libéré resultant de la réduction microbienne du sulfate (Fig. S.7). L'analyse phylogénétique des ARNr 16S a révélé la présence de bactéries capable d'utiliser le soufre et de fer, suggérant que la réduction du sulfate et du fer sont des facteurs importants pour la diminution de l'arsenic dans la phase aqueuse. En complément des informations obtenues sur la chimie de la phase aqueuse, la spectroscopie et l'identification microbienne au cours de ces expériences, un modèle thermodynamique des espèces thioarsenic a été calculé en utilisant le logiciel PHREEQC.

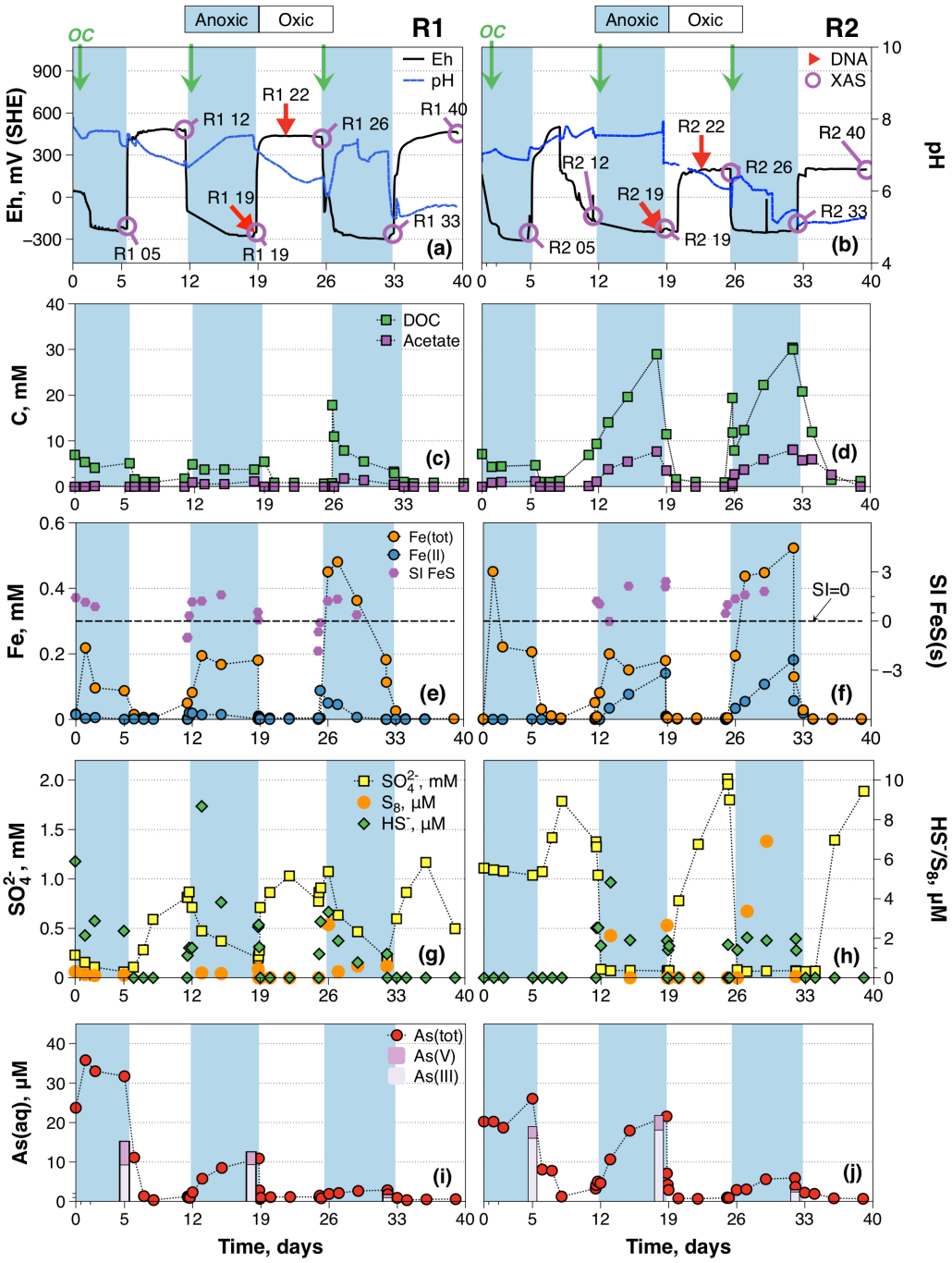

Figure S.7. Evolution du E_h, pH, S, Fe aqueux et concentration de l'arsenic en fonction du temps dans les suspensions de sédiments soumis à une oscillation d'oxydoréduction

Par conséquent, nous proposons que l'oscillation redox en milieu naturel en raison des inondations et du drainage peut potentiellement stabiliser l'arsenic dans la phase solide et limiter ainsi les concentrations aqueuses à travers plusieurs réactions microbiennes et chimiques qui influencent le cycle de l'arsenic, du fer et du soufre dans le système (Fig. S.8). Ces mécanismes comprennent l'adsorption / désorption de l'arsenic sur des

(hydr)oxydes de fer et sur ou dans du soufre solide réduit et la formation de complexe thioarsenate.

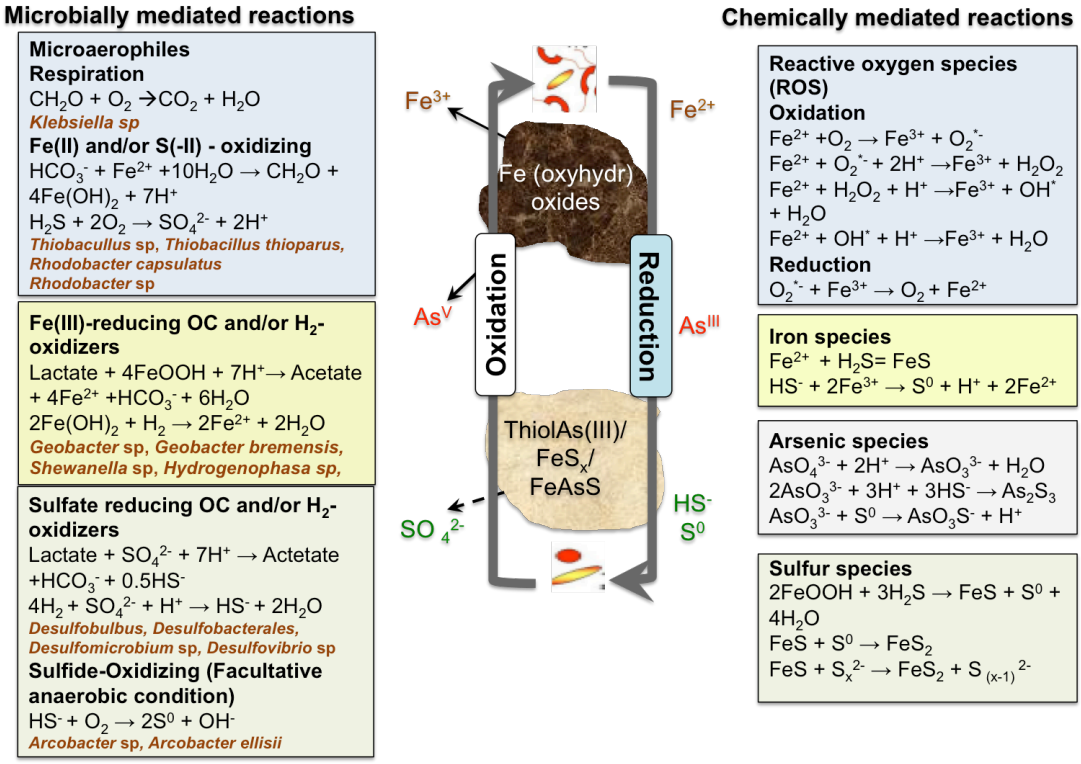

Figure S.8. Schéma de réactions chimiques et microbiennes dans le système As, Fe et S pendant l'oscillation redox

Les conditions oscillantes d'oxydoréduction ont aussi une influence sur les sédiments riches en pyrite qui, par oxydation, peuvent libérer du sulfate dans l'eau interstitielle. Les sédiments de la rivière du Delta du Mekong et de l'aquifère de la plaine inondable adjacente sont riches en pyrite. Ces sédiments ont été étudiés en regardant les effets périodiques et cumulatifs des oscillations redox temporelles sur la mobilité des As, Fe et S dans la phase solide et les mécanismes connexes de relargage d'arsenic dans les eaux souterraines. Des expériences ont été conçues pour simuler une oscillation redox sur les sédiments prélevés à 14 m (Matrice A) et 7 m (Matrice B) de profondeur en fonction des changements saisonniers du niveau des eaux souterraines. Les expériences ont consisté dans l'utilisation de suspensions riches en pyrite en poudre dans deux bioréacteurs contenant des sédiments de la matrice A et B dopés avec de l'arsenite (As^{3+}) et du sulfate (SO_4^{2-}). Les suspensions ont été soumises à un total de trois cycles redox complets impliquant des phases de purge avec N_2 / CO_2, suivi d'air comprimé et avec addition de cellobiose.

Les résultats montrent qu'il y a contamination par l'arsenic dans les nappes de sédiments deltaïques du delta du Mékong. La mobilité de l'arsenic des sédiments vers les eaux souterraines est fortement dépendante des oscillations redox et de la composition minéralogique. Dans des conditions de pH et E_h attendues, l'arsenic, le fer et le soufre peuvent subir des changements importants de spéciation. Des changements cumulatifs sur les sédiments sont attendus en raison de la stabilité minérale variable qui a un effet secondaire sur la mobilité de l'arsenic. Ces premières expériences sur des sédiments riches en pyrite montrent des changements de mobilité intra-cycle de l'As et du Fe. Pour les sédiments à haute teneur en pyrite, l'oxydation de la pyrite pourrait faire chuter le pH de la phase aqueuse qui conduirait à inhiber la réduction microbienne du sulfate, menant à une concentration de sulfate élevée et la libération d'arsenic dans les conditions réductrices à plusieurs reprises. Pour les sédiments à faible teneur en pyrite et en présence de gypse, les effets cumulatifs des cycles redox peuvent être atténués en raison des changements minéralogiques induits par des cycles successifs d'oxydo-réduction. L'hypothèse présentée prend en compte l'augmentation de l'état d'oxydation et de co-précipitation d'Arsenic-(hydr)oxydes de fer et une proportion croissante d'espèces contenant de l'As(V).

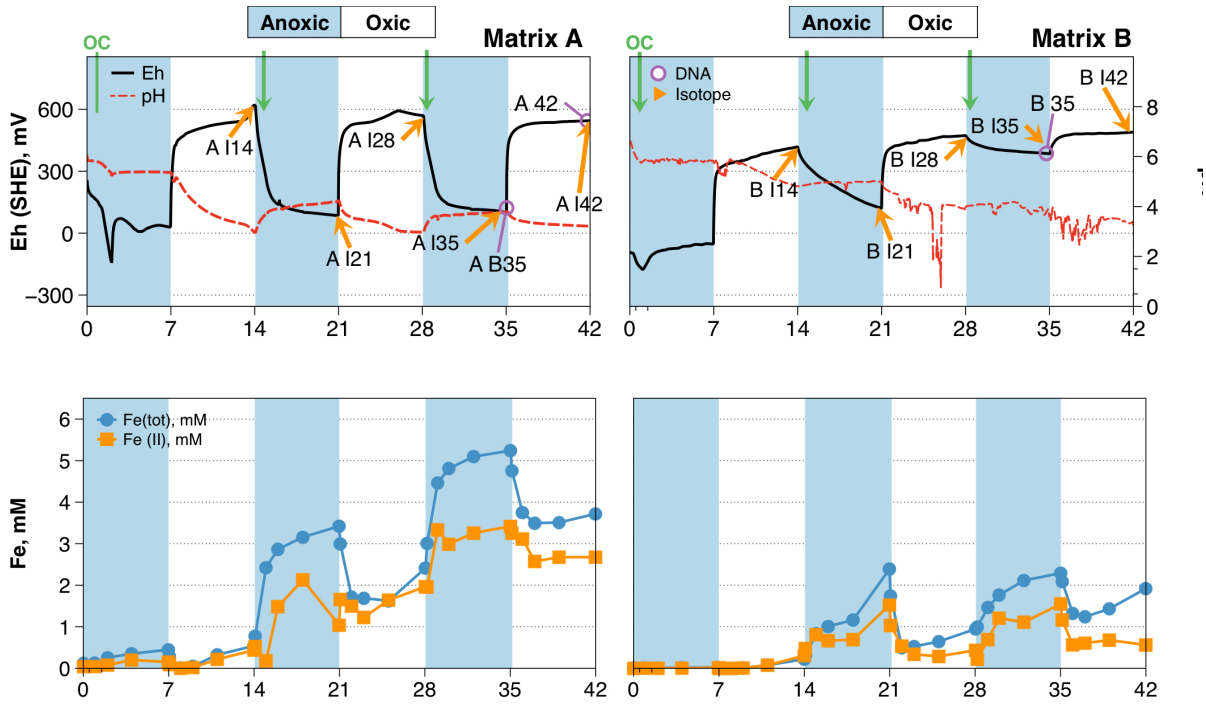

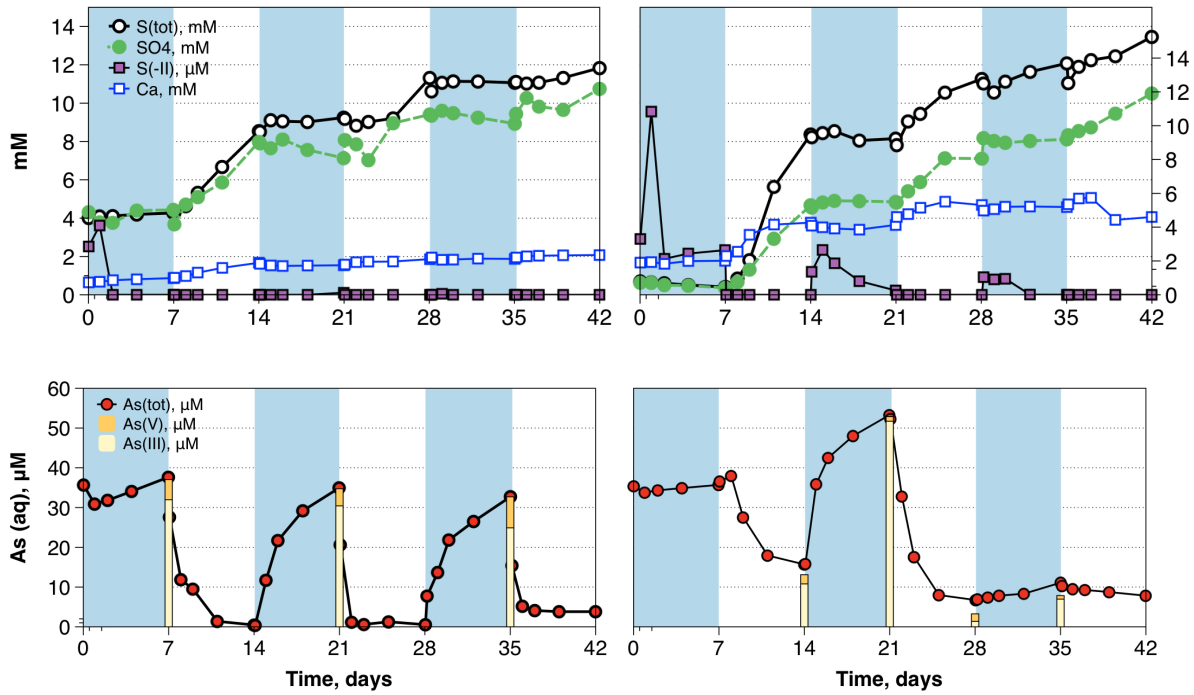

Figure S.9. Evolution des données de la phase aqueuse analysée en terme de E_h, pH, Fe(tot), Fe^{2+}, S(tot), SO_4^{2-}, et As(tot) en fonction du temps sur des sédiments à haute et basse teneur en pyrite, en suspension soumises à des oscillations d'oxydoréduction

Pour résumer, les résultats de cette thèse soulignent que la contamination par l'arsenic dans le delta du Mékong au Vietnam est alarmante et il est nécessaire d'y accorder une plus grande attention, et notamment pour les conséquences sur l'agriculture et les activités domestiques. Bien que le cycle biogéochimique de l'arsenic dans des systèmes dynamiques représente une problématique complexe, il est possible, en utilisant une combinaison de techniques, d'approcher ce problème et de renforcer notre compréhension collective de ces systèmes.

Target publication and co-authors

Title:	Arsenic release during redox oscillations in Mekong upper delta aquifers in Vietnam: a mechanistic study
Authors:	Van Phan T.H, Rizlan Bernier-Latmani, Delphine Tisserand, Fabrizio Bardelli, Manon Frutschi, Antoine Gehin, Laurent Charlet
Target journal	Journal of Science the Total Environment

Title:	Immobilization and mobilization of Arsenic induced by mineralogical changes during redox oscillations
Authors:	Van Phan T.H, Fabrizio Bardelli, Alejandro Fernandez-Martinez, Delphine Tisserand, Rizlan Bernier-Latmani, Laurent Charlet
Target journal	Journal of Hazardous Materials

Title:	Arsenic concentration in shallow aquifers linked to the electromagnetic ground conductivity: the Mekong Delta source example.
Authors:	Van Phan T.H, Timothee Bonnet, Stephane Garambois, Delphine Tisserand Fabrizio Bardelli, Rizlan Bernier-Latmani, Laurent Charlet
Target journal	Journal of Geosciences Research (accepted)

Chapter 1: Arsenic presence in the Mekong Delta Vietnam

1.1. Arsenic speciation in natural environment

Arsenic (As) is in the group 15 of the periodic table of elements together with nitrogen and phosphorus and is commonly characterized as a metalloid. The main As oxidation states in the natural environment are -III, 0, III and V, represented by arsine (AsH_3), elemental arsenic As^0, arsenite (As(III)) and arsenate (As(V)), respectively (Smedley & Kinniburgh, 2002). In natural water, it is mostly found inorganic forms (i-As) including As(III) and As(V). Organic As (o-As) as mentioned such as methylated forms can be generated and transferred through the food chain by biological activities. Arsenic is a ubiquitous element found in the atmosphere, lithosphere, hydrosphere and biosphere. The average As level in the continental crust, soil and ocean water is 2.1, 5 and 0.0023 mg/kg, respectively (Zhu et al., 2014). About 99% of As is part of the lithosphere (Matschullat, 2000). Weathering of rocks, geothermal processes and volcanic activities, mining and smelting can release As from lithosphere to the terrestrial and oceanic environments. As speciation is principally controlled by the redox environment (E_h) and the pH (Fig. 1.1). As(V) is the predominant form in the oxic environment including in the surface water and aerobic soils. Reduction of As(V) to As(III) occurs under suboxic conditions (E_h < 100 mV and neutral pH); thus, As(III) becomes the predominant form under reducing conditions, e.g. flooded soils, anoxic aquifers or anaerobic sediments. Reduction of As(V) to As(III) in soil or sediment generally leads to highly increased mobility because the latter is less strongly adsorbed by iron (oxyhydr)oxides which are common in the soil and sediment (Fendorf et al., 2010). Organic As forms may be produced by biological activity, mostly in surface water where waters are significantly impacted by industrial pollution (Smedley & Kinniburgh, 2002).

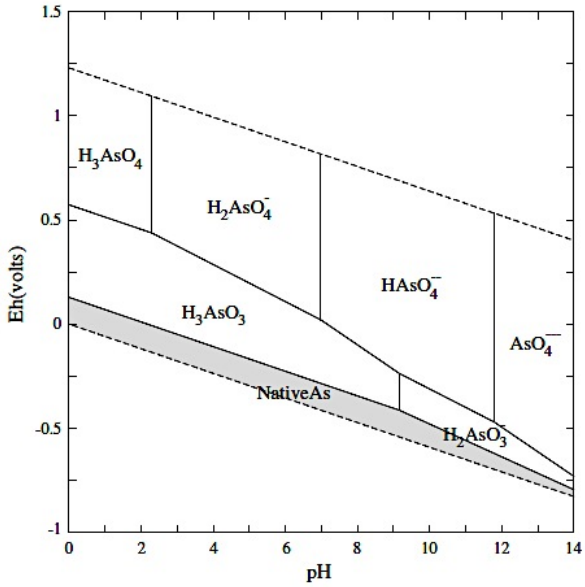

Figure 1.1. E_h-pH diagram for the system As-O-H at 25°C and 1 bar. ΣAs is set at 10^{-6} M (Grey shaded area denotes the solid phase) (Lu & Zhu, 2011; Smedley & Kinniburgh, 2002)

More than 320 minerals contain arsenic; however, only three of them, arsenopyrites (FeAsS), realgar (AsS), and orpiment (As_2S_3), are considered as As ore because the amount of As is higher in these three compounds (Hossain, 2006; Welch & Lico, 1998). In the presence of extremely high concentrations of reduced S, dissolved As-sulfide species can be significant. Reducing acidic conditions favor precipitation of As_2S_3, AsS or other sulfide minerals containing co-precipitated As (Fig. 1.2). Inorganic As species can be transformed due to redox processes as well as microbial activity. Thermodynamic calculations predict that As(V) should be dominant in all but strongly reducing groundwater. However, in reality the ratio of As(V) to As(III) can vary considerably, depending on the abundance of redox active solids, organic carbon (OC), activity of microorganisms as well as on the extent of convection and diffusion of dissolved oxygen (Smedley & Kinniburgh, 2002). Recently, thioarsenic species have been reported to play an important role for the chemistry and cycling of arsenic in sulfidic environments (Fisher et al., 2008; Planer-Friedrich et al., 2007; Planer-Friedrich & Wallschläger, 2009). However, little information exists concerning their response to changing ambient conditions such as pH, oxygen, redox potential, and temperature. The importance of abiotic and biotic catalyzed thioarsenate transformation in sulfidic systems and the involved microbes, e.g. the potential effects of sulfur metabolizing microorganisms, are so far unknown. Also the effect of sulfide (ΣS^{-2}) and elemental sulfur (S^0) are unclear. The

$S^0_{(aq)}/HS^-$ couple is expected to contribute to the redox potential in sulfidic environment where elemental sulfur is actively forming (Couture & Van Cappellen, 2011). In their review, thermodynamic data for As-O-H-S came from Lu & Zhu (2011). However, the formation constants of thioarsenic species have been revised in depth on two occasions (Helz & Tossell, 2008; Wilkin et al., 2003). Helz & Tossell (2008) proposed a preliminary thermodynamic model which predicts the concentration of As(III) and As(V) (oxy)thio-monomers as a function pH, ΣS^{-2} and $\Sigma As_{(aq)}$ at any imposed E_h. Their model predicts a significant contribution of As(V) species under highly reducing conditions. This new model allows for the existence of both As(III) and As(V) thioanions under reducing conditions. Couture & Cappellen (2011) applied this model to predict As species as a function of E_h and pH for comparison between the redox couple SO_4^{2-}/HS^- and $S^0_{(aq)}/HS^-$ (Fig. 1.3). Their modeling results suggested that in the presence of free sulfide, the oxidation of As(III) by elemental sulfur can produce thioarsenate. The formation of arsenate-sulfide complexes is thus one mechanism that helps explain an increase of solubility and mobility of As in reducing environments.

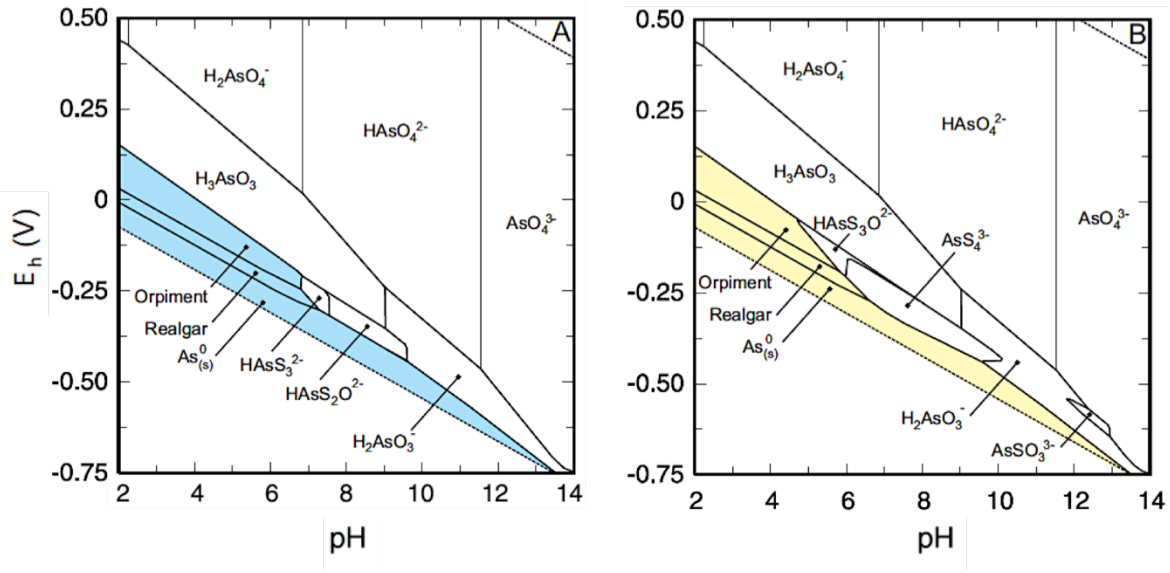

Figure 1.2. E_h-pH diagram for the system As-O-H-S at 25°C, 1bar. ΣS and ΣAs are set at 10^{-4} M and 2 x 10^{-5} M, respectively, for both diagrams. E_h was assumed to be controlled by (a) the redox couple SO_4^{2-}/HS^- (b) by the redox couple $S^0_{(aq)}/HS$, respectively (Blue and yellow shaded area denotes the solid phase) (Couture & Van Cappellen, 2011)

The effects on mineral stability and aqueous species predominance by addition of Fe to the system As-O-H-S were reported by Lu & Zhu, (2011) (Fig. 1.3). The stability range of orpiment and realgar are retracted appreciably because of the formation of arsenopyrite

(FeAsS). Thus, conversion of As speciation under S and Fe needed further investigation to examine the role of biotic and abiotic processes, comprising redox conditions and identification of microorganisms in the natural sediment.

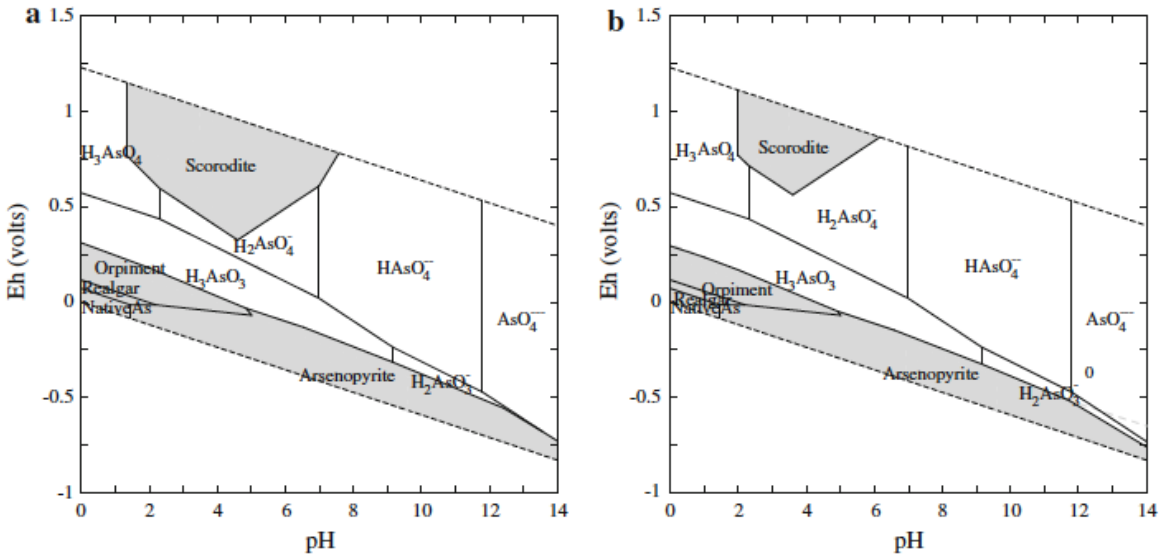

Figure 1.3. E_h-pH diagram for the system As-O-H-S-Fe at 25°C, 1bar. ΣS and ΣFe are set at 10^{-3} M and 10^{-6} M, respectively, for the both diagrams. ΣAs is (a) 10^{-3} M and (b) 10^{-5} M, respectively (Grey shaded area denotes the solid phase) (Lu & Zhu, 2011)

1.2. Arsenic distribution

High As regions are widely distributed around the world (Fig. 1.4). However, they are by no means typical for groundwater environments and only develop under special circumstances. Groundwater As problems usually result from natural sources, including young aquifers and geothermal inputs as well as from artificial activities, mostly mining actions which can occur under both oxidizing and reducing conditions in humid, temperate and arid areas.

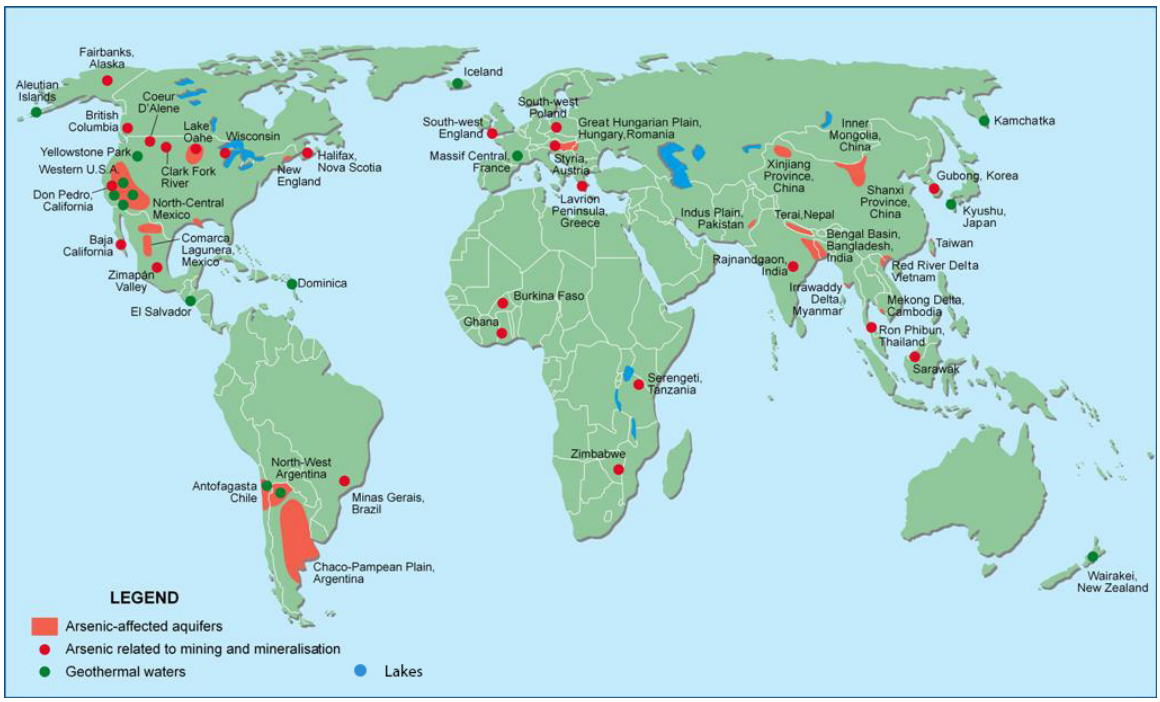

Figure 1.4. Global distribution of As in groundwater and environment related to mining, mineralisation and geothermal sources. (Smedley & Kinniburgh, 2002)

Reducing environments: Under reductive conditions, anaerobic microbial respiration is one important process contributing to the mobilization of As from host minerals (Charlet & Polya, 2006). The mobilization has probably occurred by a complex combination of redox changes brought on by deltaic sediments, including reduction of the solid phase of As to As(III), desorption of As from metal (oxyhydr)oxides. Typical occurrences of release As due to reducing conditions occur in Bangladesh (< 2500 µg/L), West Bengal (< 3200 µg/L), Taiwan (up to 1820 µg/L), Inner Mongolia (< 1740 µg/L), Red River Delta (< 3050 µg/L), and Mekong Delta River of Vietnam (up to 1500 µg/L) (Horneman et al., 2004, Majumder et al., 2014, Berg et al., 2001; Erban et al., 2013). An important question is why arsenic release occurs in reducing environments; this will be discussed in more detail in part 1.3 of As transformation.

Oxidizing environments: Arsenic-bearing minerals, including arsenic-rich pyrite, orpiment, realgar and As-associated metal sulfide such as arsenopyrite (FeAsS), can release great amounts of As when the chemical environment changes. Insoluble As-bearing minerals are rapidly oxidized by exposure to the atmosphere and As(III) is carried by runoff and groundwater flow. As(V), which mainly occurs in oxic conditions after oxidizing As(III), can get easily desorbed under these conditions. This process happens in Argentina (6 – 11500 µg/L), Mexico (8 – 620 µg/L), France (0 – 30 µg/L), United States

(up to 166 µg/L) (Nicolli et al., 1989 ; Smedley & Kinniburgh, 2002; Pili et al., 2013; Schreiber et al., 2000). Moreover, in mining activities, under oxidizing conditions arsenic bearing sulfides get oxidized and, consequently As can be released into the groundwater around mines like in Thailand (up to 5000 µg/L) (Choprapawon & Rodcline, 1987), Ghana (greater than 64 µg/L) (Smedley & Kinniburgh, 2002), United States (up to 12,000 µg/L) (Schreiber et al., 2000).

Geothermal sources: Hot springs are usually highly mineralized because they can leach elements out of rocks on their way to the surface. Arsenic concentrations in geothermal well fluids generally range from 0.1 to 10 mg/kg (Smedley & Kinniburgh, 2002). Most reservoir fluids are undersaturated with respect to FeAsS and other As minerals (Ballantyne & Moore, 1988), and then As leaching is predicted to occur rather than As precipitation. Hot springs and stream with high As content drain unprevented into the nearest catchment system and contaminate shallow aquifers by the natural upward movement of geothermal fluid and some other pollutants from human activity (Welch & Stollenwerk, 2003). As associated with geothermal waters has been reported in several parts of the world including hot springs from parts of the New Zealand, Dominica, France and United States (Hug et al., 2014; Welch & Lico, 1998; Criaud & Fouillac, 1989)

1.3. Arsenic exposure, toxicity and transformation processes

1.3.1 Human exposure pathways and metabolism of arsenic

Humans are exposed to many different forms of inorganic and organic As species in food, water and other environmental media. Routes of arsenic intake in human body are considered to be respiratory for dust and fumes, and oral for arsenic in water, soil and food (Mandal & Suzuki, 2002). As(III) and As(V) take different pathways into animals and human cells. As(III), having a structure similar to glycol, can be transported into cells through aquaglyceroporins including glycerol and urea (Liu et al., 2002). While As(V) can enter into cells through the competition with phosphate transporters (Villa-Bellosta & Sorribas, 2008). As(V) is rapidly reduced to As(III), and then undergoes multisteps in cells through arsenite methyltransferase (AS3MT) using S-adenosylmethionine (SAM) as the methyl donor, in the formation of methylated As compounds (Shankar et al., 2014). Fig. 1.5 displays the structure of several arsenicals of toxicological relevance including inorganic As (i-As) and organic As (o-As) forms are stable methylated mammalian metabolites of the inorganic As (Hughes, 2002). The metabolism of As has an important

role in its toxic effects. Challenger proposed a classical scheme below for the methylation of i-As (Challenger, 1947):

$$As(V) + 2e^- \rightarrow As(III) + CH_3 \rightarrow CH_3As(V) + 2e^- \rightarrow$$

$$CH_3As(III) + CH_3 \rightarrow (CH_3)_2\,As(V) + 2e^- \rightarrow$$

$$(CH_3)_2\,As(III) + CH_3 \rightarrow (CH_3)_3\,As(V) + 2e^- \rightarrow (CH_3)_3\,As(III)$$

where $CH_3As(V)$, monomethylarsonic acid (MMA(V)); $CH_3As(III)$, monomethylarsonous acid (MMA(III)); $(CH_3)_2As(V)$, dimethylarsinic acid (DMA(V)); $(CH_3)_2As(III)$, dimethylarsinous acid (DMA(III)); $(CH_3)_3As(V)$, trimethylarsine oxide (TMAO); $(CH_3)_3As(III)$, trimethylarsine (TMA).

Inorganic arsenic is metabolized by a sequential process involving a two-electron reduction of As(V) to As(III), followed by oxidative methylation to pentavalent organic arsenic. The predominant metabolite of i-As, DMA(V) is rapidly excreted by most mammals. TMAO is the final product in this scheme, but is found in very low amounts in urine.

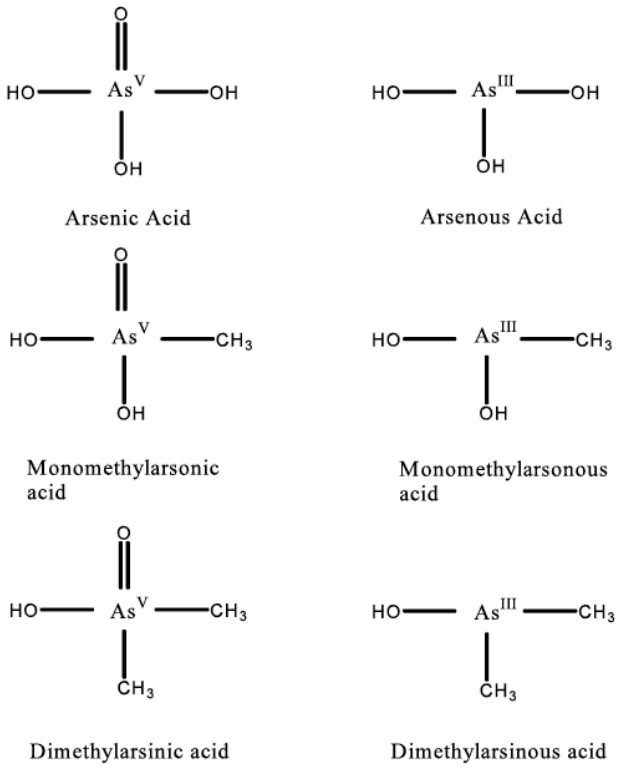

Figure 1.5. Structures of some toxicologically relevant arsenic compounds (Hughes, 2002)

In common with other biomarkers of arsenic exposure, As levels in urine may result from inhalation exposure as well as ingestion from food (rice, seafood, crops, etc.), groundwater (used as drinking water) (Zhu et al., 2014) (Fig. 1.6). As contamination of groundwater is

one of the common pathways of human exposure to i-As. Assessment of As exposure via drinking water is widely based on the measured concentrations in the drinking water and estimations of the consumed amount. Biological monitoring provides data on the absorbed dose for each individual studied using various biomarkers such as the absorbed dose of i-As in urine, blood, hair and nails. Additionally, the sum of As metabolites (i-As + MMA + DMA) in urine are also used as biomarkers of recent arsenic exposure (Mandal & Suzuki, 2002). Rice, the most popular staple in some Asian countries, is particularly efficient in accumulating arsenic into its grain. Thus, in addition to arsenic-tainted groundwater, rice is the major route of arsenic exposure for population subsisting on rice. In the reducing condition, in the rice-soil system, methylation is the key process affecting As speciation and mobility. Similar to As mobilization in sediments, Fe/As reduction under flooded conditions causes the release of arsenic to soil pore water, with As(III) as the dominant species, contributing to high arsenic accumulation in rice. Application of organic matter can enhance As release by promoting iron and As reduction.

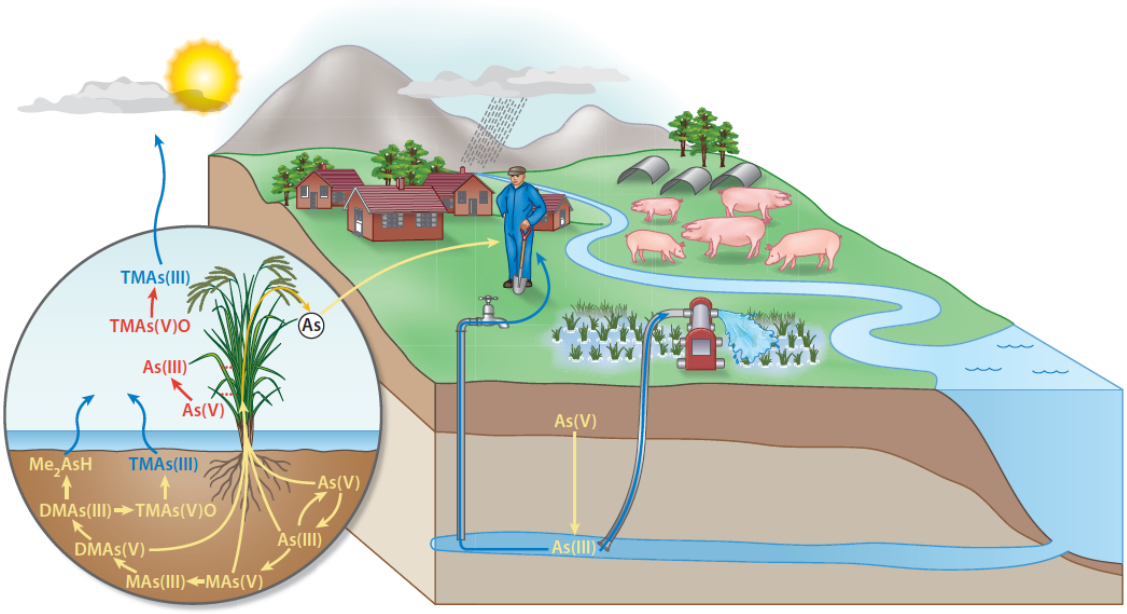

Figure 1.6. Human exposure to groundwater arsenic through drinking water and irrigation of paddy (Zhu et al., 2014)

1.3.2 Arsenic Toxicity and Standard in Drinking water

The chemical forms and oxidation state of As are more important as regards to toxicity. The relative toxicity also depends on physical state, gas, solutions, powder particle size, the rate of absorption into human cells, the rate of elimination, and the pre-existing state of the patient (Mandal & Suzuki, 2002). The toxicity of arsenicals decrease in the order: AsH_3 > i-As(III) > i-As(V) (Hindmarsh & McCurdy, 1986). Vega et al. (2001) also

reported the toxicity order of arsenicals as i-As(III) > MMAO(III) > DMA(V) > MMA(V) > i-As(V) (Vega et al., 2001). Recently, it is widely accepted that thioarsenate species may be produced by gut microbiota and to be toxic to bladder and liver cells. Dimethylmonothioarsenate (DMMTA(V)) was proposed to have the highest cellular retention and intestinal transport of all methylated species. While mono- and trithioarsenate (MTA(V) and TMA(V)) show little cellular retention like As(III) (Hinrichsen et al., 2015).

Two types of poisoning are acute and chronic toxicity. Acute arsenic poisoning is related initially to nausea, vomiting, colicky abdominal pain, profuse watery diarrhea (van Geen et al., 2002). Small amounts (< 5 mg) result in vomiting and diarrhea but resolve in 12 hours and treatment is reported not to be necessary. The lethal dose of As in acute poisoning is observed between 100 and 300 mg (Ratnaike, 2003). Long term As toxicity leads to multisystem disease and the most serious consequence is cancer. Chronic arsenic toxicity can be absorbed to accumulate in the liver, kidney, heart and lung, with smaller amounts in the muscles, nervous systems, gastrointestinal tract, spleen and lung (Ratnaike, 2003). Numerous epidemiological studies in humans have demonstrated the carcinogenic effects of inorganic arsenic from aspiration and oral exposure (Ng et al., 2003). Long-term exposure to arsenic results in chronic arsenic poisoning, namely arsenicosis. Exposure to As leads to an accumulation of As in tissues such as skin, hair and nails, resulting in various clinical symptoms such as keratosis of the hands and feet after 5 -15 years exposure (Tseng, 1977). Examples of arsenicosis and skin cancer are shown in Fig 1.7. Actually, arsenic is deposited in the keratin-rich tissues may cause black-foot disease (Chen et al., 1992). Black-foot disease (BFD) has been the most severe manifestation associated with this type exposure, which was found in Taiwan (Tseng, 1977, Lamm et al., 2006). Moreover, people occupationally exposed to arsenic and through contaminated water are reported to have an increased risk of diabetes (Tseng, 1977).

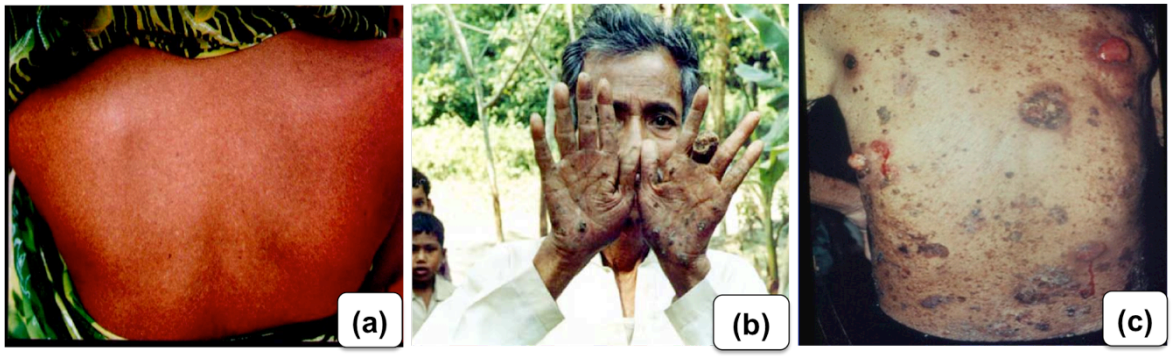

Figure 1.7. Typical skin lesions and skin cancer found in patients who have been chronically exposed to arsenic: (a) hyperpigmentation (b) keratosis, and (c) skin cancer in Southwestern Taiwan.

Cancer risk estimates attributed to As ingestion are mainly based on skin cancer risks. Other internal and more fatal cancers were also reported such as liver, lung, bladder and kidney cancers (Chen et al., 1992; Smith et al., 1992; 2009). Several epidemiological studies based on data from an area of southwestern Taiwan reported to suffer high levels of i-As in the well water supply has found elevated rates of liver cancer deaths. Table 1.1 show some mortality risk ratios for liver, lung, bladder and kidney cancer by As level in drinking water, using cancer mortality rates of the general Taiwanese population (Chen et al., 1992).

Table 1.1. Estimated mortality risk ratios for liver, lung, bladder, and kidney cancer by As concentration in drinking water in Taiwan (Chen et al., 1992)

Cancer site	Sex	Water levels, μg/L				*p*-Value for linear trend
		Background	170	470	800	
Liver	M	1.0	1.2	1.5	2.5	< 0.001
	F	1.0	1.6	2.1	3.6	< 0.001
Lung	M	1.0	1.8	3.3	4.5	< 0.001
	F	1.0	2.8	4.3	8.8	< 0.001
Bladder	M	1.0	5.1	12.1	28.7	< 0.001
	F	1.0	11.9	25.1	65.4	< 0.001
Kidney	M	1.0	4.9	11.9	19.6	< 0.001
	F	1.0	4.0	13.9	37.0	< 0.001

Standard of Arsenic in drinking water

To protect people against arsenic illnesses, the WHO encouraged to lower the drinking water quality guideline from 50 to 10 µg/l (WHO, 2004). In the meantime, most developed countries complied with this standard such as European Unions, Australia and Japan, etc. (Table 1.2). Canada is currently contemplating a further decrease to 5 µg/L. In many developing countries, including Bangladesh and Cambodia the limit of 50 µg/L is still valid. It is mainly because they have no drinking water treatment technologies to reach lower values. In Vietnam, the limit of arsenic has changed from 50 µg/L (TCVN 5502: 1991) to 10 µg/l (TCVN 5502: 2003) in 2003 and remains until now 10 µg/l (QCVN 01:2009/BYT) (Table 1.2). Nonetheless, this limit is under discussion globally as based on a 6×10^{-4} excess skin cancer risk, which is 60 times the factor normally used. In future, values fewer than 3 µg/L are targeted, because several adverse health influences are known to occur at concentration of 10 µg/L (Kapaj, Peterson, Liber, & Bhattacharya, 2006).

Table 1.2. Limitation for arsenic in drinking water

Country/Region	Standard (µg/L)
WHO guideline	10
European Union	10
USA	10
Australia	7
Canada	5
Japan	10
China	50
Bangladesh/India	50
Cambodia	50
Myanmar	50
Vietnam	10

1.3.3 As transformation in sediment and groundwater

The release of As in sediment and groundwater affected regions globally is generally seen as a natural phenomenon. Many various hypotheses presumed to explain high As concentrations in groundwater, but it is difficult to evaluate exactly which mechanisms are driving its mobilization. The interaction between dissolution/precipitation, sorption/ desorption, methylation/demethylation and oxidation/reduction of As in natural systems is summarized in Fig. 1.8 (Zhang & Selim, 2008).

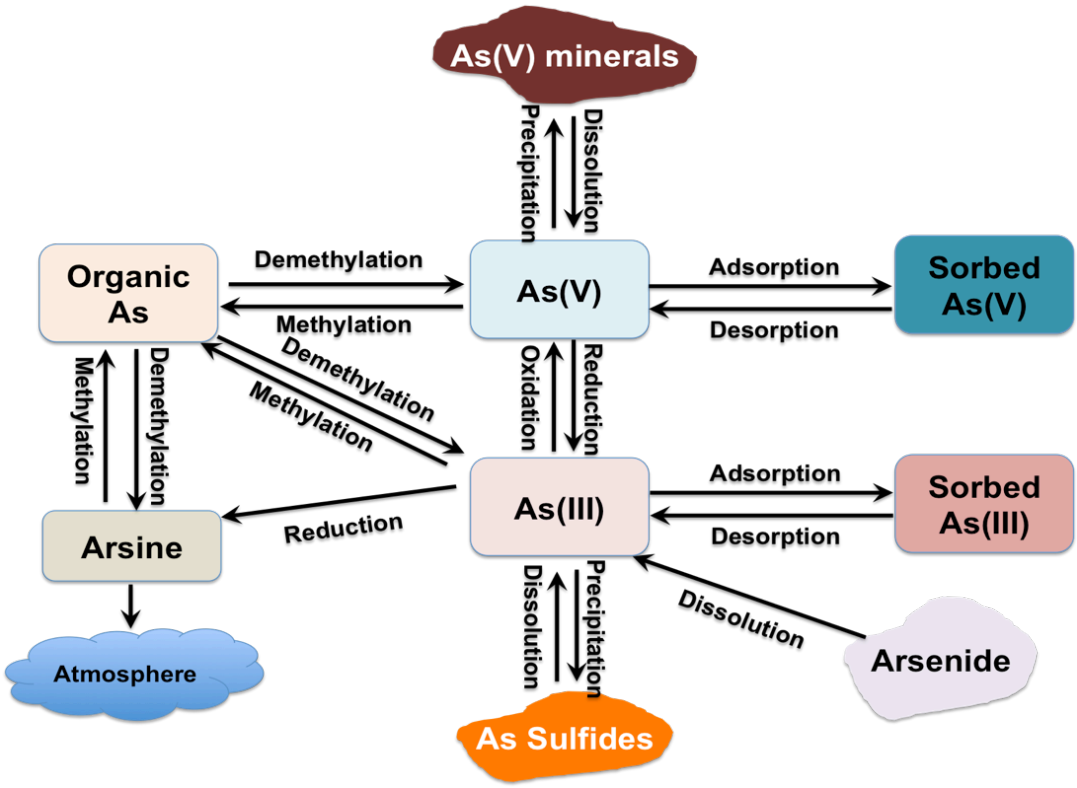

Figure 1.8. Arsenic biogeochemical cycle (Modified from Zhang & Selim, 2008)

Adsorption and Desorption processes

Adsorption reactions between As and mineral surfaces in soil and sediment are generally considered as the most important control on the concentration of aqueous As (Welch & Stollenwerk, 2003). Adsorption of As is mainly dependent on properties of the solid surface, aqueous As concentration, pH, As speciation and competing ion as well as microbial activity (BGS&DFID, 2001). Two general mechanisms for adsorption of As(V) and As(III) on a mineral surface are non-specific adsorption and specific adsorption. Non-specific adsorption, or outer-sphere surface complexation, involves the electrostatic attraction between a charged surface and an oppositely charged ion (Fig. 1.9a). The adsorbed ion resides at a certain distance from the mineral surface. Specific adsorption, also called inner-sphere complexation, connects with the formation of a coordinative complex with the mineral surface (Fig. 1.9b-d) (Cheng et al., 2009).

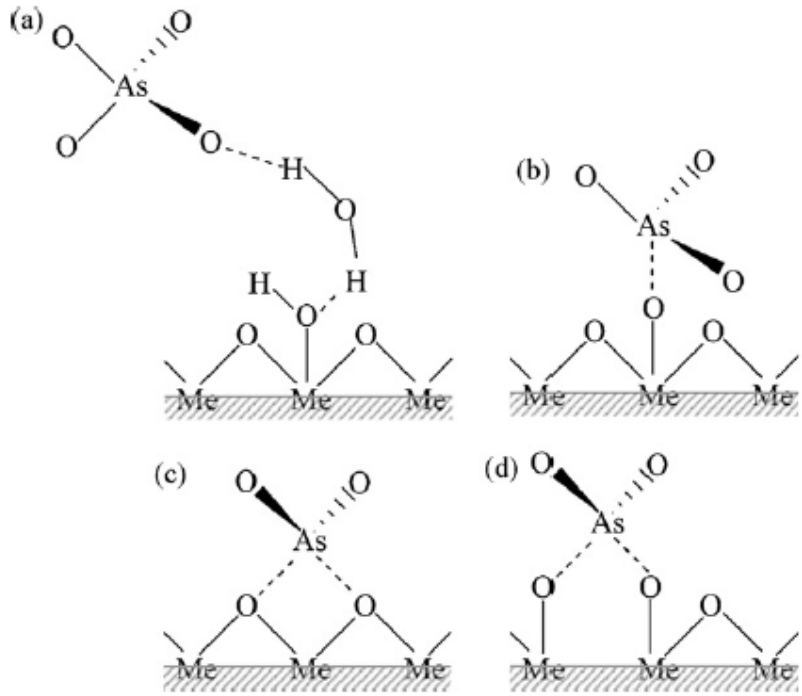

Figure 1.9. Schematic representation of structures of arsenate molecules adsorbed on metal (oxyhydr)oxides surface: (a) outer-sphere surface complexation; (b) mononuclear monodentate inner-sphere complexation; (c) mononuclear bidentate inner-sphere complexation and (d) binuclear bidentate inner-sphere complexation (Cheng et al., 2009)

As can adsorb on many soil colloids, including (oxyhydr)oxides of iron, aluminum and manganese, clay, calcium carbonate and organic matter (Cheng et al., 2009). The adsorption capacity and behavior of these minerals depend on hydration, soil pH, changes in cation coordination, isomorphous substitution and crystallinity (Fendorf et al., 2010). On one hand, mineral surface appears to be positively charged when pH in solution is below its point of zero charge (pH_{pzc}) and negatively when pH is higher than pH_{pzc} (Cheng et al., 2009). The variations of surface charge, as a function of pH for some common soil minerals are summarized in Fig. 1.10. In common pH found in the sediment and groundwater (from 5 to 9), iron and aluminum (oxyhydr)oxides and calcite are positively charged while the clay minerals are negatively charged, which suggests that the former ones are important sorption sinks for negatively charged species.

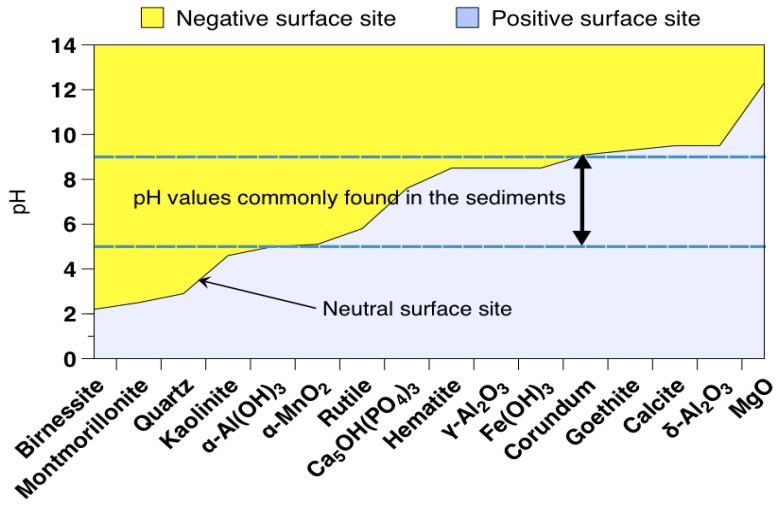

Figure 1.10. The surface charge of common mineral oxides and hydroxides as a function of pH (Cheng et al., 2009; Gorny et al., 2015)

On the other hand, charges of dissolved arsenic species originate from the association and dissociation of H^+ as a function of pH in solution (Smedley & Kinniburgh, 2002). Under the common pH condition of groundwater, As(V) is present as the negatively charged oxyanions $H_2AsO_4^-$ or $HAsO_4^{2-}$, whereas As(III) exhibit as a neutral species H_3AsO_3 (Fig. 1.11). Accordingly, electrostatic attraction can cause As(V) to be sorbed on iron, manganese, and aluminum (oxyhydr)oxides under typical soil and groundwater, while As(III) is highly mobile in such condition (Cheng et al., 2009). The contemporaneous pH dependence of both host mineral surface and As species charges may lead in complex As sorption patterns. The non-specific adsorption i-As species on the mineral surfaces depends on the charges of both the solid and the As species, both of which are pH dependent.

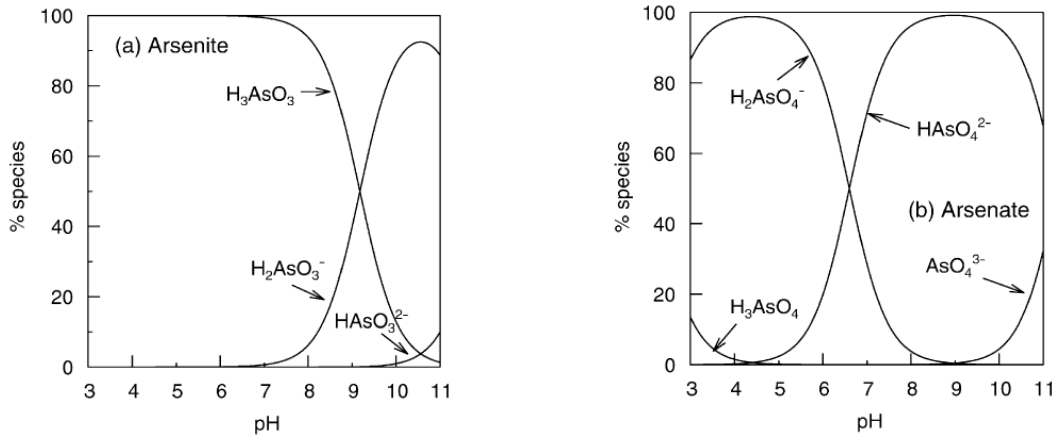

Figure 1.11. (a) Arsenite (As(III)) and (b) Arsenate (As(V)) speciation as a function of pH (ionic strength of about 0.01 M) (Smedley & Kinniburgh, 2002)

Sorption of As onto mineral particles can also be characterized macroscopically by the distribution coefficient, K_d (g/L), which defined as the ratio between the total aqueous concentration and the As solid concentration (Charlet et al., 2011). The most important sorbents of both As(III) and As(V) are metal (oxyhydr)oxides due to their large sorption capacity for a range of negatively and neutrally charged oxyanions and high surface area (Ona-nguema, 2005; Morin et al., 2009; Ona-Nguema et al., 2009; Wang et al., 2011). Many other minerals were also implicated as sorbents of arsenic in natural environments including metal carbonates such as siderite ($FeCO_3$), calcite ($CaCO_3$), metal sulfides, quartz, clays and organic clay complexes (Wolthers et al., 2005; Guo et al., 2010; Guo et al., 2007b; Charlet et al., 2011). Sorption capacities for some of these iron containing minerals are compiled in Table 1.3 (Charlet et al., 2011).

Table 1.3. K_d of As(III) and As (V) onto Fe(II)-Fe(III)-bearing phases derived from sorption edge experiments (pH 7 and 7.5) (Charlet et al., 2011)

Mineral	**Chemical formula**	**Solid, g/L**	**K_d, L/g As(III) at pH 7 (7.5)**	**K_d, L/g As(V) at pH 7 (7.5)**
Ferrihydrite	$Fe_2O_3.0.5H_2O$	0.03	85.72 (87.79)	49.3 (37.59)
Goethite	FeO(OH)	0.5	14.46 (16.1)	8.05
Mackinawite	FeS_m	0.044	2	9
Siderite	$FeCO_3$	2.5	0.28 (0.36)	3.36 (1.86)
Magnetite	Fe_3O_4	3.1	0.08 (0.20)	(8.89)
		0.5	1.85 (2.02)	-
Fougerite	$[Fe^{2+}_4Fe^{3+}_2(OH)_{12}][CO_3].3H_2O$	4.5	0.12 (0.42)	-
Vivianite	$Fe_3(PO_4)_2.8H_2O$	2.5	-	0.18 (0.18)
Muscovite	$KAl_2(AlSi_3O_{10})(F,OH)_2$	4.1	0.36 (0.13)	0.36 (0.13)
Biotite	$K(Mg,Fe)_3AlSi_3O_{10}(F,OH)_2$	4.25	0.97 (0.31)	3.4 (0.9)

Generally, iron (oxyhydr)oxides are the most widely involved natural minerals in the adsorption of As in both acidic and alkaline soils. While aluminum (oxyhydr)oxides, clay, manganese oxides, and organic matter may play some role only in acidic soils (Cheng et al., 2009). In iron-rich environments, As sorption complexes to Fe minerals often play a critical role. Iron (oxyhydr)oxides are considered to be the most important sorbents of aqueous As within oxic conditions. Sorption of As(V) onto amorphous iron oxides and goethite is more favorable than that of As(III) below pH 5 – 6, whereas, above pH 7 – 8, As(III) has a higher affinity for the solids (Dixit & Hering, 2003). Particularly, As(III) species sorb on ferrihydrite faster than As(V) with relative high As concentration and at

solution pH above 8, but As(V) adsorption is faster at low As concentration at low pH (Jain et al., 1999). In anoxic environments, iron (oxyhydr)oxides are subject to reductive dissolution by falculatively anaerobic bacteria such as *Geobacter* sp. and *Shewnella* sp. (Lovley & Phillips, 1986). As is often released under such reducing conditions as Fe(II) and As(III) species predominate (Islam et al., 2004). Geochemical and spectroscopic studies have shown that As adsorbed onto Fe sulfides is a potentially important As sequestration mechanisms in anoxic environments (Couture et al., 2013; Wolthers et al., 2005). Both As(III) and As(V) sorb on disordered mackinawite (FeS) at a fast rate and form predominantly outer-sphere complexes at the surface (Wolthers et al., 2005). However, As(III) and As(V) sorption onto Fe sulfides has received far less attention, partly because the experimental challenges. Recently, investigations on effect of dissolved organic matter (DOM) on As mobility indicates that the presence of DOM can cause release of adsorbed arsenic due to competition for sorption sites, formation of highly soluble arseno-organic complexes and reactions between organic species and As (Zhu et al., 2011). Moreover, DOM is known to catalyze both oxidation and reduction reactions, and then can promote transformation of As species and reductive desorption (Bauer & Blodau, 2006). The presence of DOM may compete with As for adsorption sites on mineral surface, hence increasing its potential bioavailability. Grafe et al. found that both humid acid (HA) and fulvic acid (FA) decreased As(V) adsorption in goethite between pH 6 and 9 from 17 to 27% compared with the absence of DOC conditions (Grafe et al., 2001).

Additionally, the mechanism of As inner sphere with iron minerals have been studying by using X-ray absorption spectroscopy. On the surface of goethite, lepidocrocite, mackinawite and pyrite, As(V) and As(III) formed bidentate inner-sphere complexes on the oxyhydroxide substrate while the complexes formed with sulfide minerals are outer sphere (Farquhar et al., 2002). Fendorf et al. (1997) and Grossl et al. (1997) reported that three types of surface complexes can form during As(V) adsorption on goethite: nonodentate surface complexes at low surface coverage; bidentate mononuclear complexes at high surface coverage; and bidentate binuclear complexes at surface coverage near monolayer capacity (Fig. 1.9b-d).

Because other anions (e.g., PO_4^{3-}, SO_4^{2-}, HCO_3^-...) have similar or higher charge densities than arsenic, they may compete for the same sorption sites on mineral surface and lead to reduced As adsorption and even desorption (Cheng et al., 2009). Adsorption isotherms of As on conditioned layered double hydroxides, particularly in Mg-Al-CO_3 hydroxide

experiment, suggested that the As(V) adsorption capacity decreases in the presence of various individual competing anions in the following order: $HPO_4^{2-} > SO_4^{2-} > CO_3^{2-} > Cl^- > NO_3^- > F^-$ (Dadwhal et al., 2011). Phosphate has similar chemical properties and behaviors as As(V), often strongly competes with As(V) for sorption sites in metal oxide surfaces such as goethite, gibbsite, kaolinite, montmorillonite, illite, and quartz (Manning & Goldberg, 1996a, 1996b; Xu et al., 1988).

Precipitation and Dissolution Processes

Formation of environmental alkaline or transition metal arsenate solid complexes as limiting minerals phases, which readily precipitate when supersaturated, may potentially control concentrations of aqueous As and change its distribution between solution and solid phase. In groundwater and sediment, As is often present in trace concentrations which is not sufficient to precipitate as arsenic minerals (Zhang & Selim, 2008). Table 1.4 summarizes the solubility product constants (K_{sp}) of some arsenic containing complexes.

Table 1.4. Solubility product constant of some arsenic containing complexes (Cheng et al., 2009)

Compound	Solubility constant (K_{sp}) at 25°C	AsO_4^{3-} concentration (mol/L)
$AlAsO_4$	1.6×10^{-16}	1.60×10^{-10}
$Ba_3(AsO_4)_2$	8.0×10^{-51}	8.94×10^{-17}
$BiAsO_4$	4.4×10^{-10}	4.40×10^{-5}
$Ca_3(AsO_4)_2$	6.8×10^{-19}	8.25×10^{-1}
$Cd_3(AsO_4)_2$	2.2×10^{-33}	4.69×10^{-8}
$CrAsO_4$	7.7×10^{-21}	7.70×10^{-15}
$Co_3(AsO_4)_2$	7.6×10^{-29}	8.72×10^{-6}
$Cu_3(AsO_4)_2$	7.6×10^{-36}	2.76×10^{-10}
$FeAsO_4$	5.7×10^{-21}	5.70×10^{-15}
$Pb_3(AsO_4)_2$	4.6×10^{-36}	2.14×10^{-9}
$Mg_3(AsO_4)_2$	2.1×10^{-20}	1.45×10^{-1}
$Mn_3(AsO_4)_2$	1.9×10^{-29}	4.36×10^{-6}
$Ni_3(AsO_4)_2$	3.1×10^{-26}	1.76×10^{-4}
$Ag_3(AsO_4)_2$	1.0×10^{-22}	1.00×10^{-4}
$Sr_3(AsO_4)_2$	8.1×10^{-19}	9.00×10^{-1}
$Zn_3(AsO_4)_2$	1.3×10^{-28}	1.14×10^{-5}
As_2S_3	2.1×10^{-22}	1.45×10^{-2}

Arsenic mobility is more controlled by co-precipitation with other major phases such as iron (oxyhydr)oxides and then by their dissolution and precipitation phases (Violante et al., 2006). Iron (oxyhydr)oxides are well known As bearing phases which are thermodynamically stable only under oxidizing conditions. The reductive dissolution of different Fe (oxyhydr)oxides, which are common in sedimentary environments, is widely accepted as a key process for the release of As into groundwater (Charlet et al., 2011;

Parsons et al., 2013). Besides, low dissolved Fe concentrations in high dissolved As regions, however, indicate that processes involved are more complicated than unique dissolution of Fe (oxyhydr)oxides with subsequent release of incorporated or adsorbed As. Processes may be caused by reabsorption of As or Fe(II) to surfaces as well as co-precipitation and transformation of Fe phases (Horneman et al., 2004; Kocar et al., 2008; Parsons et al., 2013).

In addition, arsenic minerals are shown to precipitate in scorodite ($FeAsO_4.2H_2O$) and amorphous ferric arsenate (Paktunc & Bruggeman, 2010). When As(III) is dominant, the precipitation of $CaHAsO_3$ is thought to act as a possible control on As mobility (Román-Ross et al., 2006). In the presence of sulfur and iron, As can sequester in solid phases by precipitation in arsenic sulfide minerals including orpiment (As_2S_3) and realgar (AsS), perhaps as a consequence of anaerobically bacterial activity (O'Day et al., 2004; Root et al., 2009).

Methylation and demethylation

The biological transformations of both inorganic and organic As species can be achieved by means of the bacterial activity through either detoxification or dissimilatory (Zhang & Selim, 2008). Methylation of inorganic arsenic species by aerobic and anaerobic microorganisms produces MMAA(V), DMAA(V) and TMAO. It was demonstrated that several anaerobic bacteria, methanogenic and sulfate-reducing bacteria, are accountable for arsenic methylation (Cullen & Reimer, 1989). It is widely accepted that the biomethylation goes through the Challenger pathway, where i-As and o-As undergo an alternating sequence of reduction (+ $2e^-$) and oxidative methylation (+ CH_3) reactions as schematically represented in Fig. 1.12. The sequence of this scheme is thermodynamically favored at neutral pH for redox potentials with $p_e < 0$ and methyl cation activities $pCH_3^+ < -7$ to -3 depending on the precise analyzed situation (Dombrowski et al., 2005).

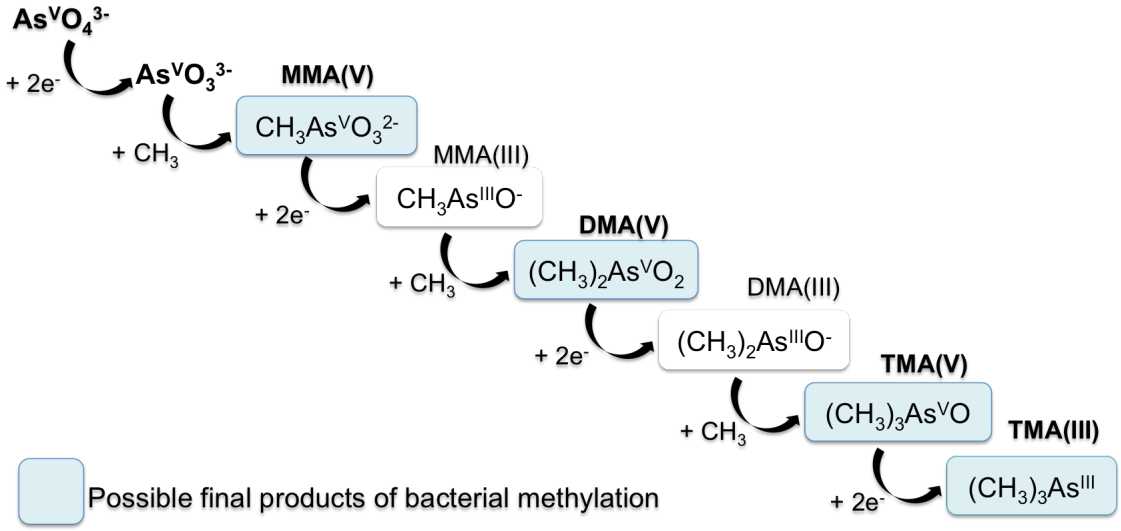

Figure 1.12. Hypothetical concept of bacterial methylation (Challenger, 1947; Dombrowski et al., 2005; Gorny et al., 2015)

As is widely cycled through i-As, methylarsenicals and other organic forms in surface waters and soils. Although biomethylation process is often received less attention than redox transformations between inorganic As(III) and As(V), methylarsenicals were reported in aquifers globally including in aquifers of West Bengal (Shraim et al., 2002), China (Lin et al., 2002), Taiwan (Lin et al., 1998), Cyprus (Christodoulidou et al., 2012), and the USA (Magu et al., 2015). Demethylarsinate (DMA(V)) concentrations correlates strongly with As(III) concentration, and less with the temperature and specific conductance of the bedrock aquifer (Magu et al., 2015).

Oxidation and Reduction processes

Redox reactions also control the mobility of As in the natural environment. Depending on the redox state of the water or sediment, i-As will either be oxidized or reduced. An E_h-pH diagram (Fig. 1.1) presents the stability of dissolved As species in either oxidizing and reducing conditions. The main oxidation states in the liquid and solid phase are V and III (Smedley & Kinniburgh, 2002). The conversion from As(III) to As(V) also occurs in nature both by chemically and biologically mediated process. The aspects will also be approached below.

Oxidation of As(III): Manganese (hydr)oxides and the bacterial activity are widely accepted to oxidize As(III) in the range of pH 5 – 9 (Jones et al., 2012; Lafferty et al., 2010, 2011). The oxidation process by Mn oxides results in As(V) complexes and production of Mn(II) and Mn(III) by reduction and disproportionation into solution and solid phase (Lafferty, 2010a, 2010b; Scott & Morgan, 1995). Particularly, this chemical

oxidation occurs in three main steps: (i) formation of an inner sphere complex between As(III) and surface sites of Mn(IV) (hydr)oxides; (ii) oxidation of As(III) to As(V) together with reduction Mn^{4+} to Mn^{2+} and (iii) successive desorption of As(V) and Mn^{2+}. The rate of reactions start fast but slows down significantly due to passivation of Mn oxides surface and highly dependent on pH conditions (Scott & Morgan, 1995).

Additionally, microbes have been shown to oxidize As(III) both as chemilithoautotropic metabolism generating energy process and as a detoxification mechanism in heterotrophic bacteria (Gihring et al., 2001; Oremland, 2003; Rhine, 2005). More than 30 species could be involved, including α-, β-, γ-, δ-, and ε-Proteobacteria; Deinocci and Archaeota (Fig. 1.13). Heterotrophic oxidation of As(III) is primarily converts As(III) encountered in the cell's outer membrane into the less toxic form as As(V). While chemolithoautotrophic arsenite oxidizes couples the oxidation of As(III) to the reduction of either oxygen or nitrate and use the energy delivered ro fix CO_2 into organic material (Oremland, 2003). Several species of oxidation As(III) was isolated and summarized in Fig. 1.13.

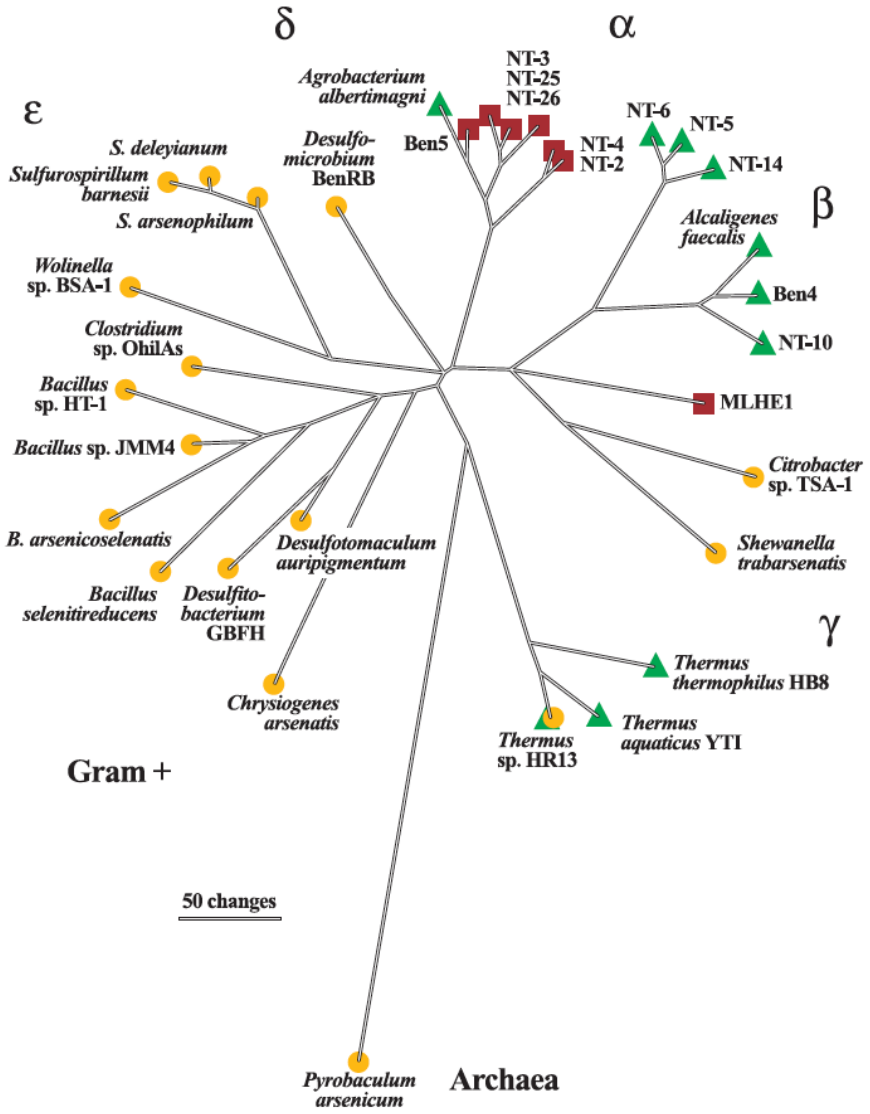

Figure 1.13. Phylogenetic trees of representative arsenic-metabolizing prokaryotics. Yellow circles indicate dissimilatory arsenate-respiring species, green triangles indicate heterotrophic oxidizers and red squares indicate chemoautotrophic arsenite oxidizers (Oremland, 2003)

The coexistence of these abiotic and biotic pathways often occurs in soil and sediment. Throughout the batch experiments, Jones et al. suggested that the rate of As(V) generation in solution was greater for the combined bath experiments, where bacteria and Mn oxides was mixed to oxidize As(III) than for either component alone (Fig. 1.14) (Jones et al., 2012)

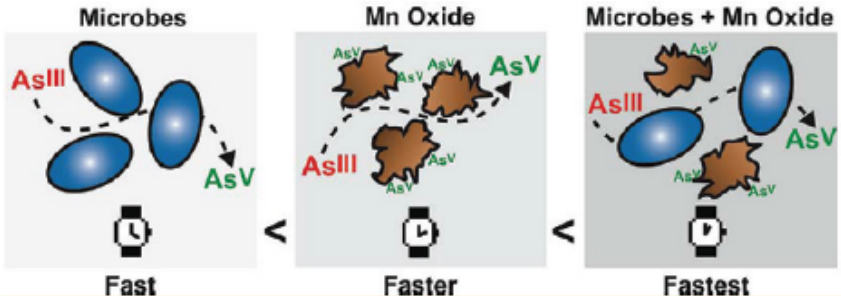

Figure 1.14. Comparison of the rate oxidation As(III) between abiotic, biotic and combinative systems (Jones et al., 2012)

Although thermodynamic data predicts that oxygen can numerically oxidize As(III), the reaction kinetic is often slow with half-times ranging from several months to a year (Smedley & Kinniburgh, 2002). Iron (oxyhydr)oxides can oxidize As(III) to As(V) in the absence of dissolved oxygen including green rust, goethite, magnetite or ferrihydrite (Planer-Friedrich & Wallschläger, 2009b; Wilkin et al., 2003). Nonetheless, the fast oxidation has been known as the photooxidation of As(III) in the presence of dissolved Fe(II) and Fe(III) (Bhandari et al., 2012) or as the photocatalytic TiO_2 (Moon et al., 2014; Zhang et al., 2015). Under the oxic condition in the presence of iron (oxyhydr)oxides, the photoinduced oxidation of As(III) produces Fe(II) and As(V), thus aqueous reactive oxygen species may lead to further oxidation of As(III) in solution (Fig. 1.15). Unlike TiO_2 and iron (oxyhydr)oxides, the oxidation of As(III) by Na-birnessite can be enhanced via irradiation with simulated solar light at pH of 5 (Shumlas et al., 2016). Other oxidants such as elemental sulfur (S^0) may oxidize As(III) to thiorarsenate species during the anoxic conditions (Burton et al., 2013; Couture et al., 2013a)

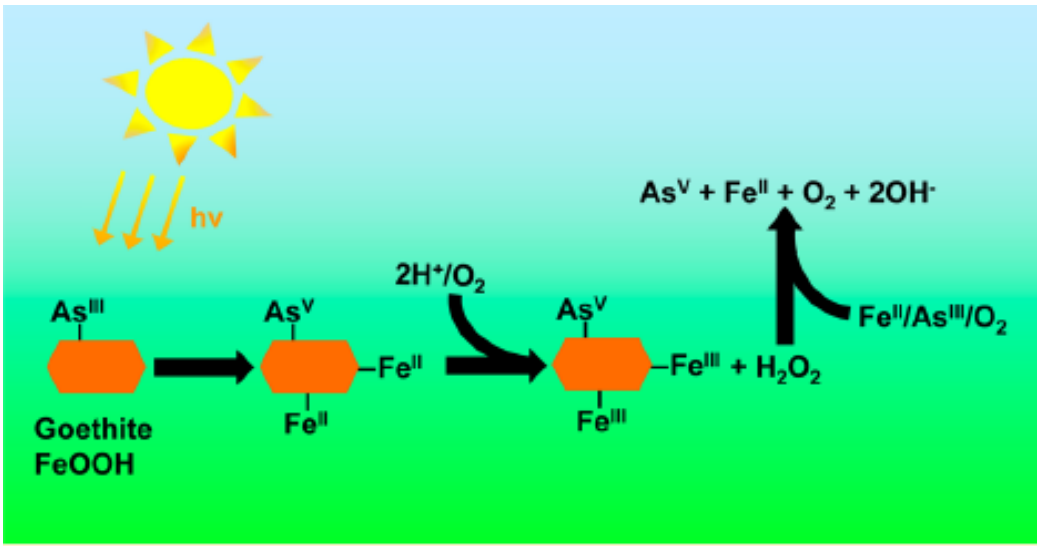

Figure 1.15. Mechanism of photooxidation of As(III) to As(V) in the presence of iron

(oxyhydr)oxides (Bhandari et al., 2012)

Reduction of As(V): The reduction As(V) process is mainly effective in the presence of reduced sulfur and microbial activities (Oremland, 2003; Rochette et al., 2000). High dissolved sulfide concentration can reduce As(V) to As(III) and several intermediate forms of thioarsenic species (Rochette et al., 2000). However, these reduction mechanisms should be studied in the future. The main factors, including pH, presence of Fe(II), S^0 and O_2 can effect the reduction of As(V). The reducing rate of As was faster at pH 4 than at pH 7 and 10 (Gorny et al., 2015). Biologically, As(V) can be reduced by some microorganisms. Two closely related representatives of the ε-Photeobacteria, including *Sulfurospirillum arsenophilum* and *Sulfurospirillum barnesii* (Fig. 1.13). These organisms can use several electron donors such as hydrogen, acetate, latace, pyruvate, butyrate, etc. (Oremland, 2003).

1.3.4 Processing affecting of redox conditions

Oxidation-Reduction (Redox) is a chemical reaction in which electrons are transferred from a donor to an acceptor. The electron donor loses electrons and increases its oxidation number or is oxidized; the acceptor gains electrons and decreases its oxidation number or is reduced. The source of electrons for biological reductions is organic matter. Redox conditions affect profoundly the mobility, toxicity, and the risk to humans by many trace metals and metalloids including As (Borch et al., 2010). Moreover, the biogeochemical behavior of other elements may be indirectly coupled to redox transformation of natural organic matter and mineral phases such as Fe oxy-hydroxides, Fe-bearing clay mineral and Fe sulfides. The sequence of redox reactions that occurs along redox gradients in time or space depends on chemical composition, microbial activity, and the redox potential, which are illustrated in Fig. 1.16 (Borch et al., 2010).

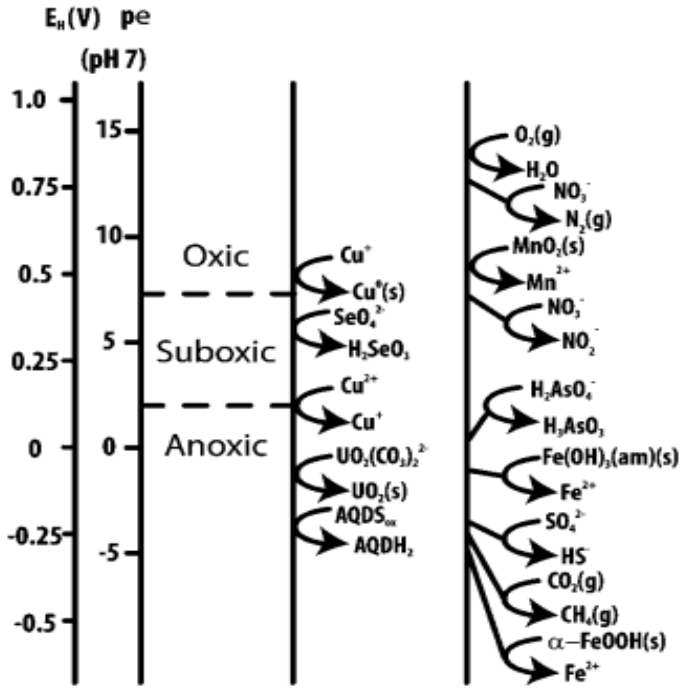

Figure 1.16. Redox ladder showing the environmentally relevant redox couples at pH 7 (Borch et al., 2010; Essington, 2004)

The reduction sequence observed commonly in pH 6.5 to 7 soils is as follows: the oxic (E_h > 421 mV), suboxic (120 < E_h < 414 mV), and anoxic conditions (E_h < 120 mV) (Essington, 2004). Depending on oxygen depletion in a sediment matrix, further changes in redox conditions are usually determined by the availability of labile organic carbon (or another suitable electron donor). Several factors affected by the redox conditions in the soil include two major factors (i) the rate of oxygen diffusion (ii) microbial metabolism of organic matter (Borch et al., 2010).

(i) Oxygen diffusion: Oxygen may also be transported from the surface to significant depth within porewater moving inside an aquifer. During periods of flooding, pores in surface soils become saturated with water and diffusion of oxygen from the atmosphere to the soil and sediment is restricted (Fig. 1.17). Soils with limited pore connectivity and low porosity can more easily become suboxic and anoxic at a shallow depth than soils with high porosity. The rate of oxygen diffusion is also controlled by the composition of the fluid occupying the pore space. In the water, the rate of oxygen diffusion occurs 10^4 times slower than in air (Ponnamperuma, 1972). Within a few hours of soil submergence, microorganisms use up the oxygen present in the water or trapped in the soil and render a submerged soil void from oxygen. Therefore seasonal changes of soil moisture can cause dramatically oscillations in oxygen concentration in sediment and thus redox profiles

(Charlet et al., 2013; Parsons et al., 2013; Couture et al., 2015). Additionally, aquifers with a high hydraulic gradient and conductivity may transport fluids very rapidly both vertically and horizontally. This can lead to the presence of oxygen-rich water at sediment layers. Hydraulic gradient can alter dramatically depending on seasonal aquifers recharge; hence deep aquifers are not supplied with oxygen through surface oxygen diffusion, are also subject to fluctuating redox zonation (Greskowiak et al., 2006).

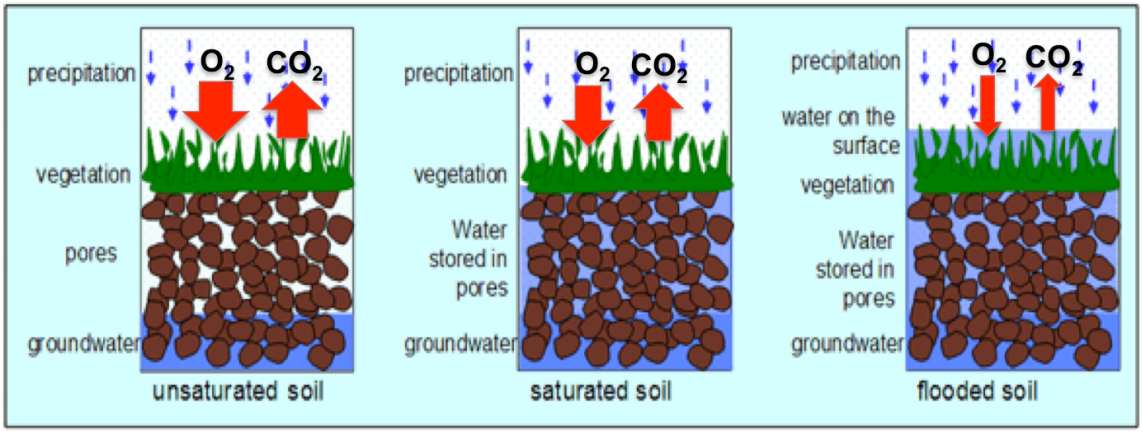

Figure 1.17. How saturated and flooded soil causes changes to redox conditions via limiting diffusion of oxygen from the surface to aerobic soil bacteria resulting in rapid oxygen depletion.

(ii) Microbial metabolism: The second factor control on redox conditions is the microbial metabolism of organic matter linked to the reduction of various terminal electron acceptors (TEA) (Parsons, 2011). In a redox reaction, the reducing agent loses electrons and the oxidizing agent accepts electrons. Depending on the type of electron acceptors used by microorganisms, microbes can be classified into variable types. Strict aerobes can only use oxygen as a terminal electron acceptor. Obligate anaerobes are actually inhibited by oxygen. Facultative anaerobes are flexible in electron acceptor usage, which maintain a supply of energy as oxygen levels decrease. The diversity of microbial and fungal facultative and obligate anaerobic microorganisms are also able to use oxygen containing compounds such as nitrate, sulfate or iron oxides to metabolize organic matter, in some cases completely to CO_2 (Lovley, 1987). The main succession of electron acceptor usage in flooded soil is as follows in Table 1.5. Fermentation is a different form of metabolism from respiration that occurs in the absence of a suitable TEA. The various products of fermentation, including lactate and acetate are released into the surrounding soil and thus become available for other anaerobic organisms. In addition, fermentation generally

reduces the soil pH, which will lead dissolution of minerals and their subsequent access by bacteria (Richardson & Vepraskas, 2001).

Table 1.5. The reduction sequence in flooded soils by microbial metabolism of organic matter using succession of electron acceptors (Stumm and Morgan, 1996)

Process	Electron haft reaction	Microbes
Aerobic respiration	$½\ O_2 + 2e^- + 2H^+ \rightarrow H_2O$	Facultative anaerobes and aerobes
Denitrification	$2NO_3^- + 12H^+ + 10e^- \rightarrow N_2 + 6H_2O$	Denitrifiers
Manganese reduction	$MnO_2 + 4H^+ + 2e^- \rightarrow Mn^{2+} + 2H_2O$	Manganese reducing bacteria
Iron reduction	$Fe(OH)_3 + 3H^+ + 2e^- \rightarrow Fe^{2+} + 2H_2O$	Iron reducing bacteria
Sulfate reduction	$SO_4^{2-} + 10H^+ + 8e^- \rightarrow H_2S + 4H_2O$	Sulfate reducing bacteria
Methane production	$CO_2 + 8H^+ + 8e^- \rightarrow CH_4 + 2H_2O$	Methanogens

As available oxygen declines, organisms can develop under anoxic conditions using alternative electron acceptors. The order in which available electron acceptors are consumed can generally be predicted by the redox potential and associated energy yields of electron pairs (Fig. 1.18). Changes in redox conditions over the time reflects the successive availability of TEA and will govern which microbes will grow up through being able to use them.

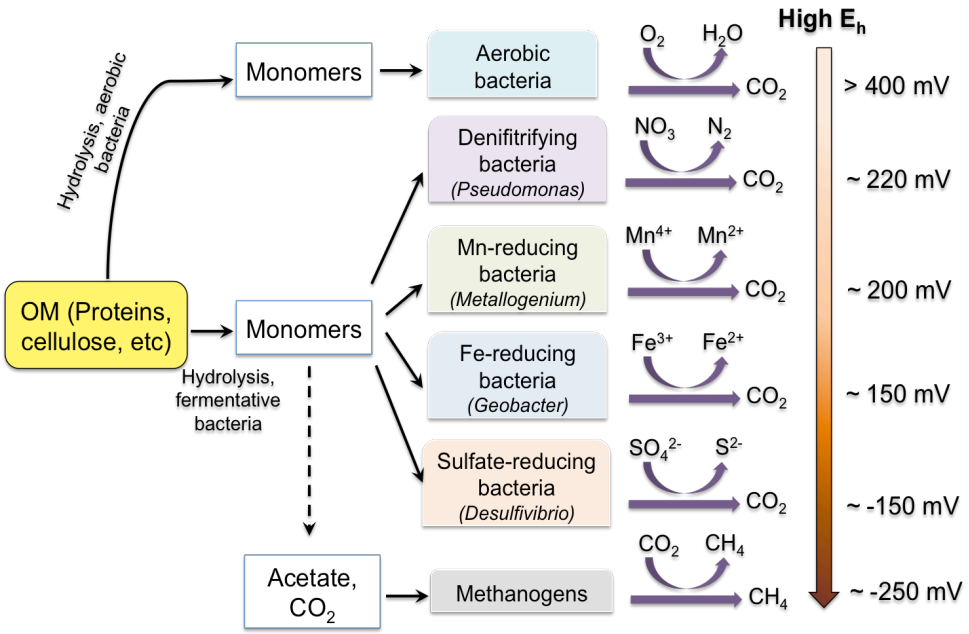

Figure 1.18. Summary of reducing sequence in soils driven by microbial metabolism of organic matter (extracted from Richardson & Vepraskas, 2001)

1.3.5 Influence of Microbial Sulfate Reduction on Arsenic mobility

The environmental fate and transport of As is thus closely related to the biogeochemical cycling of iron, sulfur and carbon (Bostick et al., 2003; Couture et al., 2013; O'Day et al., 2004; Root et al., 2009). Microorganisms play an important role in sulfur transformation. Sulfate-reducing bacteria (SRB) are anaerobic microorganisms that are widely spread in anoxic habitats, where sulfate is used as a terminal electron acceptor for degradation of organic compounds. This may lead to produce of sulfide and others reduced sulfur species such as elemental sulfur (Muyzer & Stams, 2008). In nature, sulfides produced during microbial sulfate reduction mostly reacts with metal ions, especially Fe, and largely precipitate as pyrite (FeS_2) or iron monosulfide (FeS_m) (Rickard & Iii, 2007; Wilkin et al., 2003, Rickard, 2006). Under the latter conditions, As is uptake by the adsorption on FeS_m (Wolthers et al., 2005) or through the formation of realgar ($AsS_{(s)}$) (Gallegos et al., 2008). When all the reactive Fe is transformed into Fe sulfides, the remaining free sulfide (S^{2-}) become available to complex As as As sulfide minerals such as $AsS_{(s)}$ and orpiment (As_2S_3), and the formation of thiolated As species (Fisher et al., 2008; Planer-Friedrich et al., 2010; Suess et al., 2009). Fig. 1.19 shows the summary of the primary adsorption and precipitation reactions controlling arsenic uptake and release in the As-Fe-S system relation to the dissolution/precipitation reactions, and the microbial organic matter oxidation.

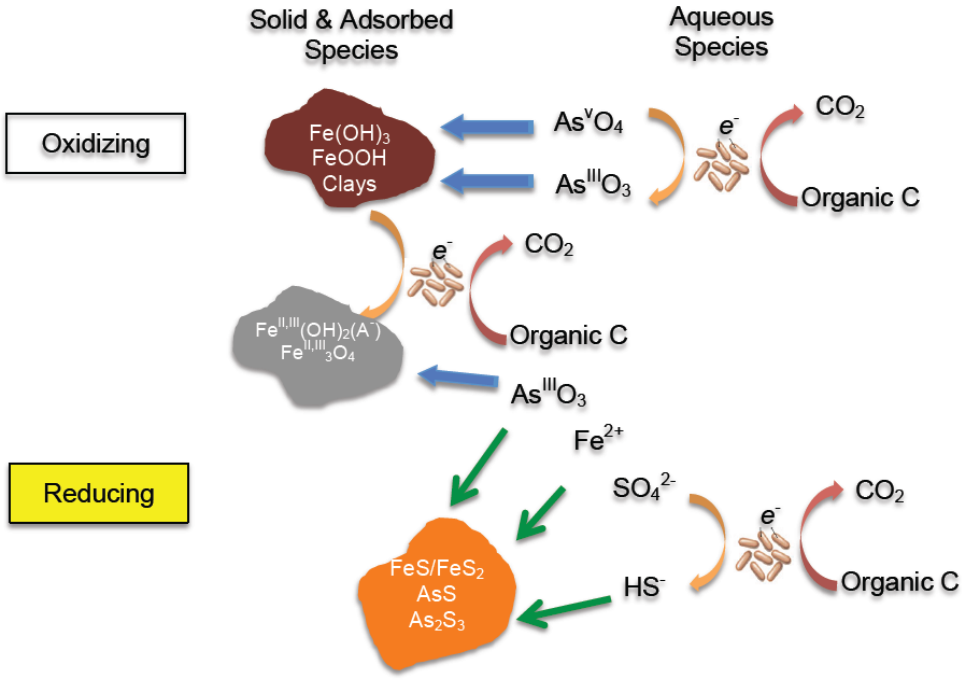

Figure 1.19. Biogeochemical model in the As-Fe-S system (O'Day et al., 2004)

On one hand, Kirk's study found that As solubility and extractability decrease under anoxic, sulfate-reducing conditions in deeper aquifer systems and thus is associated with limiting As contamination (Kirk et al., 2010). Accordingly, microbial sulfate reduction is generally thought to cause decreased As mobility in subsurface environments (Fendorf et al., 2010). On the other hand, recent studies showed that under some conditions sulfate reduction can result in increase As mobility during replacement of ferrihydrite ($Fe(OH)_3$) by mackinawite (Kocar et al., 2008). Moreover, conceptual model of the formation of As – S – Organic matter (OM) under anoxic condition is proposed by Couture et al. (2013b). In the sediment enriched in labile OM, the formation of thiols appears to be the primary sink for sulfides and others reduced S species produced by microbial sulfate reduction. This leads to enhancement of As sequestration through the formation of AsS and other thiol-bound As(III) organic matter complexes (thioAs(III)-OM), suggesting that thiols group could be used as remediation pathway for As. In sediment poor reactive OM, the dominant sink for sulfides is the formation of Fe-minerals and elemental S. The remaining sulfides are available to complex and form As sulfide minerals (Fig. 1.20)

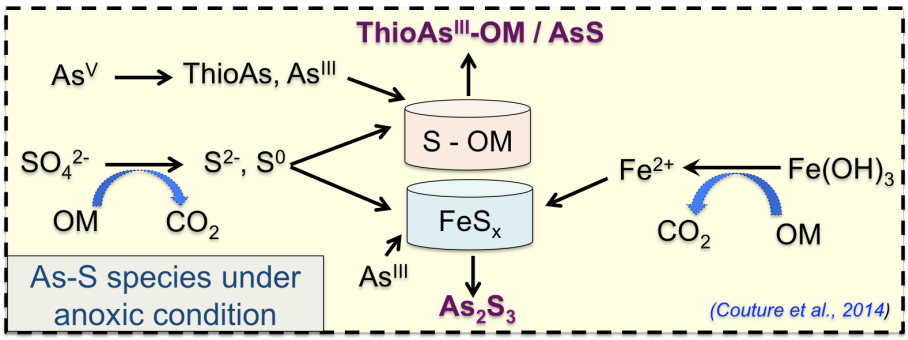

Figure 1.20. Conceptual model of the formation of As-S species under anoxic conditions. Solid lines indicate the formation of a complex; blue lines indicate organic matter (OM) oxidation reactions (Extracted from Couture et al., 2013b)

1.4. Arsenic presence in aquifers from the Mekong Delta Vietnam

1.4.1 Overview

The Mekong delta floodplain in Southern Vietnam spread out over 52,100 km^2 (Nguyen et al., 2000). At Phnom Penh, the Mekong Delta divides into two branches: the Mekong to the east and the Bassac to the south. Southward, both rivers spread out to form a delta plain. The present Mekong delta was formed during the last 6000 – 10,000 years (Holocene) (Tamura et al., 2007) and consists of alluvial sediment of marine and fluvial origin (Nguyen et al., 2000). Arsenic is a serious natural contaminant in aquifers of deltaic

Southeast Asian regions, including the Mekong Delta, where it affects the health of millions (Stanger et al., 2005; Buschmann et al., 2008a; Nguyen & Itoi, 2009; Hoang et al., 2010; Erban et al., 2013; Erban et al, 2014). Since the daily use of well water has become popular in the Mekong Delta only during the last two decades, it is expected that victims suffering from chronic arsenic poisoning will also be identified in the near future (Hanh et al., 2011; Merola et al., 2015). This is particularly true since recent findings have shown high contamination in groundwater from large areas in the Southwest Vietnam, including An Giang, Dong Thap, Long An and Tien Giang (Shinkai et al., 2007; Bang et al., 2008; Erban et al., 2013). A national survey of As in wells conducted from 2002 to 2008 by the Department of water Resources Management in Vietnam includes 42,921 observations in the Mekong Delta. This large area (>1000 km^2) has nearly 900 wells that are contaminated (Erban et al., 2013). However, the hotspot of As contamination (> 100ppb) was found in the shallow wells in the upper Mekong Delta, located near Cambodia (Fig 1.21).

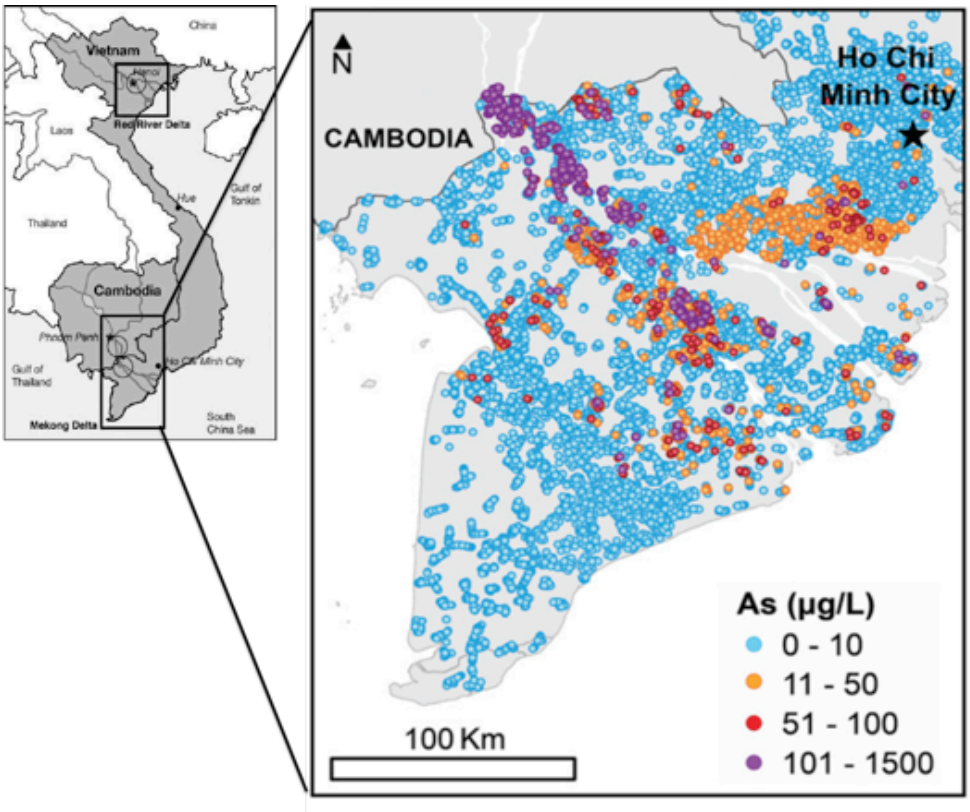

Figure 1.21. Plan view of groundwater arsenic concentration in the Mekong Delta Vietnam (Erban et al., 2013)

Additionally, Nguyen & Itoi (2009) and Hoang et al. (2010) have also reported the distribution of arsenic corresponding to areas along the Mekong River from An Giang to Can Tho province as shown in Fig. 1.22. Total dissolved As concentrations range from 1 –

741 ppb. As concentration values ranged from 1.4 – 219 ppb in several communes in An Giang including Tan Chau, Chau Phu, Long Xuyen. Arsenic concentrations exceeding 100 ppb are present at depths less than 100 m in Tan Chau. Concentration and species of As depend on redox potential (E_h). On one hand, with positive E_h values, low dissolved Fe and As concentrations are observed because of the precipitation of Fe (oxyhydr)oxides. On the other hand, high As and Fe concentrations are detected in the samples which have negative E_h values (Nguyen & Itoi, 2009). However, both the sources and release mechanisms of As to aquifers in this region remain areas of intense debate.

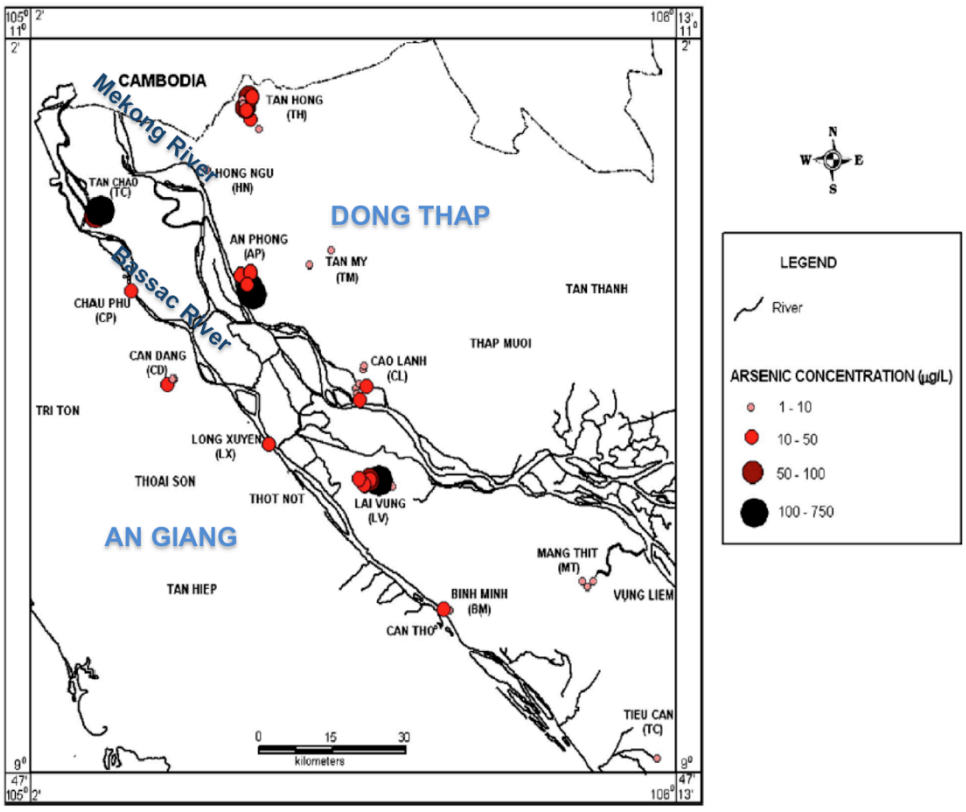

Figure 1.22. Distribution of arsenic in groundwater along the Mekong Delta River Vietnam (Nguyen & Itoi, 2009)

1.4.2 Mechanism of Arsenic Release in the Mekong Delta River

It is widely accepted that As is delivered to the delta by surface water transport from the Himalayan, and then released to pore water following burial and flooding through bioreduction of As(V)/Fe(III) oxides (Stuckey, et al., 2015a). Natural organic matter (NOM) delivered from near-surface sedimentary deposits feed dissimilatory reducing bacteria by serving as electron donors (Kocar et al., 2008; Stuckey et al., 2015a). In the Mekong Delta, in Cambodia, during the prolonged flooding stage, high primary productivity and decomposition of organic matter maintain reducing conditions. This

provides sufficient input of particulate organic C to induce long-term Fe and As reduction. Continued influx of organic matter and As-sediment to anaerobic soil results in As release. (Fig. 1.23). Effects of change in hydrology were also compared with permanently water and seasonally saturated soils. “Fresh” organic matter added to flooded soils of the seasonally wetland is rapidly degraded by the microbial community with concomitant reduction of As-bearing Fe oxides and release As to porewater. Additionally, the presence of As(V), As(III) and arsenopyrite (FeAsS) were found in the Mekong Delta by bulk X-ray absorption spectroscopy (XAS) (Stuckey et al., 2015b).

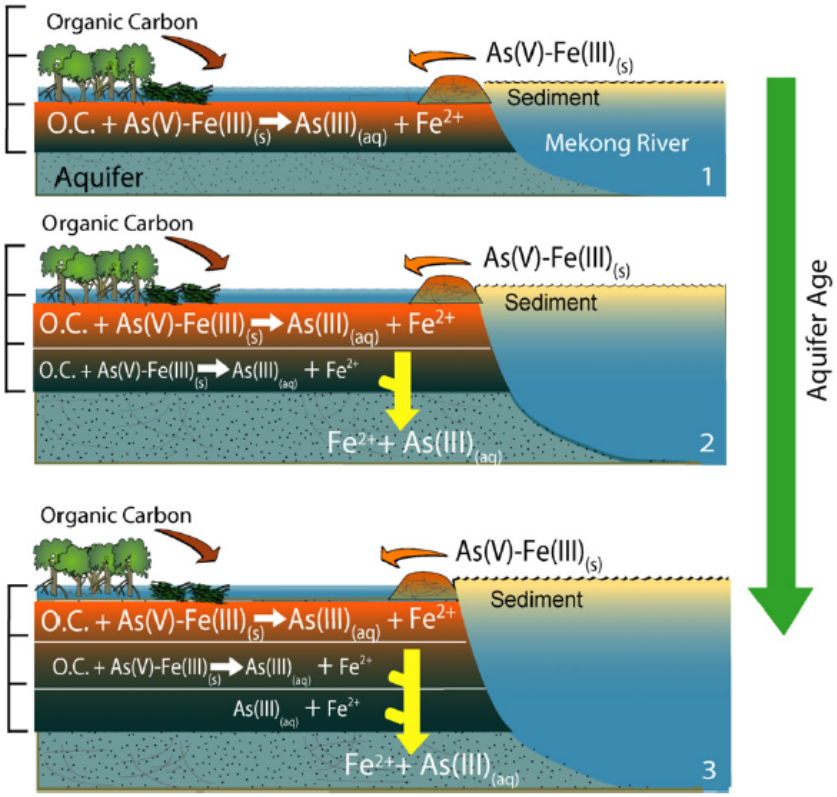

Figure 1.23. Conceptual diagram of As-bearing sediment deposition within the wetland floodplain environment (Kocar et al., 2010)

Recently, the novel As species was characterized as a carbon nanotube associated arsenic phosphate in Mekong Delta sediments by using bulk mineralogical, chemical analysis, micro-scale electron microscopy and spectroscopy, and X-ray absorption spectroscopy (Wang et al., in review). They suggested that the As-bearing nanotubes consisting of amorphous Ca-Mg phosphates could act as a long-term source of aquifers As. Additionally, the influence of dissolved S on the scale of As concentration in Mekong Delta proposed that As levels were significantly lower in the sulfate-reducing and iron-reducing zones (Buschmann & Berg, 2009; Nguyen & Itoi, 2009). Application of a binary

mixing model in Mekong Delta, As may accumulate to high level corresponding to both low levels of calculated "missing sulfate" and low actual dissolved SO_4^{2-} (Buschmann & Berg, 2009).

1.5. The Study Area – An Phu District from An Giang Province

The study site is located at An Phu district of An Giang province, Vietnam on the border with Cambodia in the upper Mekong Delta area (Fig. 1.24). The Hau River (distributary of Bassac River) and Tan Chau District bound the study area in the south and east, respectively.

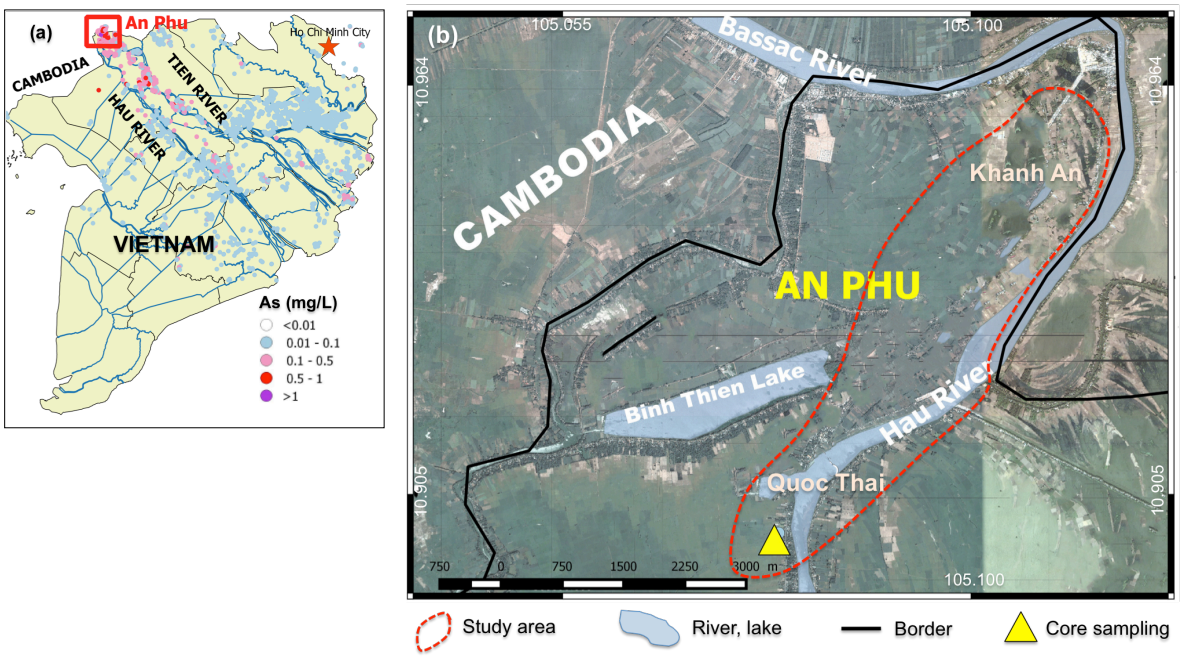

Figure 1.24. Study area maps showing (a) Location of An Phu District, An Giang, Vietnam in the upper Mekong Delta area and (b) Location of groundwater and sediment sampling area.

Most of An Phu district is a plain and is affected by the flooding season in the summer every year. During six months, rising water levels in the Mekong River due to high rainfall reach an average level of 2 – 3 meters. This prolonged flooding has major impacts on practices and production. The current land use is mostly dominated by agriculture, where cultivation of seasonal crops (rice, chili, maize, vegetables, fruits) is intensive throughout the year. This study site is located in the western part of Hau River with three crops of rice are annually grown (MARD, 2016). These crops are cultivated with a short of 2 to 4-week period between each crop. High dykes are built to prevent flooding of the rice paddies during the flood season. Irrigation for agricultural activities is entirely groundwater based

with an extraction rate peaking usually in the drainage months of January – May (Fig. 1.25).

Figure 1.25. Irrigation of vegetable fields by pumping shallow groundwater from tube wells in An Phu district

1.6. Objectives of the thesis

The objectives of the research presented in the thesis can be broadly grouped into (a) refinement of the current understanding of the process that regulates As mobilization in the shallow aquifer in An Phu and first application of geophysical tools to predict As content in the anoxic aquifer and (b) simulation of redox oscillations in the laboratory using bioreactor system to understand better key roles of sulfur biogeochemistry on mobilization of As. The specific objectives are:

i) The ability to map the spatial distribution of average soil values using geophysical methods at the field level have been well described. This includes the use of electromagnetic (EM) instruments to measure bulk soil electrical conductivity (σ_a). Estimating depths to "claypans" using electromagnetic instruments are important components for research on water quality. We find out a relationship between the clay content and As concentration in the groundwater **(Chapter 2).**

ii) Assessment of long-term geochemical controls on arsenic mobility in Vietnamese sediment to improve our understanding of redox-oscillating environments under microbial sulfate reduction **(Chapter 3)**

iii) Assessment of biogeochemical processes that regulate As mobilization during redox oscillations under acidic conditions induced by the oxidation of the mineral parts of the sediment **(Chapter 4)**

iv) Assessment of the impact of organic matter on As, S and Fe mobility during redox oscillation **(Annex)**

Chapter 2: Arsenic in shallow aquifers linked to the electrical ground conductivity: the Mekong Delta head case

Van PHAN T.H, Timothée BONNET, Stéphane GARAMBOIS, Delphine TISSERAND, Fabrizio BARDELLI, Rizlan BERNIER-LATMANI, Laurent CHARLET

Abstract

Heavy arsenic (As) contamination of groundwater is investigated in the An Giang province of Vietnam to better understand the interplay between surface sedimentology and anoxic aquifer. In particular, the present study aims to compare As concentrations measured in groundwater pumped from 40 shallow wells (< 40 m in depth) along the lower Mekong stream with surface variations of electrical conductivity measured using an electromagnetic geophysical device (EM 31). Based on the analytical results for groundwater, core sediments and geophysical data, we show the permeability and clay content of surface soil derived through EM conductivity measurement to have a positive and significant correlation (R^2 = 0.83, n = 27) with the distribution of As concentration in shallow aquifers. This indicates that the presence of soil and subsoil claypan can enhance the reducing conditions in the aquifer. The results also suggest the important role of HCO_3^-, Fe/Mn (oxyhydr)oxides and clay minerals in mobilizing As groundwater leading to a major health threat to local people of this province.

Keywords: Mekong Delta, electrical ground conductivity, arsenic, shallow aquifer, iron (oxyhydr)oxides

2.1 Introduction

Arsenic (As) contamination in groundwater has been a serious concern worldwide in recent years. Chronic exposure can adversely affect human dermal, cardiovascular, gastrointestinal, hepatic, neurological, pulmonary, renal, respiratory and reproductive systems (Mandal & Suzuki, 2002, WHO, 2004). Currently, As is recognized as a carcinogen not only causing skin cancer but also potential resulting to other internal cancers including liver, lung, bladder and kidney (Smith et al., 1992; Chen et al., 1992; Smith et al., 2009). Consequently, the present standard for drinking water supply places the upper limit of As concentration at 10 µg/L in many countries (Smedley & Kinniburgh, 2002). Some developing countries, like Bangladesh for example, have maintained the former 50 µg/L standard maximum level (Ng et al., 2003). In Vietnam, high As concentrations have been reported both in the Northern part within the Red River delta and in the Southern part within the Mekong River delta, where a large population uses As-rich groundwater for drinking and/or irrigation purposes (Agusa et al., 2007; Berg et al., 2007; Buschmann et al., 2008; Postma et al., 2010, Erban et al., 2013; Merola et al., 2015; Stuckey et al., 2015). The arsenic content has been elevated in 64% of tested people living in the Red River Delta area. Hair and urine samples had more than 1 µg/g in this part of the population, a level linked to the appearance of arsenic intoxication diseases (Agusa et al., 2014). Approximately 16 million people in Vietnam and Cambodia living in the Mekong Delta River area are therefore at risk due to elevated As concentration levels in their drinking water. Using the nail to water As ratio, Merola et al. (2015) suggested bioaccumulation of As to occur for all populations who consume groundwater. This is particularly true for residents of An Phu and Phu Tan districts, who consumed As-contaminated groundwater for 3 to 8 years, and are found to have an increased As concentration in the hair (Hoang et al., 2011). Arsenic of Southeast Asian delta aquifers derives from Himalayan sediment deposition. Once these sediments are ultimately capped with clay layer, development of anoxic condition followed by a reductive release from solid phases under reducing conditions (Polizzotto et al., 2005; Stanger et al., 2005; Stuckey et al, 2015). In the Mekong River Delta, distribution of As aqueous concentration in the shallow aquifer varies widely from 1 to 1610 µg/L (Nguyen & Itoi, 2009, Erban et al., 2013) and the average As value decreases as distance from the well to the river increases (Merola et al., 2015). Limited predictability of As concentration in a given aquifer derives from the large spatial variability observed the geology of the Mekong deltaic system. Despite underlying geological and hydrological complexities, the

interaction of multiple factors controlling As has been clarified in order to better understand how heavy As-polluted aquifer develope and therefore to reduce population exposure on the short term. Recently, a new conceptual model for As sources and sinks in Mekong delta sediment has been proposed including a mixture of As-bearing Fe (oxyhydr)oxides, As-bearing pyrite and C nanotube-associated amorphous P-Ca-Mg and (Wang et al., in review). In the redox transition zone, iron (oxyhydr)oxides are reduced and As is partially leached from the amorphous P-Ca-Mg precipitate. In the deeper layer containing pyrite, As is also leached from the amorphous precipitate, but it is at least partially immobilized by natural organic matter (NOM) as thiol-As(III) bound OM. The present study is an attempt to shed some new light on the origin of this spatial variability by applying an established and simple geophysical surveying technique, frequency electromagnetic induction to As concentration and water chemistry in Mekong Delta shallow aquifers.

Inductive electromagnetic (EM) geophysical surveys have been used widely in hydrology to map infiltration of water within near-surface formations, to estimate the extent and internal structure of shallow aquifers, and to determine the extent of groundwater contamination (Mcneill, 1990; Pellerin, 2002; Pettersson & Nobes, 2003; Aziz et al., 2008). Electrical conductivity mapping has also helped classifying soil types and sometimes to estimate depths of claypans (Doolittle et al., 1994; Doolittle et al., 2014). Because of its fast acquisition, ease of use, relative low cost, and a wealth of data collected at once, conductivity measurements performed using EM devices present immense advantages compared to soil information collected from individual cores. Instrumentsation has been improved to integrate global-positioning systems (GPS) within a data logger. EM induction sensors measure changes in the apparent electrical conductivity (EC_a) of subsurface without direct contact to the sampled material. Variations of measured EC_a are produced by changes in soil material electrical conductivity and increase with the presence of more mineralized water (salt content) and/or clay layers in the subsoil, which themselves maintain a high “cation exchange ion” content in interlayer water. Relating inductive electromagnetic conductivity and resistivity to As concentration in groundwater has been performed in Bangladesh and India (Charlet et al., 2007; Aziz et al., 2008; Métral et al., 2008; Hoque et al., 2009; Nath et al., 2010; Kumar et al., 2013). The advantages of electromagnetic methods is shorter than the array length used for conventional resistivity mappings, leading in improved spatial resolution when used in the profiling mode (Mcneill, 1990). In these studies, EM conductivity has been used to evaluate the

relationship between the permeability of surface soils and the distribution of As concentration in shallow aquifers.

The present study focus on the processes that may regulate water As concentration at shallow depth (< 40 m) in seven exploited Holocene-Miocene aquifers. Field observations extend over a 9 km^2 area in the An Phu district, An Giang province, where high As concentrations in groundwater have been reported (Erban et al., 2014; Hoang et al., 2010; Nguyen & Itoi, 2009) (Fig. 2.1). Our study compares the spatial distribution of superficial electrical conductivity measured using an electromagnetic mapping technique (EM 31) with the As concentrations in groundwater sampled from 40 shallow wells located in open fields in this region.

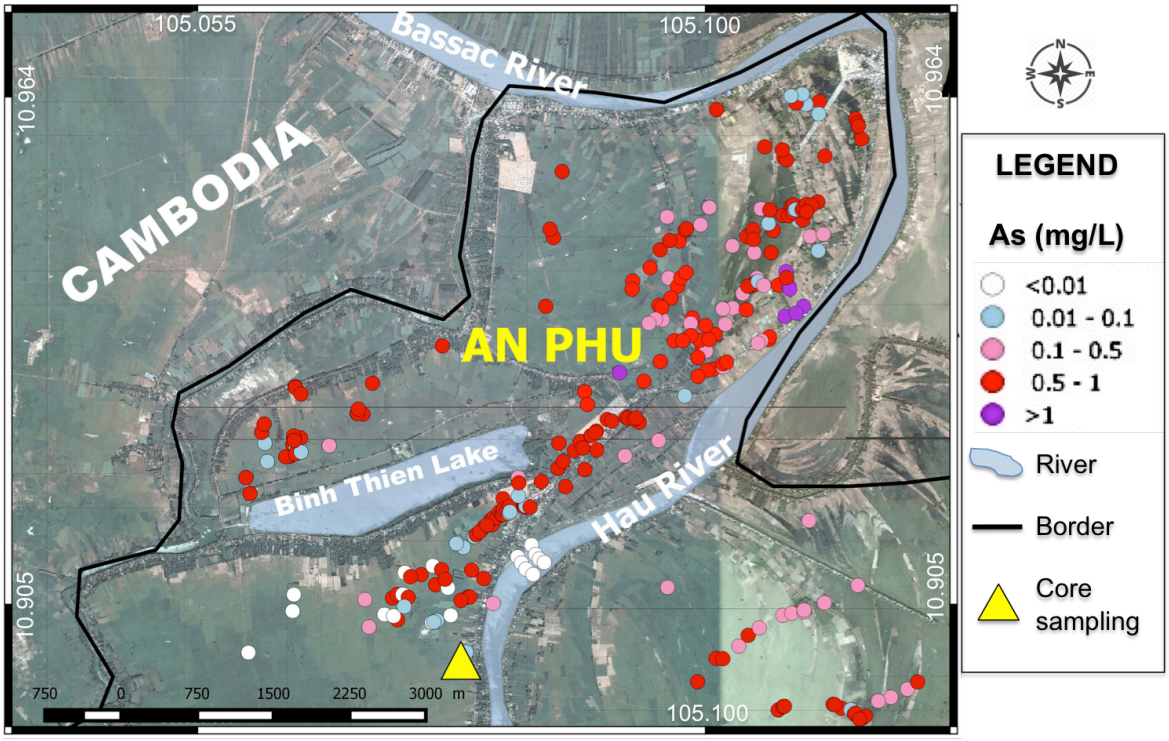

Figure 2.1. Distribution of arsenic in An Phu groundwater of An Giang province, the vicinity of Hau River of Mekong Delta (modified from Erban et al., 2013 and updated As data in January 2014 and April 2015 samplings)

2.2 Materials and methods

2.2.1 Geological and hydrogeological setting of study site

The area of lower Mekong Delta is densely populated and presents appropriate conditions for agriculture. Aquifers were formed by continental sedimentary deposits, developed in a wide Quaternary plain. Most of this region has low elevation with the range of 0 – 4 m above sea level and the delta regularly suffers of flooding originating from upper Mekong

Delta River and from tidewater. The Holocene sedimentary sequences are controlled by the changes in Late Pleistocene topography, sea level and sediment supply. Geologically, the area contains Holocene sediments mainly composed of fluvial deposits, up to 20 m thick (Nguyen et al., 2006).

2.2.2 EM 31 electromagnetic ground conductivity survey

The geophysical survey of the study area was conducted with a Geonics® EM31 instrument. This equipment consists of a transmitter coil radiating an electromagnetic field at 14.5kHz and a received coil located at the opposite end of 3.66 m long boom. By inducing an eddy current in the ground, the primary field generates a secondary electromagnetic field that is recorded by the receiving coil (Fig. 2.2). The intensity of the secondary field increases with the conductivity of the soil. This conductivity is a function of the concentration of ions dissolved in soil water as well as exchangeable ions at the solid/liquid interface and increases with clay content. The secondary field generated below the soil surface diminishes with depth. The penetration of the signal depends on the separation between the transmitting and receiving coil, the transmission frequency, and the coil orientation (Mcneill, 1990).

In our case, the maximum sensitivity with an EM31 device ranges between 2 and 5 m depths. The relation of vertical constituents between the primary and secondary fields is proportional to the conductivity (mS/m). The reproducibility of readings at a single location was generally within 0.5 mS/m. Each determination rounded to the nearest unit of mS/m was entered by hand in the field on a Compaq Pocket PC connected to a Global Positioning System (GPS) receiver using ESRI® ArcPad software. Frequency domain electromagnetic (EM) induction is used here to survey lateral variations of soil structure in the An Phu district. EM measurements were performed in April 2015 when dry season occurred in the study site to remove confounding issue of soil saturation on EM signal.

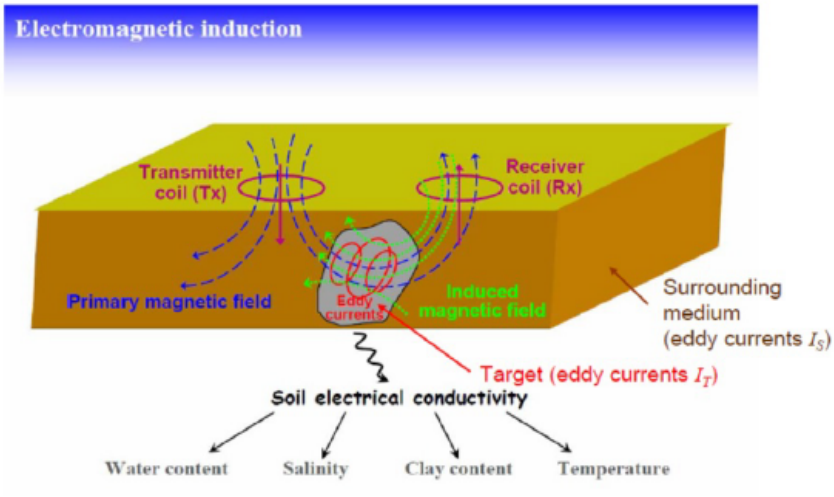

Figure 2.2. Principle of electromagnetic induction

2.2.3 Analytical methods

a. Sample preservation

Groundwater was collected from pre-existing tube wells with pipes open at the bottom in such a way as to exclude contact with the atmosphere. Samples for measurement of Fe^{2+} and S^{2-} were immediately collected with a syringe and filtered through a 0.22 µm filter membrane directly into pre-prepared colorimetric reagent solutions. For anions, a 15 mL sample was filtered into clean amber plastic bottle. For DOC measurement, a filtered 20 mL sample was acidified with 0.25 mL of concentrated HCl (37%, Sigma-Aldrich) into a special amber glass bottle. To measure major and trace elements, a filtered 15 mL sample was acidified with 0.25 mL of 65% HNO_3 (Merck, Suprapur). All samples were stored in a 4°C until analysis. In addition to groundwater samples, core sediments of the borehole, located a few km South from our study site were collected at depths ranging from 0 – 20 m (Fig. 2.1). Core samples were conserved under N_2 flow using Mylar® bag and then stored at + 4°C until analysis. Sediments from a depth of 7 m, 14 m and 16 m were characterized mineral compositions using X-ray diffraction and As bearing minerals using X-ray synchrotron technique, in particular, X-ray absorption near edge structure.

b. Analytical Techniques

Temperature, pH, electrical conductivity of water (EC) and dissolved oxygen (DO) were measured onsite using a WTW 340i multiparameter meter and a Hach sensION6 dissolved oxygen meter, respectively. Alkalinity was determined within 24 h using Gran titration (mg HCO_3^-/l) (Andersen, 2002). Samples for measurement of Fe^{2+} and S^{2-} were immediately analyzed colorimetrically with a Hach DR 2010 spectrophotometer. The

determination of major (Mg, Ca, Na, K) and trace (As, Fe, Mn, Ba, Al) cations were performed by ICP – OES (Agilent 720-ES, Varian). Dissolved anions (Cl^-, F^-, Br^-, NO_2^-, NO_3^-, PO_4^{3-}, SO_4^{2-}) were determined by ion chromatography using a Metrohm 761 Compact Ion Chromatograph with a detection limit of 0.1 mg/l and a precision better than 5%. DOC concentration was measured using a Shimazu VCSN analyzer with a detection limit of 0.3 mg/l and a precision better than 2.5%.

The major elements (Na, K, Mg, Ca, P, Fe, Mn, Al, S and total As) are identified using total acidic digestion (HNO_3 + H_2O_2 + HF, H_3BO_3 + HF) and Inductively Coupled Plasma – Optical Emission Spectrometry (ICP-OES) (Agilent 720-ES, Varian). To avoid oxidation by air, samples were loaded into glass capillaries inside a glovebox ($O_2 \leq 10$ ppm) (Jacomex). For X-ray powder diffraction (XRD) analysis, the core samples were ground using a McCrone micronizing mill, and the resulting slurry freeze dried before being prepared as a randomly oriented mount. The clay mineralogy was determined on the < 2 µm fraction. Following washing of soluble salts with pure water and removal of organic matter with H_2O_2, as described by Moore and Reynolds (1997), this fraction was extracted by centrifugation. Oriented mounts were prepared by drying the resulting suspension onto glass slides. Ethylene glycol (EG) solvation of the slides was achieved by exposing them to EG vapor at 50 °C for a minimum of 12 h. XRD patterns were recorded with a Bruker D5000/D8 powder diffractometer equipped with a SolX Si(Li) solid state detector from Baltic Scientific Instruments using CuKα_1+2 radiation. Intensities were recorded from 5 to 90° (5 s counting time per step) and from 2 to 50° (4 s counting time per step) for bulk and clay mineralogy determination, respectively.

Arsenic speciation in the sediment samples was examined by XANES at the As K-edge (11,867 eV) using the bending magnet beamline BM08 of the European Synchrotron Radiation Facility (ESRF, Grenoble, France). Samples were brought to the synchrotron facility in an anaerobic jar, mounted on the sample holders inside a glove box and then quickly transferred to the experimental chamber. To prevent beam-induced redox reactions or sample oxidation, all samples were measured in a high vacuum at low temperatures (77K). Several As references were measured along with the sediment samples in transmission mode. At the As edge, a homemade As(0) standard (zero-valent arsenic nanoparticles, Pal et al., 2012) was measured in transmission mode simultaneously with the sample spectra for accurate energy calibration. All XANES spectra were calibrated, normalized, background subtracted and the relative contributions of the different As reference compounds calculated by linear combination fitting (LCF) using the ATHENA

software package (Ravel & Newville, 2005). LCF procedure first aimed at reproducing quantitatively all the features of the spectra, using the smallest number of components. Additional components were added only if the reduced chi-square (χ^2_{red}) value lower than at least 20%, which was found to be the threshold for significantly improving the best fit. Contributions to the fits of fewer than 5% of the sum were not considered, in accordance to the error associated with the LCF procedure (Bardelli, et al., 2011; Chakraborty et al., 2010; Isaure et al., 2002). Arsenic references included: (i) $NaAsO_2$ and $NaHAsO_4$ (Sigma-Aldrich), MTA(V) (monothioarsenate), DTA(V) (dithioarsenate) and TeTA(V) (tetrathioarsenate) prepared using the method of Schwedt & Rieckhoff (1996) and optimized by Suess et al. (2009); (ii) the minerals As_2S_3, As_2S_5 (Sigma – Aldrich), As_2O_3, As_2O_5, $FeAsO_4$ (scorodite) were commercial products (Fluka or Sigma – Alrich) and FeAsS (arsenopyrite), a natural sample was provided by the Natuaral Hystory museums of the University of Florence collected from Baccu Locci (Sardinia, Italy), (iii) the complexes of As(III) and As(V) sorbed onto goethite (Farquhar et al., 2002) and (iv) the thiol As(III) bound organic matter (OM) species: glutamyl-cysteinyl-glycinyl-thiolarsenite (As(III)-Glu) synthesized using the method of Raab et al., (2004) and Langner et al. (2011).

c. Thermodynamic Calculations

Thermodynamic calculations were performed using the PHREEQC program (Parkhurst & Appelo, 1999, Appelo & Postma, 2005). The database for As species was updated according to recent data reported in the literature (Couture et al., 2010; Helz & Tossell, 2008). The program solves mass balance and chemical reaction equations and evaluates the saturation index (SI) of minerals in groundwater. In the model, pH, cations, anions, alkalinity exchange to pressure of CO_2 were used.

2.3 Results

2.3.1 Groundwater chemistry

The Piper diagram plotted for 40 samples indicates that groundwater is predominantly of Ca–HCO_3^- type (Fig. 2.3a). Bicarbonate represents up to 80% in 38 samples except for 2 samples showing 70% of Cl^-. A few groundwater samples are found to have distinct higher concentration of Na and Cl^-. The pH values are neutral to slightly alkaline (7.22 ± 0.16). Alkalinity and pH measurements, combined with carbonic acid equilibria, lead to a P_{CO2} ranging from $10^{-1.92}$ to $10^{-1.17}$ atm, with an average value of $10^{-1.54}$ atm. These results indicate additionally calcium-bicarbonate enrichment along with a sodium-bicarbonate and chloride types reported previously (Nguyen & Itoi, 2009). Other anions, in decreasing

order of concentration, are Cl^-, NO_2^- and SO_4^{2-}. SO_4^{2-} concentration values are generally low ranging from 0.07 to 13 mg/L. Sulfide concentration values were observed from 0 – 0.27 mg L^{-1}. The low concentration of SO_4^{2-} and the presence of sulfide tend to be associated with strongly reducing groundwater (Fig. 2.3a). One of the possible mechanisms to explain this observation could be related to bacterial reduction of sulfate operating in the aquifer. Total PO_4^{3-} concentrations are lower than the detection limit. EC values in groundwater range from 474 – 1774 µS/cm, which shows a slow salinity in the shallow aquifer.

For major cations, Ca^{2+} concentration is rather constant through the aquifer, with an average concentration of 82 ± 20 mg/L. The groundwater is roughly at equilibrium with calcite, representing with a saturation index (SI) ranging from -0.48 to +0.78, and an average value of +0.18. Other cations, in decreasing order of concentration, are Na^+, Mg^{2+}, K^+, Fe^{2+} and Mn^{2+} (Table 2.1). The groundwater is very hard; with an average hardness of 306 mg and minimum average of 182 mg equivalent $CaCO_3$ L^{-1} based on the sum of Ca^{2+} and Mg^{2+} concentrations. Fig 2.3b shows the groundwater is in equilibrium and slightly supersaturated with respect to both calcite and dolomite, which was found similar to the trend was reported to occur in Bangladesh and West Bengal (Nickson et al., 2000).

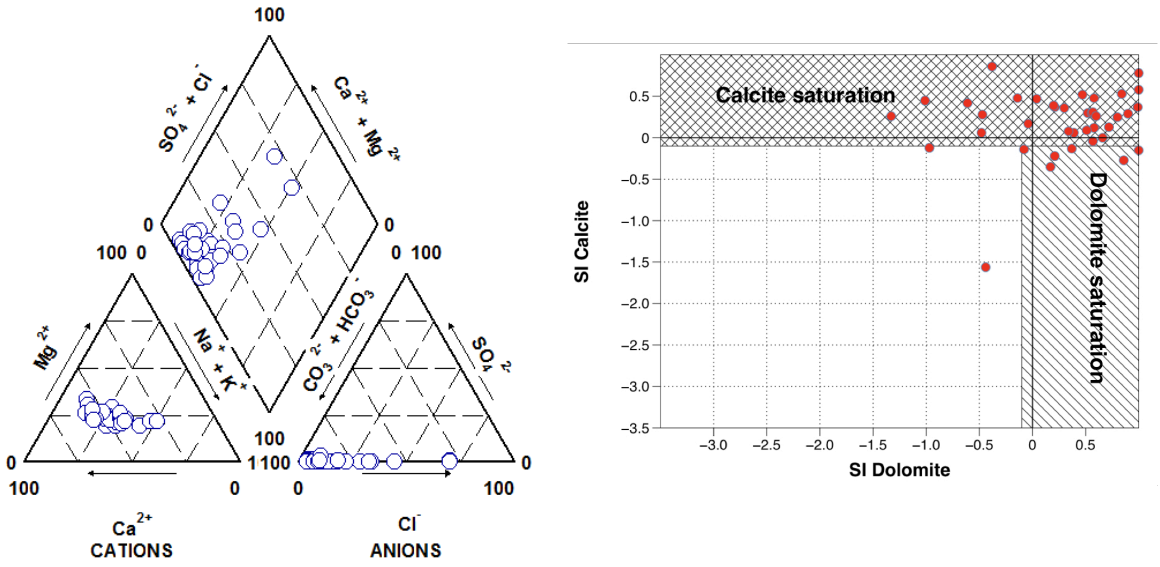

Figure 2.3 (a) The major ion composition of groundwater samples plotted on Piper diagram and (b) The groundwater is in equilibrium and slightly supersaturated with Calcite and Dolomite

Table 2.1. Chemical composition of groundwater

ID	Depth (m)	pH	EC µS/cm	DO	DOC	HS- (µg/L)	Fe	Mn	As	Na^+	K^+	Mg^{2+}	Ca^{2+}	HCO_3^-	F^-	Cl^-	NO_2^-	Br^-	NO_3^-	SO_4^{2-}
KA V1	25	7.11	841	0.74	5.89	4.00	9.50	0.77	1.02	31.02	5.69	23.11	77.70	434.96	0.09	37.58	12.42	1.34	0.03	0.23
KA V2	36	7.09	805	0.94	13.55	0.42	13.07	0.34	1.19	21.56	7.07	34.15	91.91	537.00	0.07	16.86	14.87	1.83	0.02	0.17
KA V3	25	7.01	888	0.62	9.99	6.71	15.08	0.37	1.26	20.12	5.50	24.40	74.16	484.62	0.08	14.56	13.89	1.40	0.03	0.17
KA V4	33	7.28	787	1.90	7.33	0.00	2.12	1.35	0.44	28.88	4.61	24.89	80.31	519.83	0.10	14.91	10.61	1.25	0.10	0.36
KA V5	23	7.37	975	1.72	6.66	0.66	0.22	0.62	0.43	46.11	6.83	26.15	79.45	536.60	0.11	39.55	13.71	1.36	0.06	0.20
KA V6	30	7.18	936	1.30	7.75	0.00	4.12	1.98	0.47	36.21	6.04	24.37	88.38	537.19	0.08	25.65	14.29	1.31	0.23	0.26
KA V7	40	7.18	1144	1.50	16.38	1.16	3.69	0.20	1.02	55.14	7.12	34.93	88.84	604.22	0.08	71.58	15.31	2.08	0.21	0.28
KA V8	40	7.07	1033	0.90	9.58	8.57	14.82	0.49	1.27	39.89	7.16	27.04	85.03	598.14	0.09	34.62	15.22	1.56	0.16	0.19
KA V9	28	7.07	738	1.72	3.14	1.53	9.32	1.29	0.64	49.12	3.72	17.74	79.56	357.82	0.07	45.73	9.44	1.29	0.12	0.57
KA V10	20	7.20	708	1.51	2.69	3.26	7.11	0.96	0.59	41.32	4.07	20.23	73.40	439.40	0.10	30.56	9.83	1.21	0.09	1.84
KA V11	20	7.27	775	1.88	3.75	1.40	1.29	1.46	0.52	58.27	4.00	18.76	78.12	445.77	0.00	45.27	0.00	0.00	0.00	0.07
KA V12	22	7.08	622	1.72	3.71	0.42	6.52	1.02	0.60	21.47	2.85	19.16	71.32	389.61	0.08	30.80	9.11	0.22	0.40	0.20
KA V13	23	7.12	770	1.56	4.43	0.42	8.11	1.57	0.48	20.47	2.04	13.62	52.60	325.33	0.06	36.69	10.00	0.31	0.31	0.14
KA V14	25	7.14	1248	1.69	5.45	0.79	11.18	1.23	0.89	84.22	6.38	30.33	109.61	546.03	0.07	163.07	11.42	0.73	0.58	0.07
KA V15	24	7.22	770	2.02	4.63	2.02	4.01	0.63	0.86	53.51	4.94	19.88	68.22	519.56	0.10	21.66	11.49	0.25	0.20	0.13
KA V16	27	7.26	679	2.15	2.90	0.54	1.91	1.25	0.61	40.61	4.58	19.72	66.84	446.15	0.07	19.10	10.00	0.20	0.13	0.20
KA V17	32	7.22	1007	0.74	8.94	0.91	1.89	0.18	1.08	50.28	6.09	26.80	89.40	474.44	0.09	40.27	14.22	0.54	0.17	0.41
KA V18	40	6.99	474	1.81	1.64	1.90	8.74	0.38	0.74	35.20	3.61	22.82	84.50	426.76	0.08	11.39	6.73	0.13	0.22	4.11
KA V19	25	7.28	610	2.15	3.06	1.40	2.89	1.52	0.46	39.58	3.32	16.78	59.99	390.94	0.11	11.38	8.96	0.15	0.03	2.81
KA V20	25	7.23	1365	1.34	6.12	1.53	0.06	0.81	0.59	128.59	8.02	29.85	96.85	792.21	0.07	186.80	11.67	0.82	0.04	0.23
KA V21	22	7.26	733	1.94	4.30	0.54	0.78	1.44	0.73	54.40	4.60	17.45	63.52	429.88	0.09	18.17	9.06	0.21	0.13	0.21
KA V22	28	7.44	1057	1.97	4.27	0.91	0.18	0.95	0.45	81.92	6.40	27.77	83.83	321.20	0.10	90.58	12.11	0.45	0.04	0.34
KA V23	28	7.16	831	2.50	4.63	0.17	5.31	0.26	0.88	36.16	4.53	24.65	83.64	430.40	0.07	17.93	11.85	0.23	0.07	0.24
KA V24	24	7.27	757	0.90	5.38	1.28	2.54	0.92	0.90	53.79	4.70	21.30	66.27	432.06	0.08	25.73	10.47	0.25	0.04	0.92
KA V25	24	7.09	649	1.75	4.36	0.17	1.17	0.17	0.61	39.00	3.92	15.22	47.82	467.67	0.10	11.41	9.35	0.15	0.08	0.40
KA V26	24	7.41	1015	2.47	4.57	0.42	0.41	0.65	0.42	73.67	6.07	25.42	80.56	452.85	0.12	77.77	11.24	0.41	0.04	0.33
KA V27	27	7.08	522	1.97	1.70	4.74	4.47	0.35	0.51	27.29	2.03	16.67	51.45	305.90	0.07	13.63	7.30	0.13	0.15	3.71
KA V28	20	7.26	1068	1.09	7.67	1.16	4.12	0.41	0.86	69.94	6.39	22.34	80.65	596.69	0.09	28.42	14.01	0.60	0.03	0.29
KA V29	31	7.33	1110	1.06	5.08	2.27	0.87	0.75	1.08	73.31	6.50	28.99	85.67	520.28	0.08	50.18	12.01	0.59	0.10	0.29
KA V30	24	7.37	1069	2.44	5.65	3.01	0.10	0.74	0.84	64.24	6.03	29.27	79.39	594.49	0.06	35.52	13.11	0.55	0.05	0.20
KA V31	12	6.99	1432	1.02	4.95	5.36	21.59	3.33	0.58	62.81	6.38	36.89	145.95	632.86	0.06	184.39	0.00	1.99	0.00	0.28
KA V32	12	7.41	910	1.52	5.00	2.02	0.06	1.62	0.10	31.54	5.98	28.42	92.42	429.46	0.08	28.59	12.69	1.41	10.47	13.00
KA V33	18	7.16	963	2.09	3.66	0.00	3.03	3.44	0.32	46.53	4.39	26.32	111.64	499.96	0.07	30.64	11.54	0.23	0.02	3.41
KA V34	22	7.01	1637	2.30	3.33	1.40	3.70	3.45	0.16	115.74	5.46	36.38	133.90	339.72	0.06	467.13	7.21	0.97	0.00	4.71
KA V35	30	7.25	1125	2.25	4.43	3.38	1.56	0.12	0.89	103.07	7.25	25.50	61.15	363.72	0.08	170.54	10.59	0.64	0.13	0.17
KA V36	32	7.02	1774	1.43	7.10	3.01	4.88	0.15	0.71	179.98	8.18	41.67	86.83	372.63	0.12	504.57	7.75	1.31	0.00	0.28
KA V37	30	7.64	n.a	2.99	2.70	0.91	8.26	2.48	0.55	23.65	4.45	22.41	81.72	528.67	0.10	14.01	10.31	0.13	0.04	1.08
KA V38	25	7.47	n.a	1.09	34.07	0.00	8.51	2.11	0.63	62.66	5.33	25.86	104.31	460.89	0.09	103.74	11.13	0.47	0.19	0.59
KA V39	21	7.58	n.a	1.02	6.61	0.00	9.51	0.30	0.86	32.36	5.58	24.74	87.43	542.22	0.07	11.21	12.01	0.25	3.01	0.22
KA V40	25	7.14	598	1.51	3.12	2.89	3.75	0.80	0.48	47.89	3.26	15.60	50.27	338.89	0.15	45.21	6.73	0.26	0.02	1.11

n.a: not analyzed
Concentrations in mg/l except as noted

2.3.2 Distribution of arsenic hotspots in groundwater

The distribution of As concentrations corresponding to location of groundwater in An Phu are shown in Fig. 2.4. Samples were collected at depth of 12 – 40m. Total dissolved As concentrations between 102 and 1270 µg/L, 10 – 127 times higher than WHO's guideline for As in drinking water, was observed (Table 1.1). These results suggest that all of samples are contaminated by As in Khanh An shallow aquifer. The maximum As levels appear in several wells nearest the River in the northeastern area where dissolved oxygen (DO) is present in a very low level representing with 0.62 - 0.94 mg/L. The significant Fe concentrations are detected at most areas nearest the River. The dissolution and fixation of As depend on dissolution and precipitation of Fe, controlled by the change in redox conditions with depth (Nguyen & Itoi, 2009). The processes causing changes in iron redox chemistry are important since they can affect the mobility of arsenic. One of the causes of high arsenic concentration is reductive dissolution of hydrous Fe/Mn oxides and/or release As-bearing minerals.

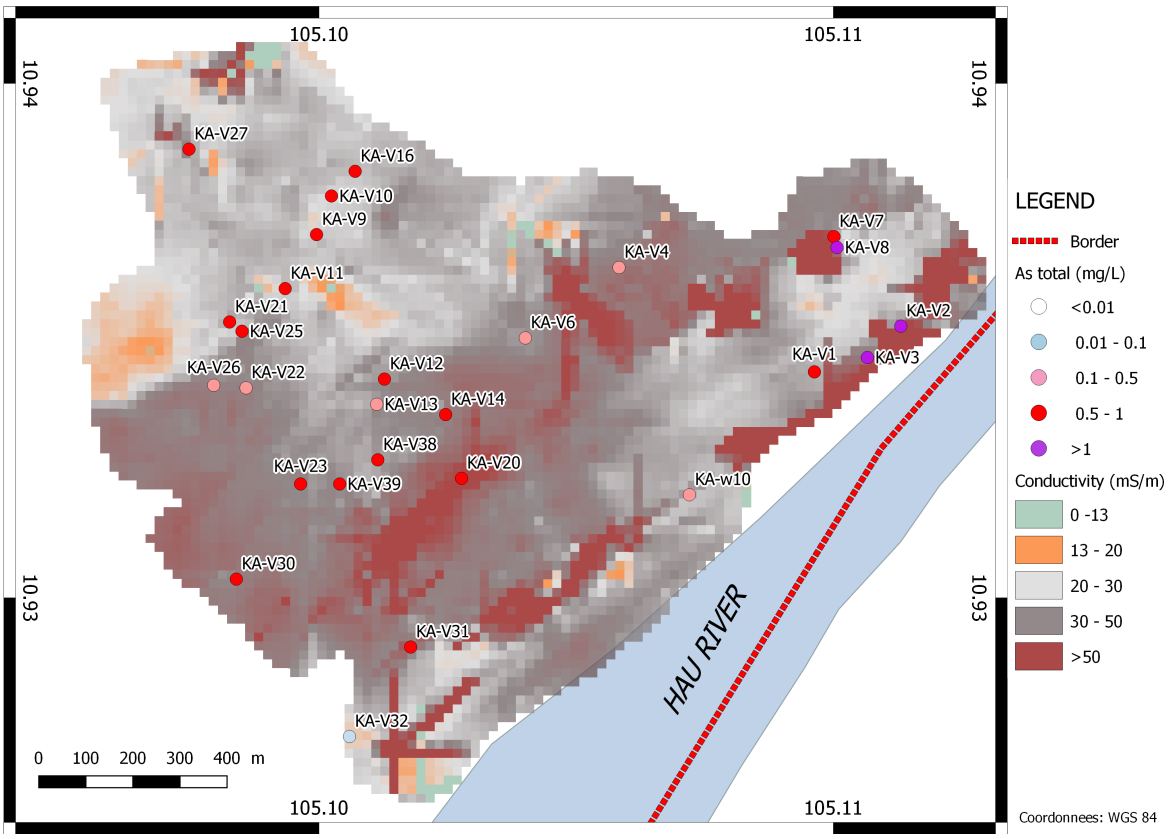

Figure 2.4. Map showing As concentrations and the electrical conductivity data distribution using EM31 device in An Phu district

2.3.3 Distribution of electrical conductivity

Electrical conductivities measured in open areas span a wide range of 15 to 200 mS/m, with an average value of 48 mS/m (n = 66,646) (Fig. 2.4). The histogram of EM conductivities tends toward high values at nearly 99% of measurements are in the 20 – 150 mS/m range. The high conductivity values exceeding more than 100 mS/m are found along the roadside where most villages are located, with shallow wells that consistently reach groundwaters with high concentration of As. Most of conductivity values for our studied site are around 40 to 50 mS/m, which indicates the presence of thick sticky clay layer in the soil. Values for EM conductivity allow distinguishing between permeable (EM < 30 mS/m) and impermeable (EM > 30 mS/m) surface layers. The majority of crops grows in low EC fields are corn, rice, and chili. Thus, the data establish the local heterogeneity with sandy soils on the west and sticky clay along the River (Fig. 2.4).

2.3.4 Thermodynamic modeling

Table 2.2 summarizes the calculated SI values of different mineral phases in Khanh An groundwater. Fe and Mn (hydr)oxides, clay minerals and organic matter play a role in

regulating As concentration. Based on PHREEQC calculation, Fe (oxyhydr)oxide minerals, such as ferrihydrite (Charlet et al., 2011), goethite (Asta et al., 2009), magnetite (Guo et al., 2007), natural/synthetic siderite (Charlet et al., 2011; Guo et al., 2011; Guo et al., 2007a) may form and then adsorb relatively large amounts of As. Mn oxides have been documented to significantly affect As adsorption (Ghosal et al., 2014; McArthur et al., 2004). In reducing conditions, As-sorbed onto Mn oxides is released, which is more favorable than Fe (oxyhydr)oxides reduction (Kelly et al., 2005). Calcite ($CaCO_3$) is also slightly oversaturated in most samples (Fig. 2.3b). The adsorption and co-precipitation mechanisms were investigated to determine which As species can be incorporated in bulk $CaCO_3$ by substitution at CO_3^{2-} sites (Román-Ross et al., 2006, Fernández-Martínez et al., 2006; SØ et al., 2008). Although two samples are at equilibrium with siderite ($FeCO_3$), the sorptive capacity of siderite towards As is as low as 0.28 L/g of As(III) and 3.36 L/g of As(V) at pH 7 (Charlet et al., 2011, Guo et al., 2007b, Jain et al., 1999). Therefore, iron (oxyhydr)oxides and carbonate clay minerals may represent an important component of the As cycle in the aquifer sediments.

Table 2.2. Saturation index of difference minerals in groundwater computed using PHREEQC.

ID	Siderite $FeCO_3$	Dolomite $Ca,Mg)CO_3$	$MnCO_3$	$CaCO_3$	$Fe(0H)_3$	Gibbsite $Al(OH)_3$	Goethite FeOOH	Hausmannite Mn_3O_4	Hematite Fe_2O_3	Jarosite	Pyrolusite MnO_2
KA V1	-6.36	0.52	0.27	0.17	3.650	1.030	9.540	3.580	21.090	-1.850	5.780
KA V2	-5.79	0.58	0.18	0.30	3.800	1.250	9.690	2.340	21.400	-1.710	4.960
KA V3	-5.74	0.04	0.10	0.12	3.840	1.090	9.730	2.140	21.470	-0.290	4.880
KA V4	-6.70	0.72	0.92	0.47	3.090	0.830	8.980	5.250	19.970	-4.180	5.900
KA V5	-7.69	0.21	0.11	0.13	2.110	0.660	8.010	2.980	18.040	-8.580	5.060
KA V6	1.27	0.56	1.01	0.37	2.740	1.010	8.640	2.270	19.280	-5.030	-5.750
KA V7	-6.48	0.57	-0.02	0.30	3.290	0.920	9.180	2.290	20.370	-3.220	4.960
KA V8	-7.02	0.17	0.22	0.31	2.600	1.100	8.490	2.730	18.980	-4.700	5.140
KA V9	-6.07	-0.97	-0.11	-0.35	3.620	1.010	9.520	1.940	21.060	-2.560	4.750
KA V10	-6.17	-0.47	0.11	-0.12	3.570	0.720	9.460	2.750	20.940	-1.970	5.000
KA V11	-6.98	0.39	0.90	0.28	2.860	0.890	8.750	5.250	19.500	-5.850	5.900
KA V12	-6.23	-0.08	0.56	0.06	3.500	0.970	9.390	3.940	20.790	-2.930	5.490
KA V13	-6.23	-0.44	0.73	-0.14	3.600	0.960	9.490	4.690	20.990	-3.050	5.730
KA V14	-5.87	-1.33	0.77	-1.56	3.760	1.020	9.650	4.300	21.300	-2.670	5.590
KA V15	-6.37	0.60	0.61	0.26	3.330	0.820	9.220	3.850	20.460	-3.890	5.450
KA V16	-6.81	0.30	0.81	0.26	3.030	0.780	8.920	5.070	19.850	-4.620	5.850
KA V17	-6.79	0.51	-0.06	0.36	3.010	0.910	8.900	2.320	19.810	-3.910	4.960
KA V18	-5.98	-0.04	0.08	0.09	3.590	1.040	9.480	2.050	20.970	0.260	4.820
KA V19	-6.68	-1.01	0.92	0.17	3.210	0.770	9.100	5.470	20.200	-1.910	5.960
KA V20	-8.08	0.80	0.65	0.45	1.500	0.950	7.390	3.730	16.790	-8.600	5.440
KA V21	-7.22	0.20	0.86	0.25	2.640	0.760	8.540	5.320	19.080	-5.770	5.920
KA V22	-8.08	0.66	0.76	0.39	2.050	0.620	7.940	5.790	17.880	-7.620	6.060
KA V23	-6.32	0.34	1.31	0.00	3.390	1.070	9.280	5.760	20.570	-2.830	6.130
KA V24	-6.70	0.37	0.68	0.08	3.120	0.830	9.010	4.340	20.040	-2.830	5.620
KA V25	-6.91	-0.14	-0.13	-0.13	2.730	1.050	8.630	1.400	19.260	-4.310	4.680
KA V26	-7.55	0.86	0.67	0.48	2.400	0.660	8.300	4.970	18.600	-6.470	5.790
KA V27	-6.51	-0.61	-0.03	-0.27	3.320	0.930	9.210	2.410	20.420	-0.900	4.980
KA V28	-6.37	0.58	0.37	0.42	3.360	0.870	9.250	3.410	20.510	-3.150	5.310
KA V29	-7.13	0.84	1.48	0.48	2.710	0.810	8.600	7.060	19.210	-5.300	6.500
KA V30	-8.02	0.99	1.51	0.53	1.800	0.720	7.690	7.070	17.390	-8.350	6.510
KA V31	1.61	0.47	1.00	0.37	-0.99	1.13	4.90	-19.67	11.81	-15.51	-6.00
KA V32	-8.52	0.90	1.05	0.52	1.540	0.70	7.43	6.33	16.86	-6.69	6.33
KA V33	-6.51	0.57	1.21	0.29	3.170	1.07	9.06	5.54	20.13	-1.45	6.05
KA V34	-6.43	-0.48	1.23	-0.04	3.170	1.20	9.06	4.87	20.12	-0.54	5.83
KA V35	-6.97	0.21	1.18	0.06	2.930	0.82	8.82	6.26	19.65	-4.56	6.25
KA V36	-6.58	-0.38	-0.58	-0.22	3.340	1.01	9.23	1.08	20.47	-2.51	4.53
KA V37	-6.29	1.45	1.46	0.86	3.750	0.47	9.64	7.74	21.29	-2.33	6.59
KA V38	-6.25	1.01	1.21	0.58	3.720	0.78	9.61	6.63	21.24	-2.24	6.29
KA V39	-6.22	1.32	0.49	0.78	3.800	0.56	9.69	4.70	21.39	-3.28	5.65
KA V40	-6.52	-0.27	0.47	-0.15	3.270	1.02	9.16	3.80	20.33	-2.15	5.42

2.3.5 Mineral composition of core samples

From the total digestion and XRD analyses of core samples, more than 30% of total mineral mass in the sediments is present as micas. Once buried in anoxic conditions, micas can adsorb As in the presence of Fe^{2+} and transform As and other pollutants into less toxic forms (Charlet et al., 2007). Pyrite is identified in all three layers of core samples, while gypsum is detected at the depth of 7 m and siderite is found at 16 m deep sediment. Low SO_4^{2-} concentration and high pyrite content in sediment demonstrate that pyrite formation occurs under the reducing condition in the aquifer.

In addition, the bulk As speciation was also determined by X-ray adsorption near-edge spectroscopy (XANES) at the European synchrotron research facility (ESRF). XANES spectra show two absorption maximum peaks at 11,869 and 11,875 eV, including As(III) and As(V) speciation (Fig. 2.5a). The O-bound As species, As(V) and As(III) sorbed onto goethite/ferrihydryrite were used in LCF. While As_2S_3, thiol-bound As(III) and FeAsS were used for S-bound As(III). However, since the XANES of these species spectra are very similar and good matches with the sediments were obtained. LCF did not allow to discriminate the actual association of As between these S-bound As(III) species. For this

reason, the best LCF results of the three layers (7, 14 and 16 m deep sediments) are summarized grouped in Fig. 2.5b.

The results of the LCF performed in the 7 m deep layer sediment indicates that As(V) adsorbed onto iron (oxyhydr)oxides represents the main species with 61% of the total solid As, along with thiol-bound As(III) or As_2S_3 (29%) and As(III) adsorbed onto (oxyhydr)oxides (13%) (Fig. 2.5b). In the deeper (14 m layer) sediment, 61% of the total As species is S-bound As. The remaining O-bound As species are 33% As(V) and 12% As(III). Thiol-bound As(III) and/or FeAsS accounted for 31% of total As in the 16m deep sediment which was also reported in Mekong Delta, Cambodia (Stuckey et al., 2015, Wang et al., submitted). The O-bound As species are 43% and 29% for As(V) and As(III), respectively.

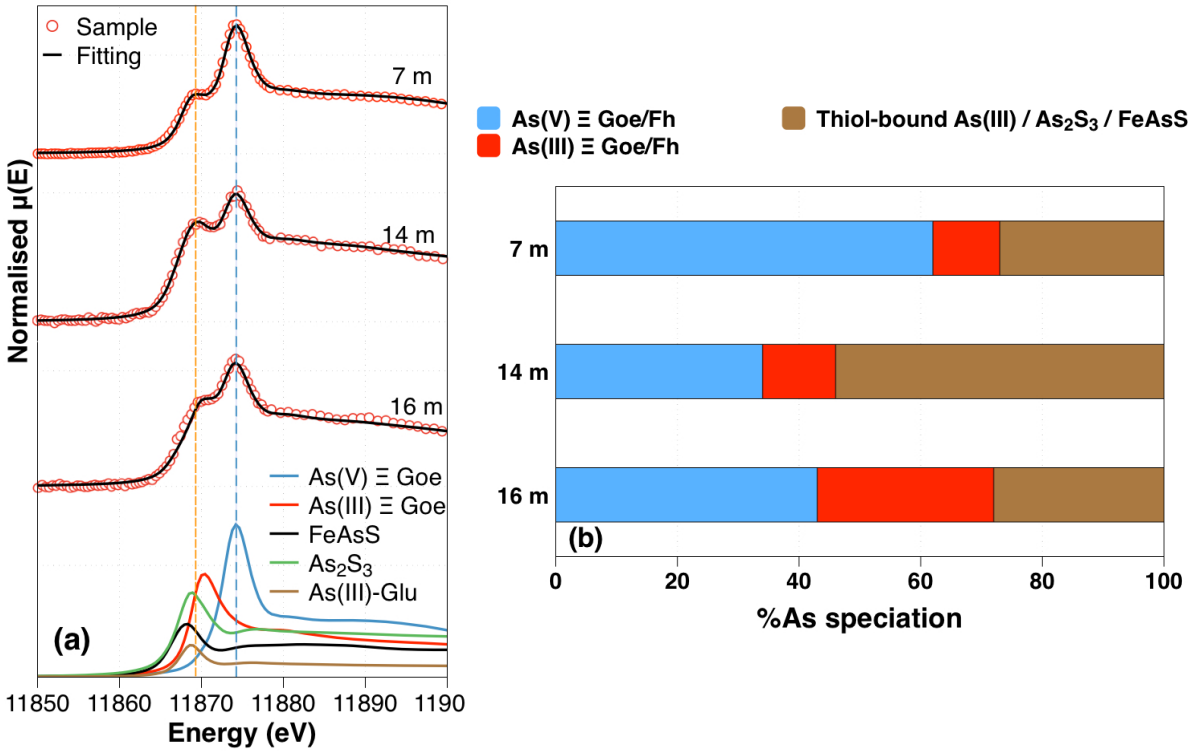

Figure 2.5. (a) Normalized As K-edge XANES spectra of sediment samples collected at 7, 14 and 16 m deep sediments and (b) Proportion of As solid phases as revealed LCF performed on corresponding XANES spectra, the error on the percentages is estimates to be in the around 10% (Bardelli et al., 2011; Isaure et al., 2002). The spectra of the samples (red circles) are reported together with the LCF curves superimposed (solid lines). The spectra of the reference compounds used for LCF (As(III)/(V)≡Goe/Fh, FeAsS, As_2S_3, As(III)–Gluthiatone) are also shown.

2.4 Discussion

2.4.1 Water chemistry and As concentration

The liberation of As often happens by reductive dissolution of iron (oxyhydr)oxides that contains As bearing forms. One problem of reductive dissolution theory is how the reductant contacts the iron (oxyhydr)oxides. Groundwater recharge is composed of both surface water rich in organic matter, which enters the aquifer all year around and rainwater, which enters the aquifer from June to November. In our data, the groundwater concentration of dissolved organic C is generally high (1.7 – 34 mg C/L), with an average concentration of 6.3 mg C L^{-1}. Concentrations of As correlates poorly with concentrations of dissolved Fe but correlate better with concentration of HCO_3^-. Fe^{2+} concentrations do not remain constant, probably because it may precipitate as $FeCO_3$. Samples with high concentrations of Fe^{2+} and HCO_3^- are oversaturated with $FeCO_3$ representing with SI of 1.3 and 1.6 in KA V6 and KA V31, respectively, and most other samples are slightly oversaturated with calcite, dolomite $(Ca,Mg)CO_3$ and $MnCO_3$ (Table. 2.2, Fig. 2.3b). Reactive transport modeling suggest the precipitation of siderite to be a reasonable option in the Red River deltaic sediment in Vietnam (Postma et al., 2007). Moreover, siderite was identified at the 16 m section in a low organic matter layer sediment which also found by Wang et al. (in submitted). Under low DO conditions, Fe oxides are likely being reductively dissolved by soluble organic matter, resulting in the groundwater recharge becoming enriched in Fe^{2+} and HCO_3^- (Nickson et al., 2000; Appelo et al., 2002; Charlet et al., 2007) following the equations below:

$$O_2 + CH_2O \rightarrow H^+ + HCO_3^-$$

$$\equiv FeH_2AsO_4 + H_2O \rightarrow \equiv OH + 2H^+ + Fe^{2+} HAsO_4^{2-}$$

$$\equiv FeH_2AsO_4 + 3H_2O + CH_2O + CaCO_3 \rightarrow \equiv OH + 6H^+ + Fe^{2+} HAsO_4^{2-} + 2HCO_3 + Ca^{2+} + 4e^-$$

The solid phase As speciation along defined recharge pathway was identified as the As-bearing iron (oxyhydr)oxide phases in the Mekong Delta (Stuckey et al., 2015). In the process shown above, soluble Fe (oxyhydr)oxides and As bearing iron minerals release into groundwater both Fe^{2+} and As, as documented in several previous studies (Hoang et al., 2010; Nguyen & Itoi, 2009). However, As concentration was not associated with total iron concentration in most of groundwater samples. The results also indicate that appreciable As-bearing Fe(III) oxides (goethite and hematite) exist in the subsoil of An Phu. Furthermore, Arsenian pyrite (FeAsS) formation reported previously in Mekong

deltaic in Vietnam and Cambodia (Stuckey et al., 2015; Wang et al., submitted) which would be a detectable source of As to groundwater only if FeAsS are oxidized. However, concentrations of SO_4^{2-} are low and indicate reduction and possibly pyrite formation, rather than oxidation. The present data suggest that total cations concentrations of Fe, Ca, Mn and Mg concentrations correlate positively with HCO_3^- concentration, indicating that simple mineral dissolution dominates the groundwater. In addition to redox processes, competition for adsorption sites at mineral surfaces (e.g., Fe/Mn (oxyhydr)oxides, clay minerals and weathered mica) may also act to mobilize As in groundwater containing high amounts of HCO_3^- (Appelo et al., 2002; Charlet et al., 2007). The displacing effect of HCO_3^- may offer an explanation for high As concentrations in Khanh An's aquifers, given that high pH and alkalinity values with average value of 7.8 mmol L^{-1}, as a consequence of high CO_2 partial pressures in the aquifer.

Another theory relates the liberation of As release to oxidation of pyrite which may contain arsenic to form jarosite (Nguyen & Itoi, 2009):

$$FeS_2 + O_2 + H_2O \rightarrow KFe_3(SO_4)_2(OH)_6 + H^+ + SO_4^{2-} \text{ and}$$

$$FeS_2(As) + O_2 + H_2O \rightarrow SO_4^{2-} + H^+ + Fe(OH)_3 + As$$

However, the saturation index calculations of jarosite are under saturated in most samples (Table 2.2). Except for one sample (KA V18) was found to saturate slightly (SI = 0.26) and difficult to detect in solid phase analysis. Additionally, the chemical data indicate that As is not released by pyrite oxidation due to the formation of FeAsS and FeS_2 in the core samples (Fig. 2.5). Wang et al. (submitted) reported the newly uncovered As species as a carbon nanotube-associated arsenic (As species P-Ca-Mg) in Mekong Delta sediments. Co-precipitation of As(V) with Ca and Mg potentially release As into aquifers In the reducing condition accompanying with cations such as Ca^{2+} and Mg^{2+}. Moreover, As(V) fraction was also interpreted as As adsorbed onto Fe/Mn (oxyhydr)oxides. The correlation strongly suggests that the As in groundwater beneath the Khanh An commune is derived from reductive dissolution Fe/Mn (oxyhydr)oxides and displacement of As by HCO_3^- from and clay minerals in sediments.

2.4.2 Relationship between Electrical Conductivity and As concentrations

Our study site is located in the region where groundwater salinity is below 1 g L^{-1} TDS (Buschmann et al., 2008). In soils with low salt content, EC_a is strongly influenced by variations in clay and moisture contents, which depends on changes in soil type and hydrology (Doolittle et al., 2014). Higher EC_a values are attributed to the presence of

higher clay content in upper (5 m) soil and wetter soil conditions (Aziz et al., 2008; Mcneill, 1990; van Geen et al., 2006); Aziz et al., 2008; Doolittle et al., 2014), but it is difficult to distinguish the respective contribution of these two factors to the high observed conductivity. However, previous studies have shown that the controlling factor in some areas is clay content, which is presented in Table 2.3 (Hedley et al, 2004, Weller et al., 2007, Aziz et al., 2008). In addition, As are also strongly adsorbed to clay particles which are transported through the river system as suspended load during the flooding stage (Nguyen & Itoi, 2009). The electrical conductivity can identify the relative distribution of fine- and coarse-grained or permeable and impermeable surface layer, which has an important control on the spatial pattern of As in groundwater. In a study performed in Bangladesh, electrical conductivity was shown to be higher than 35 mS/m, while the clay content of the soil was higher than 60% (Aziz et al., 2008). The map of EM conductivity visual comparison to the distribution of As in shallow wells is shown in Fig. 2.2. All wells in the area are contaminated by As, with an average concentration of 590 ppb (n = 40 samples). Concentrations of As in shallow aquifers tend to be lower underlying sandy soils (EM conductivity < 10 mS/m) and higher below finer-grained and high conductivity soils as shown by Métral et al. (2008) and Aziz et al. (2008). Low-As aquifers are located underneath the areas with relatively sandy surface materials and far from the River. Clay pan and finer materials act as a "cap" which prevents oxygen to enter the shallow aquifer from atmosphere, rainwater or river water and thus to enhance reducing conditions and thus increase As concentration.

Table 2.3 Correlations between electromagnetic conductivity and clay content

Place	Instrument	Prediction of clay content (%)	R^2	Reference
Klostergut Shceyern (Germany)	EM 38	Clay = - 6.4 + 0.75 EM	0.85	Weller et al., 2007
Araihazar (Bangladesh)	EM 31	Clay = - (3.97±1.5) + (0.91±0.1) EM	0.85	Aziz et al., 2008
Manawatu (New Zealand)	EM 38	Clay = - 22.496 + 1.682 EM	0.72	Hedley et al., 2004

On the basis of this calculation, we compare As and HCO_3^- contents of each shallow well with the closest electrical conductivity value. Linear regression shows a slight correlation for 27-paired measurements corresponding to an increase in As concentrations ($R^2 = 0.34$) and alkalinity ($R^2 = 0.33$) as a function of EM conductivity. Arsenic contamination in the Mekong Delta trends strongly with depth and age of the aquifer and the average value also

decreases with distance from River (Buschmann et al., 2008; Luu et al., 2009; Merola et al., 2015; Nguyen & Itoi, 2009; Erban et al., 2014). For a more quantitative comparison between groundwater and conductivity data, we return to the actual EM data by comparing the As content of each shallow well in the natural soil. To determine the relevant spatial scales, the depth of well and distance to the river, we estimate the minimum distance over which recharged water has to travel to the well (Fig. 2.6a). The correlation between electrical conductivity, the HCO_3^-/D and As/D ratios are highly significant with $R^2 = 0.83$ and 0.78 respectively (Fig. 2.6 b-c). These results confirm previous studies where high As concentrations in groundwater were correlated with high HCO_3^- concentrations (Charlet et al., 2007; Nickson et al., 2000). The displacing effect of HCO_3^- on As sorbed on Fe/Mn (oxyhydr)oxides and the rate of increasing As concentrations with the depth in shallow aquifers might depend on the clay content of surface soil inferred from EM conductivity. The observed trends in groundwater arsenic in Khanh An are consistent with known natural processes that promote contamination similar to most areas are located near Mekong Delta River and Bassac River (Kocar & Fendorf, 2012; Erban et al., 2013; Ying et al., 2015).

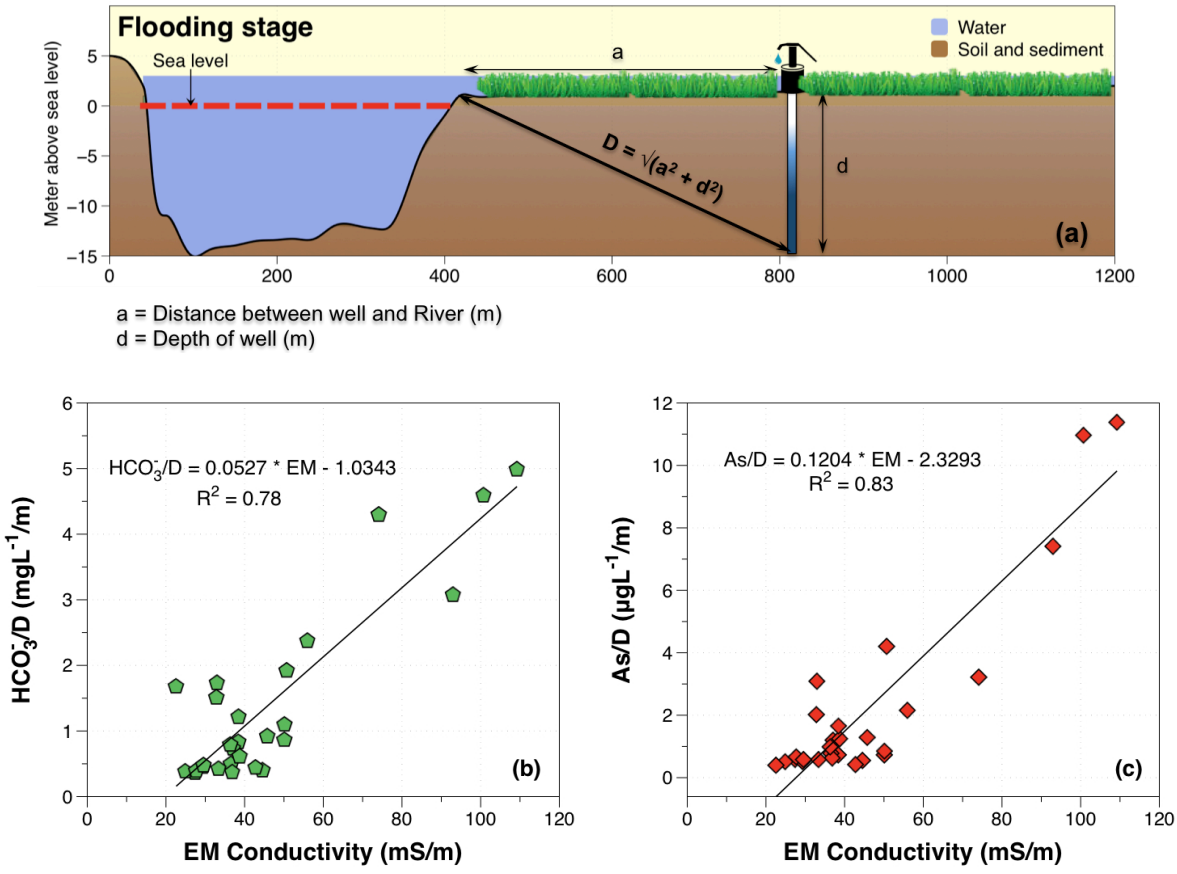

Figure 2.6. (a) Calculation of the minimum distance recharged water has to travel to the

well (D). Comparison of (b) HCO_3^-/D and (c) As/D as a function of the closet EM conductivity measurement.

2.5 Conclusion

High levels of As in tube wells are causing the greatest risk to human health in An Giang province. The solid phase As speciation suggests that As is not only in iron (oxyhydr)oxides, but also present as S-bound As(III) in the sediments. Upon reductive dissolution of iron (oxyhydr)oxides, As, Fe and high alkalinity are release in the anoxic aquifer. Electromagnetic (EM 31) investigations results from shallow subsurface from a small area in the Mekong Delta Vietnam indicated that variations in As concentration within the shallow Holocene aquifers seem to be controlled by the heterogeneity in near surface sediment and recharge of aquifers. The present geophysical data reveal a significant relationship between electrical conductivity, As and HCO_3^- concentration in shallow aquifers of Khanh An. As concentration to distance of the well to the river ratio tend to increase in high conductivity soils. Survey of conductivity and As concentration should be extended to areas of lower As concentrations and variations in hydraulic head measurement be reported monthly to estimate the recharge from horizontal and vertical permeability (Aziz et al., 2008). The challenge would also be to extend the area of the EM conductivity survey to achieve a better understanding of the correlation between As concentrations and EM measurements. The future objectives should be therefore to consider the permeability of surface soils, the distribution of groundwater ages, the vertical recharge due to precipitation, monsoonal flooding and irrigation waters and the horizontal recharge from the River. However, the present study shows that easy and cheap electrical conductivity measurements can be used to differentiate areas where this recharge may occur (low EC) from areas where it does not (high EC, high clay soil content) and where high As are favored in the underlying “sealed” aquifer.

Chapter 3: Arsenic release during redox oscillations in Mekong upper delta aquifers in Vietnam: a mechanistic study

Van PHAN T.H, Rizlan BERNIER-LATMANI, Delphine TISSERAND, Fabrizio BARDELLI, Manon FRUTSCHI, Antoine GEHIN, Laurent CHARLET

Abstract

Arsenic contamination of drinking water is a major problem in a variety of Southeast Asia delta, and in particular in the upper Mekong River Delta. The impact of seasonal wet-dry cycle linked to monsoon and irrigation generates redox oscillations in subsoil and sediment on the release of arsenic in aquifers. Long-term biogeochemical control on arsenic mobility has been investigated using batch redox oscillation bioreactor system conducted on arsenic and sulfate doped sediment. E_h oscillations between –300 mV and +500 mV were implemented by modulating an admixture of N_2/CO_2 and compressed air automatically. Carbon source (cellobiose - a mono cellulose) was added as fresh organic matter and at the beginning of each reducing cycle to stimulate the metabolism of the native microbial community. Results show that repetitive redox cycling can decrease arsenic mobility by up to 92% during reducing conditions. Phylogenetic analyses of 16S rRNA revealed the presence of sulfur and iron - cycling bacteria indicating that sulfate and iron reduction are important factors for As immobilization in the aqueous phase. The formation of aqueous sulfide ions and elemental sulfur was limited by the precipitation of mackinawite ($FeS_{m(s)}$) in this ferrous ion rich medium and then not high enough. Hence, thioarsenate species constitute was produced the arsenic load of such reductive groundwater and As(III) was sequestered on sulfur minerals rather than As(V) during microbial sulfate reduction.

Keywords: Redox oscillations, Arsenic release, Microbial sulfate reduction, S-bound As, Organic matter

3.1 Introduction

Arsenic, a well-known environmental carcinogen, is subject to a variety of mobility-altering processes (WHO IARC, 2004). WHO provisional guideline value for total As in drinking water is limited at 10µg/L. Elevated concentration of arsenic in groundwater higher than 50µg/L was reported in several Southeast Asian countries including Bangladesh, India, Cambodia, China, and Vietnam (He & Charlet, 2013; Fendorf, 2010; Kocar et al., 2008; van Geen et al., 2008; Zheng et al., 2004; Buschmann et al., 2008). In particular, the Mekong Delta floodplain stretches over 62,100 km^2 in Southern Vietnam and South Cambodia, harbors numerous wells with elevated As concentration (Buschmann et al., 2008; Nguyen et al., 2000). At Phnom Penh, the Mekong River divides into two branches, the Mekong River to the east and the Bassac River to the south. About 60% of the delta surface forms low-lying flood plains (< 2m above sea-level) with actual and potential acid sulfate soils (Stanger et al., 2005). During the monsoon season from about June to October, floodwaters from the Mekong River push water in aquifers and deposit in surrounding wetlands and rice fields. Floodwaters typically have receded by November. This results in a seasonal wet-dry cycle that generates reducing conditions (in summer and fall) and oxic conditions (in winter and spring) i.e. redox oscillations in soil and subsoil. Since As mobility is very different in oxic and anoxic conditions (Charlet & Polya, 2006), then may lead to the release of arsenic into the groundwater. A national survey of arsenic in wells conducted from 2002 to 2008 by the Department of Water Resources Management, including 42,921 observations in the Delta, shows that large areas (> 1000 km^2) of the Mekong Delta were contaminated by arsenic in nearly 900 wells (Erban et al., 2013). The dominant areas are located along the main Mekong streams from An Giang to Can Tho City (up to 1610 µg/L) (Hanh et al., 2011; Hoang et al., 2010; Nguyen et al., 2009). Our study site was selected in this area, particularly in An Phu district from An Giang province.

Many natural biogeochemical systems fluctuate regularly from oxic to anoxic conditions. The seasonal reversal of flow direction, rivers to aquifers in the wet season and aquifers to rivers in the dry season, impact the redox balance of aquifers (Benner et al., 2008; Stuckey et al., 2015). The influence of cycling within soil and aquifer in the Mekong upper Delta of Cambodia on the distribution and diversity of As(V) reductase genes (*arrA)* was described by Ying et al. (2015). Extensive flooding during monsoon seasons creates anoxic soil conditions and favors anaerobic microbial processes contributing to As mobilization. Seasonally aerobic/anaerobic cycling in Bengal and Mekong River Delta leads to the

release of As associated from pyrite and natural organic matter (NOM) including arsenic-bearing sulfides, thiol-As bound NOM (Polizzotto, et al., 2005; Stuckey et al., 2015) and reductive dissolution of As bearing iron oxyhydroxides (Nguyen & Itoi, 2009; Nickson et al., 2000). The conceptual model for As release from sediment to groundwater distinguishes three zones of Mekong sediment: seasonally flooded soils, permanently flooded soils and saturated deeper clay and sand aquifers (Stuckey et al., 2015). Fresh sediment *in situ* incubations shows slow/rapid or limited/extended As release and slow/rapid or limited/stimulation of rapid As release in seasonal/permanent wetlands.

The fate and transport of As are closely related to the biogeochemical cycling of iron, sulfur and carbon in such environments (Bostick et al., 2003; Couture et al., 2013; O'Day et al., 2004; Root et al., 2009). It is popularly agreed that As present in Mekong Delta is delivered by surface water transport of Himalayan, and then released to pore water following burial and flooding through bioreduction of As – bearing iron (oxyhydr)oxides. Natural organic matter (NOM) also transported from deposited near-surface sedimentary fuels dissimilatory reducing bacteria by serving as an electron donor (Kocar et al., 2008; Stuckey et al., 2015a). Depending on the redox oscillating conditions, sulfur can also have a significant effect on As speciation and concentration because As levels are controlled by the rate of microbial sulfate reduction, the solubility of As-bearing sulfide phases, and/or adsorption processes to sulfide minerals. Sulfate-reducing bacteria (SRB) are anaerobic microorganisms that are widespread in anoxic habitats. Microbial sulfate reduction is an energy-yielding metabolic process during which sulfate is reduced to sulfide (HS^-) and elemental sulfur ($S^0_{(aq)}$) along the oxidation of organic matter or H_2 (Barton, 1995, Muyzer & Stams, 2008). Subsequently, reduced sulfur can be used to form thiolarsenic species (Burton et al., 2013; Planer-Friedrich et al., 2007; Suess et al., 2010; Planer-Friedrich & Wallschläger, 2009) or precipitate sulfidic arsenic solids including orpiment (As_2S_3) or realgar (AsS) if concentration of As is high enough (O'Day et al., 2004; Root et al., 2009), or iron sulfide including pyrite (FeS_2), mackinawite (FeS_m) (Berner, 1984; Wilkin and Barnes, 1996; Rickard, 1997, 2006). Iron sulfide minerals can also sorb or co-precipitate with As to form As-rich pyrite or arsenopyrite (FeAsS) (Tisserand et al., 2014; Pili et al., 2013; Charlet et al., 2011; Wolthers et al., 2005; Newman et al., 1998; Rittle et al.,1995). The decrease of As solubility and extractability under iron poor anoxic sulfate-reducing conditions in deeper aquifer systems lead to reduce As contamination (Kirk et al., 2010). Accordingly, microbial sulfate reduction is generally thought to cause decreased As mobility in subsurface environments at low S^{2-} concentration (Fendorf et al., 2010). Where

sulfate-reducing bacteria are active, the sulfide produced reacts to precipitate arsenic, or co-precipitate with iron, leaving little in solution. In the absence of sulfate reduction, methanogen is the dominant type of microbial metabolism, and arsenic accumulates to high levels (Kirk et al., 2004). However, recent studies showed that under some conditions sulfate reduction can result in increased As mobility during replacement of ferrihydrite ($Fe(OH)_3$) by mackinawite (Kocar et al., 2008). A conceptual model of the formation of As – S – organic matter (As-S-OM) under anoxic condition was proposed by Couture et al. (2013b). In labile OM rich sediment, the formation of thiols appears to be the primary sink for sulfides and others reduced S species produced by microbial sulfate reduction. In the labile OM depleted sediments, the dominant sink for sulfides is the formation of Fe-minerals and elemental sulfur (Burton et al., 2013; Couture et al., 2013b; Planer-Friedrich & Wallschläger, 2009). The remaining sulfides are available to complex and form As sulfide minerals. Microbial sulfate reduction is thus expected to play a leading role in determining whether As accumulates to toxic levels and is released from sediment to groundwater during redox oscillations in natural aquifers. Two important redox active sulfur products in anoxic conditions are dissolved sulfide (H_2S and HS^-) and zero-valent sulfur or elemental sulfur ($S^0_{(aq)}$). The generation of $S^0_{(aq)}$ happens through abiotic and biotic reactions of dissolved sulfide (Steudel, 1996; Poulton et al., 2004; Couture & Cappellen, 2011). The solubility of elemental sulfur in water is very low. In the absence of $S^0_{(aq)}$ measurements, its equilibrium with respect to rhombic crystalline elemental sulfur (S_8) can be followed: $\frac{1}{8}S_8 = S^0_{(aq)}$ (log K = - 6.68) (Couture & Cappellen, 2011).

Significant attention has been paid to mechanisms responsible for arsenic mobility in sediment under microbial sulfate reductions, and to hydrological transport processes determining arsenic fluxes from sulfate-rich sediments. Moreover, it is a scarcity of experimental studies accurately isolating biogeochemical processes during the oscillating redox conditions in Vietnamese paddy fields and shallow aquifers. The role of sulfate-reducing bacteria (SRB) and sulfate-oxidizing bacteria (SOB) in As immobilization in the sediment during redox conditions remains unknown. To determine the mechanisms controlling arsenic mobility in sulfate-rich sediment of seasonally flooded soils, we investigated the As, Fe, S species generated by oscillating biogeochemical conditions and described in detail the role of bacteria in the sediment through genomic analysis. To stimulate seasonal cycles, laboratory experiments were performed using bioreactors containing sediment with equal total arsenic concentration but variable sulfate content.

3.2 Materials and methods

3.2.1 Field site characterization

Sediment sampling

The seasonally flooded sediment was sampled from the Quoc Thai commune, An Giang province of Vietnam, in a paddy soil near the Bassac (Hau) River in the dry season (January, 2014) (Fig. SI-1) where high As groundwater contamination has been reported (Erban et al., 2014; Hanh et al., 2011; Nguyen & Itoi, 2009). A sediment core was collected from a depth of 0 – 20 m, conserved under N_2 flow using Mylar® bag and then was sealed. The sediment samples were shipped in a cooler on ice and stored at +4°C until processing redox experiments. In particular, sediment from a depth of 16 m, which was collected in a peat layer, was used for this experiment.

Sediment Characterization

Prior to experiments, elemental composition was determined by total acidic digestion (HNO_3 + H_2O_2 + HF, H_3BO_3 + HF) and Inductively Coupled Plasma – Optical Emission Spectrometry (ICP-OES) (Agilent 720-ES, Varian) (Cotten et al., 1995). To avoid oxidation by air, samples were loaded into glass capillaries inside a glovebox ($O_2 \leq 10$ ppm) (Jacomex). X-Ray diffraction (XRD) measurements were performed with CoKa radiation on a Panalytical® X'Pert Pro MPD diffractometer mounted in a Debye–Scherrer configuration using an elliptical mirror to obtain a high flux parallel incident beam and an X'Celerator® detector to collect the diffracted beam. Micas, chlorite, pyrite and siderite were identified in the input sediment. Total water content was 61.74 ± 4.7 %. This sediment is a peat layer with high organic carbon (TOC/DOC) and contains pyrite. The results of the elemental and mineralogical investigation are presented in Table 3.1.

Table 3.1. Chemical characteristics of a 16 m depth sediment

Mineral (Formula)[a]	Weight Fraction (%)
Smectite	44.6
Quartz (SiO_2)	28.9
Muscovite ($KAl_2(AlSi_3O_{10})(F,OH)_2$)	11.6
Microcline ($KAlSi_3O_8$)	6.5
Albite ($NaAlSi_3O_8$)	5
Fluorapatite ($Ca_5(PO_4)_3F$)	1.7
Clinochlore ($(Mg,Fe)_5Al(AlSi_3O_{10})(OH)$)	1
Pyrite (FeS_2)	0.8
Major element chemistry	**g/kg dry sediment**
Si	125.3
Al	48.6

Fe	15.6
K	11.1
Mg	5.1
Na	3.0
Ti	2.2
Ca	0.9
S	0.7
Mn	0.1
AVS[c]	0.03
TOC[d]	32.1

[a] As determined by XRD
[b] As determined by total digestion ($HF+HNO_3+H_2O_2+H_3BO_3$) and ICP-AES
[c] As determined by the sequential extraction and UV-Vis spectroscopy
[d] As determined by loss on ignition

3.2.2 Experimental set-up and redox oscillation procedure

A redox-cycling bioreactor system based on the one described in Parsons et al. (2013) was filled with 1 L of sediment suspension (< 1 mm fraction, 100g dry soil/L) (Fig. 3.1). All glass and plastic parts were washed with 5% HNO_3 then rinsed thoroughly in ultra-pure water. The E_h and pH electrode signals were connected to FET instrumentation amplifiers with high input impedance. Two reactors were supplied with a final concentration of 50 µM of dissolved arsenite, As(III) ($NaAsO_2$ – Sigma-Aldrich). The two reactors, R1 and R2 contained 0.1 mM and 1 mM of Na_2SO_4, respectively. At the beginning of each reducing cycle, two reactors were supplied with cellobiose ($C_{12}H_{22}O_{11}$ – Sigma-Aldrich) with 8.33 mmol/L final concentration of total DOC. Input solutions were adjusted for ionic strength (I = 30 mM) using sodium chloride (NaCl - Sigma-Aldrich).

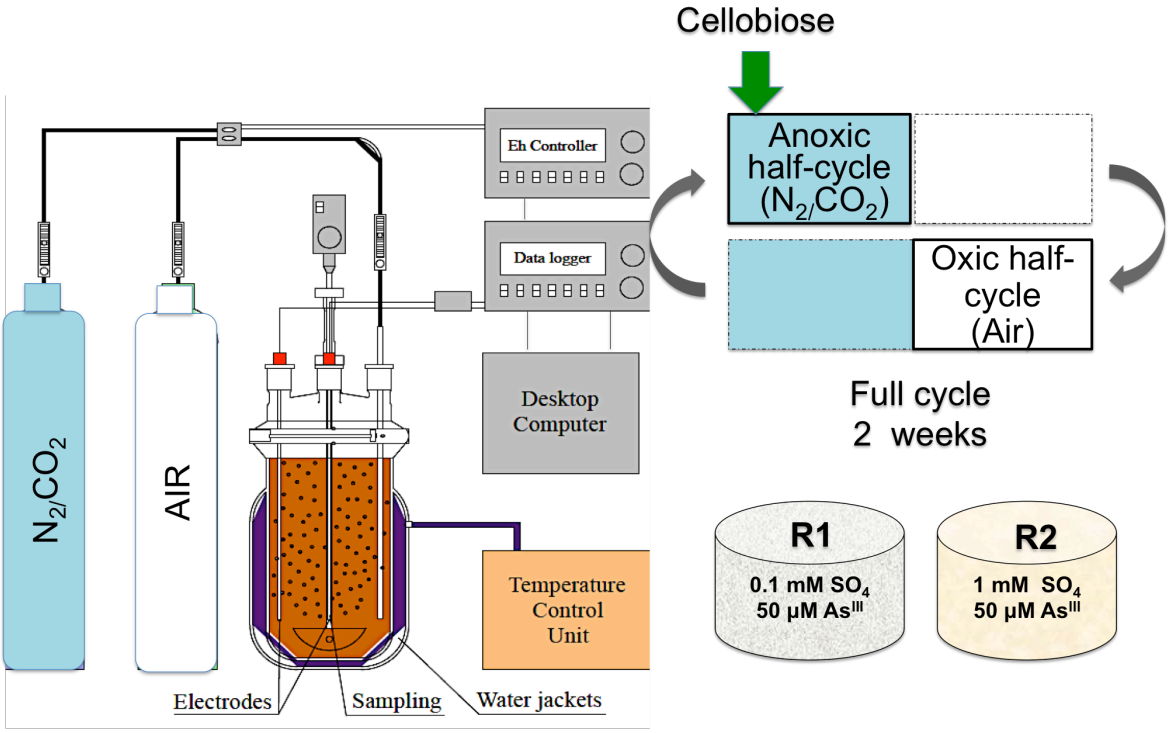

Figure 3.1 Schematic design of the redox-cycling bioreactor system including the condition for anoxic and oxic half-cycles and the inputs of R1 and R2 experiments

The suspensions were subjected to multiple cycles of reduction and oxidation to replicate flooding and draining experienced in nature and to determine the cumulative effects of the cycling on arsenic mobility during microbial sulfate reduction. E_h control was implemented by modulating the influx gas between N_2/compressed air gas admixture automatically using an Agilent switching unit and a system of solenoid valves. Redox cycles were monitored for approximately 40 days. Anoxic cycles were simulated using a N_2/CO_2 gas mixture and lasted for 7 days (half-cycle time). In the oxic cycles (7 days half cycle), the N_2/CO_2 mixture was substituted with air. The first anoxic half cycle was stimulated for 5 days. Gas flow rate and temperature were remained at a constant 30 ml/min and 30°C, respectively. A syringe was employed to inject stock reagents ($C_{12}H_{22}O_{11}$, $NaAsO_2$, or Na_2SO_4) into the system. Suspension samples were collected after day 1, 2, 3, 5, and 7 of each cycle for aqueous, microbial and solid phase analyses.

3.2.3 Aqueous Chemistry Analyses

All chemicals were analytical grades from Fluka, Sigma-Aldrich or Merck. Standards and reagents were prepared with ultra-pure water. Syringe sampled sediment suspensions were centrifuged and the supernatant filtered through 0.22 µm pore size membranes prior to all aqueous analyses. Analysis of total cations, including trace and major elements were

performed with ICP-OES (Agilent 720-ES, Varian) after dilution and acidification by HNO_3 (2%) with the detection limit of 0.1 mg/L and a precision better than 5%. DOC was determined using a Shimazu VCSN analyzer (TOC-5000, Shimadzu, France) with a detection limit of 0.3 mg/L and a precision better than 2.5%. All glassware was heated at 400°C for 3 hours avoiding DOC contamination. Major anions were analyzed by ion chromatography using a Metrohm 761 compact ion chromatography with a detection limit of 0.1 mg/L and a precision better than 5%. $[Fe^{2+}]$ and $[\Sigma S^{-2}_{(aq)}]$ was determined photometrically on the sample filtered using the Ferrozine method (Lovley & Phillips, 1986; Viollier et al., 2000, Stookey, 1970) and Cline method (Cline, 1969), respectively. The samples were then quantified by UV-Vis spectroscopy (Lambda 35, Perkin Elmer). E_h and pH were recorded every 10 seconds within the reactors using Xerolyt Solid polymer open junction electrodes. Further details of pH and E_h calculations are provided in the Supporting Information.

The amount of sulfur that remained in the solid phase at the surface in the form of elemental sulfur (S_8) was analyzed using a perchloroethylene extraction combined with High Performance Liquid Chromatography (HPLC) following the method described in McGuire & Hamers (2000). Perchloroethylene-extractable sulfur was obtained after pretreatment of unfiltered samples with 250 µL of ZnAc (5%) to precipitate free sulfide (Wan et al., 2014). Sulfide fixation allows ZnAc to react with S^{2-} as well as with S_n^{2-} ($n \geq 2$, polysulfides) leading to the precipitation of ZnS and (n-1). After 10 minutes, 4 mL of perchloroethylene was injected into 0.5 mL of suspensions. The samples were shaken for 3 hours, filtered through a 0.22µm pore size membrane. The supernatants were then analyzed by HPCL (PerkinElmer 2000 pump and auto-sampler, UV-vision detectors and software AZUR V6.0) using a C18 column (Nucleosil 100-5PAH) and isocratic elution in methanol 95% at a flow rate of 0.4 mL/min. The detection was performed at a wavelength of 265 nm.

For As speciation, a 1 mL aliquot of filtered aqueous phase was added to either a mixture of acetic acid (1%) or EDTA (1%) (Leblanc et al., 2004). Determination of inorganic (As(III), As(V)) and methylated arsenic species (monomethylarsonic acid – MMA and dimethylarsinic acid - DMA) were carried out by coupling LC (Thermo Scientific, SpectraSystem P4000) with ICP-MS with the internal standard Ge (Thermo Scientific, XSeries 2) according to the method described by Bohari et al. (2001). The LC system consisted of Varian ProStar gradient solvent delivery system equipped with a 100µL injection loop (Interchim). An anion-exchange column (Hamilton, PRP-X100) and an

eluent 30mM $(NH_4)_2HPO_4/NH_4H_2PO_4$ (pH = 8.1) was conducted at a flow rate of 1 mL/min. The detection limit was 0.09 µg/L for As(III), 0.06 µg/L for DMA, 0.04 µg/L MMA and 0.41 µg/L for As(V), with a precision better than 5%.

3.2.4 Microbial Community Analysis

In order to characterize the microbial community, samples were collected at the end of the reduced cycle and the middle of the oxidized cycle in both reactors (Fig. 1 (a-b)). The overall approach entails bacterial sequencing as a function of time and geochemical conditions. A suspension of 0.25 grams suspension was used for DNA extraction. Total genomic DNA (gDNA) was extracted using the PowerSoil® DNA Isolation kit (MO BIO Laboratories, Carlsbad, USA). The extractions were performed according to the manufacturer's manual. The DNA quantification was determined using a Nanodrop 1000 Spectrophotometer (Thermo Fisher Scientific, USA). Following DNA extraction, amplification of the DNA coding for 16S rRNA was performed by polymerase chain reaction (PCRs) using the 0.2 µmol L^{-1} of each 28f (forward) and 519r (reverse) primer (Fan et al., 2012). PCRs were performed with the Biometra T3 Thermocycler (Germany) in 50 µL total volume using the following cycling conditions: 95°C for 5.5 min, 50°C for 1 min, 68°C for 1 min after that 34 cycles of 95°C for 30 sec/cycle, and followed by a final incubation step at 68°C for 10 min. PCR products were visualized on an agarose gel, and the 16S rRNA band excised and then purified using the Wizard® SV Gel and PCR Clean-Up System (Promega, USA). The concentration of PCR products was examined using a Nanodrop prior to DNA sequencing. The amplicons were sent to a facility for the sequencing at Research and Testing Laboratory (Texas, USA). The data shows the taxonomic information with a minimum confidence of 97%.

3.2.5 Solid-phase Characterization

Solid-phase samples were collected from the two reactors at the end of the redox cycles indicated in Fig. 3.2a-b. Samples were flash-frozen in liquid N_2 and kept at -80°C until XAS analysis. Sulfur speciation in the sediment samples was examined by XANES (X-Ray absorption near edge structure) at the S K-edge (2,472 eV) at the XAFS beamline of the Elettra synchrotron (Trieste, Italy). The X-ray energy resolution was achieved by a Si(111) monochromator calibrated relative to the white line of a $Na_2S_2O_{3(s)}$ standard (Sigma-Aldrich) at 2,471.64 eV. Spectra were collected in fluorescence mode using a solid-state Si detector. Arsenic speciation in the sediment samples was examined by XANES at As K-edge (11,867 eV) at the bending magnet beamline BM08 of the European

Synchrotron Radiation Facility (ESRF, Grenoble, France). Samples were brought to the synchrotron facilities in an anaerobic jar and mounted on the samples holder inside a glove box, and then quickly transferred in the experimental chamber. To prevent beam-induced redox reactions or sample oxidation, all samples were measured in a high vacuum at low temperatures (80K). Several As and S references were measured along with the sediment samples in transmission mode. At the As edge, a homemade As(0) standard (zero-valent arsenic nanoparticles, Pal et al., 2012) was measured in transmission mode simultaneously with the sample spectra for accurate energy calibration. At the S K-edge, a commercial elemental sulfur reference was measured in fluorescence mode before each scan.

All XANES spectra were calibrated, normalize, and background subtracted, and the relative contributions of the different S and As reference compounds were calculated by linear combination fitting (LCF) using the ATHENA software package (Ravel & Newville, 2005). LCF procedure aimed at reproducing quantitatively all the features of the spectra, using the smallest number of components. Additional components were added only if the reduced chi-square (χ^2_{red}) value lowered by at least 20%, which was found to be the threshold for significantly improving the best fit. Contributions to the fits of fewer than 5% of the sum were not considered, in accordance to the error associated with the LCF procedure (Bardelli et al., 2011; Chakraborty et al., 2010; Isaure et al., 2002). The suite of sulfur references included: FeS_2 (pyrite), S_8 (elemental sulfur), SO_4^{2-} (sulfate) and RSO_2O^- (sulfonates). Arsenic references include: (i) $NaAsO_2$ and $NaHAsO_4$ (Sigma-Aldrich), MTA(V) (monothioarsenate), DTA(V) (dithioarsenate) and TeTA(V) (tetrathioarsenate) prepared using the method of Schwedt & Rieckhoff (1996) and optimized by (Suess et al., 2009); (ii) the minerals As_2S_3, As_2S_5 (Sigma – Aldrich), As_2O_3, As_2O_5, FeAsS (arsenopyrite) and $FeAsO_4$ (scorodite) (iii) the sorption complexes of As(III) and As(V) sorbed onto goethite (Farquhar et al., 2002) and (iv) the thiol-bound As(III) species: glutamyl-cysteinyl-glycinyl-thiolarsenite (As(III)-Glu) synthesized using the method of (Raab et al., 2004; Langner et al., 2011) (see Supporting information for more details in references used)

To complement the S K-edge XANES results, AVS (acid-volatile sulfide) measurement was operationally defined with a new designed system developed and optimized in our laboratory (Tisserand et al., In Prep.). AVS extraction was based on a purge and trap method (Allen et al., 1993). The method relies on the conversion of sulfur compounds within dry sediments that are first purged with HCl to generate volatile H_2S secondly trapped with NaOH. Finally, a complexation is done by adding a diamine reagent to the

trapped solution to form a methylene blue molecule (Cline, 1969), quantified by UV spectroscopy at 670 nm. Calibration was performed by the same method using Na_2S solution at 10mM. This AVS purge and trap methods were carried out within airtight Teflon reactors under continuous flow of nitrogen to avoid oxidation of sulfide. A quantity of 0.18 to 0.50 g of sediment previously freeze-dried underwent AVS extractions and quantification.

3.2.6 Thermodynamic Modeling

Thermodynamic calculations were performed using the PHREEQC program (Parkhurst & Appelo, 1999). E_h values were converted into p_e (negative logarithm of the theoretical electron activity) using the Nernst Equation ($E_h = 0.059 \times p_e$). The following calculations were performed: (i) thermodynamic aqueous species distribution during the anoxic half cycles, and (ii) the saturation state ($SI = \log IAP/K_{sp}$) at each sampling point with respect to solid arsenic, sulfur and iron phase. The database for As species was updated according to the data reported in the literature (Helz & Tossell, 2008). The added species included As(III) species, such as $H_nAsO_3^{n-3}$ (As(III) – arsenite), $H_nAsO_4^{n-3}$, $H_nAsSO_2^{n-3}$ (MTA(III) – monothioarsenite), $H_nAsS_2O^{n-3}$ (DMAs(III) – dithioarsenite), H_nAsS_3 (TTA(III) – trithioarsenite), and $As^{(V)}$ species, such as $H_nAsO_4^{n-3}$ (As(V) – arsenate), $H_nAsSO_3^{n-3}$ (MTA(V) – monothioarsenate), $H_nAsS_2O_2^{n-3}$ ($DTAs^{(V)}$ – dithioarsenate), $H_nAsS_3O^{n-3}$ (TTA(V) – trithioarsenate) and $H_nAsS_4^{n-3}$ (TeTA(V) – tetrathioarsenate). Their reactions and equilibrium constants are summarized in Table SI-1 (Couture et al., 2010; Helz & Tossell, 2008; Keller et al., 2014).

3.3 Results

3.3.1 Aqueous chemistry

Results of the aqueous phase of experiments carried out in reactors R1 and R2, containing respectively with 0.1 mM and 1 mM of sulfate, are summarized in Fig. 3.2.

E_h and pH cycling. The reducing and oxidizing steps can be clearly identified by E_h and pH parameters (Fig. 3.2. a-b). E_h ranges from -300 mV, in anoxic half-cycles, to +500 mV, in oxic half-cycles, for both reactors. E_h and pH underwent repeatedly cycling in the low sulfate reactor (R1). However, in the high sulfate reactor (R2), the oxidizing condition was not full attained in all oxic half-cycles. Reducing cycles were characterized by a decrease in E_h and an increase in both pH and in the Fe^{2+} concentration, while the oxidizing half cycles showed opposite trends (Fig. 3.2a-b). Intra-cycle E_h changes were similar to the E_h -monitoring studies of flooded soils and previous redox oscillating experiments (Couture et

al., 2015; Parsons et al., 2013; Ponnamperuma, 1972; Thompson et al., 2006). The pH values varied within the range of 5.2 to 7.8. In the reductive processes, we interpret the decrease in E_h as being driven by the consumption of successive terminal electron acceptors, such as Fe^{3+} and SO_4^{2-}, and of DOC by the microbial community (Essington, 2004), which resulted in hydroxide (OH^-) production and pH increase.

DOC cycling. DOC was manually replenished by adding cellobiose, a byproduct of microbial hydrolysis of cellulose under both anoxic an oxic condition in soils (Lynd et al., 2002; Schellenberger et al., 2011), at the beginning of each anoxic cycle. In R1 (low sulfate), bacteria present in the suspension are expected to consume cellobiose and produce short organic acids such as lactate and acetate, as well as carbon dioxide, during both oxidation and reduction cycles, via aerobic respiration and fermentation (Castillo et al., 2013). The consumption of sulfate can be attributed to its reduction coupled to organic carbon oxidation (Canfield et al., 1998). The presence of sulfide and acetate in the reducing cycles was associated with lower concentrations of DOC and sulfate (Fig. 3.2 c-g). In R2 (high sulfate), [DOC] increased during each anoxic half-cycle, indicating that dissolved organic matter (DOM) was released in the sediment under reducing conditions (Grybos et al., 2009). Three hypotheses can be proposed to explain the observed data: i) the reductive dissolution leads to the release of OM bound to iron oxyhydroxides; ii) the increase in pH values accompanying reduction reactions results in OM desorption (Ponnamperuma, 1972; Thompson et al., 2006; Grybos et al., 2009); or iii) the production of DOM during reduction of microbial biomass present in sediment. The rate of biomass solubilization of particulate organic matter (POM) or the hydrolysis of POM may exceed rates of DOC consumption by heterotrophic bacteria (Parsons et al., 2013). During the oxic half-cycles, the bacterial consumption may occur at a higher rate, resulting in a decrease of [DOC] in both reactors.

Total Fe and Fe^{2+} cycling. [Fe] and [Fe^{2+}] increased in the reducing cycles, consistently with the reduction reaction of labile Fe-oxides (Essington, 2004; Thompson et al., 2006). During the oxic cycles, [Fe^{2+}] dropped when E_h values were increased indicating that all the Fe^{2+} originating from initial pyrite oxidation and iron (oxyhydr)oxides was oxidized to Fe^{3+}, which precipitated as poorly soluble phases, such as goethite (α-FeOOH) and ferrihydrite ($Fe_2O_3.0.5H_2O$). Furthermore, thermodynamic predictions suggest that in anoxic sulfidic conditions, mackinawite (FeS) is the first iron sulfide to precipitate, and it constitutes a major component of the empirically defined "acid volatile sulfides" (AVS) (Rickard & Morse, 2005). The saturation index of FeS (SI > 0) was calculated using

PHREEQC in both reactors (SI = logIAP/K_{sp}, where IAP is the ion activity product and K_{sp} is the solubility) and is reported in Fig. 3.2 (e-f). Fe^{3+} in aqueous phase was also analysed after adding hydroxylamine soludtion. However, there was no evidence of Fe^{3+} production in the solution. The difference between total [Fe] and [Fe^{2+}] was probably organic Fe complexes which was mentioned during iron reducing such as Fe(III)-citrate and Fe(III) oxalate (Langner et al., 2011; Rickard & Iii, 2007)

SO_4^{2-}, HS^- and S_8 cycling. [SO_4^{2-}] decreased during the anoxic half-cycles and increased during the oxic half-cycles and reached to about 1.1 mM in R1 and 2 mM in R2, repectively, which were greater than 1 mM, compared to adding SO_4^{2-} of 0.1 mM at R1 and 1 mM at R2 probably due to natural pyrite oxidation (Fig. 3.2 g-h). Additionally, complete [HS^-] depletion was observed during oxidation cycles, while in reduction cycles, [HS^-] varied in the range between 0.8 - 8.7 µM in R1, and 1.4 - 4.8 µM in R2 (Fig. 3.2 i-j). Low [S^0] were detected in supernatants because the elemental sulfur is typically associated with the solid phase ($S_{8(s)}$) (McGuire & Hamers, 2000; Wan et al., 2014). [$S_{8(s)}$] was found in the suspension at concentration ranges between 0.06 – 8.7 µM and 0.1 – 2.7 µM in R1 and R2, respectively. This finding suggests that sulfate reduction and sulfide formation were followed by oxidation to sulfur and sulfate. Sulfide produced may react with Fe-oxides present in the sediment to produce iron sulfide minerals (Appelo and Postma, 2005), following for example the reaction path:

$$2FeOOH + 3HS^- \rightarrow 2FeS + S^0 + H_2O + 3OH^-$$

This reaction implies the reduction of iron oxide by S^{2-}, which is generally, a rapid process (Canfield et al., 1998). While part of the sulfide reduces Fe^{3+} and produces S^0, the remaining dissolved sulfide precipitates as FeS with representing of AVS (1.82 and 0.17 µmol/g dry soil in R1 and R2, respectively) (Table 2.2).

As cycling. Intra-cycle mobilization of $As_{(aq)}$ was observed during the anoxic half cycles. Particularly, As was released in the initial anoxic half-cycle, representing up to 32 µM and 27 µM in R1 and R2, respectively, and then sequestered in the solid phase in subsequent anoxic cycles. Conversely, oxidizing conditions re-immobilized As, returning to a base-level of approximately 1 µM in both R1 and R2. The As decreasing trend and the concomitant increasing in E_h were observed (Fig. 3.2 i-j). When oxic conditions prevail, the most thermodynamically favorable arsenic species was As(V) ($H_2AsO_4^-$ and $HAsO_4^{2-}$). As(V) is potentially retained by iron oxides such as goethite (α-FeOOH) and ferrihydrite ($Fe_2O_3.0.5H_2O$) (Couture et al., 2013; Essington, 2004). An alternative mechanism

explaining the release of arsenic in reducing conditions include the dissolution of As-bearing iron (oxyhydr)oxides (Laing et al., 2009; Molinari et al., 2013). Reducing condition were established during the anoxic half-cycles, which favors the formation of arsenite (H_3AsO_3). Successive redox cycles resulted in 92% and 83% removal of As in R1 and R2, respectively. In the presence of iron minerals, the sequestration may involve the formation of precipitates of Fe (oxyhydr)oxides and/or Fe sulfides such as FeOOH, FeS and FeS_2 and subsequent As adsorption (Couture et al., 2010, 2013; Charlet et al., 2011; Wolthers et al., 2005).

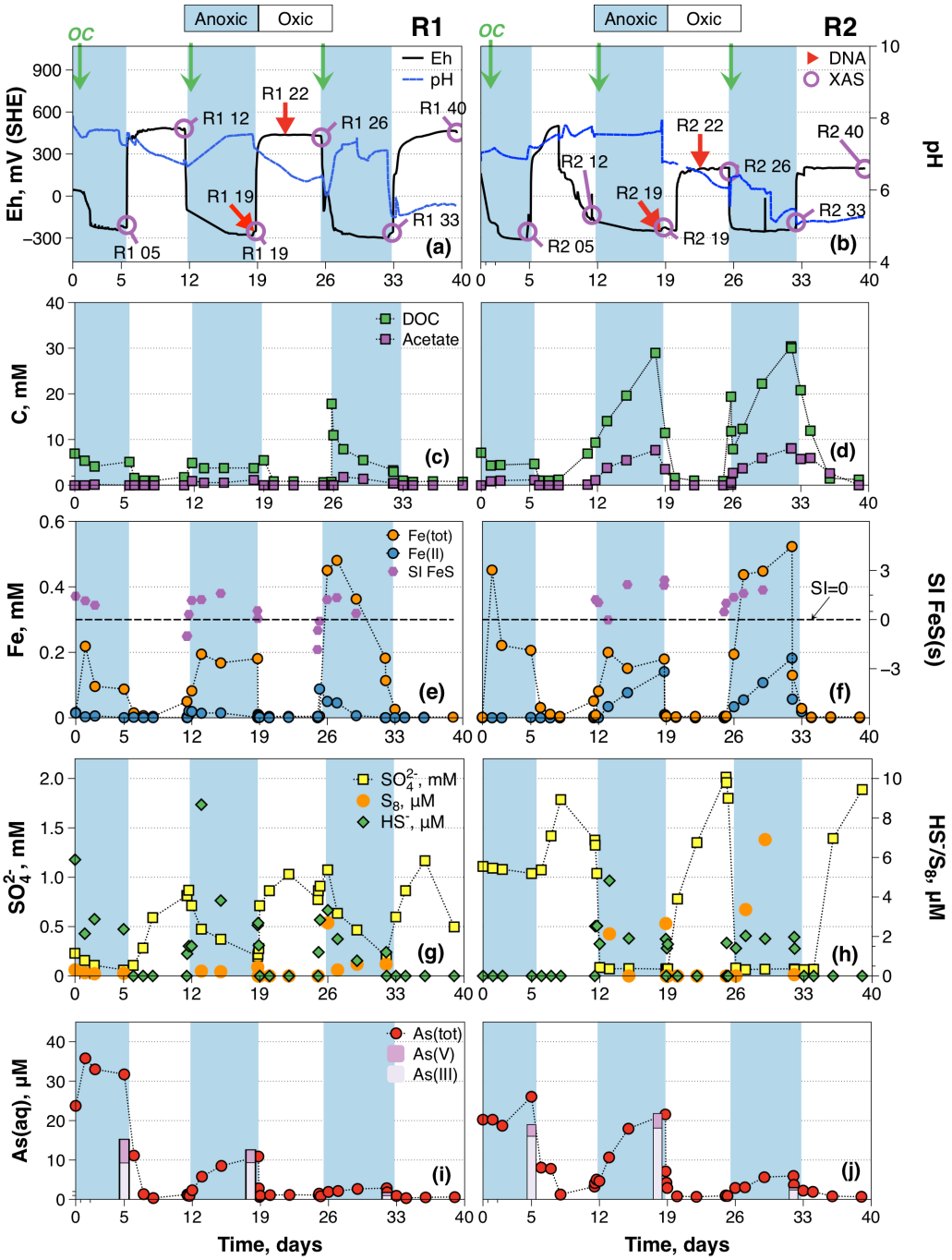

Figure 3.2**.** Aqueous chemistry measured E_h and pH (a-b), DOC and acetate (c-d), Fe(tot) and Fe^{2+} (e-f), S(tot) and SO_4^{2-}, HS^- and S_8 (g-h), As(tot), As(V) and As(III) (i-j) data with time in reactor R1, 0.1 mM and R2, 1.0 mM of SO_4^{2-}. Blue and white shaded areas indicate periods with anoxic and oxic half-cycles, respectively. Sampling points for S K-edge XANES and microbial community analysis are shown on the E_h curve (As and S K-edge XANES = open purple circles, 16S rRNA = red arrows), cellobiose (OC) adding points = green arrows, and saturation index of porewaters (e-f) with respect to $FeS_{m(s)}$

3.3.2 Microbial Community Analysis

Bacterial 16S rRNA sequence libraries were generated from the DNA extracted on day 19 (anoxic, R1- or R2-19) and 22 (oxic, R1- and R2-22), as shown by the red arrows in the Fig. 3.2a-b. Numerous bacterial phyla identified in the microbial community during the reducing and oxidizing phases mainly consist of Proteobacteria including alpha-, beta-, gamma-, delta- and epsilon-proteobacteria classes, bacteroidetes and Firmicutes class (Fig. 3.3a).

In anoxic half-cycles, phylotypes closely related to *Arcobacter* sp*.,* were the largest group in R1, representing more than 60% of the operational taxonomic units (OTUs), while they accounted for approximately 1% in R2 (Fig. 3.3b). Members of the family Campylobacteraceae, *Arcobacter* sp. may be exposed to oxic-anoxic fluctuations and significant sulfide levels (Wirsen et al., 2002). Generally, these bacteria are responsible for sulfide oxidation under microaerophilic conditions (Wirsen et al., 2002). The bacteria belonging to iron-reducing species mainly consisted of *Geobacter* sp. and *Geobacter bremensis* (Das & Caccavo, 2001; Snoeyenbos-West et al., 2000). *Geobacter* species were enriched in the two experiments (R1 and R2) during reducing cycles, representing 3.6 and 6.3% of microbial communities at R1 and R2, respectively. In addition, sequences for other extensively studied Fe(III) reducing microorganisms such as *Shewanella* species were also identified. *Shewanella xiamenensis* is one of the metal reducing bacteria that have the ability to use various terminal electron acceptors to survive in anoxic conditions (Ng et al., 2015). OTUs of *Shewanella xiamenensis* were more abundant in both R1 and R2 during reducing than during oxidizing cycles. Phylotypes related to sulfate-reducing bacteria (SRB), including *Desulfobulbus* sp*., Desulfomicrobium* sp. and *Desulfovibrio* sp. were detected in both reactors with higher contributions at reactor R2 than reactor R1 (Fig. 3.3a). Most of the members in the family Desulfobacterales were described as thermophilic sulfate reducing bacteria and potentially consumed these fermentation products such as

lactate, acetate (Muyzer & Stams, 2008; Pokorna & Zabranska, 2015). Typically, carbon compounds are incompletely oxidized to acetate by SRB, which may explain the accumulation of acetate under anoxic conditions in R2 and, to lesser extent in R1.

In the oxic half-cycles, phylotypes related to iron and sulfur-oxidizing bacteria such as *Thiobacillus thipoarus* were detected indicating the microbial oxidation of Fe^{2+} and S^{2-} or reduced sulfurs (Hedrich & Johnson, 2011). Phototrophic iron oxidizers such as *Rhodobacter* sp. that potentially use reduced sulfur compounds (S^0, HS^-, $S_2O_3^{2}$), H_2, or organic compounds as electron donors, were also identified. These organisms do not require phototrophic growth. They can also grow either chemoautotrophically or chermoheterotrophically. Additionally, the genus *Hydrogenophaga* sp., are facultatively autotrophic hydrogen-oxidizing bacteria (Willems et al., 1989). During the oxic half-cycle, the presence of *Hydrogenophaga* sp. suggests the potential accumulation of H_2 during the previous anoxic half-cycle. *Geobacter* species were also detected during oxic half-cycles, representing 7.2 and 26.1% at R1 and R2, respectively (Fig. 3.3b). *Geobacter* species were previously considered strict anaerobes (Caccavo et al., 1994; Lin et al., 2004). However, in recent years, evidence of the use of oxygen as a terminal electron acceptor by some *Geobacter* species has emerged as has their ability to reduce O_2 under microaerophilic conditions (Lin et al., 2004; Parsons et al., 2013). Sulfate-reducing bacteria (SRB) such as *Desulfovibrio* sp. were observed in oxic half-cycles. The species, like *Geobacter* species, can survive oxygen exposure and also contain enzymes to reduce oxygen (Cypionka, 2001).

Finally, the presence of many heterotrophic bacteria, capable of operating under both aerobic and anaerobic conditions, such as *Klebsiella* sp., *Methylobacterium* sp., and *Parabacteroides* sp. may account for the oxidation of OM during both phases (Eller & Frenzel, 2001; Franciscon et al., 2009). Other heterotophic bacteria, facultative OM respiring bacteria, take a prominent part of the overall community in both reactors representing from 17 – 45% of total OTUs (Fig. 3.3b). These distributions are consistent with the higher organic matter content was reduced during the oxidizing cycles and acetate production during the reducing cycles.

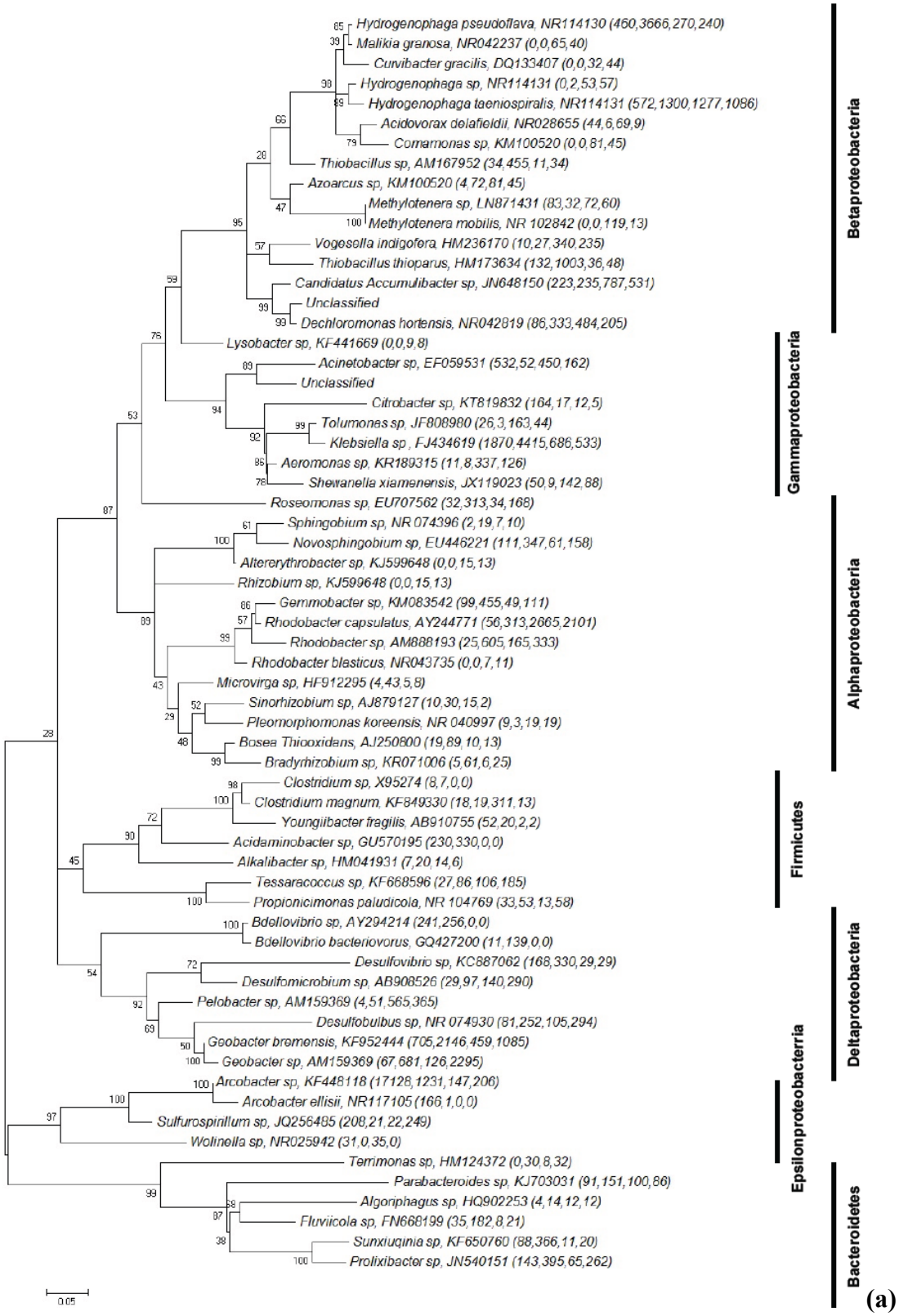
Hydrogenophaga pseudoflava, NR114130 (460,3666,270,240)
Malikia granosa, NR042237 (0,0,65,40)
Curvibacter gracilis, DQ133407 (0,0,32,44)
Hydrogenophaga sp, NR114131 (0,2,53,57)
Hydrogenophaga taeniospiralis, NR114131 (572,1300,1277,1086)
Acidovorax delafieldii, NR028655 (44,6,69,9)
Comamonas sp, KM100520 (0,0,81,45)
Thiobacillus sp, AM167952 (34,455,11,34)
Azoarcus sp, KM100520 (4,72,81,45)
Methylotenera sp, LN871431 (83,32,72,60)
Methylotenera mobilis, NR 102842 (0,0,119,13)
Vogesella indigofera, HM236170 (10,27,340,235)
Thiobacillus thioparus, HM173634 (132,1003,36,48)
Candidatus Accumulibacter sp, JN648150 (223,235,787,531)
Unclassified
Dechloromonas hortensis, NR042819 (86,333,484,205)
Lysobacter sp, KF441669 (0,0,9,8)
Acinetobacter sp, EF059531 (532,52,450,162)
Unclassified
Citrobacter sp, KT819832 (164,17,12,5)
Tolumonas sp, JF808980 (26,3,163,44)
Klebsiella sp , FJ434619 (1870,4415,686,533)
Aeromonas sp, KR189315 (11,8,337,126)
Shewanella xiamenensis, JX119023 (50,9,142,88)
Roseomonas sp, EU707562 (32,313,34,168)
Sphingobium sp, NR 074396 (2,19,7,10)
Novosphingobium sp, EU446221 (111,347,61,158)
Altererythrobacter sp, KJ599648 (0,0,15,13)
Rhizobium sp, KJ599648 (0,0,15,13)
Gemmobacter sp, KM083542 (99,455,49,111)
Rhodobacter capsulatus, AY244771 (56,313,2665,2101)
Rhodobacter sp, AM888193 (25,605,165,333)
Rhodobacter blasticus, NR043735 (0,0,7,11)
Microvirga sp, HF912295 (4,43,5,8)
Sinorhizobium sp, AJ879127 (10,30,15,2)
Pleomorphomonas koreensis, NR 040997 (9,3,19,19)
Bosea Thiooxidans, AJ250800 (19,89,10,13)
Bradyrhizobium sp, KR071006 (5,61,6,25)
Clostridium sp, X95274 (8,7,0,0)
Clostridium magnum, KF849330 (18,19,311,13)
Youngiibacter fragilis, AB910755 (52,20,2,2)
Acidaminobacter sp, GU570195 (230,330,0,0)
Alkalibacter sp, HM041931 (7,20,14,6)
Tessaracoccus sp, KF668596 (27,86,106,185)
Propionicimonas paludicola, NR 104769 (33,53,13,58)
Bdellovibrio sp, AY294214 (241,256,0,0)
Bdellovibrio bacteriovorus, GQ427200 (11,139,0,0)
Desulfovibrio sp, KC887062 (168,330,29,29)
Desulfomicrobium sp, AB908526 (29,97,140,290)
Pelobacter sp, AM159369 (4,51,565,365)
Desulfobulbus sp, NR 074930 (81,252,105,294)
Geobacter bremensis, KF952444 (705,2146,459,1085)
Geobacter sp, AM159369 (67,681,126,2295)
Arcobacter sp, KF448118 (17128,1231,147,206)
Arcobacter ellisii, NR117105 (166,1,0,0)
Sulfurospirillum sp, JQ256485 (208,21,22,249)
Wolinella sp, NR025942 (31,0,35,0)
Terrimonas sp, HM124372 (0,30,8,32)
Parabacteroides sp, KJ703031 (91,151,100,86)
Algoriphagus sp, HQ902253 (4,14,12,12)
Fluviicola sp, FN668199 (35,182,8,21)
Sunxiuqinia sp, KF650760 (88,366,11,20)
Prolixibacter sp, JN540151 (143,395,65,262)
0.05
Betaproteobacteria
Gammaproteobacteria
Alphaproteobacteria
Firmicutes
Deltaproteobacteria
Epsilonproteobacterria
Bacteroidetes

(a)

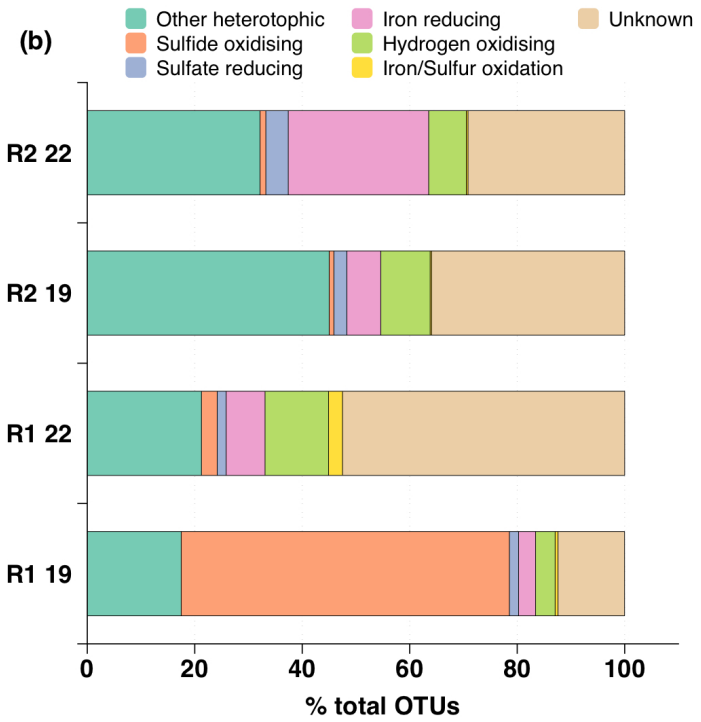

Figure 3.3. (a) Maximum likelihood phylogenetic tree showing full sequences obtained from the reactors, which retrieved from the GenBank database and (b) Distribution of microbial 16S rRNA gene sequences at four samples (R1-19, R1-22, R2-19 and R2-22). Numbers in brackets are the number of OTUs from the R1 and R2 at the various times points that shared 97% or greater identify to the displayed sequence. The bootstrap values at the left are percentages out of 1000 replicate. Sequences generated in this study were excluded from bootstrap analysis, and added to the phylogenetic tree using the software MEGA version 6.06. Scale bar represents 0.05 substitutions per nucleotide position.

3.3.3 Solid sulfur and arsenic analysis

Solid sulfur speciation

LCF of the XANES spectra at the S K-edge revealed that the majority of S accumulated in R1 and R2 as FeS_2, S_8 and SO_4^{2-} (Fig. 3.4 and Table 3.2). Most S was in the form of FeS_2 and S_8 during the anoxic cycles, except for the second anoxic cycle in R1 (R1 19), which contained FeS. In addition, AVS values indicated the possible presence of FeS representing of 1.82 μmol/g dry soil during the second anoxic cycles in R1 (Table 3.2). However, extracted AVS is not equivalent to FeS and originated from complex minerals such as FeS and greigite (Fe_3S_4) without significant release of sulfide from pyrite (Rickard

& Morse, 2005). Both S K-edge XANES and S_8 extraction analyses indicated the occurrence of elemental sulfur formation.

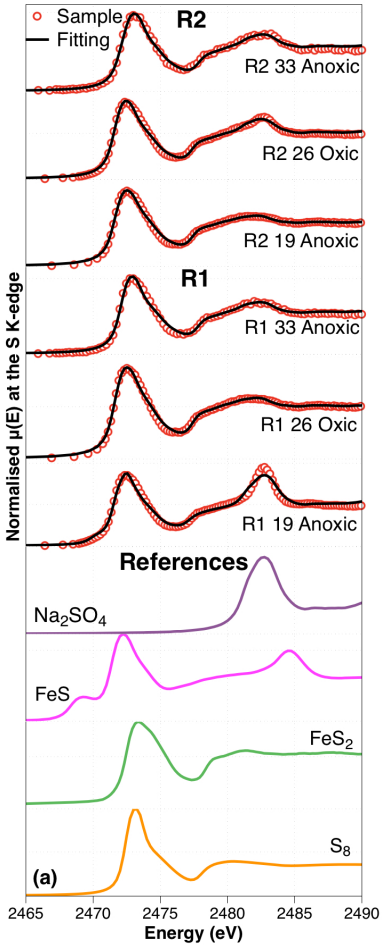

Table 3.2. Solid-phase sulfur speciation. Proportion of S solid phases revealed in the sediment samples by LCF performed on the corresponding XANES spectra. The error on the percentages estimated to be about 10%, according to Bardelli et al. (2011) and Isaure et al. (2002). The acid volatile sulfide (AVS, µmol/g of dry soil) was calculated from sequential extractions. The reduced chi-square (χ_ν^2) of the LCF is also reported.

Sample	AVS (µmol/g)	LCF (%)				χ^2
		SO_4	$S(\alpha)_8$	FeS	FeS_2	
R1 19	1.817	30	43	31	-	0.0036
R1 26	-	15	15	-	66	0.0041
R1 33	-	15	38	-	54	0.0018
R2 19	0.167	9	22	-	68	0.0059
R2 26	-	18	26	-	56	0.0085
R2 33	-	17	33	-	60	0.0472

Figure 3.4. Normalized S K-edge XANES spectra of sediment samples collected from reactors R1 (0.1 mM SO_4^{2-}) and R2 (1 mM SO_4^{2-}) at the end of each anoxic or oxic half-cycles, as shown in Fig. 3.2. The spectra of the samples (open circles) are reported together with the LCF curves superimposed (solid lines). The spectra of the reference compounds used for LCF (SO_4, S_8, FeS, FeS_2) are also shown. All spectra are vertically shifted for clarity.

Solid Arsenic Speciation

To determine the effect of redox cycling on solid arsenic speciation, X-ray absorption spectra were recorded at the As K-edge on sediments sampled at the end of each half-cycle for both reactors and initial sediment. Five species were found to be necessary to reproduce the samples spectra (Fig. 3.5a). The initial sediment included As(V), As(III)-sorbed goethite and FeAsS, as these compounds were needed for the LCF fit to reproduce the As K-edge XANES spectra of 13 samples in the natural sediment and two reactors (Fig. 3.5b-

c). The limit of XANES analysis is able to detect species that are present in amount higher than 5 – 10% and distinguish only species with sufficiently different spectral features. For the initial sediment, As(V), As(III) sorbed on iron (oxyhydr)oxides and S-bound As and/or arsenian pyrite (FeAsS). FeAsS, which was previously identified from the Mekong Delta in Cambodia, typically in the peat sediments (Stuckey et al., 2015) and pyrite-poor clay layers (Wang et al., submitted). A S-bound As(III) species was also detected in the study site, which corresponds rather to As(III) to thiol groups than to amorphous As_2S_3 precipitates (Wang et al., submitted). The liner combination fitting showed the presence of an admixture of As(III) and As(V) species in all samples, with an increase in the proportion of As(V) over As(III) during the oxidizing cycles. In the last oxic cycle, the difference of As(V) and As(III) is quite small (57% (or 53%) of As(V) and 44% (or 47%) of As(III)). In R1, in the anoxic half cycles, and partly also in oxic half cycles, 6 – 15 % of the total As solid phase was attributed to As_2S_3 or thiol-bound As(III) or FeAsS (Fig. 3.5b). In R2, LCF suggested that S-bound As compound contributed by 7 – 15% of the total As (Fig. 3.5c; Table 3.3).

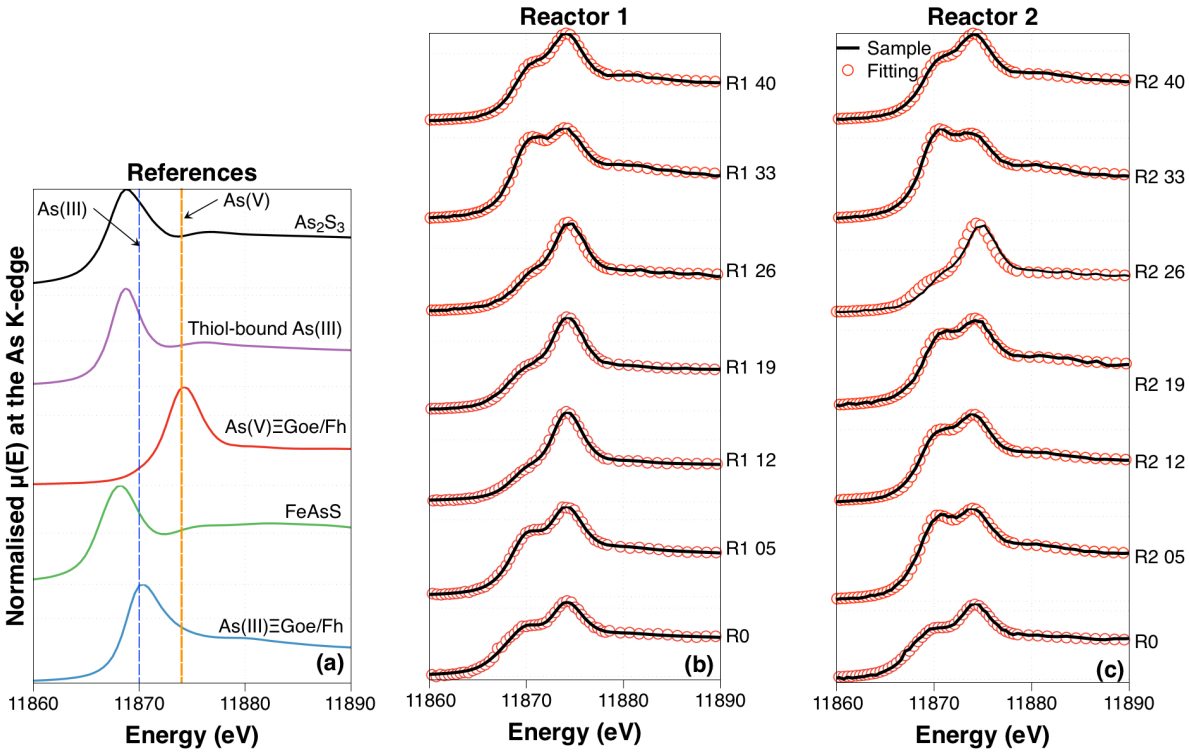

Figure 3.5. (a) The spectra of the reference compounds used for LCF (As(III/V) goethite, FeAsS, As_2S_3, thiol-bound As(III) are shown. Normalized As K-edge XANES spectra of sediment samples collected from (b) reactors R1 (0.1 mM SO_4^{2-}) and (c) R2 (0.1 mM SO_4^{2-}) at the end of each anoxic or oxic half cycle, as shown in Fig. 3.2. The spectra of the samples (open circles) are reported together with the LCF curves superimposed (solid lines). All

spectra are vertically shifted for clarity.

Table 3.3. Proportion of As solid phases in the initial sediment sample (R0) and in sediments extracted from bioreactors (R1 and R2) as revealed by LCF performed on the corresponding XANES spectra. According to Bardelli et al. (2011) and Isaure et al. (2002) the error on the percentages is estimated to be in the around 10%.

Sample	LCF (%)			χ^2
	As(V)≡Goe/Fh	As(III)≡Goe/Fh	Thiol bound As(III)/FeAsS/As_2S_3	
R0	43	29	28	0.0020
R1 05	48	38	14	0.0004
R1 12	77	19	< 10	0.0009
R1 19	66	21	15	0.0004
R1 26	74	20	< 10	0.0016
R1 33	39	56	< 10	0.0006
R1 40	57	44	< 5	0.0006
R2 05	37	54	16	0.0007
R2 12	45	53	10	0.0010
R2 19	37	59	< 10	0.0009
R2 26	74	16	14	0.0005
R2 33	30	66	< 5	0.0007
R2 40	53	47	< 5	0.0008

3.4 Discussion

3.4.1 Microbial sulfate reduction and elemental sulfur formation

The analytical results of porewater and microbial analysis at both reactors suggest the occurrence of iron and SO_4^{2-} reduction during the anoxic half-cycles. Sulfate-reducing bacteria (e.g. *Desulfobulbus* sp., *Desulfomicrobium* sp. and *Desulfovibrio* sp.) and iron-reducing microorganisms (e.g. *Geobacter* sp., *Shewanella* sp.) are detected, supporting the microbial origin of SO_4^{2-} and Fe reduction. Coincidentally, [Fe^{2+}] and [HS^-] were released repeatedly during three anoxic half-cycles in both high and low sulfate contents. These results seem to indicate an increasing trend in iron and sulfate reduction activities at high sulfate concentration. Additionally, the presence of *Arcobacter* sp. and S_8 during the anoxic half-cycles support that S^0 accumulated in the environment. Many sulfur-oxidizing organisms produce internal or external elemental sulfur in the form of hydrophilic spherical globules that can serve as an energy reserve when hydrogen sulfide availability decreases (Steudel, 1989). The mechanism for the accumulation of elemental S in the sediment is the precipitation from $S^0_{(aq)}$ during the oxidation of $S^{-2}_{(aq)}$ by metals capable of cycling between two different oxidation states, such as iron (Steudel, 1996). In the case of

sulfide oxidation by iron (oxyhydr)oxides, oxidized sulfur dominates over elemental sulfur or sulfide species, and the Fe^{2+} released may react with additional dissolved sulfide to produce $FeS_{(s)}$ (Poulton et al., 2004; Wolthers et al., 2005). This is expected that an important removal of sulfate from the sediments could be by microbial sulfate reduction during the reducing conditions. Microbially and chemically mediated processes can reduce to S^{2-}, and then may precipitate as FeS and FeS_2 (slow formation). Moreover, sulfide may be re-oxidized to intermediate S species such as S^0, which is known to microbially disproportionate (Fig. 3.6).

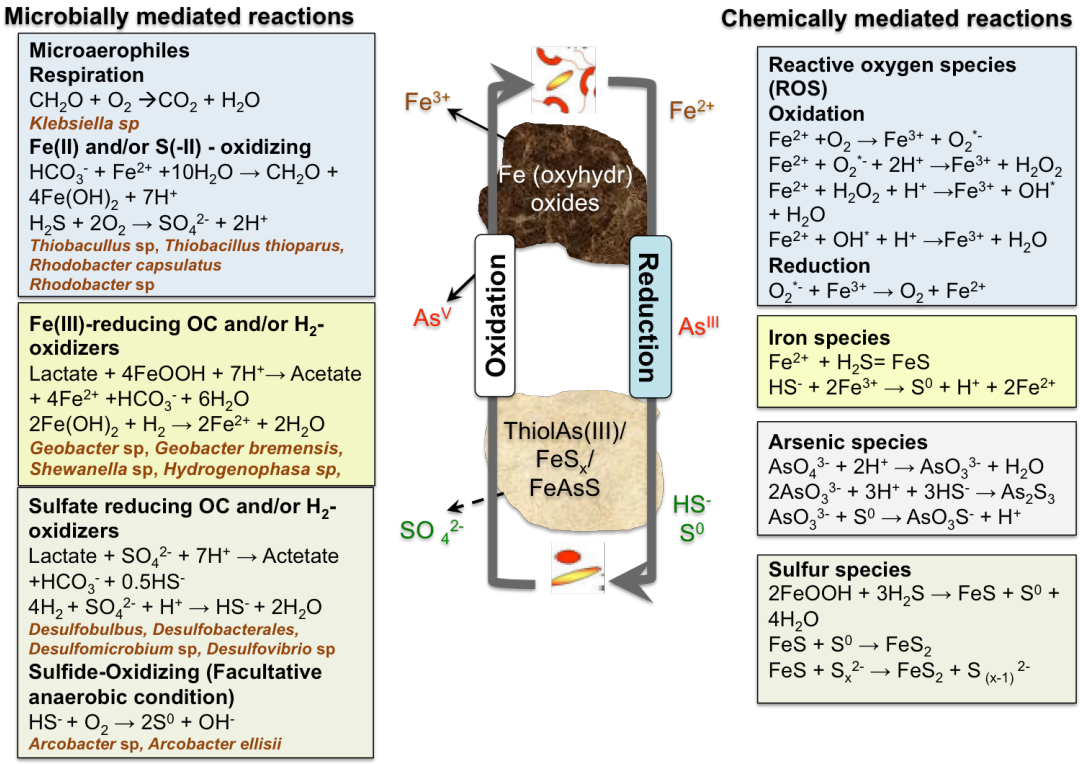

Figure 3.6. Schematic of the different microbially and chemically mediated reactions during redox experiments (see Supporting Information for calculation in PHREEQC).

3.4.2 Mechanism of As immobilization during redox oscillation

Reactions controlling As release under oxic cycles

As a first step in investigating the mechanism responsible for As removal during the oxic half-cycles, we calculated the saturation index. This calculation indicates that aqueous phases were over saturated (SI ≥ 4.5) with respect to arsenic pentoxide (As_2O_5). However, As_2O_5 is relatively unstable in the environment. Calculations, performed at pH values of 5.5 – 5.7, indicated that 0 – 80% of As_2O_5 may form in both R1 and R2 during the oxic half-cycles. In addition, its adsorption to freshly formed Fe (oxyhydr)oxides is the most likely mechanism to explain its removal from aqueous phase. Many studies have

demonstrated the important role of As adsorption onto Fe (oxyhydr)oxides (Nickson et al., 2000; Root et al., 2007; van Geen et al., 2003). Linear combinations of the XANES spectra also showed that As(V) sorbed onto an iron (oxyhydr)oxide presented was the main As solid phase species in R1 and R2 representing with 45 – 74% and 48 – 77%, respectively (Fig. 6b-c; Table 3.3). Altogether, these results suggest As immobilization during the oxidizing conditions is controlled by the adsorption on Fe (oxyhydr)oxides.

Reactions controlling As release under anoxic conditions

FeAsS and amorphous S-bound As(III) were previously identified in the natural organic matter layers and pyrite-poor clay sediments from the Mekong Delta in Cambodia (Stuckey et al., 2015, Wang et al., submitted). In this study, the XAS results suggest that the initial sediment contained As(III)/As(V) bearing iron oxyhydroxide, FeAsS and/or thiol bound As(III). Under anaerobic conditions, microbially driven oxidation of organic matter coupled to the dissimilatory reductive dissolution of As-bearing iron oxyhydroxide can cause the transfer of arsenic from the solid to the aqueous phase (Anawar et al., 2003; Hoque et al., 2009; Horneman et al., 2004; Nickson et al., 2000). The thermodynamic calculations using PHREEQC updated with thioarsenic species are shown in Fig. 3.7. Based on the latest constants, As speciations are expected to be dominated by As(III), MTA(V), TTA(V) and TeTA(V) both at low (R1) and high (R2) sulfate contents (Burton et al., 2013) (Fig. 3.7). Moreover, to test the precipitation of pure As phases, as reported in O'Day et al. (2004), we calculated the SI of the aqueous phase at each sampling point with respect to these solids (Table SI 1. 61-70). The aqueous phase was over saturated with respect to realgar, orpiment, and amorphous As sulfide ($As_2S_{3(s)}$) (SI $\geq$ 0.7) when [S^{-2}] $\geq$ 2.5 µM and in the pH range 3.2 - 7.5 (Fig. 3.7). In range of experimental pH (5.5 – 8), 0 – 30% and 0 – 60% of total aqueous As were predicted to precipitate as AsS and As_2S_3 in R1 and R2, respectively (Fig. 3.7a-c). In fact, when arsenic concentration reach micromolar levels, orpiment (As_2S_3) stability is predicted at low [Fe^{2+}] and high [S^{2-}] and when Fe^{3+} is in excess, realgar (AsS) could be formed (O'Day et al., 2004). Our finding show that, under the anoxic half-cycles, As solid species could refer to S-bound As(III) which also mentioned as As bearing minerals in the presence of S and Fe(III) organic complexes. However, the realgar spectra were really different from our samples. In the presence of high Fe(III) bound NOM and low Fe(III) (hydr)oxides, As was completely coordinated to S groups of NOM at slightly acidic pH (5.5 – 6). The sequestration of As(III) by organic S from natural OM through the formation of thiol-bound As has been reported only recently in peat samples and flow-through reactor sediments (Couture et al., 2013a, Hoffmann et

al., 2012; Langner et al., 2011). The LCF at the As K-edge were not conclusive in discriminating between As_2S_3 and thiolAs(III)-OM (Fig. 3.5a). The LCF revealed the presence of 7 – 15 % thiol bound As(III) and/or FeAsS in the anoxic half-cycles (Fig. 3.5b-c; Table 3.3). In OM-rich sediment, sulfate reduction process may control on As sequestration through the formation of thiol bound As(III) complexes.

Arsenic sequestration onto $FeS_{(s)}$ was examined in previous work (Bostick & Fendorf, 2003; Wilkin et al., 2003; Wolthers et al., 2005). The adsorption of As onto disordered mackinawite (FeS_m) was best predicted by linear adsorption isotherms with K_d (K_d = $[As_{(abs)}]/[As_{(aq)}]$ values of 2 and 9 $L.g^{-1}$ for As(III) and As(V) at pH 7.4, respectively (Wolthers et al., 2005). A saturation index was calculated with respect to disordered mackinawite using the K_{sp} value of $10^{-3.5}$ provided by Rickard (2006). The results indicate sthat aqueous phase was over saturated with respect to disordered mackinawite (Fig. 3.2e-f). Moreover, the equilibrium of aqueous phase is consistent with AVS measurements in both reactors at the end of the anoxic half-cycles (Table 3.2). LCF of the XANES spectra at the S K-edge indicated that the majority of S accumulated in R1 was in the form of S_8 and FeS during the second anoxic half-cycle. The estimated K_d values corresponding to As removal was 1.8 $L.g^{-1}$ at the second of anoxic half-cycle in R1. This value is similar to the value of 2 $L.g^{-1}$ reported by Wolthers et al. (2005). In R2, over these two cycles, the aqueous phase was saturated with respect to FeS_m. However, it should be stressed that both results of AVS and S solid phase speciation, S_8 were present instead of FeS_m during anoxic half-cycles. The generation of S^0 through the abiotic reaction of dissolved sulfide with iron oxyhydroxides can be represented by:

$$2Fe(OH)_3 + HS^- + 5H^+ \rightarrow 2Fe^{2+} + S^0 + 6H_2O$$

Thus, when microbial sulfate reduction occurs in the presence of reactive Fe^{3+} minerals phase after oxic half-cycles, the accumulation of dissolved Fe^{2+} is prevented by the precipitation of Fe sulfides (Fig. 3.2-f), two sulfur redox couples can potentially influence E_h values in the aqueous phase including, SO_4^{2-}/HS^- and S^0/HS^- (Couture & Cappellen, 2011). At high $[SO_4^{2-}]$, the transformation of FeS into FeS_2 through the reaction of FeS with intermediate sulfur species such as S^0 and S_x^{2-} or H_2S has been proposed to follow the reaction paths in laboratory experiments (Berner, 1970; Raiswell & Berner, 1985; Hurtgen et al., 1999): $FeS + S^0 \rightarrow FeS_2$ or $FeS + S_x^{2-} \rightarrow FeS_2 + S_{(x-1)}^{2-}$ (Fig. 3.6).

However, LCF fit of As K-edge shows that As(III) bearing iron (oxyhydr)oxides is the main species during the anoxic half-cycles, representing 21 – 38% in R1, and 54 – 66% in

R2. The persistence of As(III) under oxidizing conditions also indicates that oxidation process was probably strongly kinetically controlled (Parsons et al., 2013). On the contrary, As(III) adsorption onto iron (oxyhydr)oxides was favored with respect to As(V) during reducing cycles. This is consistent with the dissolution of As(V)-bearing iron (oxyhydr)oxides predicted by the PHREEQC model and with the reduction of As(V) to As(III) either directly by arsenic reducing bacteria, or indirectly due to chemical reduction (Fig. 3.6).

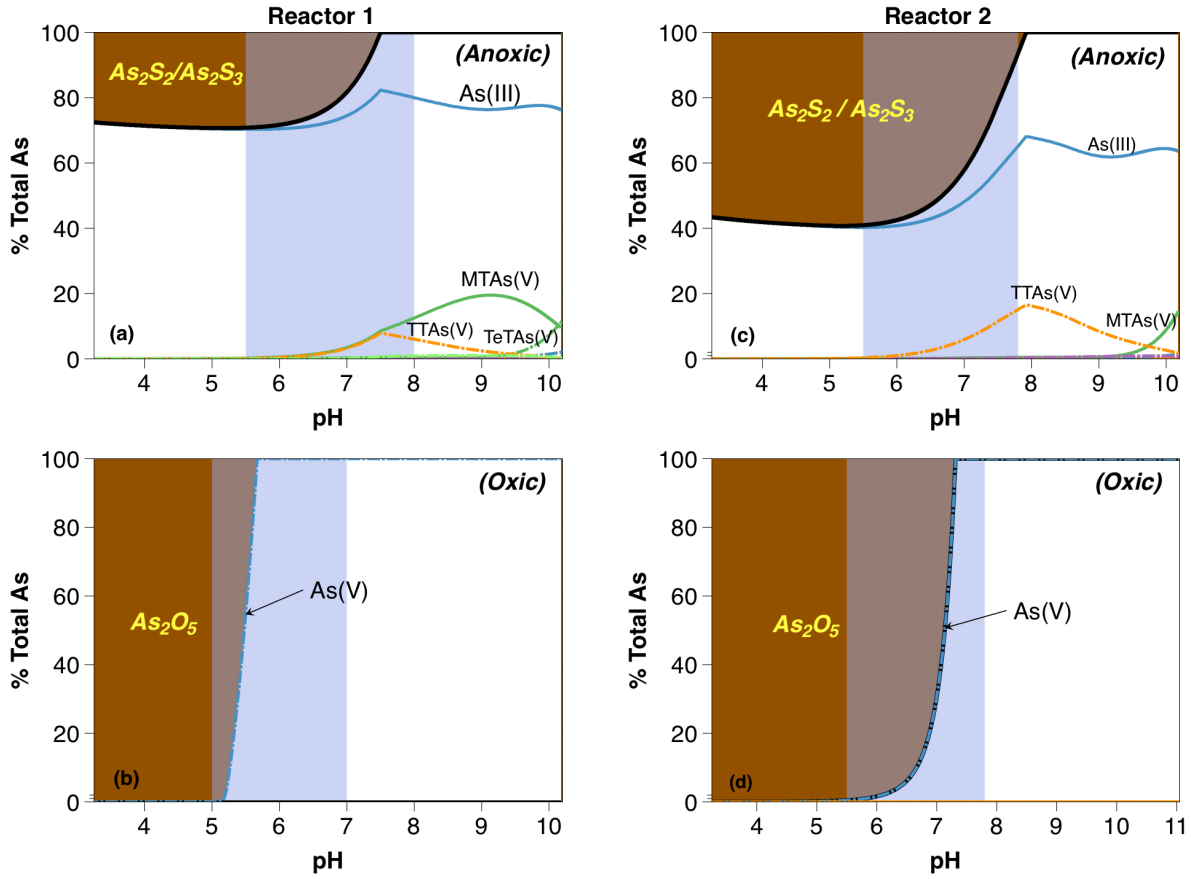

Figure 3.7. Thermodynamically aqueous (white region) and solid (brown region) As speciation with R1 in the anoxic (a) and oxic cycle (b) ($\Sigma As = 50 \times 10^{-6}$ and $\Sigma S = 100 \times 10^{-6}$ (M) and R2 in the anoxic (c) and oxic cycle (d) ($\Sigma As = 50 \times 10^{-6}$ and $\Sigma S = 1000 \times 10^{-6}$ (M) using PHREEQC code. The blue vertical areas represent pH values of anoxic/oxic half-cycles.

3.5 Conclusion

This study aimed to better understand whether the high As concentrations detected in the aquifer in An Giang can be attributed to redox dynamics. The effects of cumulated sulfate-rich sediment redox cycles on microbial community and arsenic mobility in As contaminated sediments were investigated in laboratory batch bioreactors. Previous studies

on the floodplain soils demonstrated that the As concentration in porewater decreased after flooding was due to the physical removal of arsenic by receding floodwater and trapping of As within minerals, OM composition and microbial activity. Based on present results, we proposed that sulfur and iron biogeochemistry play a key role in the fate of As in deltaic sediments during redox oscillations occurring upon monsoon or irrigation flooding. Particularly, the results indicate that: (i) As is released during the reducing conditions but is sequestered during the sulfate reduction leading to a new control of a sulfur-rich phase on As release according to S and As K-edge XANES spectroscopic results; (ii) As adsorbs/desorbs on iron (oxyhydr)oxides and on/within reduced solid sulfur; (iii) thiolAs (III) bound organic matter complexes potentially form in; and (iv) the observed decreased mobility of aqueous As over subsequent cycles can be attributed to fermentation during anoxic periods and respiratory consumption during oxic periods under microbial activity. Although previous studies have shown that in the reducing cycles As is released to the pore waters by reductive dissolution of iron (oxyhydr)oxides, the present work demonstrates that microbial sulfate reduction has potential to stabilize As during redox oscillations. To conclude, the results of the redox cycling experiments support more for As immobilization based on the combined impact of surface hydrology and microbial degradation of OM in seasonally saturated sediments in Mekong Delta, Vietnam.

Acknowledgements

The authors acknowledge the financial support of the doctoral scholarship from University Grenoble-Alpes, France. This study has been conducted under the framework of CARE-RESCIF initiatives. We give special thanks to Y. Wang, M. P. Asta, M. C. Reid from EPFL, Le-Phu Vo, Quoc-Tuc Dinh and Phuoc-Dan Nguyen from HCMUT for help with collecting sediment and fieldwork in Vietnam, L. Spadini and M-C Morel in LTHE for IC and S_8 analysis. We also thank E. Markelova, A. Fernandez-Martinez for experimental and analytical support. The As aqueous species were analyzed on Plateforme AETE – HydroSciences/OSU OREME, Montpellier, France. We also thank Francesco D'Acapito and Giovanni Lepore for the assistance during XAS measurements at the LISA beamline at the ESRF (BM08), and Giuliana Aquilanti for the assistance at the XAFS beamline at the Elettra synchrotron.

Supplementary information Chapter 3

Arsenic release during redox oscillations in Mekong upper delta aquifers in Vietnam: a mechanistic study

S.1 Studied sampling

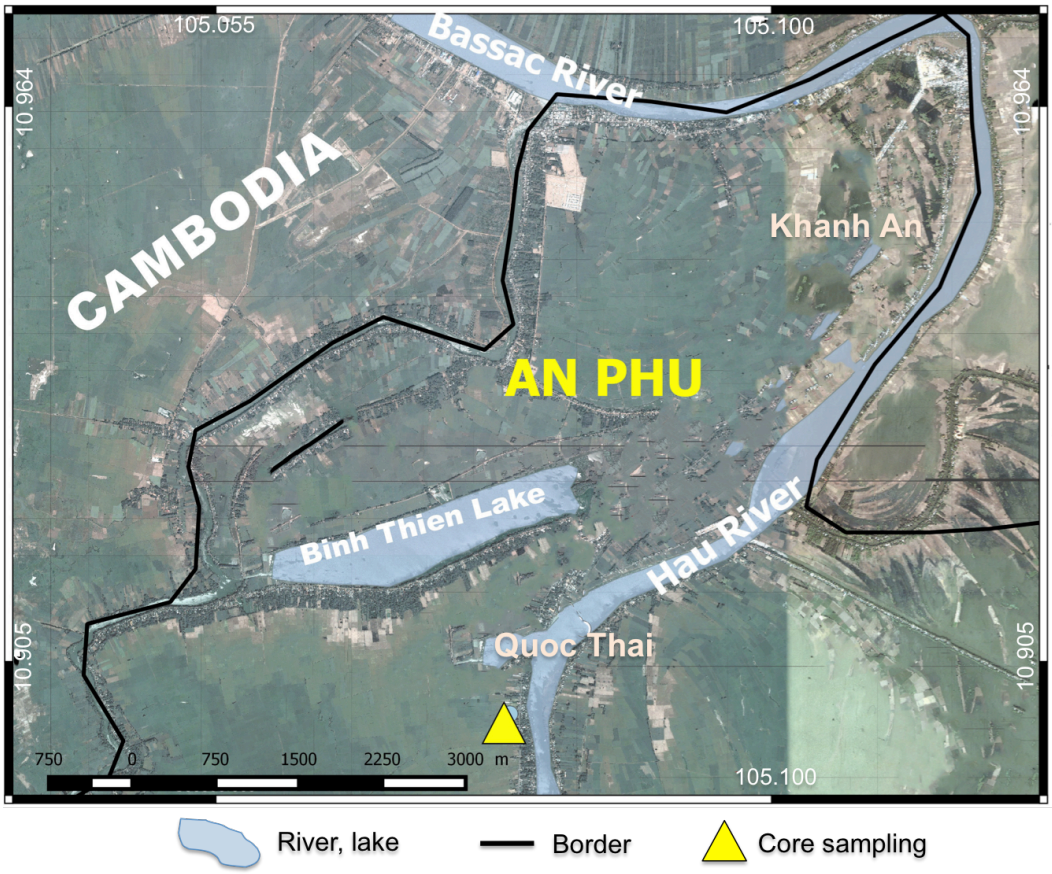

Figure S3.1. Maps the sampling location in An Phu commune marked with a yellow triangle, in the vicinity of Mekong Delta River.

S.2 Materials and methods

d. Detail on the redox cycling reactor setup

A two part Pyrex® glass reactor system was used, previously designed in Parsons et al. (2013). E_h and pH data were recorded every 10 seconds and the influx gas was changed between N_2:CO_2 (392 ppm) and compressed air via the Agilent switching unit, a relay board and a system of solenoid valves. Solid polymer open junction Xerolyt electrodes (Mettler-Toledo, France) were selected for their long-term measurement. A three-point calibration was performed for the pH electrodes (pH of 4, 7 and 10) at the start and end of experiments showing that electrode response had not shifted more than 0.02 pH units

during experiments. Measured E_h recordings were converted to a redox potential with respect to the Standard Hydrogen Electrode (SHE) by normalization using redox standard solution (220 mV). The calculated difference at the start of experiments was equal to the electrode manufacturer specification of 207 mV (temperature of 30°C).

e. Thermodynamic modeling

Table S3.1. Summary of As equilibrium reactions and constants applied in this study for aqueous As speciation using PHREEQC

No	Reaction	Log*K*	Reference
Electron transfer			
1	$AsO_4^{3-} + 2e^- + 2H^+ = AsO_3^{3-} + H_2O$	2.17	a
2	$S^0_{(aq)} + H^+ + 2e^- = HS^-$	4.57	a
3	$SO_4^{2-} + 9H^+ + 8e^- = HS^- + 4H_2O$	33.65	a
4	$HS^- + H^+ = H_2S$	6.99	a
5	$HS^- = S^{2-} + H^+$	-18.97	a
Ionization			
6	$AsO_3^{3-} + H^+ = HAsO_3^{2-}$	13.99	b
7	$AsO_3^{3-} + 2H^+ = H_2AsO_3^-$	27.53	b
8	$AsO_3^{3-} + 3H^+ = H_3AsO_3$	36.8	b
9	$AsO_4^{3-} + H^+ = HAsO_4^{2-}$	11.8	a
10	$AsO_4^{3-} + 2H^+ = H_2AsO_4^-$	18.79	a
11	$AsO_4^{3-} + 3H^+ = H_3AsO_4$	21.09	a
Complexation			
12	$AsO_4^{3-} + 2H^+ + Fe^{2+} = FeH_2AsO_4^+$	5.15	c
13	$AsO_4^{3-} + H^+ + Fe^{2+} = FeHAsO_4^0$	6.1	c
14	$AsO_4^{3-} + Fe^{2+} = FeAsO_4^-$	-13.6	c
Sulfidation			
Monothioarsenite - MTA(III)			
15	$AsO_3^{3-} + HS^- + 4H^+ = H_3AsSO_2 + H_2O$	45.7	d
16	$AsO_3^{3-} + HS^- + 3H^+ = H_2AsSO_2^- + H_2O$	42	d
17	$AsO_3^{3-} + HS^- + 2H^+ = HAsSO_2^{2-} + H_2O$	27.9	d
Dithioarsenite - DTAs(III)			
18	$AsO_3^{3-} + 2HS^- + 5H^+ = H_3AsS_2O + 2H_2O$	56.5	d
19	$AsO_3^{3-} + 2HS^- + 4H^+ = H_2AsS_2O^- + 2H_2O$	52.8	d

20	$AsO_3^{3-} + 2HS^- + 3H^+ = HAsS_2O^{2-} + 2H_2O$	44.2	d
Trithioarsenite - TrTAs(III)			
21	$AsO_3^{3-} + 3HS^- + 6H^+ = H_3AsS_3 + 3H_2O$	69	d
22	$AsO_3^{3-} + 3HS^- + 5H^+ = H_2AsS_3^- + 3H_2O$	65.3	d
23	$AsO_3^{3-} + 3HS^- + 3H^+ = HAsS_3^{2-} + 3H_2O$	56.7	d
Monothioarsenate - MTAs(V)			
24	$AsO_4^{3-} + HS^- + 4H^+ = H_3AsSO_3 + H_2O$	39.1	d
25	$AsO_4^{3-} + HS^- + 3H^+ = H_2AsSO_3^- + H_2O$	35.8	d
26	$AsO_4^{3-} + HS^- + 2H^+ = HAsSO_3^{2-} + H_2O$	25.6	d
27	$AsO_4^{3-} + HS^- + H^+ = AsSO_3^{3-} + H_2O$	17.6	d
Dithioarsenate - DTAs(V)			
28	$AsO_4^{3-} + 2HS^- + 5H^+ = H_3AsS_2O_2 + 2H_2O$	46.2	d
29	$AsO_4^{3-} + 2HS^- + 4H^+ = H_2AsS_2O_2^- + 2H_2O$	48.6	d
30	$AsO_4^{3-} + 2HS^- + 3H^+ = HAsS_2O_2^{2-} + 2H_2O$	41.5	d
31	$AsO_4^{3-} + 2HS^- + 2H^+ = AsS_2O_2^{3-} + 2H_2O$	30.7	d
Trithioarsenate - TTAs(V)			
32	$AsO_4^{3-} + 3HS^- + 6H^+ = H_3AsS_3O + 3H_2O$	56.7	d
33	$AsO_4^{3-} + 3HS^- + 5H^+ = H_2AsS_3O^- + 3H_2O$	58.3	d
34	$AsO_4^{3-} + 3HS^- + 4H^+ = HAsS_3O^{2-} + 3H_2O$	56.9	d
35	$AsO_4^{3-} + 3HS^- + 3H^+ = AsS_3O^{3-} + 3H_2O$	46.1	d
Tetrathioarsenate - TeTAs(V)			
36	$AsO_4^{3-} + 4HS^- + 7H^+ = H_3AsS_4 + 4H_2O$	66.3	d
37	$AsO_4^{3-} + 4HS^- + 6H^+ = H_2AsS_4^- + 4H_2O$	68.6	d
38	$AsO_4^{3-} + 4HS^- + 5H^+ = HAsS_4^{2-} + 4H_2O$	67.1	d
39	$AsO_4^{3-} + 4HS^- + 4H^+ = AsS_4^{3-} + 4H_2O$	61.9	d
Polysulfide species			
40	$S^0_{(aq)} + HS^- = S_2^{2-} + H^+$	-4.48	e
41	$2S^0_{(aq)} + HS^- = S_3^{2-} + H^+$	2.92	e
42	$3S^0_{(aq)} + HS^- = S_4^{2-} + H^+$	10.34	e
43	$4S^0_{(aq)} + HS^- = S_5^{2-} + H^+$	17.25	e
44	$5S^0_{(aq)} + HS^- = S_6^{2-} + H^+$	23.74	e
45	$6S^0_{(aq)} + HS^- = S_7^{2-} + H^+$	29.84	e
46	$7S^0_{(aq)} + HS^- = S_8^{2-} + H^+$	35.97	e

47	$S^0_{(aq)} + HS^- = HS_2^-$	5.25	e
48	$2S^0_{(aq)} + HS^- = HS_3^-$	10.75	e
49	$3S^0_{(aq)} + HS^- = HS_4^-$	16.97	e
50	$4S^0_{(aq)} + HS^- = HS_5^-$	23.28	e
51	$5S^0_{(aq)} + HS^- = HS_6^-$	29.25	e
52	$6S^0_{(aq)} + HS^- = HS_7^-$	35.02	e
53	$7S^0_{(aq)} + HS^- = HS_8^-$	40.91	e
54	$S^0_{(aq)} + HS^- + H^+ = H_2S_2$	10.36	e
55	$2S^0_{(aq)} + HS^- + H^+ = H_2S_3$	15.06	e
56	$3S^0_{(aq)} + HS^- + H^+ = H_2S_4$	20.88	e
57	$4S^0_{(aq)} + HS^- + H^+ = H_2S_5$	26.89	e
58	$5S^0_{(aq)} + HS^- + H^+ = H_2S_6$	32.89	e
59	$6S^0_{(aq)} + HS^- + H^+ = H_2S_7$	38.50	e
60	$7S^0_{(aq)} + HS^- + H^+ = H_2S_8$	44.31	e
Precipitation reactions			
61	$2As^{V}O_4^{3-} + 6H^+ = As_2O_{5(s)} + 3H_2O$	61.95	a
62	$2As^{V}O_4^{3-} + 3Fe^{2+} = Fe_3(AsO_4)_{2(s)}$	34.41	b
63	$2As^{III}O_3^{3-} + 6H^+ = As_2O_{3(s)}$ (arsenolite) $+ 3H_2O$	77.92	a
64	$2As^{III}O_3^{3-} + 6H^+ = As_2O_{3(s)}$ (claudetite) $+ 3H_2O$	77.95	a
65	$2As^{III}O_3^{3-} + 3H^+ + 3HS^- = As_2S_3$ (orpiment) $+ 6H_2O$	122.8	a
66	$2As^{III}O_3^{3-} + 3H^+ + 3HS^- = As_2S_3$ (orpiment, amorphous) $+ 6H_2O$	121.4	a
67	$As^{III}O_3^{3-} + 4H^+ + HS^- = AsS_{(s)}$ (realgar) $+ 2.5H_2O + 0.25O_2$	36.9	a
68	$Fe^{2+} + HS^- = FeS_m$ (mackinawite, disordered) $+ H^+$	3.5	f
69	$3Fe^{2+} + 3HS^- + S^0 = Fe_3S_4$ (greigite) $+ 3H^+$	13.2	g
70	$Fe^{2+} + 2HS^- = FeS_2$ (pyrite) $+ 2e^- + 2H^+$	16.4	g

Reference a: Nordstrom et al. (2014); b: Keller et al. (2014); c: Whiting (1992), d: Helz & Tossell (2008); e: Kamyshny et al. (2009), f: Rickard (2006), g: Davison (1991)

f. Reference Preparation

Table S3.2. List of As K-edge and S K-edge reference compounds analyzed by XANES

No	Compound	Chemical formula	Source/synthesis reference

1	Sodium arsenite	$NaAsO_2$	Sigma - Aldrich
2	Sodium arsenate dibasic hetahydrate	$Na_2HAsO_4.7H_2O$	Sigma - Aldrich
3	Monothioarsenate - $MTAs^{(V)}$	$Na_3AsO_3S.7H_2O$	Schwedt & Rieckhoff (1996)
4	Dithioarsenate $DMAs^{(V)}$	$Na_3AsO_2S_2.7H_2O$	Schwedt & Rieckhoff (1996)
5	Realgar	AsS	Alfa-Aesar
6	Orpiment	As_2S_3	Sigma – Aldrich
7	Arsenian pyrite	FeAsS	Natural samples*
8	Glutamyl-cysteinyl-glycinyl-thioarsenite	$As(C_{10}H_{17}N_3O_6S)_{2.6}(OH)_{0.6}$	Raab et al. (2004)
9	As^{III}≡goethite	As^{III}=α-FeOOH	Farquhar & Livens (2002)
10	As^{V}≡Goethite	As^{V}=α-FeOOH	Farquhar & Livens (2002)
11	As^{III}≡Jarosite	$As^{III}=KFe^{3+}_3(OH)_6(SO_4)_2$	Baron and Palmer (1996)
12	As^{V}≡Jarosite	$As^{V}=KFe^{3+}_3(OH)_6(SO_4)_2$	Baron and Palmer (1996)
13	Arsenolite/Claudetite	As_2O_3	Fluka
14	Arsenic pentoxide	As_2O_5	Sigma – Aldrich
15	Elemental sulfur	S_8	Sigma – Aldrich
16	Pyrite	FeS_2	Alfa Aesar
17	Mackinawite	FeS_m	Scheinost et al. (2008)
18	Sodium sulfate	Na_2SO_4	Sigma – Aldrich

* a natural sample was provided by the Natuaral Hystory museums of the University of Florence collected from Baccu Locci (Sardinia, Italy)

As(0)

Aqueous freshly prepared solution of $NaBH_4$ stored at 4°C was sued for reducing $As^{(III)}$ to $As^{(0)}$. The reduction was carried out on aqueous sodium arsenite ($NaAsO_2$) already maintained at pH 7-9 under ambient condition (Pal et al., 2012). As(III) solution (0.5 mM) was mixed with 3.0 mL of distilled water to maintain the concentration of arsenic in the range 0.1 – 0.5 mM and to this was added 150 µl of 0.1 M ice-cold $NaBH_4$ solution. On addition of $NaBH_4$ solution the pH of the medium increases slightly. The mixtures were allowed to stand at room temperature for 2 h when yellowish-brown colored $As^{(0)}$ sol appeared. The solution was then heated to 60°C for 15 min, and cooled to room temperature.

$Na_3AsO_3S.7H_2O$ (Monothioarsenate - MTA(V))

Monothioarsenate was synthesized from As^{III} and elemental sulfur (S^0) using method of Schwedt & Rieckhoff (1996) under alkaline conditions. A 1.44-g amount of sulfur (0.045 mol S) was added to a mixture of 5.00 g of As_2O_3 (0.050 mol As) and 6.00 g of NaOH

(0.150 mol Na) in 20 ml of water and the solution was heated to 100°C. After 2 h, the excess of sulfur was filtered off and the solution was cooled slowly to 4°C. Colorless needle-shaped crystals were obtained (yield of $Na_3AsO_3S.7H_2O$: 0.038 mol, 76%). The rest of the solvent was removed under vacuum.

$Na_3AsO_2S_2.7H_2O$ (Dithioarsenate - DTA(V))

A 5.76 g amount of sulfur (0.180 mol S) was added to a mixture of 5.00 g of As_2O_3 (0.050 mol As) and 6.00 g of NaOH (0.150 mol Na) in 20 ml of water. Then, the solution was heated to 70°C (Schwedt & Rieckhoff, 1996). After 2 days, the excess of sulfur was filtered off and the solution was cooled slowly to 4°C. Colorless rhombic crystals were obtained (yield of $Na_3AsO_2S_2.7H_2O$: 0.023 mol, 46%). The crystals were dried under vacuum for 1 h.

$Na_3AsS_4.8H_2O$ (Tetrathioarsenate - TeTA(V))

The procedure described by Schwedt and Rieckhoff (1996) did not yield tetrathioarsenate. Therefore, it will be synthesized in an entirely different manner using (Suess et al., 2009). As_2S_5 was synthesized by dissolving 41.9 g of $Na_2HAsO_4.7H_2O$ in 500 mL of ultra-pure water and adding 500 mL of concentrated HCl, and bubbling H_2S gas vigorously through the solution for 10 min. The precipitate was allowed to settle for 1 h, and then it was filtered and washed with UPW. The As_2S_5 was dried over P_2O_5 under vacuum for the weekend but did not dry completely. This material (20.9g) was added to a mixture of 49.4g of $Na_2S.9H_2O$ and 8.1 g of NaOH in 600 mL of UPW, which yielded a golden-colored solution that appeared to contain colloidal matter. This solution was filtered and 300 mL of ethanol was added, and the precipitate was allowed to form at 4°C overnight.

The thiolAs(III) bound OM species (glutamyl-cysteinyl-glycinyl-thioarsenite)

It was synthesized following Langner et al. (2011) and Raab et al. (2004). The synthesis involved stirring the reagents for 12 h at room temperature under nitrogen. Dissolve 1.17 g $Na_2HAsO_4.7H_2O$ (Sigma-Aldrich) and 5 g Reduced Glutathione (GSH) (Sigma-Aldrich) in 10 mL ultra-pure water (0.375 mmol As and 1.6 mmol GSH). The reaction mixture was then mixed with 30 mL methanol and the resulting precipitate was filtered and dried at room temperature.

As(III) sorbed on Goethite

A procedure for synthesizing Goethite has been described in detail by Drissi et al. (1995). The precipitation of ferrous hydroxide was performed by mixing solutions of ferrous sulfate ($FeSO_4.7H_2O$) (Sigma-Aldrich) and mixture of NaOH – $NaHCO_3$. This process produced a buffering of the pH between 10 and 11. A 0.065 g of $NaAsO_2$ (0.5 mM of As^{III}) was put into 1 L of ultra-water, and adjusted pH = 5.5 - 6.5 by NaOH 0.01 M (Farquhar et al.,

2002). A solution of As(III) was contacted with 0.15 g Goethite. The phases were separated in 15 minutes by centrifuging at a speed of 3000 rpm.

As(V) sorbed on Goethite

A 0.093 g of $Na_2HAsO_4.7H_2O$ (0.5 mM of As(V)) was put into 1 L of ultra-water, and adjusted pH from 5.5 to 6.5 by NaOH 0.01 M. Afterwards, a 15 mL of solution As(V) was contacted with 0.15g Goethite (Farquhar et al., 2002)

As(V) sorbed on Schewertmannite

Schwertmannite was synthesized using the method of Fernandez-Martinez et al. (2010). A solution containing ferric chloride and 50 sodium sulfate was prepared and heated to 60°C in a beaker under magnetic stirring at 350 rpm for 12 min. The produced suspension was cooled to room temperature and dialysed for a period of 30 days and subjected to X-ray diffraction (XRD) analysis. In a 100 mL flask, 50 mL of solutions containing 0.5 mmol of $Na_2HAsO_4.7H_2O$ was mixed with 150 mg of dried schwertmannite products. After the pH of schwertmannite suspension was adjusted to 3 – 4 by addition of H_2SO_4 or NaOH, the flask was stirring in at 120 rpm, room temperature in 24 h to allow maximum As(V) sorption.

Mackinawite (FeS_m)

Mackinawite was synthesized using method of Scheinost et al. (2008). The mackinawite (FeS) suspension (Fe_{tot} = 0.3 M) was prepared by mixing 100 mL of a 0.6 M Fe^{2+} solution ($Fe(NH_4)_2(SO_4)_2\times4H_2O$) with 100 mL of a 0.6M S^{2-} solution Na_2S (60 – 62%). Two solutions are mixed in the glove box and leave them stirring for 2 days. And then the solution is vacuum-filtered them and rinsed the solids while in the filter with milliQ water inside the glove box. Finally, the pellet was dried at the glove box atmosphere.

g. Transport and Preparation of the samples to ESRF

The samples were dried inside the glove box at room temperature and the powder was deposited on porous membranes and then sealed in Kapton® tape both sides inside the glove box. The samples were mounted on a multi-slot sample holder inside a glove box in an external laboratory in ISTerre, Grenoble, and the sample holder brought at the Elettra/ESRF inside an anaerobic jar. The membranes were exposited to air only for the time required to fix the sample holder in the vacuum chamber and start the vacuum pump, which took less than half minute, and, however, the membranes remain sealed with Kapton® all time.

S.3 Full bacterial phylogenetic plots results

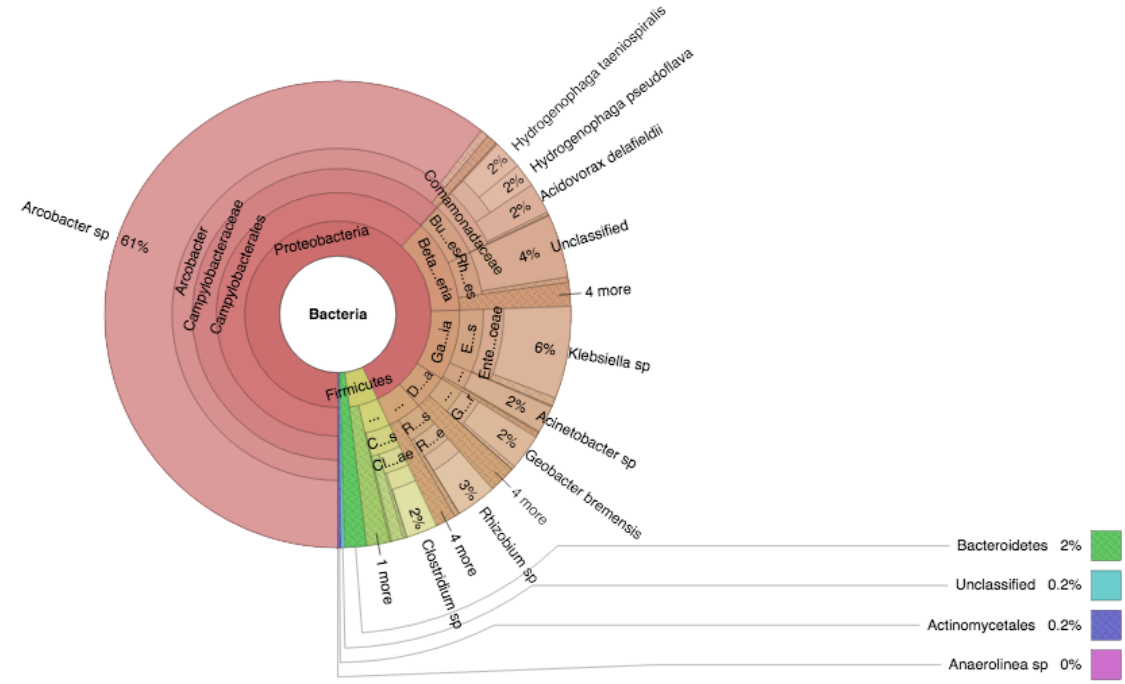

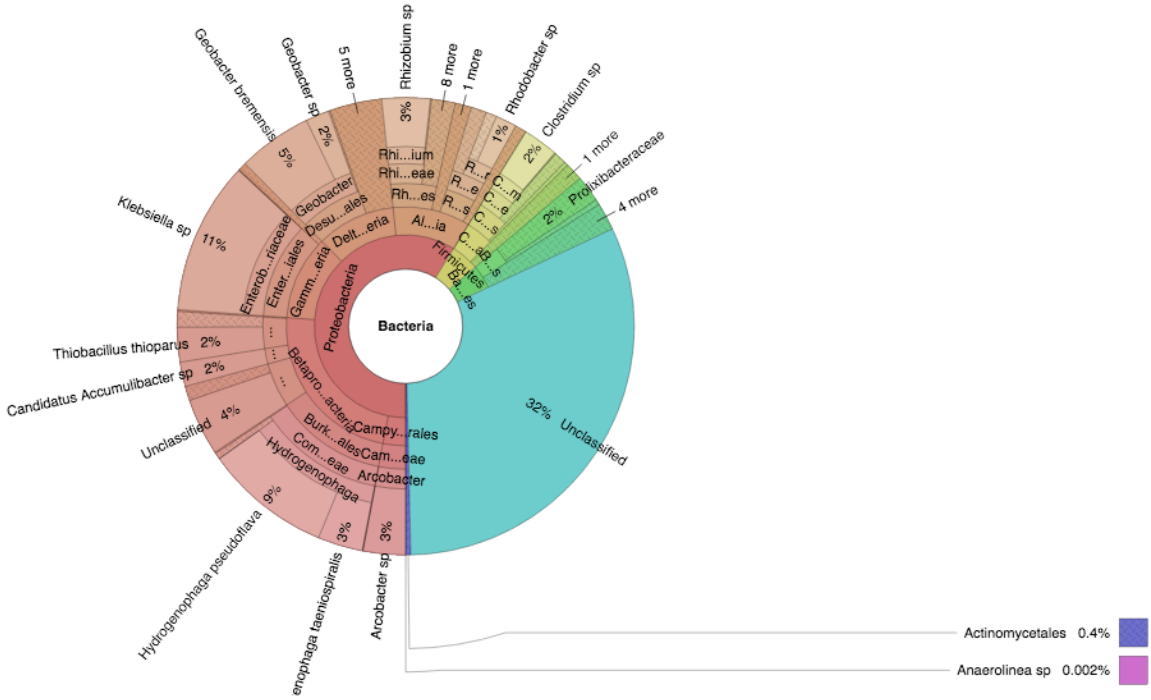

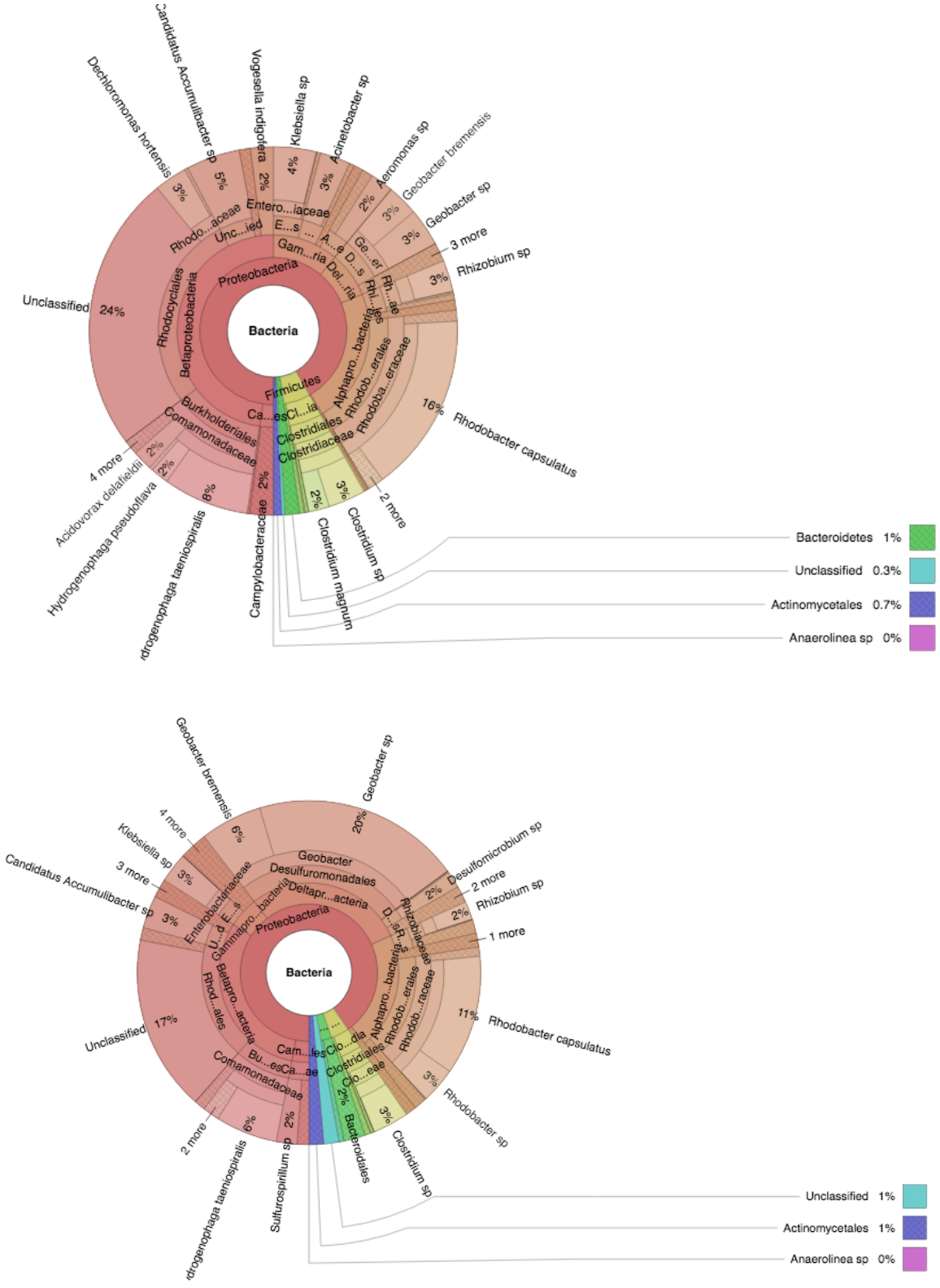

Figure S3.2. Complete representation of bacterial phylogenetic trees, using Krona plots, of sample R1 19, R1 22, R2 19, and R2 22. The considered phylogenetic levels from the center to the outside are: Kingdom, Phylum, Class, Order, Family, and Genus.

Chapter 4: Immobilization and mobilization of Arsenic induced by mineralogy changes during redox oscillations

Van PHAN T.H, Fabrizio BARDELLI, Alejandro FERNANDEZ-MARTINEZ, Delphine TISSERAND, Rizlan BERNIER-LATMANI, Laurent CHARLET

Abstract

The cumulative effects of periodic redox oscillations on the mobility of As, Fe and S to groundwater in pyrite rich sediments from the Mekong Delta River were investigated. Experiments were designed to simulate redox oscillations in the substrate in the 14 m and 7 m depth sediments occurring due to seasonal changes in groundwater levels. Investigations consisted of powdered pyrite rich suspensions were used in two reactors containing these two sediments added with arsenite (As^{3+}) and sulfate (SO_4^{2-}). These suspensions were subjected to three full-redox cycles entailing phases of nitrogen/CO_2, compressed air sparging and cellobiose addition. The results show that the immobilization/mobilization of arsenic is strongly dependent on the effect of redox potential and it is ultimately controlled by the mineralogy. Based on a series of measurements of major, minor and trace element concentrations, As, Fe and S speciation and S-O-isotope ratios, we propose a primary source for sulfate release from pyrite oxidation and gypsum dissolution. At high pyrite content, pyrite oxidation lead to low pH of the aqueous solutions preventing microbial sulfate reduction during the anoxic conditions. Arsenic (As) was mobilized under anoxic conditions and was reversibly sequestered via the absorption process, whereas sulfur (S) was released regardless of anoxic or oxic conditions. At low pyrite content and in the presence of gypsum, the immobilization of dissolved arsenic (As) was observed across cycles.

Keywords: redox oscillation, pyrite oxidation, gypsum dissolution, arsenic mobilization, isotope sulfur and oxygen

4.1 Introduction

Many countries lowered their limit for As concentration in drinking water following the WHO guideline value of 10 µg/L (Smedley & Kinniburgh, 2002). In Vietnam, a large number of wells are contaminated by high As concentrations from the Red Delta and Mekong Delta River (Berg et al., 2001; Stanger et al., 2005; Nguyen et al., 2006; Agusa et al., 2007; Hoang et al., 2010; Erban et al, 2013). In the Red Delta, groundwater As concentration varies in a range from 1 to 3000 µg/L (Berg et al., 2001; Winkel et al., 2010) whereas in the Mekong Delta the range is 1 – 1610 µg/L (Erban et al., 2013; Nguyen & Itoi, 2009; Stanger et al., 2005). Naturally occurring arsenic originates from the Upper Mekong Basin and it is mobilized by chemical and microbial-induced reductive dissolution of iron oxides from the Himalayan As-bearing alluvial sediments (Fendorf et al., 2010; Winkel et al., 2010; Merola et al., 2015; Stuckey et al., 2015). Annual flooding in the Mekong Delta or inundation of swamplands lead to reducing conditions in the aquifers of this area (Stanger et al., 2005). During this time, Fe included in sand from the Mekong River and sulfide originating from seawater SO_4 reduction combine with each other to form sulfide minerals, usually pyrite (FeS_2) (Brinkman et al., 1993). Soils that include pyrite are called "potential acid sulfate soils (ASS)" have a major influence on the biogeochemical cycles of Fe, S and As. In these systems, natural acidity-consuming processes are capable of promoting iron and sulfate reduction potentially form iron sulfide minerals (Burton et al., 2008). Whereas a number of previous studies addressing flooding in acid sulfate soils have focused on the changes in soil acidity, iron, sulfur and arsenic geochemistry (Konsten et al., 1994; Burton et al., 2008), only a limited number of studies have documented Fe and S mobilization during redox oscillations, and the corresponding behavior of As has not been addressed (Couture et al., 2015; Parsons et al., 2013).

The origin of sulfate in the environment can be determined by the sulfur isotope signatures of sulfur originated from different sources (Balci et al., 2007; Pili et al., 2013; Tisserand et al., 2014). As pyrite may contain significant amounts of arsenic, sulfur isotopes may thus be used to link As concentration measured in water with a potential pyrite source. Fractionation of ^{34}S and ^{32}S between sulfide and sulfate, and of ^{18}O and ^{16}O between sulfate and water have been the focus of much attention in studies on acid mine drainage. Pyrite can be oxidized by molecular oxygen from dissolved atmospheric O_2 and H_2O (Eq. 4.1) or ferric iron (Eq. 4.2) - (Eq. 4.3) (Lipfert et al., 2007).

$$FeS_2 + 3.5O_2 + H_2O \rightarrow Fe^{2+} + 2SO_4^{2-} + 2H^+ \quad \text{(Eq. 4.1)}$$

$$Fe^{2+} + 0.25O_2 + H^+ \rightarrow Fe^{3+} + 0.5H_2O \quad \text{(Eq. 4.2)}$$

$$FeS_2 + 14Fe^{3+} + 8H_2O \rightarrow 15Fe^{2+} + 2SO_4^{2-} + 16H^+ \quad \text{(Eq. 4.3)}$$

Studies on pyrite-rich sediments have focused on changes in soil acidity and iron sulfur geochemistry (Burton et al., 2008; Lipfert et al., 2007). These studies suggest that the profound changes observed in the abundance of iron-sulfur phases may influence As mobility. The present study is part of a comprehensive research project aimed at investigating the immobilization and mobilization of As concentrations in shallow aquifers located in the An Phu district, near the Mekong Delta River (Vietnam) (Fig. 4.1a). This study contains the results of a set of lab-scale experiments on As release induced by redox oscillations. The redox changes are stimulated by a carbon pulse (cellobiose input) together with 7 days of anoxia, and are subsequently followed by 7 days of oxic periods. The experiments were performed on two sediment matrices, namely Matrix A and B, using a system of bioreactors. Matrix A originates from a sediment layer at 14 m depth sediments in the redox transition zone and is characterized by poor NOM and high pyrite content. Matrix B, which was collected at 7 m depth in paleo-mangrove layers, is characterized by moderate NOM and low pyrite content (Fig. 4.1b-c). This particular approach was to force systematic redox oscillations while applying a comprehensive geochemical behavior of Fe, S, organic matter and As. Additionally, isotopes of S and O have been applied to study the redox sensitive sulfur and arsenic cycling.

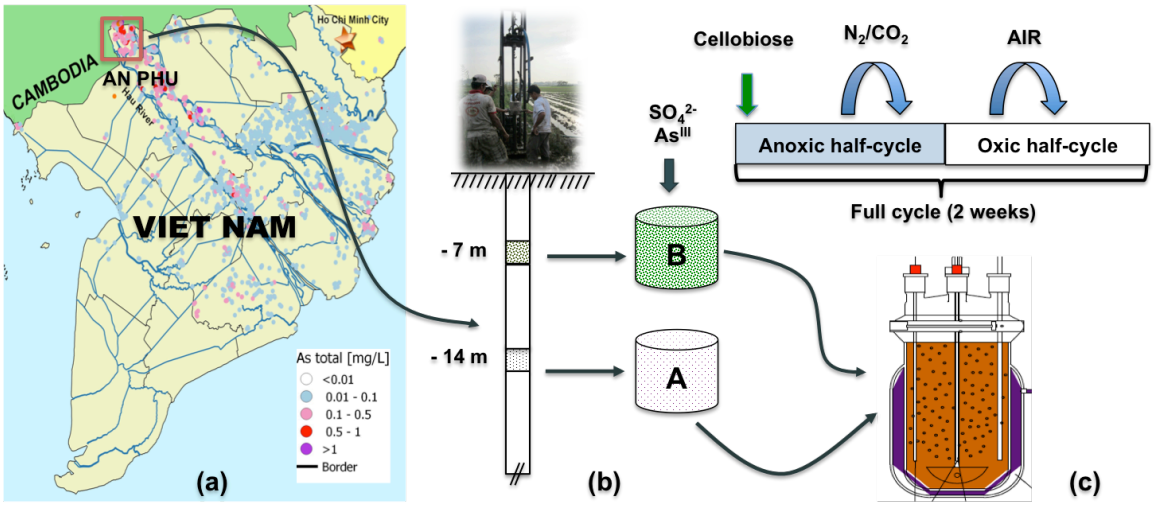

Figure 4.1. (a) Studied site, (b) scheme showing the depth of sampled sediments: 14 m of matrix A and 7 m of matrix B (c) Scheme of the bioreactors showing duration and influx gas in anoxic half-cycle and oxic half-cycle

4.2 Method and materials

4.2.1 Sampling site and sediment characteristics

The sediments in the present study were sampled in January 2014 from the An Phu district of the An Giang province, near the Mekong Delta River (Fig. 4.1a). The core sediments were sampled at 7 m and 14 m deep sediments under anoxic conditions by using a high-flow N_2 stream and then transported back to France in sealed Mylar® bags. Anoxic conditions were necessary to preserve the acid surface layer. Elemental composition of the sediment samples was determined by total acidic digestion followed by inductively coupled plasma optical emission spectroscopy (ICP-OES) analysis. The bulk mineralogy, analyzed by X-Ray Diffraction (XRD) revealed that the major minerals are quartz, muscovite, mica, chlorite, kaolinite, and albite. Data on the chemical and mineralogical composition of the sediments are presented in Table 4.1 (Matrix A: 14 m deep layer; Matrix B: 7 m deep layer). Moreover, Fe quantitative speciation of the two initial matrices evaluated using Fe K-edge XAS data by Wang et al. submitted suggested that Matrix A includes moderate NOM (1.2 – 1.9% w/w), high pyrite content (3.7% w/w) (Table 4.1) and Matrix B represents oxic sediments undergoing a redox transition with traces of pyrite (0.8% w/w).

Table 4.1. Mineralogical composition and major elements of Matrix A (14 deep layer) and B (7 deep layer) sediments

Mineral - Formula[a]	Matrix A	Matrix B
	Weight Fraction (%)	
Quartz - SiO_2	23.2	27.2
Muscovite - $K_{0.86}Al_{1.94}(Al_{0.965}Si_2O_{10})(OH)_{1.744}.F_{0.256}$	38.3	33.0
Mica – $KAl_{2.2}(SiAl)_{0.975}O_{10}(OH)_{1.72}O_{0.28}$	2.6	17.5
Chlorite – $(Mg_5Al)(AlSi_3)O_{10}(OH)_8$	4.7	6.3
Kaolinite - $Al_2(Si_2O_5)(OH)_4$	2.9	15.8
Albite – $NaAlSi_3O_8$	4.3	9.6
Gypsum – $CaSO_4.2H_2O$	nd	2.7
Microcline – $KAlSi_3O_8$	4.7	2.6
Pyrite - FeS_2	3.7	≈ 1

Major element chemistry[b]	g/kg dry sediment	
Si	99.5	77.1
Al	40.0	29.0
Fe	19.7	14.1
K	8.2	6.1
Mg	3.8	2.8
Na	2.5	2.4
Ti	1.6	1.3
Ca	0.7	1.3
S	9.7	12.1
Mn	0.2	0.1

[a] As determined by XRD

[b] As determined by total digestion ($HF+HNO_3+H_2O_2+H_3BO_3$) and ICP-OES

4.2.2 Experimental redox oscillation scenarios

Contaminants were prepared using a solution of high purity analytical standards of $NaAsO_2$ (≥ 98%, Sigma-Aldrich) and Na_2SO_4 to obtain a final concentration 50 µmol L^{-1} of As(III) and 1 mmol L^{-1} of SO_4^{2-}. Experiments were performed with two reactors containing 1L of the pre-equilibrated sediment suspension containing either Matrix A (14 m deep sediment) or Matrix B (7 m deep sediment). The stock solutions of As(III) and SO_4^{2-} were mixed and injected to the slurry. Cellobiose ($C_{12}H_{22}O_{11}$ – Sigma-Aldrich) additions were done at the start of each anoxic phase at same concentration of dissolved organic carbon (DOC) in the aquifer during the seasonal flooding (100 mgC L^{-1} or 8.3 mmol L^{-1}).

Batch experiments were performed using a bioreactor system described by Parsons et al. (2013) and Couture et al. (2015). Each reactor was filled with 1 L of the As(III) and SO_4^{2-} added sediment suspension (< 1 mm fraction), 100 g L^{-1} (dry weight equivalent). Electrodes and mechanical agitators were installed through the reactor cap and a water jacket was used to maintain a constant temperature of 25°C.

The suspension was sampled on days 1, 2, 3, 5, and 7 of each half-cycle. 20 ml of suspension was sampled on the first day and 16 ml of suspension was sampled in the other days through a connection on the top of the reactor by pulling with the syringe connected to a sampling tube. The syringe and the tube were purged with either air or nitrogen (depending on oxic or anoxic half cycle). Under anoxic sampling, the suspension was

transferred to a glove box (Jacomex, $O_2 \leq 10$ ppm) in order to avoid O_2 exposure from the atmosphere. On day 1 of every cycle, 5 ml of slurry from the 20 ml samples were used for microbial analysis, and the rest of the suspension was centrifuged at 8500 rpm for 20 minutes to separate the solid from the aqueous phase. The supernatant was then passed through a 0.22µm filter to ensure that no particles were present during supernatant removal. The supernatant and the solid pellet were frozen immediately in liquid nitrogen and stored at -80°C for microbial analysis and XRD or XAS, respectively.

4.2.3 Aqueous chemistry analysis

Aqueous samples for cations and DOC analysis were acidified with HNO_3 and HCl, respectively. Anions were stored at 4°C until analysis. All chemicals were analytical grades from Fluka, Sigma-Aldrich or Merck. Standards and reagents were prepared with 18MΩ cm^{-1} water (Millipore). Syringe sampled sediment suspensions were centrifuged and the supernatant filtered to 0.22 µm prior to all aqueous analysis. Analysis of total cations Fe, Mn, S and As concentrations were performed with ICP-OES (Varian 720-ES) after dilution and acidification by HNO_3. DOC concentration was determined using a Shimadzu VCSN analyzer with a detection limit of 0.3 mg/L and a precision better than 2.5%. All glassware was heated at 400°C for 3 hours before use to avoid DOC contamination. Major anions were analyzed by ion chromatography using a Metrohm 761 Compact ion chromatography with a detection limit of 0.1 mg/L and a precision better than 5%. Fe^{2+}, Fe^{3+} and $\Sigma S_{(aq)}^{-2}$ was determined photometrically on the filtered sample using the ferrozine method modified by (Lovley & Phillips, 1986; Viollier et al., 2000; Stookey, 1970) and Cline method (Cline, 1969), respectively, and then quantified by UV-Vis spectroscopy (Lambda 35, Perkin Elmer). E_h and pH were recorded every 2 minutes within the reactors using Xerolyt Solid polymer open junction electrodes.

For analyses on aqueous As species, a 1 mL aliquot of filtered aqueous sample was added to either a mixture of acetic acid (1%) or EDTA (1%) (Leblanc et al., 2004). Determination of inorganic (As(III), As(V)) and methylated arsenic species (MMA and DMA) was carried out by coupling liquid chromatography (LC) (Thermo Scientific, SpectraSystem P4000) with ICP-MS with internal standard Ge (Thermo Scientific, X7 Series II) (Bohari et al., 2001). The LC system consisted of Varian ProStar gradient solvent delivery system equipped with a 100 µL injection loop (Interchim), a pre-column PRP-X100 and a 10µm x 25 cm x 4.1 mm (Hamilton, PRP-X100) anion-exchange column eluted with 30mM $(NH_4)_2HPO_4/NH_4H_2PO_4$ (Merk) (pH = 8.1). The detection limit was 0.09 µg/L for As(III),

0.06 µg/L for DMA, 0.04 µg/L MMA and 0.41 µg/L for As(V), with a precision better than 5%.

4.2.4 Adenosine tri-phosphate (ATP) and Microbial Community Analysis

Adenosine tri-phosphate (ATP), often described as the "energy currency" of all living cells (Karl, 1980), is a parameter that can be used as an independent and complementary method for viability assessment. ATP was measured using the Bacter-Glo™ Microbial Cell Viability Assay (G8233; Promega Corporation, Dübendorf) and a Lumar LB 9507 luminometer (Berthold Technologies, Bad Wildbad, Germany). The BacTiter-Glo™ reagent was prepared according to the manufacturers. The prepared reagent was stored in the dark at -20°C until ATP analysis, but never exceeding 2 weeks of storage. The protocol of ATP analysis was optimized following the method of Hammes et al. (2010). A luminescence-based ATP kit/protocol can detect ATP concentration as low as 0.0001 nM with a standard deviation of < 5%. After shaking, 100 µl of the slurry samples were added to 100 µl of ATP reagent, incubated 5 minutes at room temperature and RLU (relative light units) was recorded using a luminometer. ATP concentrations in mol were obtained by using a calibration curve of ATP standard (BioTherma Luminescent Assays, 45-051 ATP Standard 10 µM 5 mL, Sweden). Measurement of ATP was done in duplicate.

Additionally, pyrosequencing was performed on suspension samples collected at the end of anoxic and oxic half-cycles in both matrices in order to characterize the microbial community and identify organisms that were metabolically active. Total genomic DNA (gDNA) was extracted from 0.25 g of suspension using the PowerSoil® DNA Isolation kit (MO BIO Laboratories, Carlsbad, USA) according to the manufacturer's instructions. A Nanodrop 1000 Spectrophotometer (Thermo Fisher Scientific, USA) was used for the DNA quantification using the wavelength ratio of A260/A280. Following DNA extraction, amplification of the DNA coding for 16S rRNA was performed by polymerase chain reaction using the 0.2 µmol L^{-1} of bacteria/archaeal primers 515f (forward)/ 806r (reverse) (Caporaso et al., 2012). PCRs were performed with the Lightcycler® 480 (Roche) in 12.5-µL total volume with the following thermal cycling protocol: 50°C for 2 minutes, 95°C for 10 minutes, 35 cycles of 95°C for 15 seconds/cycle, and followed by a final incubation step at 60°C for 1 minute. PCR products were visualized on an agarose gel, and the 16S band excised and then purified using the Wizard® SV Gel and PCR Clean-Up System (Promega, USA). CT (threshold cycle), the intersection between an amplification curve and a threshold line, was used to measure concentration of targets in the qPCR reaction

and to calculate copy counts. The amplicons were sent to a facility (Research and Testing Laboratory (Texas, USA) for pyrosequencing. The data shows the taxonomic information with a minimum confidence of 97%.

4.2.5 S and O isotopic analysis

All aqueous samples were acidified with HCl 3M to pH = 4.2 in order to remove HCO_3^- and CO_3^{2-}. Samples were then heated at 200°C to ensure complete removal of CO_2 and to prevent $BaCO_3$ co-precipitation with Ba^{2+}. Dissolved sulfate was precipitated as $BaSO_4$ by adding a 5% $BaCl_2$ solution prior to oxygen and sulfur isotopes analysis performed with an isotope-ratio mass spectrometer (IRMS) coupled in continuous-flow mode to an EuroVector elemental analyzer (Brenot et al., 2007). Determination of oxygen isotopes in water was performed by IRMS after standard CO_2 equilibration. Isotope analyses are reported in per mil notation (‰) with reference to the Vienna Canyon Diablo Troilite standard (VCDT) for sulfur ($\delta^{34}S_{SO4}$) and to the Vienna Standard Mean Ocean Water (VSMOW) for oxygen ($\delta^{18}O_{SO4}$ and $\delta^{18}O_{H2O}$). The barium sulfate NBS 127 international reference material has an isotopic composition of 20.3‰.

Sulfur isotope analysis of sediments ($\delta^{34}S_m$) was performed by using IRMS following the method modified by Brenot et al. (2007). 0.5 g of sediment was sufficient to get a complete combustion under O_2 in the reactor and to obtain a SO_2 peak signal (Brenot et al., 2007). Isotopic ratios of both oxygen and sulfur are reported in per mil deviation relative to a "delta zero" standard according to Eq. (5)

$$\delta\ (‰) = (R_{sample} / R_{standard})\ -1] \times 1000$$

where R represents the ratio $^{18}O/^{16}O$ or $^{34}S/^{32}S$ both for aqueous $\delta^{34}S_{SO4}$ and for solid $\delta^{34}S_m$. For convenience, fractionations are also often expressed simply as the isotope difference, are approximately equivalent to ε as defined in $\varepsilon_{A-B} = \delta_A - \delta_B$, with units of ‰ (Canfield, 2001).

4.2.6 Solid phase analysis

Powder XRD analysis was conducted for initial sediments and on days 35 and 42 at the end of the last oxic and anoxic half-cycles for both matrix A and B. Less than 1 mm size sediments were analyzed using Bruker D5000 equipped with a Kevex Si(Li) solid detector and a Cu $K_{\alpha 1+2}$ radiation source. Intensities were recorded at 25°C over an angular range of 2 – 80° 2θ and using a counting time of 3 seconds per step.

Sulfur speciation in the sediment samples was examined by XANES (X-Ray absorption near edge structure) spectroscopy at the S K-edge (2472 eV) at the XAFS beamline of the Elettra synchrotron (Trieste, Italy). The X-ray energy resolution was achieved by a Si(111) monochromator calibrated relative to the white line of a $Na_2S_2O_{3(s)}$ standard (Sigma-Aldrich) at 2,471.64 eV. Spectra were collected in fluorescence mode using a single element solid-state Si detector. Arsenic speciation in the sediment samples was examined by XANES spectroscopy at As K-edge (11867 eV) at the bending magnet beamline BM08 of the European Synchrotron Radiation Facility (ESRF, Grenoble, France). Samples were brought to the synchrotron facilities in an anaerobic jar and mounted on the sample holder inside a glove box and transferred to the experimental chamber. All samples were measured in a high vacuum at low temperature (77K) to prevent beam-induced redox reactions. At the S edge, a commercial elemental sulfur reference was measured in fluorescence mode before each scan. At the As K-edge, a homemade As(0) standard (zero-valent arsenic nanoparticles, Pal et al., 2012) was measured in transmission mode simultaneously with sample spectra for accurate energy calibration.

XANES spectra were energy calibrated, normalized and background subtracted using standard procedures (Ravel & Newville, 2005). The relative contributions of the different S and As reference compounds to the sample spectra were determined by linear combination fitting (LCF) using the ATHENA software package (Ravel & Newville, 2005). The LCF procedure first aimed at reproducing quantitatively all the features of the spectra, using the smallest number of components, and removing those contributing to less than 5% of the sum, i.e. by an amount lower than the error associated with this method (~10%) (Bardelli, et al., 2011; Chakraborty et al., 2010; Isaure et al., 2002). Visually similar fits were further evaluated by selecting those with the lowest R-factor values, and permutations were tested by selecting the combinations that lowered the reduced Chi-square (χ^2_{red}) values by at least 20%, which corresponded to a significant improvement. The suite of reference sulfur materials included was as follows: FeS_2 (pyrite), S_8 (elemental sulfur) and SO_4^{2-} (sulfate). The set of As references included $NaAsO_2$ and $NaHAsO_4$ (Sigma-Aldrich), As_2O_3, As_2O_5, FeAsS (arsenopyrite) and $FeAsO_4$ (scorodite) and the sorption complexes of As(III) and As(V) sorbed onto iron oxyhydroxides (Farquhar et al., 2002), As(III) and As(V) sorbed on jarosite (Kendall et al., 2013) and As(V) sorbed on schwertmanite (Fernandez-Martinez et al., 2010).

4.2.7 Geochemical modeling

The geochemical code, PHREEQC and PhreePlot including the thermodynamic database WATEQ4F.DAT was updated with a schwermannite K_{sp} values of $10^{18 \pm 2.5}$ as presented by Bigham et al. (1996) to calculate the distribution of Fe species (Appelo & Postma, 2005; Kinniburgh & Cooper, 2011).

4.3 Results

4.3.1 Aqueous phase behavior during redox oscillation

The results of the aqueous phase analyses performed during the redox cycling experiments are presented in Fig. 4.2. The experiments lasted for 42 days and included six half-cycles. E_h (SHE) and pH were continuously monitored and DOC, Fe(tot), Fe^{2+}, S(tot), SO_4^{2-}, and As(tot) were measured by sampling the suspension at regular intervals.

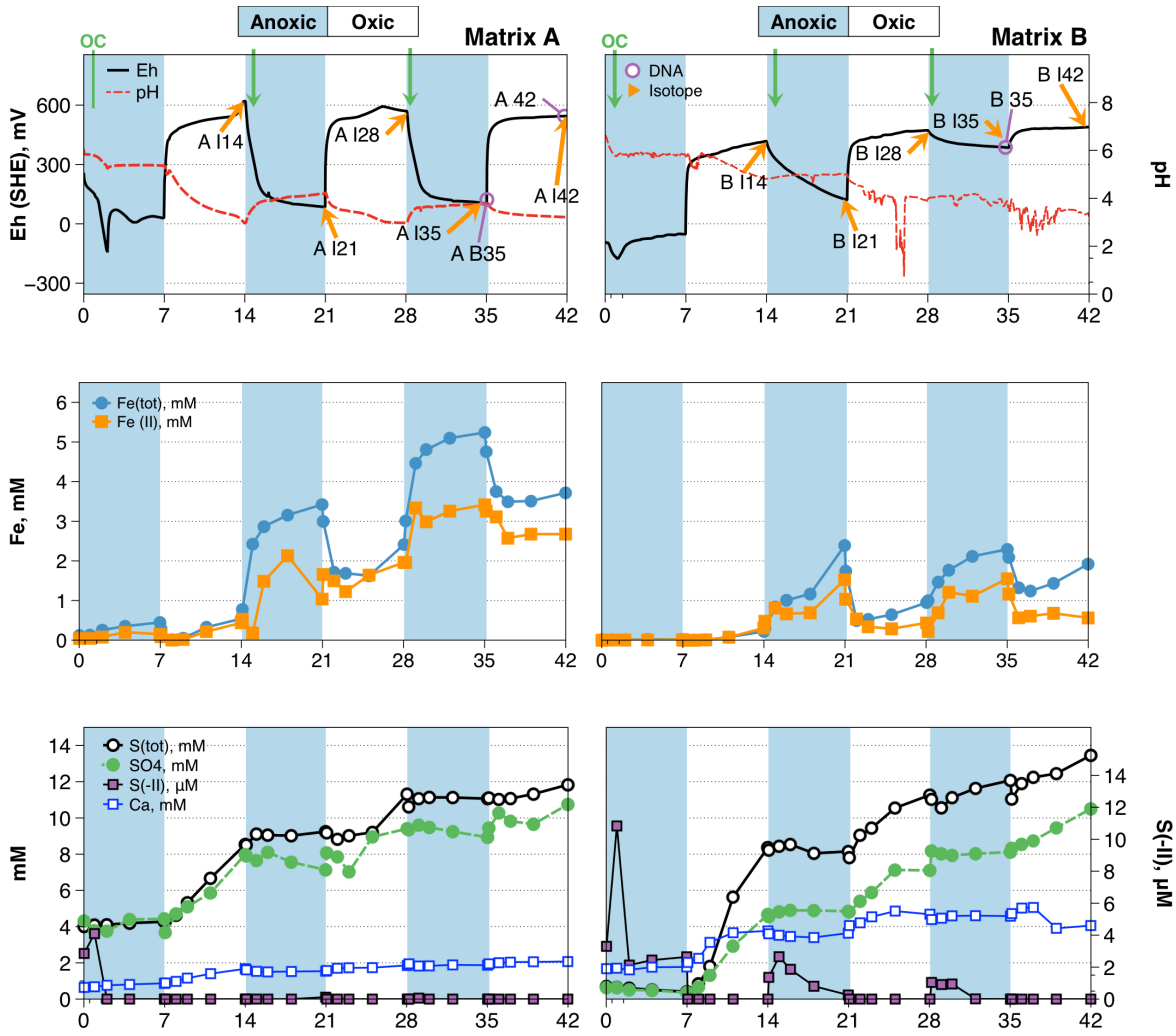

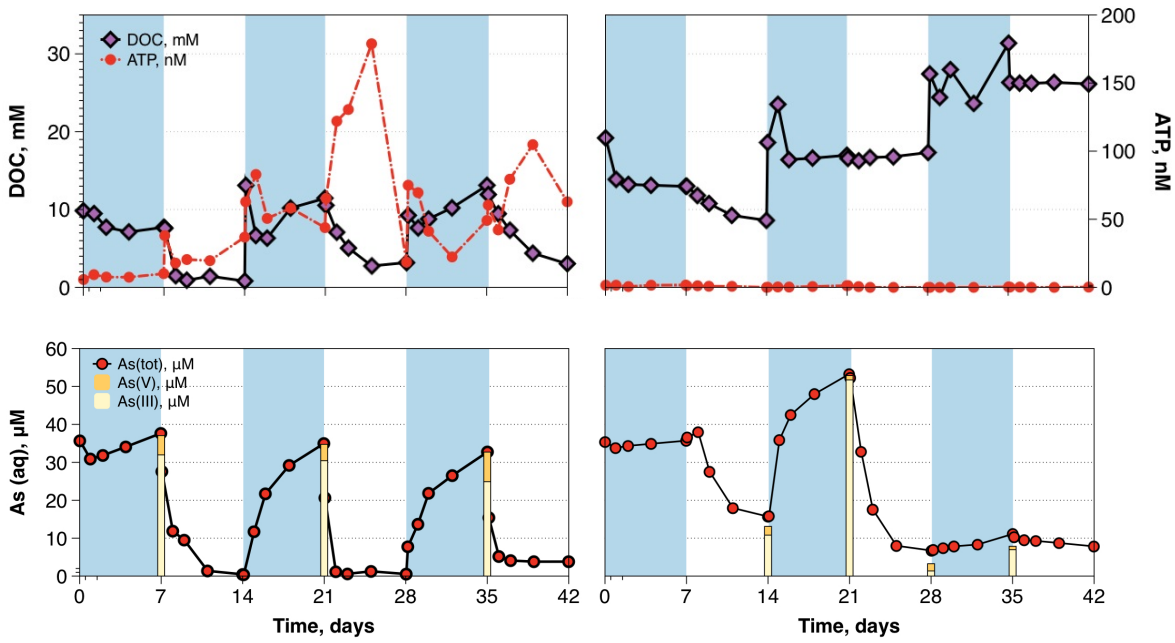

Figure 4.2. Aqueous chemistry measured E_h (SHE), pH, DOC, Fe(tot), Fe^{2+}, S(tot), SO_4^{2-}, and As(tot) data with time in Matrix A and Matrix B. Blue and white shaded areas indicate periods of anoxic and oxic half-cycles, respectively. The green arrows show the cellobiose additions at the beginning of each anoxic period. Sampling points for microbial communities and isptopic analysis are shown on E_h-pH diagrams (isotopic analysis = orange arrow, 16S rRNA = purple open circles).

E_h and pH cycling. Oscillation of the redox conditions between -130 mV and +600 mV was observed in both reactors during the experiments (Fig. 4.2). In particular, for Matrix A, E_h was 600 mV during the oxic half-cycles, dropped to -130 mV in the first anoxic half-cycles, and decreased to 100 mV in subsequent anoxic half-cycles. In Matrix B, an increase to 550 mV of E_h was recorded during oxic half-cycles. E_h values dropped in minimum of -200 mV at the first day and gradually changed from -100 mV at the end of the first anoxic half-cycle to +100 mV in the second and to + 400 mV in the last anoxic half-cycle.

The pH value of the initial suspension in Matrix A was approximately 6 and dropped to 5 at the end of the first anoxic half cycle. In subsequent cycles, the pH increased from 3 to 4 during the anoxic half cycles and decreased from 4 to 3 during the oxic half cycles. While, in matrix B, pH decreased from 6.5 to 5.7 after 1 day and remained constant during the first anoxic half-cycle. In the subsequent oxic half-cycle, pH values were fluctuated dramatically, in particular, pH of 5 decreased and suddenly dropped to fewer than 2 in the second and varied between 2.5 and 4 in the last half-cycle. The pH value slightly slightly

increased from 4.7 to 4.9 in the second half-cycle and oscillated between 3.6 and 4.1 in the last anoxic half cycle.

Iron cycling. High Fe(tot) and Fe^{2+} concentration in anoxic conditions are indicative of iron reduction in the sediment. In Matrix A, this represented values ranging from 0.16 – 5.2 mM and 0.04 – 4.7 mM for Fe(tot) and Fe^{2+}, respectively. Cycling of redox conditions led to an increase in the released iron to the solution from one anoxic half cycle to the other. Previous studies reported that the co-precipitating of Fe (oxyhydr)oxides under oxidizing condition leads to a decrease of Fe^{2+} and Fe(tot) during the oxidizing periods (Phan et al., in submitted; Couture et al., 2015; Parsons et al., 2013; Thompson et al., 2006). The present data show Fe(tot) and Fe^{2+} drop after one day in oxic conditions, and then a slight increase until the end of the first oxic half-cycle. The overall increasing trend in both concentrations shows that the ability of reductive dissolution during the anoxic periods is much higher than the co-precipitation during the oxic periods. Similar trends are observed in matrix B, with an overall lower increase of Fe(tot) and Fe^{2+} concentrations than for Matrix A. The two maximum concentrations of 2.5 mM (Fig. 4.2) can be correlated with the pyrite content in both reactors: higher values of dissolved iron are found in Matrix A where pyrite amount in higher.

Sulfur release. In Matrix A, S(tot) and SO_4^{2-} concentrations increase dramatically in the oxic half cycles and remain stable during the anoxic half-cycles. During the reactor experiments sulfate reduction was limited even if the initial SO_4^{2-} concentration in the sediment was high and equal 4 mM including 3 mM released from natural sediment and 1 mM from initial addition. Sulfide concentration was always lower than the detection limit indicating that no sulfate reduction occurred during anoxic half-cycles.

In matrix B, a production of S^{2-} in the first anoxic half cycle and in early subsequent haft cycles was observed (Fig. 4.2). SO_4^{2-} and S(tot) decreased, while S^{2-} was produced in the first anoxic half cycle up to a maximum concentration of 10.8 µM. The slight decrease of sulfate and corresponding release of aqueous sulfide during the last anoxic half-cycles suggest that microbial sulfate reduction may still occur. However, as in experiments conducted in Matrix A, sulfate reduction after the first full cycle was limited, probably due to the duration of reducing cycles and to the acidic conditions. During oxic half-cycles, SO_4^{2-} ions were released due to either solid sulfide oxidation or rather to the gypsum dissolution as gypsum was present in the initial Matrix B sediment (confirmed X-ray

diffraction), and as SO_4^{2-} concentration was partly matched by Ca^{2+} ion concentration increase (Fig. 4.2).

DOC consumption and microbial activity. An amount of 8.33 mM of cellobiose was added every two weeks at the beginning of anoxic half cycles to stimulate bacteria in the bioreactor systems (Fig. 4.2). In matrix A, DOC increased slightly during each anoxic half cycle indicating that rates of microbially mediated solubilization of particulate organic matter (POM) exceeded rates of DOC consumption by heterotrophic metabolism (Parsons et al., 2013). DOC decreased during each oxic half-cycle because of respiration, oxidation of Fe^{2+}, S and As. Addition of organic substrates to acidic systems usually initiates or stimulates sulfate reduction. This effect was observed in a variety of systems with different substrates (for example acetate, lactate, ethanol and various complex organic matter sources (Koschorreck, 2008). However, it has also been reported that in some cases, substrate addition had no effect or even inhibited sulfate reduction (Gyure et al., 1990).

In matrix B, DOC decreased in the first oxic half-cycle because of respiration and of oxidation of Fe^{2+}, S, and As. However, it seems that bacteria were not appreciably active, as indicated by ATP monitoring. ATP concentrations remained at a low levels compared with an acutely oscillation of Matrix A (Fig. 4.2). It is likely that a large diversity of enzymes is produced in matrix A, which do not the case in matrix B (Yaginuma et al., 2014). Sulfate reduction occurred during the first anoxic cycle and the HS^- concentration varied from 1.5 to 10.8 µM. Sulfur compounds in any oxidized form are, under anaerobic conditions, inevitably reduced to sulfides, which depending on the fermentation conditions, can result in production of gaseous hydrogen sulfide (H_2S) (Pokorna & Zabranska, 2015). The pH 6-7 in the first anoxic half cycle reduces the proportion of non-dissociated species from 9 to 50% and hence the proportion of H_2S that may escape to a gas phase. Sulfides in the undissociated state are often toxic to microorganisms because it reacts with metal ions and functional groups of electron carrier systems (Koschorreck, 2008; Pokorna & Zabranska, 2015). Inhibition of all bacteria by H_2S may explain the lack of DOC consumption and low ATP values in matrix B.

Arsenic mobility. In matrix A, As is released from the sediment during anoxic half cycles and is re-immobilized during oxidizing half cycle. When oxic conditions overcome, As is predominantly present as As(V) and is strongly associated with poorly crystalline Fe (oxyhydr)oxides and As-rich ferric oxides (Couture et al., 2015; Parsons et al., 2013). Under the present redox conditions, bacterial reduction of ferric (oxyhydr)oxides release

As (Lipfert et al., 2007; Molinari et al., 2013; Parsons et al., 2013). The sequestration of dissolved As across cycles noted in previous redox-oscillating experiments was not observed (Phan et al., in submitted). Instead, As was refilled every anoxic half-cycle. This behavior is likely controlled by pH conditions, dissolutions of Fe oxides, and dissolved sulfate depletion, suggesting microbial sulfate reduction. In previous experiments, SO_4^{2-} was reduced and the pH remained in the ranges 5.5 to 8 (Phan et al., submitted), while here SO_4^{2-} was continuously released cycle after cycle.

In matrix B, As(tot) concentrations decreased in the first oxic half cycle, increased in the first and second anoxic half cycles, and was sequestered in the last anoxic half cycle. During the oxic cycle, at high values of E_h (400 – 570 mV), As(V) is the major dissolved As species, and it can be strongly retained by soil surfaces (Essington, 2004) (Fig. 4.2). In the third anoxic half cycle, a high E_h value suggests that As may be mainly present as As(V).

4.3.2 Microbial Community

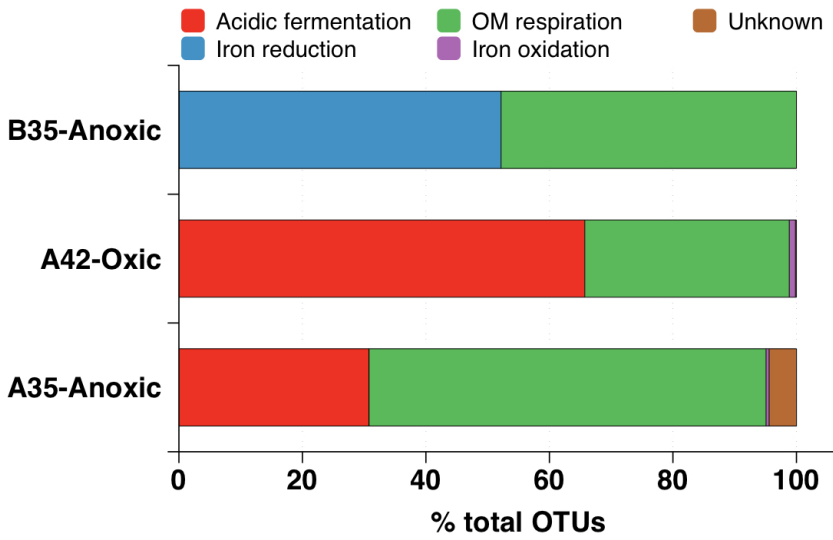

Figure 4.3. Results of microbial analysis of 16S rRNA for selected samples at Matrix A and Matrix B in function of potential metabolism at the various time points: A35 (anoxic half-cycle), A42 (oxic half-cycle) and B35 (anoxic half-cycle). Red: acidic fermenters (*Streptococcus* sp.); Green: aerobic OM-respiring bacteria (Acidobacteria, *Rhodoplanes* sp.); Blue: iron-reducing bacteria (*Geobacter* sp.); Purple: Iron-oxidising bacteria (*Thiobacillus* sp.)

Four samples were collected in the last anoxic and oxic half-cycle in both A and B matrices, but the 16S rRNA sequences were detected only in three samples (A 35 and A 42 in Matrix A and B35 in Matrix B). The potential metabolism results are shown in Fig. 3.

The array of bacterial phyla identified mainly consists of Antinobacteria and Firmicutes, with contributions from Proteobacteria, including alphaproteobacteria, betaproteobacteria and gammaproteobacteria and deltaproteobacteria classes.

At the oxidizing cycles of Matrix A, fermenting bacteria, facultative acidic OM respiring microorganisms such as *Streptococcus* sp. are observed representing 64% of the total OTUs. They are able to ferment carbohydrates, producing mainly lactic acid without producing biogas and have complex nutritional requirements (Gobbetti & Calasso, 2014). *Streptococcus* sp. also belongs to *Lactobacillus acidophilus*. In the presence of organic matter, they are considered as lactic acid bacteria with optimal pH values of 5.5 - 6.5 (Rault et al., 2009). Additionally, members of Acidobacteria, *Granulicatella* sp. Are able to ferment organic matter to produce lactic acid, are attributed with 12.3 % (Christensen & Facklam, 2001). Regardless of the change to reducing conditions, *Streptococcus* sp. remained a dominant species in Matrix A.

ATP values in Matrix B were very low, but it was still possible to identify bacterial population in the last anoxic half-cycle. Sequences of the 16S rRNA gene, which belongs to iron-reducing bacteria, were also detected. *Geobacter* sp. represented more than 52% of the microbial community during the reducing condition. Finally, members of the Actinobacteria genus, common in fermenting or respiring organic compounds, occupy a large amount of the total population in both matrices. Actinobacteria employ a variety of metabolic mechanisms, although no photosynthetic members are known. In soils, they behave much like fungi, decomposing organic matter (Servin et al., 2008).

4.3.3 Solid phase characterization

a. X-ray diffraction

XRD analysis revealed the presence of pyrite in both Matrix A (A 00) and Matrix B (B 00) initial sediment samples and in all anoxic and oxic cycle samples. Moreover, it confirmed that Matrix B diffractograms displayed gypsum in the initial sediment sample (B 00), but the absence of this mineral at the deposit of Matrix B sediments after redox experiments (B 35 and B 42) (Fig. 4.4). While, gypsum was not found at both original and experimental samples at Matrix A. Moreover, XRD analysis evidence the precipitation of schwermannite at both anoxic (B 35) and oxic (B 42) haft-cycle solid samples, but not in the original Matrix B samples. This suggests that precipitation of schwermannite starts in the second oxic half-cycle and remains in subsequent cycles.

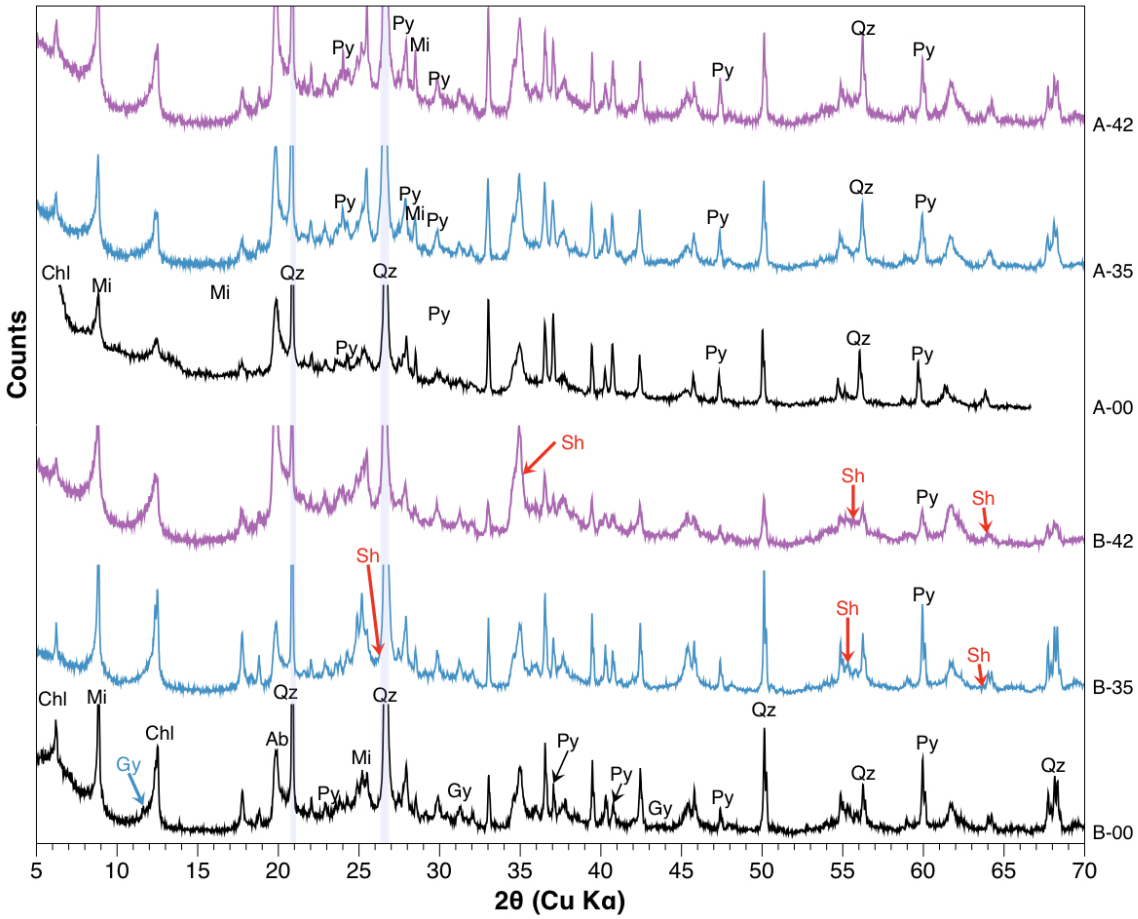

Figure 4.4. X-ray diffraction patterns for samples taken at the end of the last anoxic and oxic half-cycles in Matrix A (A) and Matrix B (B). Chl: Chlorite, Mi: Mica; Ab: Albite, Qz: Quartz, Sch: schwertmanite; Py: Pyrite; Gy: Gypsum

b. Solid sulfur speciation

S K-edge XANES spectra are presented in Fig. 4.5 and the results of linear combination fitting (LCF) summarized in Table 4.2. XAS is broadly consistent with XRD data and demonstrates that pyrite was the dominant sulfide mineral phase at the end of the redox experiments, constituting 71 – 80 % and 53 – 55 % of the total sulfur in Matrix A and Matrix B, respectively. In Matrix A, during the reducing conditions, E_h values were in the range between -100 and 0 mV, and [HS^-] was below the detection limit. A sulfidic solution containing HS^- and SO_4^{2-} has at equilibrium -300 to -200 mV of theoretical E_h values. Generally, E_h value increases with increasing $S^0_{(aq)}$ concentration, until solution reaches equilibrium with S_8, beyond which $S^0_{(aq)}$ no longer accumulates in the aqueous phase (Couture & Cappellen, 2011). The presence of particulate elemental sulfur (S^0) and pyrite grain coatings as byproducts of pyrite oxidation has previously been reported (Bouffard et al., 2006; Sasaki et al., 1995). Another possibility is the formation of a layer rich in

elemental sulfur resulting either from non-stoichiometric oxidation of pyrite with preferential dissolution of iron or from disproportionation of thiosulfate ($S_2O_3^{2-}$), sulfite (SO_3^{2-}) into elemental sulfur and sulfate (Canfield, 2001; Sasaki et al., 1995).

LCFs results show that pyrite is also detected at levels of 53 to 55% of total sulfur in Matrix B (Fig. 4.5, Table 4.2). SO_4^{2-} is present in the range between 11 and 15% of total S in the last oxic and anoxic half-cycles, suggesting that sulfate compounds such as schwermannite could resist oxic/anoxic cycles. Although microbial sulfate reduction was limited after the initial anoxic half-cycle, iron reduction was observed during the subsequent anoxic half-cycles. The formation of other sulfur species may explain the difference between total S and sulfate solid during the reducing conditions. Elemental sulfur (S_8) is also detected in a 22% to 30% range corresponding to oxic and anoxic half-cycles, respectively.

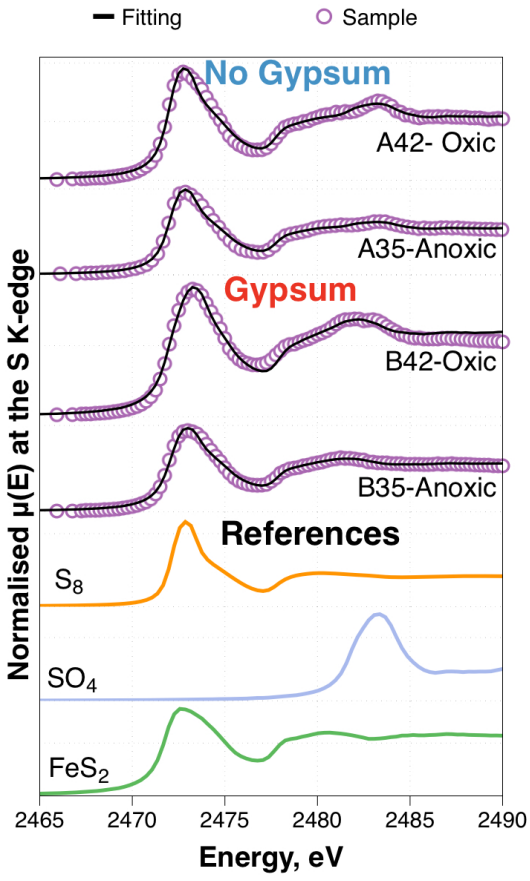

Figure 4.5. Normalized spectra XANES at the S K-edge (lines) and LCF curves (points) in samples of matrix A and B at the end of the last anoxic (day 35) and oxic (day 42) half cycle. Spectra of the reference compounds used for LCF (SO_4, S_8, FeS_2) are also shown. All spectra are vertically shifted for clarity

Table 4.2. Solid-phase sulfur speciation, proportion of S solid phases in sediment samples and obtained by LCF performed on the corresponding XANES spectra are shown. The error on percentages is estimated to be about 10%, according to Bardelli et al. (2011) and Isaure et al. (2002). The reduced chi-square (χ_ν^2) of the LCF is also reported.

Sample	LCF (%)			χ^2
	%FeS_2	%S_8	%SO_4	
A35 (anoxic)	71	30	< 5	0.0016
A42 (oxic)	80	22	< 5	0.0024
B35 (anoxic)	55	39	11	0.0016
B42 (oxic)	53	37	15	0.0019

c. Solid arsenic speciation

To identify the As-bearing phase in the sediment of Matrix A and Matrix B, As oxidation state was investigated by As K-edge X-ray absorption near-edge structure (XANES). XANES spectra exhibit two absorption maxima at about 11,869 and 11,875 eV. The first absorption peak corresponds to a mixture of S-bound As(III) (at 11,869.5 eV) (Wang et al., 2008) and O-bound As(III) (at 11,871.3 eV), while the second one corresponds to O-bound As(V) (Wang et al., 2011) (Fig. 4.6). For the later, three O-bound As(V) species, As(V) sorbed onto goethite/ferrhydryrite, jarosite, and schwertmannite were used in LCF. However, since the XANES spectra of these species are very similar, good matches with the experimental samples were obtained regardless on the As/S-iron(hydr)oxide spectrum used. Therefore, LCF did not allow to distinguish the actual association of As with any three of the above mentioned iron(hydr)oxides. The same applies for the thiol-bound As(III) and As_2S_3 references in Matrix A. For these reasons, these species are shown as grouped species in Table 4.3. On the other hand, the goethite/ferrhydryrite reference was used for As(III), because of the difficulty to obtain a sufficient amount of As(III) adsorbed onto jarosite and schwertmanite

The results of the LCF performed in Matrix A sediment indicated that 61% of the total As species is S-bound As. As_2S_3 and thiol-bound As(III) have similar spectra, and it is therefore difficult to distinguish them by LCF. Nevertheless, Wang et al. (in submitted) reported that the actual As speciation should correspond rather to As(III) bound to thiols

group than to amorphous As_2S_3. The remaining O-bound As species are therefore 33% As(V) and 12% As(III). Thiol-bound As(III) present in the initial sediment disappeared during the first oxic cycle. In oxic cycles, O-bound As(V) adsorbed on iron (hydr)oxides is the main species ranging between 88 – 100%, and decreasing to 60 – 67% of total As during oxic half-cycles. O-bound As(III) adsorbed on iron (hydr)oxides represents 0 – 14% during oxic half cycles and 34 – 35% during anoxic half-cycles (Table 4.3).

In Matrix B, As(V) adsorbed onto iron (oxyhydr)oxides represents the main species with 61% of the total solid As, along with thiol-bound As(III) or As_2S_3 (29%) and As(III) adsorbed onto iron (oxyhydr)oxides (13%) (Table 4.3). The formation of thiol-bound As(III) increased in the first anoxic half-cycle, where microbial sulfate reduction occurred (Fig. 4.6), reaching 66% of total As. The thiol-bound As(III) species decreased in the subsequent half-cycles. Remarkably, after the second oxic half-cycle, O-bound As(V) became the main species accounting for 82 – 86% of total As, regardless to oxidizing or reducing conditions.

Table 4.3. Proportion of As solid phases revealed in the sediment samples by LCF performed on the corresponding XANES spetra. The error on the percentages is estimated to be about 10%, according to Bardelli et al. (2011) and Isaure et al. (2002).

Condition	Sample	LCF (%)			χ^2
		As(V)≡Goe/Fh/Jar/Sch	As(III) ≡Goe/Fh	As(III)-Glu/As_2S_3	
Initial	**A 00**	**33**	**12**	**61**	**0.0013**
Oxic	A 14	88	14	0	0.0014
Anoxic	A 21	60	34	0	0.0010
Oxic	A 28	100	0	0	0.0015
Anoxic	A 35	67	35	0	0.0013
Oxic	A 42	90	10	0	0.0002
Initial	**B 00**	**61**	**13**	**29**	**0.0017**
Anoxic	B 07	0	33	66	0.0003
Oxic	B 14	63	24	13	0.0002
Anoxic	B 21	42	40	17	0.0003
Oxic	B 28	84	10	< 5	0.0008
Anoxic	B 35	82	10	10	0.0007
Oxic	B 42	86	6	< 5	0.0004

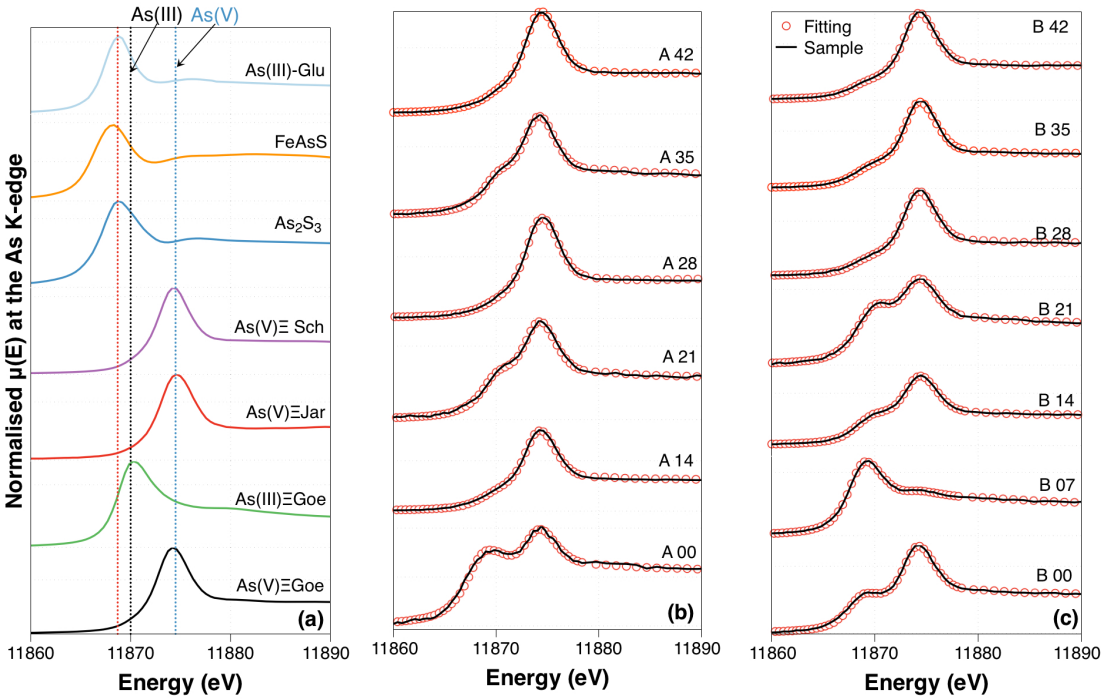

Figure 4.6. (a) The spectra of the reference compounds used for LCF. Normalized As K-edge XANES spectra of sediment samples collected from (b) Matrix A and (c) Matrix B at the end of each anoxic and oxic half-cycles. The spectra of the samples (solid lines) are reported together with the LCF curves superimposed (open circles).

4.3.4 Sulfur and oxygen isotopes

X-ray diffraction patterns of selected initial sediment samples revealed that pyrite is the dominant S-bearing minerals in Matrix A, while gypsum and less pyrite were detected in Matrix B. During the redox oscillation, sulfate concentration increased regardless of the reducing or oxidizing conditions. Isotopic analysis of $\delta^{34}S_m$, $\delta^{34}S_{SO4}$ and $\delta^{18}O_{SO4}$ were used to retrieve the origin of sulfide and sulfate source and, therefore, to unravel the relation with As mobilization in two reactor experiments (Pili et al., 2013; Tisserand et al., 2014).

a. Sulfur isotopes

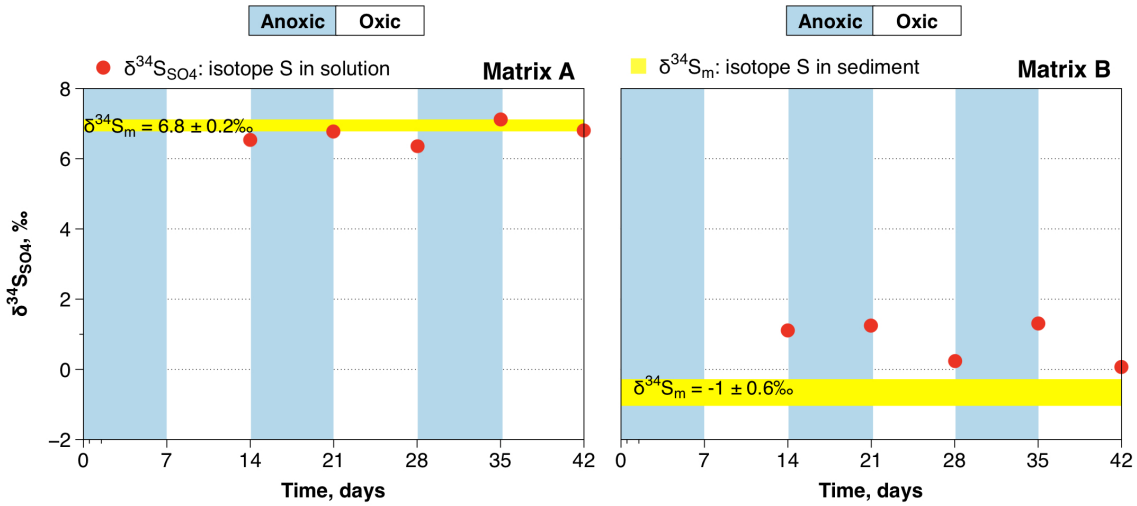

Figure 4.7. Sulfur isotope composition of sulfate in solutions and sediments at Matrix A (left) and Matrix B (right) during the redox cycling experiment. Red dots: $\delta^{34}S$ of sulfate in the solution; Yellow line: $\delta^{34}S$ of sulfur in the sediments

The isotopes data of $\delta^{34}S_m$ (solid phase) and $\delta^{34}S_{SO4}$ (aqueous phase) are clearly different between Matrix A and Matrix B sediments. In Matrix A, the average $\delta^{34}S_m$ value ranged was 6.8 ± 0.2 ‰, while those for Matrix B shown – 1 ± 0.6 ‰ (Fig. 4.7). The average $\delta^{34}S_{SO4}$ values are 6.49 ± 0.17 ‰ and 0.8 ± 0.5‰ in Matrix A and Matrix B, respectively. Unlike correlation demonstrated in Pili et al. (2013), $\delta^{34}S_{SO4}$ values and As concentration tend to be negatively, but not significantly correlated with each other. This may be due to As being added as an external source at the beginning of experiments. The production of SO_4^{2-} from pyrite is known to be associated with a small fractionation of the sulfur isotopes (referred as $\varepsilon^{34}S_{SO4-m} = \delta^{34}S_{SO4} - \delta^{34}S_m$), typically between -1.8 ‰ and +0.8‰ (Heidel & Tichomirowa, 2011; Balci et al., 2012). In our experiments, the apparent $\varepsilon^{34}S_{SO4-m}$ can be calculated from isotope composition of water samples collected during redox experiments where sediment pellets are also samples. We obtain small values as expected from pyrite oxidation literature data with $\varepsilon^{34}S_{SO4-m}$ ranging between – 0.57 ‰ and +0.04 ‰ (Fig. 4.7). Additionally, oxidation experiments with Fe(III) suggest a small fractionation of the sulfur isotopes with typical values of $\varepsilon^{34}S_{SO4-m}$ of - 0.75 ± 0.02‰ in both biotic and abiotic conditions (Balci et al., 2007; Mazumdar et al., 2008). Although the $\delta^{34}S_{SO4}$ values increase slightly during all anoxic cycles, most of $\delta^{34}S_{SO4}$ values agreed with $\delta^{34}S_m = 6.8 \pm 0.2$. Microbial sulfate reduction will preferentially reduce the lighter S isotope (^{32}S), resulting in an increase in $\delta^{34}S_{SO4}$ (Canfield, 2001), but the increase of $\delta^{34}S_{SO4}$ was low in

our case. On contrary, the $\delta^{34}S_{SO4}$ values decrease during oxic half-cycles (Fig. 4.7) probably due to an increase of lighter S isotope. Thurston et al. (2010) and Balci et al. (2007) concluded from their chalcopyrite (CuFeS) and pyrite (FeS_2) oxidation experiments suggeting ^{32}S is enriched in sulfate relative to the sulfide, resulting in a decrease $\delta^{34}S_{SO4}$ and $\varepsilon^{34}S_{SO4-m} < 0$ ‰ in during the abiotic oxidation by ferric ion due to the formation of intermediate sulfur species such as elemental sulfur. In Matrix A, the isotope sulfur data summarize that the origin of SO_4^{2-} could be from pyrite oxidation by both O_2 in abiotic conditions or Fe(III) in biotic and abiotic system.

In Matrix B, the increase in $\delta^{34}S_{SO4}$ values suggests the lighter S isotope (^{32}S) reduce during anoxic-half cycles. Contrarily, $\delta^{34}S_{SO4}$ values decrease during oxic half-cycles due to ^{32}S is enriched in sulfate (Fig. 4.7). Moreover, the fractionation sulfur isotope ($\varepsilon^{34}S_{SO4-m}$) values are larger with 1.03 – 2.27‰ compared to that values in Matrix A, which are not associated with only pyrite oxidation. Large depletions of sulfide in ^{34}S have been observed during other processes such as the disproportionation of sulfur intermediate compounds such as sulfite and elemental sulfur (Canfield, 2001).

b. Oxygen isotopes

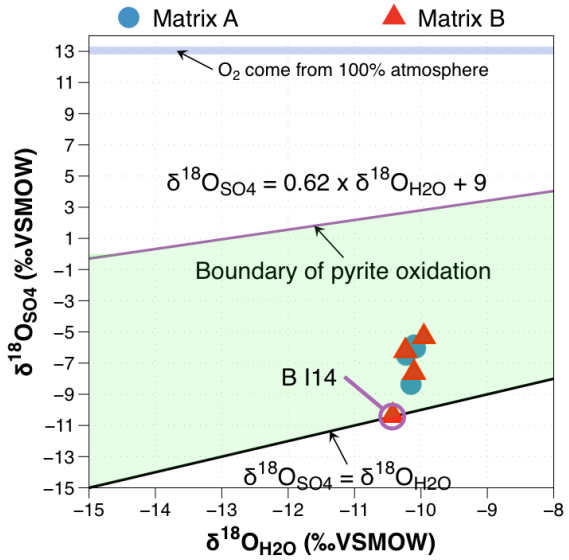

Figure 4.8. Experimental data for $\delta^{18}O_{SO4}$ as a function of $\delta^{18}O_{H2O}$ during oxic half-cycles at Matrix A (Blue circles) and Matrix B (Red triangles). The upper boundary of the green area, $\delta^{18}O_{SO4} = 0.62 \times \delta^{18}O_{H2O} + 9$, has a slope based on the regression of the submersed sulfide experiments (Stempvoort & Krouse, 1994). The lower boundary, where $\delta^{18}O_{SO4} = \delta^{18}O_{H2O}$ is inferred lower limit for all oxygen of SO_4^{2-} derived from water.

Low sulfate concentration in the first anoxic half-cycle did not allow the analysed of $\delta^{18}O_{SO4}$ and $\delta^{18}O_{H2O}$. $\delta^{18}O_{H2O}$ values remained constant at approximately -10.2‰ (agreed with ± 0.18), similar to the average value in groundwater (Pili et al., 2004). The $\delta^{18}O_{SO4}$ values were observed in the range -8.36 to -5.79 ‰ and -10.36 to -5.3 ‰ in Matrix A and Matrix B, respectively. According to reactions (2) and (4), oxygen in sulfate may originate from the oxidizing half-cycle derived molecular oxygen and water. The higher the $\delta^{18}O_{SO4}$ value is the lower the water-derived oxygen proportion will be. A precise quantification of the water-derived oxygen proportion can be obtained, following the equation (Stempvoort & Krouse, 1994):

$$\delta^{18}O_{SO4} = X(\delta^{18}O_{H2O} + \varepsilon_{SO4-H2O}) + (1 - X)(\delta^{18}O_{O2} + \varepsilon_{SO4-O2})$$

Where $\delta^{18}O_{SO4}$, $\delta^{18}O_{H2O}$ and $\delta^{18}O_{O2}$ are the oxygen isotope compositions of sulfate, water, and molecular oxygen ($\delta^{18}O_{O2}$ = 23.5‰, Kroopnick & Craig, 1976), respectively. X and (1-X) are the relative proportions of water-derived and molecular oxygen in sulfate. $\varepsilon_{SO4-H2O}$ is the oxygen isotope enrichment between sulfate and water which normally ranges from 2.3‰ to 4.0‰ for abiotic pyrite oxidation under acidic conditions (Balci et al., 2007; Mazumdar et al., 2008; Taylor et al., 1984). A plot of $\delta^{18}O_{H2O}$ versus $\delta^{18}O_{SO4}$ for redox cycling experiments in Matrix A and Matrix B is shown in Fig. 4.8. Most of the oxygen data are contained within the green area, which indicates that SO_4^{2-} may form during the abiotic and biotic oxidation of pyrite (Stempvoort & Krouse, 1994). However, a sample at the first oxic half-cycle in Matrix B has similar values between $\delta^{18}O_{H2O}$ and $\delta^{18}O_{SO4}$ ($\varepsilon_{SO4-H2O} \approx 0$) suggesting no oxygen is derivered from water or molecular O_2 to enrich SO_4^{2-} probably due to no pyrite oxidation occur.

4.4 Discussion

4.4.1 Pyrite oxidation and sulfate reducing inhibition during the redox oscillation

The analytical results of pore water of Matrix A suggest that sulfate was released to not balance by a consumption of SO_4^{2-} during anoxic half cycles. It is evident that the presence of dissolved oxygen may caused iron oxidation to Fe^{3+}. Pyrite could be oxidized to form Fe^{2+} (Lipfert et al., 2007; Yacob et al., 2013), depending strongly on reactive minerals, oxygen and water. Based on theoretical consideration and previous experiments, regardless of pH conditions, Fe^{3+} rather than O_2, is the primary agent responsible for direct abiotic oxidation of pyrite, and possibly for oxidation of intermediate elemental sulfur (S_8) (Johnson et al., 2012). The difference between total Fe and Fe^{2+} during the oxic half-cycle in Matrix A indicates that Fe^{3+} may exist in the aqueous phase. In the absence of Fe^{3+}, the

oxidation of pyrite is extremely slow in acidic media (Singer & Stumm, 1970, Moses et al., 1987). Moreover, S isotope data indicate sulfur isotope enrichment processes between sulfate in solution and sulfide in sediment due to a small fractionation of S isotope (ε_{SO4-m} < 0.0‰) (Balci et al., 2007; Heidel & Tichomirowa, 2011; Thurston et al., 2010). The O isotope data also suggest that oxygen originated from water or molecular oxygen can contribute for pyrite oxidation. Therefore, sulfate potentially originates from pyrite oxidation by Fe^{3+} and/or O_2 during the biological processes in Matrix A.

As a result, pyrite oxidation may generate a decrease in pH (≈ 3) during the oxic half-cycle and presumably allow an acidophilic pyrite oxidizing community to develop. The drop in pH seems to prevent the development of sulfate reducing bacteria during the anaerobic phases (Koschorreck, 2008). Microbial community analyses suggest the absence of iron and sulfate reducing bacteria along with the presence of acidic respiring OM bacteria (*Streptococcus* sp.) in Matrix A during redox cycling experiments. A very small quatity of *Thiobacillus* sp. (24 OTUs), which was previously reported to oxidize pyrite was identified in Matrix A. Haikarainen et al. (2011) shows that *Streptococcus* sp. are able to oxidize Fe^{2+} to Fe^{3+} to protect microorganisms from oxidative damage. Moreover, others suggest that oxidants such as hydrogen peroxide (H_2O_2) can be produced by several members of the genus *Streptococcus* under aerobic growth conditions (Xu et al., 2014). Presumably, FeS_2 and Fe^{2+} may be oxidized to Fe^{3+} by forming hydroxyl radicals with H_2O_2 according to the Fenton reaction (Haikarainen et al., 2011). Thus, some acidophiles are able to oxidize pyrite to generate sulfate and other sulfurs such as elemental sulfur, which detected in solid phases by S K-edge XANES (Fig. 4.9).

4.4.2 Iron reduction and sulfate mineral dissolution

The general soil type of the area sampled were previously shown as contain trace minerals like gypsum (Post & Sloane, 1971). The analytical data of Matrix B suggest the occurrence of some sulfide production through sulfate reduction in the initial anoxic half-cycle, which disappeared and unrecovered after moving to oxic half cycle. Iron-reducing bacteria in the sediment were identified. Isotopic analyses of sulfur and oxygen indicate that sulfate release may not only be related to pyrite but also to the dissolution of other sulfate minerals. The presence of gypsum in the initial sediment and the increasing of Ca^{2+} and SO_4^{2-} concentration in Matrix B maybe related to gypsum dissolution (Postma, 1983).

$CaSO_4.2H_2O \rightarrow Ca^{2+} + SO_4^{2-} + 2H_2O$, $\log K = -4.60$

The saturation state of pore water for gypsum for Matrix B is shown in Fig. 4.9 at equilibrium constant of log$K$ = - 4.60 at 25°C (Wigley, 1973). The added SO_4^{2-} and SO_4^{2-} originated gypsum concentration are higher than total aqueous SO_4^{2-} concentration during fisrt anoxic half-cycle probably due to microbial sulfate reduction. Moreover, during the first oxic half-cycle, the fractionation values of oxygen between sulfate and water suggested no oxygen derives from water or molecular oxygen into sulfate leading the absence of pyrite oxidation here. Coincidentally, the saturation state (IAP/K) of gypsum is lower than 1, refects subsaturation or dissolution process. The saturation state of gypsum increases and reaches equilibrium after two full cycles (Fig. 4.9). S isotope data did not allow distinguishing all sources of sulfate in Matrix B due to the mixture of many factors including pyrite oxidation, gypsum dissolution, added sulfate, disproportination of sulfur intermediate compounds and schwertmannite precipitation. However, chemical data evidenced gypsum dissolution and then mixed with pyrite oxidation at Matrix B.

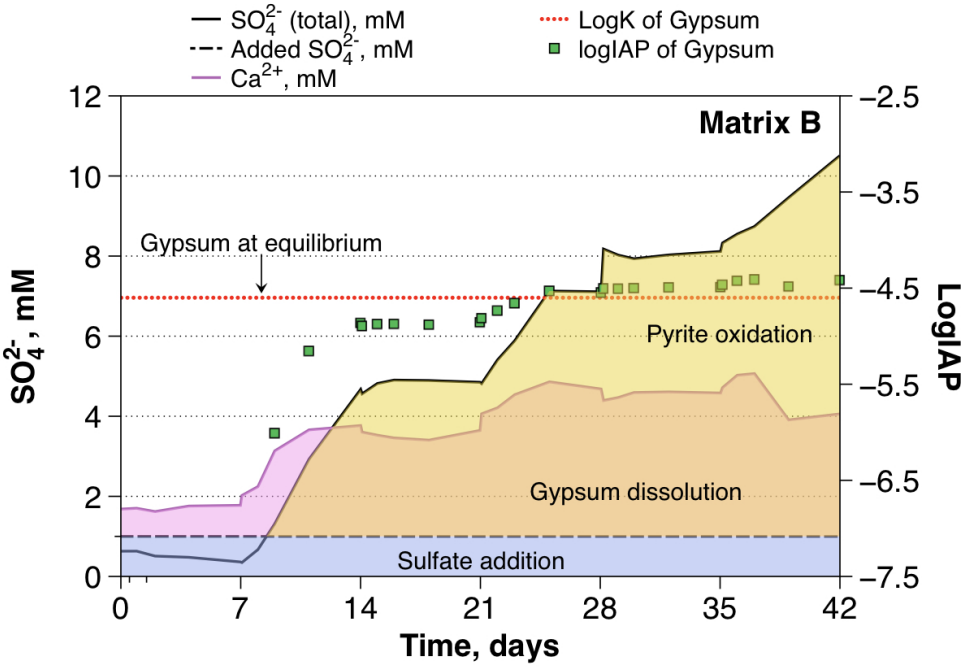

Figure 4.9. Origins of aqueous sulfate with the saturation state of pore waters at Matrix B sediments for gypsum

4.4.3 Geochemical control on As mobility

When oxic conditions prevail, As is predominantly present as As(V) and is strongly associated with poorly crystalline iron (oxyhydr)oxides and As-rich ferric oxides (Couture et al., 2015; Parsons et al., 2013). In matrix A, sorption processes remove more than 90% of total As in each oxic half-cycle. Upon the transition to anoxic conditions following the

addition of DOC, iron reduction and a concomitant drop in E_h are observed, and microbial reduction of As-bearing iron (oxyhydr)oxides leads to an increased mobilization of As in the aqueous phase (Stuckey et al., 2015). LCF results of As K-edge also suggest that As(V) was the dominant species during oxidizing conditions with an increase in the ratio of As(V) to As(III). On the contrary, the proportion of As(III) sorbed on iron (oxyhydr)oxides rise during the reducing conditions. Our previous study has shown evidence of the association of As sequestration with sulfate reduction during the redox oscillation (Phan et al., submitted). In the present study, in absence of microbial sulfate reduction, the anaerobic phases of subsequent redox oscillation never lead to the effective immobilization of As.

Additionally, when exposed to air during oxic half-cycles, Fe^{2+} is readily oxidized to Fe^{3+}, and secondary Fe precipitates may form, increasing the acidity (Jönsson et al., 2005). The composition of these secondary precipitates is determined by the composition of the aqueous phase, with pH and SO_4^{2-} as main variables. At pH < 3 and high SO_4^{2-} concentration, jarosite ($K,Na,H_3O[Fe_3(OH)_6(SO_4)_2]$) may form, whereas at neutral pH, ferrihydrite ($Fe_2O_3.1.8H_2O$) and goethite (α-FeOOH) are known to precipitate (Bigham, 1996; Regenspurg et al., 2004). At pH values between 3.0 and 4.0 and sulfate concentrations between 1000 and 3000 mg/L, schwertmannite is a Fe(III)-oxyhydroysulfate that forms commonly in water (Acero et al., 2006), according to:

$$8\ Fe^{3+} + SO_4^{2-} + 14H_2O \leftrightarrow Fe_8O_8(OH)_{5.5}(SO_4)_{1.25} + 22H^+ + 8e^-$$

The IAP values for schwertmannite were calculated with Fe^{3+} and SO_4^{2-} activities using the PHREEQC code and the WATEQ4F database with pH, E_h and total aqueous components as input variables and the updated equilibrium constant of schwertmannite was used (Bigham et al., 1996). The observed SI (saturation index) for schwertmannite was 42.33 ± 1.1 for the sample within the pH range of 2.0 to 3.5 in the second oxic half-cycle where sulfate concentration values range from 790 – 1000 mg/L. The observed IAP for schwertmannite is in agreement with the K_{sp} value of $10^{18\pm2.5}$ reported by Bigham et al. (1996). The transformation of schwertmannite to goethite releases acidity, and may inhibit sulfate reduction in the sediment and support an acidic iron cycle at the sediment-water interface (Peine et al., 2000). PhreePlot simulations show that goethite and schwertmannite are probably predominant forms of iron (oxyhydr)oxides in Matrix B, whereas only goethite potentially precipitated in Matrix A (Fig. 4.10). Moreover, the formation of schwertmannite was also observed by XRD analysis in the matrix B at both last anoxic and

oxic half-cycle samples. Schwertmannite is a metastable phase, and has been formed firstly after Fe^{2+} oxidation, and then transform with time into goethite and at low pH and in the presence of monovalent cations, also to jarosite (Regenspurg et al., 2004; Acero et al., 2006). It is widely accepted that As is depleted in solution as schwermanite is transformed into goethite plus jarosite (Burton et al., 2009). Howerver, LCF of As K-edge did not allow distinguishing the actual association of As with a specific iron (hydr)oxides. The constant proportion of As(V) sorbed on iron (oxyhydr)oxides indicate an increase of dissolved As(V) absorption across cycles after the second oxic half-cycle. Instead of the observation that As is replenished every cycle in Matrix A, while oxidizing conditions were dominant in Matrix B, and As was sequestered on iron (oxyhydr)oxides phase.

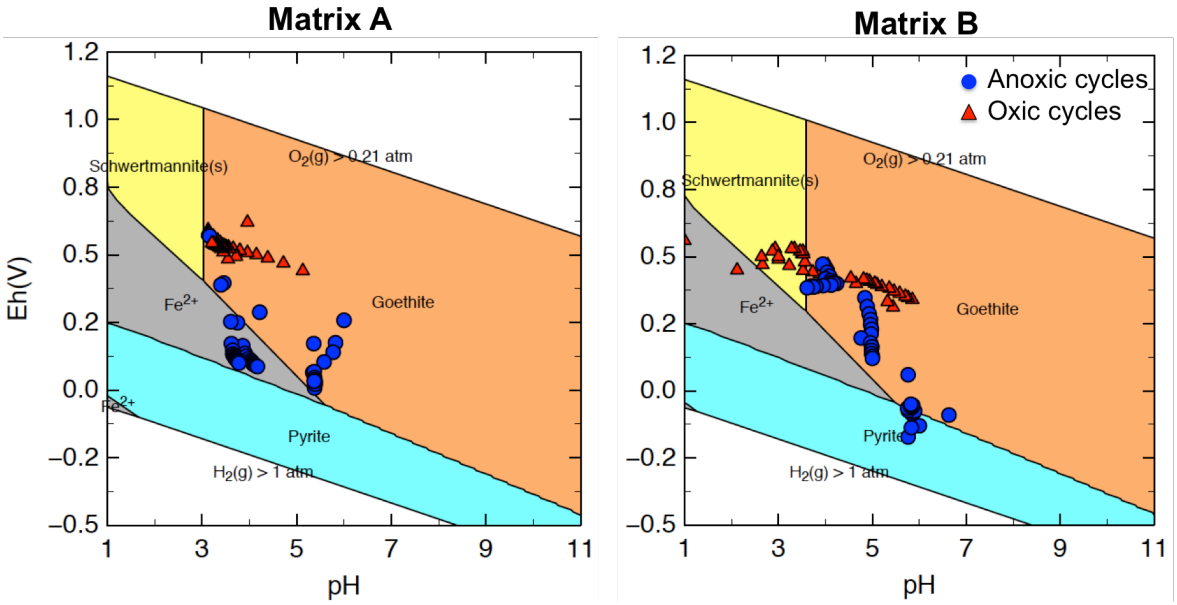

Figure 4.10. Variation in E_h/pH during redox oscillations (blue circle = anoxic half-cycle value; red triangle = oxic half cycle value) in Matrix A (left) and Matrix B (right) compared to the areas of stability for Fe^{2+}, schwertmannite, pyrite and goethite

4.5 Conclusion

The mobility of As from sediment to groundwater is strongly depending on the redox oscillations and sediment mineralogy. Under the observed pH and E_h conditions, it is expected for As, Fe and S to undergo significant changes to their speciation. Additionally cumulative changes of the substrate are expected due to the varying mineral stability that has a second any effect on As mobility. In high pyrite content sediment (Matrix A), pyrite oxidation and pH drop in aqueous solution lead to an inhibition of microbial sulfate reduction, high sulfate concentrations and release of As during reducing conditions. In low pyrite content in presence of gypsum (Matrix B), the accumulative effects of redox cycling

potentially sequester As in solid phase due to cumulative mineralogical changes induced by successive redox cycles. The hypothesis is presented including increase in oxidizing conditions and co-precipitations of As with iron (oxyhydr)oxides and/or iron oxyhydroxysulfate and increase in proportion of As(V) species.

Chapter 5: Conclusion, Perspectives and Future research

5.1 Conclusion

5.1.1 High arsenic concentration from the Mekong Delta in Vietnam

Arsenic is a well-known carcinogen and in Vietnam, An Phu district, a part of the Mekong Delta aquifer, is a hotspot of arsenic contamination. In chapter 2, an investigation of the distribution of arsenic and electrical conductivity in An Phu aquifer is presented and leads to several key conclusions. First, groundwater contamination by arsenic in this region is alarming. All 40 well samples have been found to have As concentration exceeding 16 to 120 times the standard level of drinking water (10 μg/L). The second conclusion concerns the source of the heavy arsenic contamination. As is not only present in As bearing iron (oxyhydr)oxides near the sediment surface, but also in other As-bearing phases such as clay and organic matter since As binds thiol groups bound OM complex. However, due to the low total number of sample cores and the limitated access to X-ray absorption near edge structure, we cannot fully distinguish all the arsenic species present in Mekong Delta sediments. What was clear from the present study is that the distribution of As was dependent on one key physicochemical variable: As aqueous concentration tends to increase in high conductivity soils. Using an electromagnetic geophysical device (EM 31), we show a positive and significant correlation between the electrical conductivity and the As concentration to well-river distance ratio and alkalinity to well-river distance ratio. The electrical conductivity investigation is a user-friendly and less expensive technique for the exploration of subsurface lithology and can be productive in identifying the hydrogeological framework of the area. The results also suggest the important role of alkalinity, iron/manganese (oxyhydr)oxides and clay minerals in mobilization of heavy aqueous As concentrations in the An Giang province.

5.1.2 The importance of redox cycling effects in a sediment-groundwater system

The study site is under a regular flooding and drainage cycle, created by alternating wet-dry seasons. In turn, this generates redox oscillations in soil and subsoil. Hence, the results presented in Chapters 3 and 4 of this thesis clearly show that the repetitive oscillation of redox conditions can result in additional cumulative effect on partition coefficients due to kinetic controls on mineralogy and microbial communities. Very few investigations into

arsenic cumulative effects of redox oscillating conditions exist and fewer still have formally considered effects of bulk mineralogical changes and pH conditions. Under batch experimental conditions multiple cycles of reduction and oxidation are clearly shown to result in the attenuation of aqueous As concentration suggesting that redox cycling may be an effective form of natural sequestration of As in the environment.

5.1.3 Key biogeochemical processes observed

Arsenic binding during microbial sulfate reduction under redox oscillations

Dissolved organic matter in porewater has been linked to the liberation of arsenic in shallow anoxic aquifers and paddy field soils by many recent studies. In chapter 3, the cycling of dissolved organic matter (cellobiose) is attributed to fermentation during anoxic periods and respiration during oxic periods under microbial activity. For the sulfate rich sediment, the fluctuation from oxic to anoxic conditions, sulfate-reducing bacteria using organic matter or hydrogen, as a source of energy is able to convert sulfate into sulfide and reduced elemental sulfur. Phylogenetic analysis of 16S rRNA revealed the presence of sulfur and iron – cycling bacteria suggesting sulfate and iron reduction are important factors for As sequestration in the aqueous phase. Although As is released from sediment to pore water by reductive dissolution of As-bearing Fe(III) (oxyhydr)oxides of seasonally flooded soils, microbial sulfate reduction has a potential to stabilize As in the sulfidic solid phase as shown by the observed redox cycle cumulative effects on As mobility. These mechanisms include adsorption/desorption of As on iron (oxyhydr)oxides and on or within reduced solid sulfur and formation of thiols As complex.

Pyrite oxidation leads to low pH, inhibits sulfate-reducing bacteria and releases arsenic

In chapter 4, the redox cycling experiment containing pyrite rich sediment showed that microbial sulfate reduction was inhibited by the low pH value and high sulfate and iron concentrations in both oxic and anoxic conditions. The pyrite in the 14 m deep sediment (Matrix A) was oxidized during oxic half-cycles, leading to a drop in pH value and allowing to develop acidophilic pyrite oxidizing microbial community. Although microbial sulfate reduction has been observed in previous works performed on acidic lakes, wetlands, acidic sulfate soils and bioreactors, phylogenetic trees based on 16S rRNA indicated the presence of the large species variety in acidic fermentative bacteria and the absence of sulfate-reducing bacteria. That obviously explains the high sulfate, low pH, high acetate and undetectable sulfide concentration during the following reducing cycles in this experiment. Hence, these bacteria prevent the development of sulfate reducing

condition during the anaerobic phases of redox oscillation experiments. The low pH values suppress the viability of many organisms that utilize specific metabolic strategies. Additionally, pyrite oxidation generates large amount of precipitated iron (oxyhydr)oxides favoring iron reduction once anaerobic conditions are established. As a consequence, As was released from As-bearing iron (oxyhydr)oxides during the anoxic conditions repeatedly.

Origin of sulfate production and impact of mineralogy on arsenic mobility during redox oscillation

Pyrite (FeS_2) is the most abundant metal sulfide in nature and, therefore, has a major influence on iron, sulfur and arsenic biogeochemistry and cycles. In Mekong Delta sediments, pyrite precipitation was observed by X-ray diffraction (XRD) from 14 m deep (matrix A) and 7 m deep layers (Matrix B). To better understand the origin of sulfate production in pyrite rich sediment during redox oscillation experiments, the isotopes of oxygen and sulfur ($\delta^{18}O$ and $\delta^{34}S$) were determined. The results presented in Chapter 4 suggest that Fe^{3+} is potentially the primary oxidant for pyrite in the deep layer (Matrix A) as often observed in acid mine drainage, even in the presence of dissolved oxygen during the oxic periods and high sulfate concentration originating from pyrite oxidation. Sulfate was consumed slightly during the anoxic periods and produced mostly by dissolution of gypsum in the shallow layer (Matrix B). The high sulfate concentration, low pH (3 – 4) and suboxic conditions (E_h > 450 mV) in the last full cycle may lead to iron (oxyhydr)oxides sulfate minerals such as schwermannite and goethite formation in Matrix B. These minerals could retard the mobility of arsenic by decreasing its solubility.

5.2 Perspectives

5.2.1 Monsoonal influence on arsenic distribution in groundwater linked to S cycling

Under regular flooding and drainage, As distribution maybe linked to S cycling under redox oscillations in the natural environment. The sediment-groundwater system becomes seasonally anoxic in the flooded soils near the Mekong Delta River (Stuckey et al., 2015). Moreover, this condition would be increased by irrigation with shallow groundwater, which is common practice in the study area, especially during the dry season, and by influx of river water to the aquifer during flooding. The distribution of sulfur and sulfate concentration is also different between low and high As concentration areas (Nguyen & Itoi, 2009). Extending sampling is needed to better evidence the role of sulfur in As

mobilization in An Giang groundwater. Also, water samples should be collected during the pre-monsoon and post-monsoon season. Comparison of a seasonal variation with groundwater geochemical factors could explain better the redox oscillation in the nature and the role of sulfur in As mobilization from An Giang groundwater.

5.2.2 Aqueous thioarsenate species measurement

Microbial sulfate reduction caused important changes in arsenic speciation, especially the formation of aqueous thioarsenate. In this thesis, As K-edge XANES showed that the thiol-bound As(III) and/or arsenic sulfide mineral phase (orpiment) may form during the redox oscillating experiment. In recent years, aqueous thioarsenates have been shown to be important arsenic species in reductive sulfidic waters. Thioarsenate also occurs in iron-rich ground waters (Suess et al., 2011). The preservation of thioarsenate in high iron media has been studied. All methods using acidification, flash-freezing, or EDTA addition fail to preserve thioarsenate in such matrices. In pure water, thioarsenate is only stable for 21 days when the samples are first preserved by flash-freezing and cryo-stored with an addition of EtOH (1% v/v) and with minimal anoxic headspace (Suess et al., 2011). Arsenic-sulfur speciations could then be measured by an Ion Chromatography coupled an ICP-MS. Storage and preservation of thioarsenate were difficult to perform in our case because redox experiments lasted 42 to 56 days and samples were collected every day and the nearest IC – ICP – MS was far away. Additionally, periods of flooding on the Mekong Delta can last more than 4 months; comparatively periods of reduction in bioreactor suspensions of up to 7 days were short and may not have been sufficient to allow sampling for thioarsenate analyses. The ideal case would be the development of portable IC-ICP-MS to be used both in the field and in the laboratory.

5.2.3 Analysis of sulfate-reducing bacteria

The present work was limited to the identification of the general microbial communities variety by using 16S rRNA analysis, but functional genomic analysis was not performed. To understand better the role of sulfate-reducing bacteria (SRB), more powerful approach for the detection of SRB could be used as well as looking for so-called functional genes which encode enzymes that play an important part in the sulfate-reduction pathway, such as *dsrAB* (Muyzer & Stams, 2008), which encodes the dissimilatory sulfide reductase. Many methods have been developed to detect SRB in natural samples such as DNA microarray, fluorescence *in situ* hybridization (FISH), quantitative real-time PCR, RNA-sequencing (Wolf, 2013). PCR primers set for the 16S rRNA gene of six phylogenetic

groups of SRB has been designed and used by Daly et al. (2000). The SRB-specific 16S rDNA primers and probes should be further developed and applied for investigating SRB population composition and change in relation to reducing and oxidizing cycles in the lab and in the field. Furthermore, cloning *dsr* gene fragments could also be used to analyze the diversity of SRBs in many different habitats as was done in few previous studies (Dar et al., 2007; Hug et al., 2014; Muyzer & Stams, 2008).

5.2.4 Kinetic modeling

A mix kinetic-equilibrium model was introduced in PHREEQC and used in previous studies of redox oscillation experiments (Couture et al., 2015; Parsons et al., 2013). In principle, each half-cycle is imposed by alternating the headspace and dissolved gas composition between $N_{2(g)}$ and $O_{2(g)}$ while carrying over the solution chemistry, exchanger, adsorbent composition and solid phase compounds. Following evidence from 16S rRNA, aqueous phase and solid phase analysis, we mostly identified biogeochemical processes by capturing key features (E_h, DOC, Fe, S and As) of the observed time series. Hence, model parameters taken from the literature could help to increase the confidence that a process is correctly identified when the model reproduces both the trends and magnitude of changes in the observation. However, the equilibrium constants of thiolAs(III) bound organic matter formations were not available. Thermodynamic calculation of arsenic speciation in this thesis suggests that thioarsenic may play an important role for the formation of thiolAs complexes or solids. Therefore, the rate of precipitation of these species should be studied in the future to help predict the influence on As speciation and concentration via the formation of thioarsenic species by computing tools.

5.3 Further work

5.3.1 Improvements to sampling and experimental design

Although the bioreactor system model was designed to represent complex natural system, it always entails a degree of modifications. Significant improvements could be made to the experimental design and alternative methodologies used during this thesis in order to more accurately represent natural conditions in Vietnam.

One of the key simplifications of the suspended sediment systems used within this work is the fermentation of organic matter and the reduction of sulfate during the anoxic conditions. As discussed in Chapter 2, sulfate is present in most of the samples and its concentrations vary with time in the area. The initial sulfate and arsenic concentration was added following the high concentration of sulfate in the environment. However, $N_2/CO_{2(g)}$

and O_2 were not measured imposed as real conditions. Dissolved oxygen should be controlled during the redox experiment. Similar to E_h, pH electrodes, oxygen electrode should be installed into the bioreactor system to simulate the real level of dissolved oxygen in the natural groundwater.

Additionally, the formation of H_2S and H_2 needs to be determined both in the lab during the redox oscillation as well as in the field. As mentioned in chapter 3, H_2 can be used as an electron donor for some sulfate reducing bacteria. Through the hydrolysis of organic macromolecules, H_2 could be formed during the anaerobic condition. The presence of *Hydrogenophaga* sp., which is facultative autotrophic hydrogen-oxidizing bacteria, suggests the potential accumulation of H_2 during anoxic half-cycles. Dissolved hydrogen could be measured by headspace equilibration method as described by Bagnoud et al. (Bagnoud et al., 2016) or by using a dissolved hydrogen sensor following the method of Takeshita et al. (1993). The formation of H_2S gas also plays an important role during the microbial sulfate reduction. As mentioned in Chapter 4, in the redox cycling rector containing the 7 m deep sediment sample (Matrix B), high dissolved sulfide concentration was produced during the initial anoxic half-cycle, which did not occur in the subsequent anoxic half-cycles. In addition, low ATP concentration suggests that bacterial community was not active during the experiment. Free sulfide may be toxic to all bacteria because it reacts with metal ions and functional groups of electron carrier system, amino acid and metabolic coenzymes. Furthermore, H_2S may negatively affect cells by precipitating essential trace metals as metal sulfide. Compared to other bacteria, SRB have H_2S as major product of their energy metabolism. H_2S gas could be detected by trapping in a NaOH solution similar to AVS methodology and quantified using UV spectroscopy at 670 nm or by H_2S sensors.

A further key change of the experimental system is the sulfate reducing bacteria scenarios. The observations suggest that As sequestration is enhanced under microbial sulfate reduction, thus it would be worth to perform a comparison of abiotic (sterile) and biotic conditions. Normally, sterility of the abiotic reactor could be achieved by high temperature sterilization (>100^{o}C) of sediment or the use of microbial inhibitors such as sodium azide (NaN_3), streptomycin and kanamycin sulfate or sodium molybdate (Yadav & Archer, 1989) or γ – ray sterilisation. In parallel, a second reactor experiment could be performed well defined sulfate reducers such as *Desulfotomaculum nigrificans,* NCIMB 8395*; Desulfobulbus propionicus,* DSM 2032*; Desulfobacterium autotrophicum,* DSM 3382*; Desulfobacter curvatus,* DSM 3379*; Desulfosarcina variabilis,* DSM 2060*; Desulfovibrio*

desulfuricans, DSM 642. Addition of organic matter would be done in the beginning of every anoxic phase. Similarly, aqueous phase, solid phase and metagenomic analyses would be performed to better clarify effects of sulfate reducing bacteria on As mobility.

5.3.2 Applicability of findings to microbial sulfate reduction to natural environments in the Mekong Delta

The experimental redox cycling and sulfate reduction aspects of this thesis were conducted on one type of low pyrite and on two types of high pyrite sediments in the An Giang province of the Mekong delta. Microbial sulfate reduction was observed in the low pyrite aquifer sample where As concentration was stabilized in the sediment through the formation of thiol group complexes and the increasing of sorption on iron (oxyhydr)oxides and iron sulfide. One logical continuation of this research theme would be to apply the same methodology to soil and sediment *in situ*. This may shed light on the importance of S cycling in the release of As, and specifically the role of thioarsenate in As mobilization in the sulfate-reducing groundwater from the Mekong Delta.

5.3.3 Arsenic removal in the groundwater for drinking water and agriculture

Previous investigation of a number of affected sites in Vietnam has given people a better understanding of the As contamination problem and As removal from groundwater. Most information is mainly focus on the Red River Delta. Household sand filters are the most popular system in the Vietnamese rural area due to low operation costs, their simplicity and locally available construction material. An increasing number of rural households are using simple sand filters to remove Fe because of its “bad taste”. However, a sand filter system always requires the presence of iron in water and in filter where soils are often mixed with sand. Therefore, this is not a technology meeting drinking water standard in all cases. Several research groups have experimentally investigated As removal by coagulation with ferric chloride, co-precipitation enhanced by solar oxidation or TiO_2, adsorption onto preformed hydrous ferric oxide (HFO), iron oxide coated sand, or zerovalent iron or injection of PO_4^{3-}, or mixed with gypsum and organic matter in the aquifer. From this thesis, we show heavy As contamination in one of Southwestern Vietnamese province, a vicinity of Mekong Delta River. Therefore, government should pay more attention to domestic and agricultural activities in this region which both could be affected by As from groundwater use. More researches should be focused on optimizing and applying on the removal As technologies in Mekong Delta region in the future.

Reference

Acero, P., Ayora, C., Torrentó, C., & Nieto, J.-M. (2006). The behavior of trace elements during schwertmannite precipitation and subsequent transformation into goethite and jarosite. *Geochimica et Cosmochimica Acta*, *70*(16), 4130–4139. http://doi.org/10.1016/j.gca.2006.06.1367

Agusa, T., Kubota, R., Kunito, T., Tu, B. M., Pham, T. K. ., Chamnan, C., … Tanabe, S. (2007). Arsenic Pollution in Groundwater of Vietnam and Cambodia: A Review. *Biomed Res Trace Elements*, *18*(1), 35–47.

Agusa, T., Pham, T. K. T., Vi, M. L., Duong, H. A., Tanabe, S., Pham, H. V, & Berg, M. (2014). Human exposure to arsenic from drinking water in Vietnam. *Science of the Total Environment*, *488–489*, 562–569. http://doi.org/10.1016/j.scitotenv.2013.10.039

Allen, H. E., Fu, G., & Deng, B. (1993). Analysis of acid-volatile sulfide (AVS) and simultaneously extracted metals (SEM) for the estimation of potential toxicity in aquatic sediments. *Environmental Toxicology and Chemistry*, *12*, 1441–1453.

Anawar, H. M., Akai, J., Komaki, K., & Terao, H. (2003). Geochemical occurrence of arsenic in groundwater of Bangladesh: sources and mobilization processes. *Geochemical Exploration*, *77*, 109–131. http://doi.org/10.1016/S0375-6742(02)00273-X

Andersen, C. B. (2002). Understanding Carbonate Equilibria By Measuring Alkalinity in Experimental and Natural Systems. *Geoscience Education*, *50*(4), 389–403.

Appelo, C. A. J., & Postma, D. (2005). *Geochemistry, groundwater and pollution* (2nd ed.). Bakema, Leiden, New York.

Appelo, C. A. J., Van Der Weiden, M. J. J., Tournassat, C., & Charlet, L. (2002). Surface complexation of ferrous iron and carbonate on ferrihydrite and the mobilization of arsenic. *Environmental Science and Technology*, *36*(14), 3096–3103. http://doi.org/10.1021/es010130n

Asta, M. P., Cama, J., Martínez, M., & Giménez, J. (2009). Arsenic removal by goethite and jarosite in acidic conditions and its environmental implications. *Journal of Hazardous Materials*, *171*(1–3), 965–972. http://doi.org/10.1016/j.jhazmat.2009.06.097

Aziz, Z., Geen, A. Van, Stute, M., Versteeg, R., Horneman, A., Zheng, Y., … Ahmed, K. M. (2008). Impact of local recharge on arsenic concentrations in shallow aquifers inferred from the electromagnetic conductivity of soils in Araihazar, Bangladesh. *Water Resources Research*, *44*, 1–15. http://doi.org/10.1029/2007WR006000

Bagnoud, A., Leupin, O., Schwyn, B., & Bernier-Latmani, R. (2016). Rates of microbial hydrogen oxidation and sulfate reduction in Opalinus Clay rock. *Applied Geochemistry*, *72*, 42–50. http://doi.org/10.1016/j.apgeochem.2016.06.011

Balci, N., Mayer, B., Shanks, W. C., & Mandernack, K. W. (2012). Oxygen and sulfur isotope systematics of sulfate produced during abiotic and bacterial oxidation of sphalerite and elemental sulfur. *Geochimica et Cosmochimica Acta*, *77*, 335–351. http://doi.org/10.1016/j.gca.2011.10.022

Balci, N., Shanks, W. C., Mayer, B., & Mandernack, K. W. (2007). Oxygen and sulfur isotope systematics of sulfate produced by bacterial and abiotic oxidation of pyrite. *Geochimica et Cosmochimica Acta*, *71*(15), 3796–3811. http://doi.org/10.1016/j.gca.2007.04.017

Ballantyne, J. M., & Moore, J. N. (1988). Arsenic geochemistry in geothermal systems. *Geochimica et Cosmochimica Acta*, *52*, 475–483.

Bang, S., Thi, H. H., Kim, K., Nguyen, M. H., & Dang, D. M. (2008). Arsenic-Contaminated Groundwater in the Mekong River Delta of Vietnam. *Proceedings of the International Syposia On Geoscience Resources and Environments of Asian Terranes*, 24–27.

Bardelli, F., Cattaruzza, E., Gonella, F., Rampazzo, G., & Valotto, G. (2011). Characterization of road dust collected in Traforo del San Bernardo highway tunnel: Fe and Mn speciation. *Atmospheric Environment*, *45*(35), 6459–6468. http://doi.org/10.1016/j.atmosenv.2011.07.035

Barton, L. L. (1995). *Biotechnology Handbooks 8 - Sulfate-Reducing Bacteria*. (T. Atkinson & R. F. Sherwood, Eds.). Springer Science.

Bauer, M., & Blodau, C. (2006). Mobilization of arsenic by dissolved organic matter from iron oxides, soils and sediments. *Science of the Total Environment*, *354*, 179–190. http://doi.org/10.1016/j.scitotenv.2005.01.027

Benner, S. G., Polizzotto, M. L., Kocar, B. D., Ganguly, S., Phan, K., Ouch, K., … Fendorf, S. (2008). Groundwater flow in an arsenic-contaminated aquifer, Mekong Delta, Cambodia. *Applied Geochemistry*, *23*(11), 3072–3087. http://doi.org/10.1016/j.apgeochem.2008.06.013

Berg, M., Stengel, C., Pham, T. K. T., Pham, H. V, Sampson, M. L., Leng, M., … Fredericks, D. (2007). Magnitude of arsenic pollution in the Mekong and Red River Deltas - Cambodia and Vietnam. *Science of the Total Environment*, *372*, 413–425. http://doi.org/10.1016/j.scitotenv.2006.09.010

Berg, M., Tran, H. C., Nguyen, T. C., Pham, H. V, Schertenleib, R., & Giger, W. (2001). Arsenic contamination of groundwater and drinking water in Vietnam: a human health threat. *Environmental Science & Technology*, *35*(13), 2621–6. Retrieved from http://www.ncbi.nlm.nih.gov/pubmed/11452583

Bernardez, L. A., de Andrade Lima, L. R. P., Ramos, C. L. S., & Almeida, P. F. (2012). A Kinetic Analysis of Microbial Sulfate Reduction in an Upflow Packed-Bed Anaerobic Bioreactor. *Mine Water Environ*, *31*, 62–68. http://doi.org/10.1007/s10230-012-0170-z

Berner, R. A. (1970). Sedimentary Pyrite Formation. *American Journal of Science*, *268*, 1–23.

BGS&DFID. (2001). *Arsenic contamination of groundwater in Bangladesh*. *BGS Technical Report*.

Bhandari, N., Reeder, R. J., & Strongin, D. R. (2012). Photoinduced Oxidation of Arsenite to Arsenate in the presence of goethite. *Environmental Science & Technology*, *46*, 8044–8051.

Bigham, J. M. (1996). Influence of pH on mineral speciation in a bioreactor simulating acid mine drainage. *Applied Geochemistry*, *11*(583), 845–849.

Bigham, J. M., Swertmann, S. J., Traina, S. J., Winland, R. L., & Wolf, M. (1996). Schwertmannite and the chemical modeling of iron in acid sulfate waters. *Geochimica et Cosmochimica Acta*, *60*(12), 2111–2121.

Bohari, Y., Astruc, A., Astruc, M., Cloud, J., & Angot, A. P. (2001). Improvements of hydride generation for the speciation of arsenic in natural freshwater samples by HPLC-HG-AFS. *Analytical Atomic Spectrometry*, *16*, 774–778. http://doi.org/10.1039/b101591p

Borch, T., Kretzschmar, R., Kappler, A., Cappellen, P. Van, Ginder-Vogel, M., Voegelin, A., & Campbell, K. (2010). Biogeochemical Redox Processes and their Impact on Contaminant Dynamics. *Environmental Science and Technology*, *44*, 15–23.

Bostick, B. C., & Fendorf, S. (2003). Arsenite sorption on troilite (FeS) and pyrite (FeS2). *Geochimica et Cosmochimica Acta*, *67*(5), 909–921. http://doi.org/10.1016/S0016-7037(02)01170-5

Bouffard, S. C., Rivera-Vasquez, B. F., & Dixon, D. G. (2006). Leaching kinetics and stoichiometry of pyrite oxidation from a pyrite-marcasite concentrate in acid ferric sulfate media. *Hydrometallurgy*, *84*, 225–238. http://doi.org/10.1016/j.hydromet.2006.05.008

Brenot, A., Carignan, J., France-Lanord, C., & Benoît, M. (2007). Geological and land use control on δ34S and δ18O of river dissolved sulfate: The Moselle river basin, France. *Chemical Geology*, *244*(1–2), 25–41. http://doi.org/10.1016/j.chemgeo.2007.06.003

Brinkman, Nguyen, B. V., Tran, K. T., Do, P. H., & van Mensvoort, M. E. F. (1993). Sulfidic materials in the Western Mekong Delta, Vietnam. *Catena*, *20*, 317–331.

Burnol, A., Garrido, F., Baranger, P., Joulian, C., Dictor, M., Bodénan, F., … Charlet, L. (2007). Decoupling of arsenic and iron release from ferrihydrite suspension under reducing conditions : a biogeochemical model, *18*(2), 1–18. http://doi.org/10.1186/1467-4866-8-12

Burton, E. D., Bush, R. T., Johnston, S. G., Watling, K. M., Hocking, R. K., Sullivan, L. A., & Parker, G. K. (2009). Sorption of As(V) and As(III) to Schwertmannite. *Environmental Science & Technology*, *43*(24), 9202–9207.

Burton, E. D., Bush, R. T., Sullivan, L. a., Johnston, S. G., & Hocking, R. K. (2008). Mobility of arsenic and selected metals during re-flooding of iron- and organic-rich acid-sulfate soil. *Chemical Geology*, *253*, 64–73. http://doi.org/10.1016/j.chemgeo.2008.04.006

Burton, E. D., Johnston, S. G., & Planer-Friedrich, B. (2013). Coupling of arsenic mobility to sulfur transformations during microbial sulfate reduction in the presence and absence of humic acid. *Chemical Geology*, *343*, 12–24. http://doi.org/10.1016/j.chemgeo.2013.02.005

Buschmann, J., & Berg, M. (2009). Impact of sulfate reduction on the scale of arsenic contamination in groundwater of the Mekong, Bengal and Red River deltas. *Applied Geochemistry*, *24*(7), 1278–1286. http://doi.org/10.1016/j.apgeochem.2009.04.002

Buschmann, J., Berg, M., Stengel, C., Winkel, L., Sampson, M. L., Trang, P. T. K., & Viet, P. H. (2008). Contamination of drinking water resources in the Mekong delta floodplains: Arsenic and other trace metals pose serious health risks to population. *Environment International*, *34*(6), 756–764. http://doi.org/10.1016/j.envint.2007.12.025

Caccavo, F., Lonergan, D. J., Lovley, D. R., Mark, D., Stolz, J. F., & McInerney, M. J. (1994). Geobacter sulfurreducens sp.nov, a hydrogen- and acetate-oxidizing dissimilatory metal-reducing microorganism. *Applied and Environmental Microbiology*, *60*(10), 3752–3759.

Canfield, D. E. (2001). *Biogeochemistry of Sulfur Isotopes*. http://doi.org/10.2138/gsrmg.43.1.607

Canfield, D. E., Thamdrup, B., & Fleischer, S. (1998). Isotope fractionation and sulfur metabolism by pure and enrichment cultures of elemental sulfur-disproportionating bacteria. *Limnology and Oceanography*, *43*(2), 253–264. http://doi.org/10.4319/lo.1998.43.2.0253

Caporaso, J. G., Lauber, C. L., Walters, W. a, Berg-Lyons, D., Huntley, J., Fierer, N., … Knight, R. (2012). Ultra-high-throughput microbial community analysis on the Illumina HiSeq and MiSeq platforms. *International Society for Microbial Ecology*, *6*(8), 1621–1624. http://doi.org/10.1038/ismej.2012.8

Castillo Martinez, F. A., Balciunas, E. M., Salgado, J. M., Domínguez González, J. M., Converti, A., & Oliveira, R. P. D. S. (2013). Lactic acid properties, applications and production: A review. *Trends in Food Science & Technology*, *30*, 70–83. http://doi.org/10.1016/j.tifs.2012.11.007

Chakraborty, S., Bardelli, F., & Charlet, L. (2010). Reactivities of Fe(II) on Calcite: Selenium Reduction. *Environmental Science & Technology*, *44*(4), 1288–1294.

Challenger, F. (1947). Biological methylation. *Advanced in Enzymology and Related Areas of Molecular Biology*, *12*, 429–491. http://doi.org/10.1039/qr9550900255

Charlet, L., Chakraborty, S., Appelo, C. A. J., & Roman-ross, G. (2007). Chemodynamics of an arsenic "'hotspot'" in a West Bengal aquifer: A field and reactive transport modeling study. *Applied Geochemistry*, *22*, 1273–1292. http://doi.org/10.1016/j.apgeochem.2006.12.022

Charlet, L., Markelova, E., Parsons, C., & Madé, B. (2013). Redox oscillation impact on natural and engineered biogeochemical systems: chemical resilience and implications for contaminant mobility. *Procedia Earth and Planetary Science*, *7*, 135–138. http://doi.org/10.1016/j.proeps.2013.03.048

Charlet, L., Morin, G., Rose, J., Wang, Y., Auffan, M., Burnol, A., & Fernandez-martinez, A.

(2011). Reactivity at (nano)partical-water interfaces, redox processes, and arsenic transport in the environment. *Comptes Rendus Geoscience*, *343*(2–3), 123–139. http://doi.org/10.1016/j.crte.2010.11.005

Charlet, L., Morin, G., Rose, J., Wang, Y., Auffan, M., Burnol, A., & Fernandez-Martinez, A. (2011). Reactivity at (nano)particle-water interfaces, redox processes, and arsenic transport in the environment. *Comptes Rendus Geoscience*, *343*, 123–139. http://doi.org/10.1016/j.crte.2010.11.005

Charlet, L., & Polya, D. A. (2006). Reducing Groundwaters in Southern Asia: An Environmental Health Disaster. *Elements*, *2*, 91–96.

Chen, C. J., Chen, C. W., Wu, M. M., & Kuo, T. L. (1992). Cancer potential in liver, lung, bladder and kidney due to ingested inorganic arsenic in drinking water. *British Journal of Cancer*, *66*(5), 888–92. http://doi.org/10.1038/bjc.1992.380

Cheng, H., Hu, Y., Luo, J., Xu, B., & Zhao, J. (2009). Geochemical processes controlling fate and transport of arsenic in acid mine drainage (AMD) and natural systems. *Journal of Hazardous Materials*, *165*, 13–26. http://doi.org/10.1016/j.jhazmat.2008.10.070

Choprapawon, C., & Rodcline, A. (1987). *Chronic arsenic poisoning in Ronpiboll Nakhon Sri Thammarat, the Southern Province of Thailand*. (C. O. Albernathy, Ed.). Chapman & Hall.

Christensen, J. J., & Facklam, R. R. (2001). Granulicatella and Abiotrophia species from human clinical specimens. *Journal of Clinical Microbiology*, *39*(10), 3520–3523. http://doi.org/10.1128/JCM.39.10.3520

Christodoulidou, M., Charalambous, C., Aletrari, M., Kanari, P. N., Petronda, A., & Ward, N. I. (2012). Arsenic concentrations in groundwaters of Cyprus. *Journal of Hydrology*, *468–469*, 94–100. http://doi.org/10.1016/j.jhydrol.2012.08.019

Cline, J. D. (1969). Spectrophotometric determination of hydrogen sulfide in natural waters. *Limnology and Oceanography*, *14*(3), 454–458. http://doi.org/10.4319/lo.1969.14.3.0454

Cotten, J., Le Dez, A., Bau, M., Caroff, M., Maury, R. C., Dulski, P., … Brousse, R. (1995). Origin of anomalous rare-earth element and yttrium enrichments in subaerially exposed basalts: Evidence from French Polynesia. *Chemical Geology*, *119*, 115–138. http://doi.org/10.1016/0009-2541(94)00102-E

Couture, R.-M., Gobeil, C., & Tessier, A. (2010). Arsenic, iron and sulfur co-diagenesis in lake sediments. *Geochimica et Cosmochimica Acta*, *74*(4), 1238–1255. http://doi.org/10.1016/j.gca.2009.11.028

Couture, R.-M., Rose, J., Kumar, N., Mitchell, K., Wallschläger, D., & Van Cappellen, P. (2013). Sorption of arsenite, arsenate, and thioarsenates to iron oxides and iron sulfides: a kinetic and spectroscopic investigation. *Environmental Science & Technology*, *47*(11), 5652–9. http://doi.org/10.1021/es3049724

Couture, R.-M., Wallschläger, D., Rose, J., & Van Cappellen, P. (2013a). Arsenic binding to organic and inorganic sulfur species during microbial sulfate reduction: a sediment flow-through reactor experiment. *Environmental Chemistry*, *10*(4), 285. http://doi.org/10.1071/EN13010

Couture, R.-M., Wallschläger, D., Rose, J., & Van Cappellen, P. (2013b). SI: Arsenic binding to organic and inorganic sulfur species during microbial sulfate reduction: a sediment flow-through reactor experiment. *Environmental Chemistry*, *10*(4), 285. http://doi.org/10.1071/EN13010

Couture, R., & Cappellen, P. Van. (2011). Reassessing the role of sulfur geochemistry on arsenic speciation in reducing environments. *Journal of Hazardous Materials*, *189*(3), 647–652. http://doi.org/10.1016/j.jhazmat.2011.02.029

Couture, R. M., Charlet, L., Markelova, E., Madé, B., & Parsons, C. T. (2015). On–Off Mobilization of Contaminants in Soils during Redox Oscillations. *Environmental Science &*

Technology, *49*, 3015–3023. http://doi.org/10.1021/es5061879

Criaud, A., & Fouillac, C. (1989). The distribution of arsenic (III) and arsenic (V) in geothermal waters: Examples from the Massif Central of France, the Island of Dominica in the Leeward Islands of the Caribbean, the Valles Caldera of New Mexico, U.S.A., and southwest Bulgaria. *Chemical Geology*, *76*(3–4), 259–269. http://doi.org/10.1016/0009-2541(89)90095-8

Cullen, W. R., & Reimer, K. J. (1989). Arsenic Speciation in the Environment. *Environmental Science and Technology*, *89*, 713–764.

Cypionka, H. (2001). Periplasmic oxygen reduction by Desulfovibrio species. *Archives of Microbiology*, *176*, 306–309. http://doi.org/10.1007/s002030100329

Dadwhal, M., Sahimi, M., & Tsotsis, T. T. (2011). Adsorption Isotherms of Arsenic on Conditioned Layered Double Hydroxides in the Presence of Various Competing Ions. *I&EC Research*, *50*, 2220–2226.

Daly, K., Sharp, R. J., & Mccarthy, A. J. (2000). Development of oligonucleotide probes and PCR primers for detecting phylogenetic subgroups of sulfate-reducing bacteria, 1693–1705.

Dar, S. A., Yao, L., Van Dongen, U., Kuenen, J. G., & Muyzer, G. (2007). Analysis of diversity and activity of sulfate-reducing bacterial communities in sulfidogenic bioreactors using 16S rRNA and dsrB genes as molecular markers. *Applied and Environmental Microbiology*, *73*(2), 594–604. http://doi.org/10.1128/AEM.01875-06

Das, A., & Caccavo, F. (2001). Adhesion of the dissimilatory Fe(III)-reducing bacterium Shewanella alga BrY to crystalline Fe(III) oxides. *Current Microbiology*, *42*(3), 151–154. http://doi.org/10.1007/s002840010195

Dixit, S., & Hering, J. G. (2003). Comparison of As(V) and As(III) sorption onto iron oxide minerals: Implications for arsenic mobility. *Environmental Science and Technology*, *37*(18), 4182–4189. http://doi.org/10.1021/es030309t

Dombrowski, P. M., Long, W., Farley, K. J., Mahony, J. D., Capitani, J. F., & Di Toro, D. M. (2005). Thermodynamic analysis of arsenic methylation. *Environmental Science and Technology*, *39*(7), 2169–2176. http://doi.org/10.1021/es0489691

Doolittle, J. A., Brevik, E. C., Doolittle, J. A., & Brevik, E. C. (2014). The use of electromagnetic induction techniques in soils studies. *Geoderma*, (223–225), 33–45.

Doolittle, J. A., Sudduth, K. A., Kitchen, N. R., & Indorante, S. J. (1994). Estimating depths to claypans using electromagnetic induction methods. *Soil and Water Conservation*, *49*(6), 572–575.

Du Laing, G., Chapagain, S. K., Dewispelaere, M., Meers, E., Kazama, F., Tack, F. M. G., … Verloo, M. G. (2009). Presence and mobility of arsenic in estuarine wetland soils of the Scheldt estuary (Belgium). *Journal of Environmental Monitoring*, *11*(4), 873. http://doi.org/10.1039/b815875d

Eller, G., & Frenzel, P. (2001). Changes in Activity and Community Structure of Methane-Oxidizing Bacteria over the Growth Period of Rice. *Applied and Environmental Microbiology*, *67*(6), 2395–2403. http://doi.org/10.1128/AEM.67.6.2395

Erban, L. E., Gorelick, S. M., & Fendorf, S. (2014). Arsenic in the Multi-aquifer System of the Mekong Delta, Vietnam: Analysis of Large-Scale Spatial Trends and Controlling Factors. *Environmental Science & Technology*, *48*(11), 6081–6088. http://doi.org/10.1021/es403932t

Erban, L. E., Gorelick, S. M., Zebker, H. a, & Fendorf, S. (2013). Release of arsenic to deep groundwater in the Mekong Delta, Vietnam, linked to pumping-induced land subsidence. *Proceedings of the National Academy of Sciences of the United States of America*, *110*(34), 13751–6. http://doi.org/10.1073/pnas.1300503110

Essington, M. (2004). *Soil and water chemistry an integrative approach*. CRC Press, Boca Raton.

Fan, L., McElroy, K., & Thomas, T. (2012). *Reconstruction of ribosomal RNA genes from*

metagenomic data. *PLoS ONE*.

Farquhar, M. L., Charnock, J. M., Livens, F. R., & Vaughan, D. J. (2002). Mechanisms of Arsenic Uptake from aqueous solution by interaction with Goethite, Lepidocrocite, Mackinawite, and Pyrite: An X-ray Absorption Spectroscopy Study. *Environmental Science and Technology*, *26*, 1757–1762.

Fendorf, S., Eick, M. J., Grossl, P. R., & Sparks, D. L. (1997). Arsenate and Chromate Retention Mechanisms on Goethite. 1. Surface Structure. *Environmental Science & Technology*, *31*(2), 315–320.

Fendorf, S., Nico, P. S., Kocar, B. D., Yoko, M., & Tufano, K. J. (2010). *Arsenic chemistry in soils and sediments*. Lawrence Berkeley National Laboratory.

Ferna, D. C., Rodriguez, N., Go, F., & Amils, R. (2003). Geological record of an acidic environment driven by iron hydrochemistry : The Tinto River system. *Geophysical Research*, *108*, 1–15. http://doi.org/10.1029/2002JE001918

Fernández-Martínez, A., Román-Ross, G., Cuello, G. J., Turrillas, X., Charlet, L., Johnson, M. R., & Bardelli, F. (2006). Arsenic uptake by gypsum and calcite: Modelling and probing by neutron and X-ray scattering. *Physica B: Condensed Matter*, *385–386*, 935–937. http://doi.org/10.1016/j.physb.2006.05.276

Fernandez-Martinez, A., Timon, V., Romaman-Ross, G., Cuello, G. J., Daniels, J. E., & Ayora, C. (2010). The structure of schwertmannite, a nanocrystalline iron oxyhydroxysulfate. *American Mineralogist*, *95*(8–9), 1312–1322. http://doi.org/10.2138/am.2010.3446

Fisher, J. C., Wallschläger, D., Planer-Friedrich, B., & Hollibaugh, J. T. (2008). A new role for sulfur in arsenic cycling. *Environmental Science & Technology*, *42*(1), 81–5.

Franciscon, E., Zille, A., Fantinatti-Garboggini, F., Silva, I. S., Cavaco-Paulo, A., & Durrant, L. R. (2009). Microaerophilic-aerobic sequential decolourization/biodegradation of textile azo dyes by a facultative Klebsiella sp. strain VN-31. *Process Biochemistry*, *44*(4), 446–452. http://doi.org/10.1016/j.procbio.2008.12.009

Gallegos, T. J., Han, Y. S., & Hayes, K. F. (2008). Model predictions of Realgar precipitation by reaction of As(III) with synthetic Mackinawite under anoxic conditions. *Environmental Science & Technology*, *42*, 9338–9343.

Ghosal, U., Sikdar, P. K., & Mcarthur, J. M. (2014). Palaeosol Control of Arsenic Pollution: The Bengal Basin in West Bengal, India. *Groundwater*, *53*(4), 588–599. http://doi.org/10.1111/gwat.12251

Gihring, T. M., Druschel, G. K., Maccleskey, R. B., Hamers, R. J., & Banfield, J. F. (2001). Rapid Arsenite Oxidation by Thermus aquaticus and Thermus thermophilus : Field and Laboratory Investigations. *Environmental Science & Technology*, *35*(19), 3857–3862.

Gobbetti, M., & Calasso, M. (2014). *Streptococcus*. *Encyclopedia of Food Microbiology* (Vol. 3). http://doi.org/10.1016/B978-0-12-384730-0.00324-4

Gorny, J., Billon, G., Lesven, L., Dumoulin, D., Madé, B., & Noiriel, C. (2015). Arsenic behavior in river sediments under redox gradient: A review. *Science of the Total Environment*, *505*, 423–434. http://doi.org/10.1016/j.scitotenv.2014.10.011

Grafe, M., Eick, M. J., & Grossl, P. R. (2001). Adsorption of arsenate (V) and arsenite (III) on goethite in the presence and absence of dissolved organic carbon. *Soil Science Society of America Journal*, *65*(V), 1680–1687. http://doi.org/10.2136/sssaj2001.1680

Greskowiak, J., Prommer, H., Massmann, G., & Nützmann, G. (2006). Modeling seasonal redox dynamics and the corresponding fate of the pharmaceutical residue phenazone during artificial recharge of groundwater. *Environmental Science and Technology*, *40*(21), 6615–6621. http://doi.org/10.1021/es052506t

Grossl, P. R., Eick, M., Sparks, D. L., Goldberg, S., & Ainsworth, C. C. (1997). Arsenate and

Chromate retention mechanisms on goethite. 2. Kinetic Evaluation Using a Pressure-Jump Relaxation Technique. *Environmental Science and Technology*, *31*(2), 321–326.

Grybos, M., Davranche, M., Gruau, G., Petitjean, P., & Pédrot, M. (2009). Increasing pH drives organic matter solubilization from wetland soils under reducing conditions. *Geoderma*, *154*, 13–19. http://doi.org/10.1016/j.geoderma.2009.09.001

Guo, H., Li, Y., & Zhao, K. (2010). Arsenate removal from aqueous solution using synthetic siderite. *Journal of Hazardous Materials*, *176*, 174–80. http://doi.org/10.1016/j.jhazmat.2009.11.009

Guo, H., Li, Y., Zhao, K., Ren, Y., & Wei, C. (2011). Removal of arsenite from water by synthetic siderite: behaviors and mechanisms. *Journal of Hazardous Materials*, *186*, 1847–54. http://doi.org/10.1016/j.jhazmat.2010.12.078

Guo, H., Stüben, D., & Berner, Z. (2007a). Adsorption of arsenic(III) and arsenic(V) from groundwater using natural siderite as the adsorbent. *Journal of Colloid and Interface Science*, *315*(1), 47–53. http://doi.org/10.1016/j.jcis.2007.06.035

Guo, H., Stüben, D., & Berner, Z. (2007b). Arsenic removal from water using natural iron mineral-quartz sand columns. *The Science of the Total Environment*, *377*, 142–51. http://doi.org/10.1016/j.scitotenv.2007.02.001

Haikarainen, T., Paturi, P., Linde, J., Haataja, S., Meyer-klaucke, W., Finne, J., & Papageorgiou, A. C. (2011). Magnetic properties and structural characterization of iron oxide nanoparticles formed by Streptococcus suis Dpr and four mutants. *Biological Inorganic Chemistry*, *16*, 799–807. http://doi.org/10.1007/s00775-011-0781-z

Hammes, F., Goldschmidt, F., Vital, M., Wang, Y., & Egli, T. (2010). Measurement and interpretation of microbial adenosine tri-phosphate (ATP) in aquatic environments. *Water Research*, *44*(13), 3915–3923. http://doi.org/10.1016/j.watres.2010.04.015

Hanh, H. T., Kim, K. W., Bang, S., & Hoa, N. M. (2011). Community exposure to arsenic in the Mekong river delta, Southern Vietnam. *Journal of Environmental Monitoring*, *13*(7), 2025–32. http://doi.org/10.1039/c1em10037h

He, J., & Charlet, L. (2013). A review of arsenic presence in China drinking water. *Journal of Hydrology*, *492*, 79–88. http://doi.org/10.1016/j.jhydrol.2013.04.007

Hedley, C. B., Yule, I. J., Eastwood, C. R., Shepherd, T. G., & Arnold, G. (2004). Rapid identification of soil textural and management zones using electromagnetic induction sensing of soils. *Australian Journal of Soil Research*, *42*(4), 389–400. http://doi.org/10.1071/SR03149

Hedrich, S., Schlomann, M., & Barrie Johnson, D. (2011). The iron-oxidizing proteobacteria. *Microbiology*, *157*(6), 1551–1564. http://doi.org/10.1099/mic.0.045344-0

Heidel, C., & Tichomirowa, M. (2011). The isotopic composition of sulfate from anaerobic and low oxygen pyrite oxidation experiments with ferric iron - New insights into oxidation mechanisms. *Chemical Geology*, *281*, 305–316. http://doi.org/10.1016/j.chemgeo.2010.12.017

Helz, G. R., & Tossell, J. A. (2008). Thermodynamic model for arsenic speciation in sulfidic waters : A novel use of ab initio computations. *Geochimica et Cosmochimica Acta*, *72*, 4457–4468. http://doi.org/10.1016/j.gca.2008.06.018

Hindmarsh, J. T., & McCurdy, R. F. (1986). Clinical and Environmental Aspects of Arsenic Toxicity. *Critical Review in Clinical Laboratory Sciences*, *23*(4), 315–347. http://doi.org/10.3109/10408368609167122

Hinrichsen, S., Geist, F., & Planer-friedrich, B. (2015). Inorganic and Methylated Thioarsenates Pass the Gastrointestinal Barrier. *Chemical Research in Toxicology*, *28*, 1678–1680. http://doi.org/10.1021/acs.chemrestox.5b00268

Hoang, T. H., Bang, S., Kim, K.-W., Nguyen, M. H., & Dang, D. M. (2010). Arsenic in groundwater and sediment in the Mekong River delta, Vietnam. *Environmental Pollution*, *158*, 2648–58. http://doi.org/10.1016/j.envpol.2010.05.001

Hoffmann, M., Mikutta, C., & Kretzschmar, R. (2012). Bisulfide reaction with natural organic matter enhances Arsenite sorption: Insights from X-ray Absorption Spectroscopy. *Environmental Science & Technology*, *46*, 11788–11797. http://doi.org/dx.doi.org/10.1021/es302590x

Hoque, M. A., Khan, A. A., Shamsudduha, M., Hossain, M. S., Islam, T., & Chowdhury, S. H. (2009). Near surface lithology and spatial variation of arsenic in the shallow groundwater: Southeastern Bangladesh. *Environmental Geology*, *56*(8), 1687–1695. http://doi.org/10.1007/s00254-008-1267-3

Horneman, A., van Geen, A., Kent, D. V, Mathe, P. E., Zheng, Y., Dhar, R. K., … Ahmed, K. M. (2004). Decoupling of As and Fe release to Bangladesh groundwater under reducing conditions. Part I: Evidence from sediment profiles. *Geochimica et Cosmochimica Acta*, *68*(17), 3459–3473. http://doi.org/10.1016/j.gca.2004.01.026

Hossain, M. F. (2006). Arsenic contamination in Bangladesh - An overview. *Agriculture, Ecosystems & Environment*, *113*, 1–16. http://doi.org/10.1016/j.agee.2005.08.034

Hug, K., Maher, W. A., Stott, M. B., Krikowa, F., Foster, S., & Moreau, J. W. (2014). Microbial contributions to coupled arsenic and sulfur cycling in the acid-sulfide hot spring Champagne Pool, New Zealand. *Frontiers in Microbiology*, *5*(569), 1–15. http://doi.org/10.3389/fmicb.2014.00569

Hughes, M. F. (2002). Arsenic toxicity and potential mechanisms of action. *Toxicology Letters*, *133*, 1–16.

Hurtgen, M. T., Lyons, T. W., Ingall, E. D., & Cruse, A. M. (1999). Anomalous enrichments of iron monosulfide in euxinic marine sediments and the role of H2S in iron sulfide transformations: Examples from Effingham inlet, Orca Basin, and the Black Sea. *American Journal of Science*, *299*, 556–588.

Isaure, M.-P., Laboudigue, A., Manceau, A., Sarret, G., Tiffreau, C., Trocellier, P., … Chateigner, D. (2002). Quantitative Zn speciation in a contaminated dredged sediment by μ-PIXE, μ-SXRF, EXAFS spectroscopy and principal component analysis. *Geochimica et Cosmochimica Acta*, *66*(9), 1549–1567. http://doi.org/10.1016/S0016-7037(01)00875-4

Islam, F. S., Gault, A. G., Boothman, C., Polya, D. A., Charnock, J. M., Chatterjee, D., & Lloyd, J. R. (2004). Role of metal-reducing bacteria in arsenic release from Bengal delta sediments. *Nature*, *430*, 68–71. http://doi.org/10.1038/nature02638

Jain, A., Raven, K. P., & Loeppert, R. H. (1999). Arsenite and arsenate adsorption on ferrihydrite: Surface charge reduction and net OH- release stoichiometry. *Environmental Science and Technology*, *33*(8), 1179–1184. http://doi.org/10.1021/es980722e

Johnson, D. B., Kanao, T., & Hedrich, S. (2012). Redox transformations of iron at extremely low pH: fundamental and applied aspects. *Frontiers in Microbiology*, *3*(96), 1–13. http://doi.org/10.3389/fmicb.2012.00096

Jones, L. C., Lafferty, B. J., & Sparks, D. L. (2012). Additive and competitive effects of bacteria and mn oxides on arsenite oxidation kinetics. *Environmental Science and Technology*, *46*(12), 6548–6555. http://doi.org/10.1021/es204252f

Jönsson, J., Persson, P., Sjöberg, S., & Lövgren, L. (2005). Schwertmannite precipitated from acid mine drainage: Phase transformation, sulphate release and surface properties. *Applied Geochemistry*, *20*, 179–191. http://doi.org/10.1016/j.apgeochem.2004.04.008

Kamyshny, J. A., Borkenstein, C. G., & Ferdelman, T. G. (2009). Protocol for quantitative detection of elemental sulfur and polysulfide zero-valent sulfur distribution in natural aquatic samples. *Geostandards and Geoanalytical*, *33*(3), 415–435.

Kapaj, S., Peterson, H., Liber, K., & Bhattacharya, P. (2006). Human health effects from chronic arsenic poisoning- Areview. *Environmental Science and Health Part A*, *41*(10), 2399–428. http://doi.org/10.1080/10934520600873571

Karl, D. M. (1980). Cellular nucleotide measurements and applications in microbial ecology. *Microbiological Reviews*, *44*(4), 739–796. http://doi.org/0146-0749/80/04-0739/58

Keller, N. S., Stefa, A., & Sigfusson, B. (2014). Arsenic speciation in natural sulfidic geothermal waters. *Geochimica et Cosmochimica Acta*, *142*, 15–26. http://doi.org/10.1016/j.gca.2014.08.007

Kelly, W. R., Holm, T. R., Wilson, S. D., & Roadcap, G. S. (2005). Arsenic in Glacial Aquifers : Sources and Geochemical Controls. *Groundwater*, *43*(4), 500–510.

Kendall, M. R., Madden, A. S., & Elwood, M. E. (2013). Effects of arsenic incorporation on jarosite dissolution rates and reaction products. *Geochimica et Cosmochimica Acta*, *112*, 192–207. http://doi.org/10.1016/j.gca.2013.02.019

King, G. M., Howes, B. L., & Dacey, J. W. H. (1985). Short-term endproducts of sulfate reduction in a salt marsh: Formation of acid volatile sulfides, elemental sulfur, and pyrite. *Geochimica et Cosmochimica Acta*, *49*, 1561–1566. http://doi.org/10.1016/0016-7037(85)90261-3

Kinniburgh, D., & Cooper, D. (2011). *PhreePlot Creating graphical output with PHREEQC*. http://www.phreeplot.org, last updated July 21, 2014.

Kirk, M. F., Holm, T. R., Park, J., Jin, Q., Sanford, R. A., Fouke, B. W., & Bethke, C. M. (2004). Bacterial sulfate reduction limits natural arsenic contamination in groundwater. *Geology*, *32*(11), 953–956. http://doi.org/10.1130/G20842.1

Kirk, M. F., Roden, E. E., Crossey, L. J., Brealey, A. J., & Spilde, M. N. (2010). Experimental analysis of arsenic precipitation during microbial sulfate and iron reduction in model aquifer sediment reactors. *Geochimica et Cosmochimica Acta*, *74*, 2538–2555. http://doi.org/10.1016/j.gca.2010.02.002

Kocar, B. D., Borch, T., & Fendorf, S. (2010). Arsenic repartitioning during biogenic sulfidization and transformation of ferrihydrite. *Geochimica et Cosmochimica Acta*, *74*, 980–994. http://doi.org/10.1016/j.gca.2009.10.023

Kocar, B. D., & Fendorf, S. (2012). Arsenic Release and Transport in Sediments of the Mekong Delta. *Environmental Pollution and Ecotoxicology*, 117–124.

Kocar, B. D., Polizzotto, M. L., Benner, S. G., Ying, S. C., Ung, M., Ouch, K., … Fendorf, S. (2008). Integrated biogeochemical and hydrologic processes driving arsenic release from shallow sediments to groundwaters of the Mekong delta. *Applied Geochemistry*, *23*(11), 3059–3071. http://doi.org/10.1016/j.apgeochem.2008.06.026

Konsten, C. J. M., Breemen, N. V, Suping, S., Aribawa, I. B., & Groenenberg, J. E. (1994). Effects of Flooding on pH of Rice-Producing, Acid Sulfate Soils in Indonesia. *Soil Sci. Soc. Am. J.*, *58*, 871–883. http://doi.org/10.2136/sssaj1994.03615995005800030035x

Koschorreck, M. (2008). Microbial sulphate reduction at a low pH. *FEMS Microbiology Ecology*, *64*, 329–342. http://doi.org/10.1111/j.1574-6941.2008.00482.x

Kroopnick, P., & Craig, H. (1976). Oxygen isotope fractionation in dissolved oxygen in the deep sea. *Earth and Planetary Science Letters*, *32*, 375–388. http://doi.org/10.1016/0012-821X(76)90078-9

Kumar, P., Avtar, R., Kumar, A., Singh, C. K., Tripathi, P., Senthil, K. G., & Ramanathan, A. L. (2014). Geophysical approach to delineate arsenic hot spots in the alluvial aquifers of Bhagalpur district, Bihar (India) in the central Gangetic plains. *Applied Water Science*, *4*, 89–97. http://doi.org/10.1007/s13201-013-0133-y

Lafferty, B. J., Ginder-Vogel, M., & Sparks, D. L. (2010). Arsenite oxidation by a poorly crystalline manganese-oxide 1. Stirred-flow experiments. *Environmental Science and*

Technology, *44*(22), 8460–8466. http://doi.org/10.1021/es102013p

Lafferty, B. J., Ginder-Vogel, M., & Sparks, D. L. (2011). Arsenite oxidation by a poorly-crystalline manganese oxide. 3. Arsenic and manganese desorption. *Environmental Science and Technology*, *45*(21), 9218–9223. http://doi.org/10.1021/es201281u

Lafferty, B. J., Ginder-Vogel, M., Zhu, M., Livi, K. J. T., & Sparks, D. L. (2010). Arsenite oxidation by a poorly crystalline manganese-oxide. 2. Results from X-ray absorption spectroscopy and X-ray diffraction. *Environmental Science and Technology*, *44*(22), 8467–8472. http://doi.org/10.1021/es102016c

Lamm, S. H., Engel, A., Penn, C. A., Chen, R., & Feinleib, M. (2006). Arsenic cancer risk confounder in Southwest Taiwan data set. *Environmental Health Perspectives*, *114*(7), 1077–1082. http://doi.org/10.1289/ehp.8704

Langner, P., Mikutta, C., & Kretzschmar, R. (2011). Arsenic sequestration by organic sulphur in peat. *Nature Geoscience*, *5*(1), 66–73. http://doi.org/10.1038/ngeo1329

Leblanc, M., Casiot, C., Bruneel, O., & Personne, J. (2004). Arsenic oxidation and bioaccumulation by the acidophilic protozoan, Euglena mutabilis, in acid mine drainage (Carnoules, France). *Science of the Total Environment*, *320*, 259–267. http://doi.org/10.1016/j.scitotenv.2003.08.004

Lin, N., Tang, J. I. E., & Bian, J. (2002). Characteristics of environmental geochsmistry in the arsneiasis area of the inner Mongolia of China. *Environmental Geochemistry and Health*, *24*, 249–259.

Lin, T. H., Huang, Y. L., & Wang, M. Y. (1998). Arsenic species in drinking water, hair, fingernails, and urine of patients with blackfoot disease. *Toxicology and Environmental Health A*, *53*, 85–93. http://doi.org/10.1080/009841098159376

Lin, W. C., Coppi, M. V, & Lovley, D. R. (2004). Geobacter sulfurreducens Can Grow with Oxygen as a Terminal Electron Acceptor Geobacter sulfurreducens Can Grow with Oxygen as a Terminal Electron Acceptor. http://doi.org/10.1128/AEM.70.4.2525

Lipfert, G., Sidle, W. C., Reeve, A. S., Ayuso, R. A., & Boyce, A. J. (2007). High arsenic concentrations and enriched sulfur and oxygen isotopes in a fractured-bedrock ground-water system. *Chemical Geology*, *242*, 385–399. http://doi.org/10.1016/j.chemgeo.2007.04.003

Liu, Z., Shen, J., Carbrey, J. M., Mukhopadhyay, R., Agre, P., & Rosen, B. P. (2002). Arsenite transport by mammalian aquaglyceroporins AQP7 and AQP9. *PNAS*, *99*(9), 6053–6058.

Lovley, D. R. (1987). Organic matter mineralization with the reduction of ferric iron: a review. *Geomicrobiology Journal*, *5*(3), 375–399.

Lovley, D. R., & Phillips, E. J. P. (1986). Organic Matter Mineralization with Reduction of Ferric Iron in Anaerobic Sediments. *Applied and Environmental Microbiology*, *51*(4), 683–689.

Lu, P., & Zhu, C. (2011). Arsenic Eh-pH diagrams at 25oC and 1 bar. *Environmental Earth Sciences*, *62*(8), 1673–1683. http://doi.org/10.1007/s12665-010-0652-x

Luu, T. T. G., Sthiannopkao, S., & Kim, K. W. (2009). Arsenic and other trace elements contamination in groundwater and a risk assessment study for the residents in the Kandal Province of Cambodia. *Environment International*, *35*(3), 455–460. http://doi.org/10.1016/j.envint.2008.07.013

Lynch, S. F. L., Batty, L. C., & Byrne, P. (2014). Environmental risk of metal mining contaminated river bank sediment at redox-transitional zones. *Minerals*, *4*, 52–73. http://doi.org/10.3390/min4010052

Lynd, L. R., Weimer, P. J., Willem, H. van Z., & Isak, P. S. (2002). Microbial Cellulose Utilization: Fundamentals and Biotechnology. *Microbiology and Molecular Biology Reviews*, *66*(3), 506–577. http://doi.org/10.1128/MMBR.66.3.506

Magu, S. C., Kirk, M. F., Daigle, A. R., Hinkle, S. R., & Jin, Q. (2015). Substantial contribution of

biomethylation to aquifer arsenic cycling. *Nature Geoscience*, 2–5. http://doi.org/10.1038/NGEO2383

Majumder, S., Nath, B., Sarkar, S., Chatterjee, D., Roman-Ross, G., & Hidalgo, M. (2014). Size-fractionation of groundwater arsenic in alluvial aquifers of West Bengal, India: the role of organic and inorganic colloids. *The Science of the Total Environment*, *468–469*, 804–12. http://doi.org/10.1016/j.scitotenv.2013.08.087

Mandal, B. K., & Suzuki, K. T. (2002). Arsenic round the world: a review. *Talanta*, *58*, 201–35.

Manning, B. A., & Goldberg, S. (1996a). Modeling arsnate competitive adsorption on kaolinite, monmorillonite and illite. *Clays and Clay Minerals*, *44*(5), 609–623.

Manning, B. A., & Goldberg, S. (1996b). Modeling Competitive Adsorption of Arsenate with Phosphate and Molybdate on Oxide Minerals. *Soil Sci. Soc. Am. J.*, *60*, 121–131.

MARD. (2016). *Subproject on enhancing the ability of adaptation and water management for the upper part of Bassac River in An Phu district An Giang province*.

Matschullat, J. (2000). Arsenic in the geosphere - A review. *Science of the Total Environment*, *249*(1–3), 297–312. http://doi.org/10.1016/S0048-9697(99)00524-0

Mazumdar, A., Goldberg, T., & Strauss, H. (2008). Abiotic oxidation of pyrite by Fe(III) in acidic media and its implications for sulfur isotope measurements of lattice-bound sulfate in sediments. *Chemical Geology*, *253*, 30–37. http://doi.org/10.1016/j.chemgeo.2008.03.014

McArthur, J. M., Banerjee, D. M., Hudson-Edwards, K. A., Mishra, R., Purohit, R., Ravenscroft, P., … Chadha, D. K. (2004). Natural organic matter in sedimentary basins and its relation to arsenic in anoxic ground water: the example of West Bengal and its worldwide implications. *Applied Geochemistry*, *19*, 1255–1293. http://doi.org/10.1016/j.apgeochem.2004.02.001

McGuire, M. M., & Hamers, R. J. (2000). Extraction and Quantitative Analysis of Elemental Sulfur from Sulfide Mineral Surfaces by High-Performance Liquid Chromatography. *Environmental Science & Technology*, *34*(21), 4651–4655. http://doi.org/10.1021/es0011663

Mcneill, J. D. (1990). *Use of Electromagnetic Methods for Groundwater Studies. Geotechnical and Environmental Geophysics* (Ward SN). Society of Exploration Geophysicists, Tulsa, UK.

Merola, R. B., Hien, T. T., Quyen, D. T. T., & Vengosh, A. (2015). Arsenic exposure to drinking water in the Mekong Delta. *Science of the Total Environment*, *511*, 544–552. http://doi.org/10.1016/j.scitotenv.2014.12.091

Métral, J., Charlet, L., Bureau, S., Mallik, S. B., Chakraborty, S., Ahmed, K. M., … van Geen, A. (2008). Comparison of dissolved and particulate arsenic distributions in shallow aquifers of Chakdaha, India, and Araihazar, Bangladesh. *Geochemical Transactions*, *9*. http://doi.org/10.1186/1467-4866-9-1

Molinari, A., Guadagnini, L., Marcaccio, M., Straface, S., Sanchez-Vila, X., & Guadagnini, A. (2013). Arsenic release from deep natural solid matrices under experimentally controlled redox conditions. *Science of the Total Environment*, *444*, 231–40. http://doi.org/10.1016/j.scitotenv.2012.11.093

Moon, G., Kim, D., Kim, H., Bokare, A. D., & Choi, W. (2014). Platinum-like Behavior of Reduced Graphene Oxide as a Cocatalyst on TiO_2 for the Efficient Photocatalytic Oxidation of Arsenite. *Environmental Science & Technology Letters*, *1*(2), 185–190. http://doi.org/10.1021/ez5000012

Morin, G., Wang, Y., Ona-Nguema, G., Juillot, F., Calas, G., Menguy, N., … Brown, G. E. (2009). EXAFS and HRTEM evidence for As(III)-containing surface precipitates on nanocrystalline magnetite: Implications for as sequestration. *Langmuir*, *25*(16), 9119–9128. http://doi.org/10.1021/la900655v

Moses, C. O., Kirk Nordstrom, D., Herman, J. S., & Mills, A. L. (1987). Aqueous pyrite oxidation by dissolved oxygen and by ferric iron. *Geochimica et Cosmochimica Acta*, *51*, 1561–1571.

http://doi.org/10.1016/0016-7037(87)90337-1

Muyzer, G., & Stams, A. J. M. (2008). The ecology and biotechnology of sulphate-reducing bacteria. *Nature Reviews. Microbiology*, *6*(6), 441–454. http://doi.org/10.1038/nrmicro1892

Nath, B., Mallik, S. B., Stüben, D., Chatterjee, D., & Charlet, L. (2010). Electrical resistivity investigation of the arsenic affected alluvial aquifers in West Bengal, India: Usefulness in identifying the areas of low and high groundwater arsenic. *Environmental Earth Sciences*, *60*(4), 873–884. http://doi.org/10.1007/s12665-009-0224-0

Ng, I.-S., Ndive, C. I., Zhou, Y., & Wu, X. (2015). Cultural optimization and metal effects of Shewanella xiamenensis BC01 growth and swarming motility. *Bioresources and Bioprocessing*, *2*(1), 28. http://doi.org/10.1186/s40643-015-0055-7

Ng, J. C., Wang, J., & Shraim, A. (2003). A global health problem caused by arsenic from natural sources. *Chemosphere*, *52*(9), 1353–9. http://doi.org/10.1016/S0045-6535(03)00470-3

Nguyen, K. P., & Itoi, R. (2009). Source and release mechanism of arsenic in aquifers of the Mekong Delta , Vietnam. *Journal of Contaminant Hydrology*, *103*, 58–69. http://doi.org/10.1016/j.jconhyd.2008.09.005

Nguyen, K. P., Itoi, R., & Nguyen, T. V. (2006). Arseniferous groundwater in relation with geochemical conditions , Mekong Delta , Vietnam Division of Hydrogeology and Engineering Geology for the south of Vietnam ,. In *Environment, Ecosystems and Development* (pp. 19–27).

Nguyen, V. L., Ta, T. K. O., & Tateishi, M. (2000). Late holocene depositional environments and coastal evolution of the Mekong River Delta, Southern Vietnam. *Journal of Asian Earth Sciences*, *18*(4), 427–439. http://doi.org/10.1016/S1367-9120(99)00076-0

Nickson, R. T., Mcarthur, J. M., Ravenscroft, P., Burgess, W. G., & Ahmed, K. M. (2000). Mechanism of arsenic release to groundwater, Bangladesh and West Bengal. *Applied Geochemistry*, *15*(4), 403–413. http://doi.org/10.1016/S0883-2927(99)00086-4

Nicolli, H. B., Suriano, J. M., Gomez Peral, M. A., Ferpozzi, L. H., & Baleani, O. A. (1989). Groundwater contamination with arsenic and other trace elements in an area of the pampa, province of Cordoba, Argentina. *Environmental Geology and Water Sciences*, *14*(1), 3–16. http://doi.org/10.1007/BF01740581

Nordstrom, D. K., Majzlan, J., & Königsberger, E. (2014). Thermodynamic Properties for Arsenic Minerals and Aqueous Species. *Mineralogy & Geochemistry*, *79*, 217–255.

O'Day, P. a, Vlassopoulos, D., Root, R., & Rivera, N. (2004). The influence of sulfur and iron on dissolved arsenic concentrations in the shallow subsurface under changing redox conditions. *Proceedings of the National Academy of Sciences of the United States of America*, *101*(38), 13703–8. http://doi.org/10.1073/pnas.0402775101

Ona-Nguema, G., Morin, G., Juillot, F., Calas, G., & Brown Jr, G. E. (2005). EXAFS Analysis of Arsenite Adsorption onto Two-Line Ferrihydrite, Hematite, Goethite, and Lepidocrocite. *Environmental Science and Technology*, *39*, 9147–9155.

Ona-Nguema, G., Morin, G., Wang, Y., Menguy, N., Juillot, F., Olivi, L., … Brown, G. E. (2009). Arsenite sequestration at the surface of nano-Fe(OH)2, ferrous-carbonate hydroxide, and green-rust after bioreduction of arsenic-sorbed lepidocrocite by Shewanella putrefaciens. *Geochimica et Cosmochimica Acta*, *73*(5), 1359–1381. http://doi.org/10.1016/j.gca.2008.12.005

Oremland, R. S. (2003). The Ecology of Arsenic. *Science*, *300*, 939–944. http://doi.org/10.1126/science.1081903

Paktunc, D., & Bruggeman, K. (2010). Solubility of nanocrystalline scorodite and amorphous ferric arsenate: Implications for stabilization of arsenic in mine wastes. *Applied Geochemistry*, *25*(5), 674–683. http://doi.org/10.1016/j.apgeochem.2010.01.021

Pal, A., Saha, S., Maji, S. K., Kundu, M., & Kundu, A. (2012). Wet-chemical synthesis of spherical arsenic nanoparticles by a simple reduction method and its characterization. *Advanced Materials Letters*, *3*(3), 177–180. http://doi.org/10.5185/amlett.2011.9305

Parkhurst, B. D. L., & Appelo, C. A. J. (n.d.). USER'S GUIDE TO PHREEQC (VERSION 2)—A COMPUTER PROGRAM FOR SPECIATION, AND INVERSE GEOCHEMICAL CALCULATIONS, (Version 2).

Parkhurst, B. D. L., & Appelo, C. A. J. (1999). *User's guide to PhreeqC (Version 2) - A computer program for speciation, batch-reaction, one-dimensional transport, and inverse geochemical calculations*. U.S. Department of the Interior, U.S. Geological Survey.

Parsons, C. (2011). *Distribution et mobilité de l'arsenic dans les sols: Effets de cycles redox successifs*. *PhD Thesis, UJF*.

Parsons, C. T., Couture, R.-M., Omoregie, E. O., Bardelli, F., Greneche, J.-M., Roman-Ross, G., & Charlet, L. (2013). The impact of oscillating redox conditions: Arsenic immobilisation in contaminated calcareous floodplain soils. *Environmental Pollution*, *178*, 254–63. http://doi.org/10.1016/j.envpol.2013.02.028

Peine, A., Tritschler, A., & Ku, K. (2000). Electron flow in an iron-rich acidic sediment — evidence for an acidity-driven iron cycle. *Limnology and Oceanography*, *45*(5), 1077–1087.

Pellerin, L. (2002). Applications of electrical and electromagnetic methods for environmental and geotechnical investigations. *Surveys in Geophysics*, *23*, 101–132. http://doi.org/10.1023/A:1015044200567

Pettersson, J. K., & Nobes, D. C. (2003). Environmental geophysics at Scott Base: Ground penetrating radar and electromagnetic induction as tools for mapping contaminated ground at Antarctic research bases. *Cold Regions Science and Technology*, *37*(2), 187–195. http://doi.org/10.1016/S0165-232X(03)00037-5

Pili, É., Perrier, F., & Richon, P. (2004). Dual porosity mechanism for transient groundwater and gas anomalies induced by external forcing. *Earth and Planetary Science Letters*, *227*, 473–480. http://doi.org/10.1016/j.epsl.2004.07.043

Pili, E., Tisserand, D., & Bureau, S. (2013). Origin, mobility, and temporal evolution of arsenic from a low-contamination catchment in Alpine crystalline rocks. *Journal of Hazardous Materials*, *262*, 887–895. http://doi.org/10.1016/j.jhazmat.2012.07.004

Planer-Friedrich, B., London, J., McCleskey, R. B., Nordstrom, D. K., & Wallschläger, D. (2007). Thioarsenates in geothermal waters of Yellowstone National Park: determination, preservation, and geochemical importance. *Environmental Science & Technology*, *41*(15), 5245–51.

Planer-Friedrich, B., Suess, E., Scheinost, A. C., & Wallschläger, D. (2010). Arsenic speciation in sulfidic waters: reconciling contradictory spectroscopic and chromatographic evidence. *Analytical Chemistry*, *82*(24), 10228–35. http://doi.org/10.1021/ac1024717

Planer-Friedrich, B., & Wallschläger, D. (2009a). A critical investigation of hydride generation-based arsenic speciation in sulfidic waters. *Environmental Science & Technology*, *43*(13), 5007–13.

Planer-Friedrich, B., & Wallschläger, D. (2009b). A critical investigation of hydride generation-based arsenic speciation in sulfidic waters. *Environmental Science & Technology*, *43*(13), 5007–13. Retrieved from http://www.ncbi.nlm.nih.gov/pubmed/19673299

Pokorna, D., & Zabranska, J. (2015). Sulfur-oxidizing bacteria in environmental technology. *Biotechnology Advances*, *33*(6), 1246–1259. http://doi.org/10.1016/j.biotechadv.2015.02.007

Polizzotto, M. L., Harvey, C. F., Sutton, S. R., & Fendorf, S. (2005). Processes conducive to the release and transport of arsenic into aquifers of Bangladesh. *Proceedings of the National Academy of Sciences*, *102*(52), 18819–18823.

Ponnamperuma, F. N. (1972). The Chemistry of Submerged Soils. *Advances in Agronomy*, *24*, 29–96. http://doi.org/10.1016/S0065-2113(08)60633-1

Post, J. L., & Sloane, R. L. (1971). The nature of clay soils from the Mekong Delta, An Giang province, South Vietnam. *Clays and Clay Minerals*, *19*, 21–29.

Postma, D. (1983). Pyrite and siderite oxidation in swamp sediments. *Soil Science*, *34*, 163–182.

Postma, D., Larsen, F., Minh Hue, N. T., Duc, M. T., Viet, P. H., Nhan, P. Q., & Jessen, S. (2007). Arsenic in groundwater of the Red River floodplain, Vietnam: Controlling geochemical processes and reactive transport modeling. *Geochimica et Cosmochimica Acta*, *71*(21), 5054–5071. http://doi.org/10.1016/j.gca.2007.08.020

Postma, D., Thi, N., Hue, M., & Thanh, M. (2010). Mobilization of arsenic and iron from Red River floodplain sediments , Vietnam. *Geochemical Transactions*, *74*, 3367–3381. http://doi.org/10.1016/j.gca.2010.03.024

Poulton, S. W., Krom, M. D., & Raiswell, R. (2004). A revised scheme for the reactivity of iron (oxyhydr) oxide minerals towards dissolved sulfide. *Geochimica et Cosmochimica Acta*, *68*(18), 3703–3715. http://doi.org/10.1016/j.gca.2004.03.012

Raab, A., Meharg, A. A., Jaspars, M., & Genney, R. (2004). Arsenic–glutathione complexes - their stability in solution and during separation by different HPLC modes. *Journal of Analytical Atomic Spectrometry*, *19*, 183–190.

Raiswell, R., & Berner, R. a. (1985). Pyrite formation in euxinic and semi-euxinic sediments. *American Journal of Science*. http://doi.org/10.2475/ajs.285.8.710

Ratnaike, R. N. (2003). Acute and chronic arsenic toxicity. *Postgraduate Medical Journal*, *79*(933), 391–396.

Rault, A., Bouix, M., & Béal, C. (2009). Fermentation pH influences the physiological-state dynamics of Lactobacillus bulgaricus CFL1 during pH-controlled culture. *Applied and Environmental Microbiology*, *75*(13), 4374–4381. http://doi.org/10.1128/AEM.02725-08

Ravel, B., & Newville, M. (2005). Athena, Artemis, Hephaestus: Data analysis for X-ray absorption spectroscopy using Ifeffit. *Journal of Synchrotron Radiation*, *12*(4), 537–541. http://doi.org/10.1107/S0909049505012719

Regenspurg, S., Brand, A., & Peiffer, S. (2004). Formation and stability of schwertmannite in acidic mining lakes. *Geochimica et Cosmochimica Acta*, *68*(6), 1185–1197. http://doi.org/10.1016/j.gca.2003.07.015

Rhine, E. D. (2005). Environmental Microbes Can Speciate and Cycle Arsenic. *Environmental Science & Technology*, *39*(24), 9569–9573.

Richardson, J. L., & Vepraskas, M. J. (2001). *Wetland soils: Genesis, hydrology, landscapes and classification*. Lewis.

Rickard, D. (2006). The solubility of FeS. *Geochimica et Cosmochimica Acta*, *70*(23), 5779–5789. http://doi.org/10.1016/j.gca.2006.02.029

Rickard, D., & Iii, G. W. L. (2007). Chemistry of Iron Sulfides. *Chem. Rev*, *44*, 514–562.

Rickard, D., & Morse, J. W. (2005). Acid volatile sulfide (AVS). *Marine Chemistry*, *97*, 141–197. http://doi.org/10.1016/j.marchem.2005.08.004

Rigby, P. A., Dobos, S. K., Cook, F. J., & Goonetilleke, A. (2006). Role of organic matter in framboidal pyrite oxidation. *Science of the Total Environment*, *367*, 847–854. http://doi.org/10.1016/j.scitotenv.2004.10.011

Robertson, F. N. (1988). Arsenic in groundwater under oxidizing, south-west United States. *Environmental Geochemistry and Health*, *11*, 171–185.

Rochette, E. A., Bostick, B. C., Li, G., & Fendorf, S. (2000). Kinetics of arsenate reduction by dissolved sulfide. *Environmental Science and Technology*, *34*(22), 4714–4720.

http://doi.org/10.1021/es000963y

Román-Ross, G., Cuello, G. J., Turrillas, X., Fernández-Martínez, A., & Charlet, L. (2006). Arsenite sorption and co-precipitation with calcite. *Chemical Geology*, *233*, 328–336. http://doi.org/10.1016/j.chemgeo.2006.04.007

Root, R. A., Dixit, S., Campbell, K. M., Jew, A. D., Hering, J. G., & O'Day, P. A. (2007). Arsenic sequestration by sorption processes in high-iron sediments. *Geochimica et Cosmochimica Acta*, *71*, 5782–5803. http://doi.org/10.1016/j.gca.2007.04.038

Root, R. A., Vlassopoulos, D., Rivera, N. A., Rafferty, M. T., Andrews, C., & O'Day, P. A. (2009). Speciation and natural attenuation of arsenic and iron in a tidally influenced shallow aquifer. *Geochimica et Cosmochimica Acta*, *73*(19), 5528–5553. http://doi.org/10.1016/j.gca.2009.06.025

Sasaki, K., Tsunekawa, M., Ohtsuka, T., & Konno, H. (1995). Confirmation of a sulfur-rich layer on pyrite after oxidative dissolution by Fe(lll) ions around pH 2. *Geochimica et Cosmochimica Acta*, *59*(15), 3155–3158. http://doi.org/10.1016/0016-7037(95)00203-C

Scheinost, A. C., Kirsch, R., Banerjee, D., & Fernandez-martinez, A. (2008). X-ray absorption and photoelectron spectroscopy investigation of selenite reduction by Fe(II)-bearing minerals. *Contaminant Hydrology*, *102*, 228–245. http://doi.org/10.1016/j.jconhyd.2008.09.018

Schellenberger, S., Drake, H. L., & Kolb, S. (2011). Functionally redundant cellobiose-degrading soil bacteria respond differentially to oxygen. *Applied and Environmental Microbiology*, *77*(17), 6043–8. http://doi.org/10.1128/AEM.00564-11

Schreiber, M. E., Simo, J. a., & Freiberg, P. G. (2000). Stratigraphic and geochemical controls on naturally occurring arsenic in groundwater, eastern Wisconsin, USA. *Hydrogeology Journal*, *8*(2), 161–176. http://doi.org/10.1007/s100400050003

Schwedt, G., & Rieckhoff, M. (1996). Separation of thio- and oxothioarsenates by capillary zone electrophoresis and ion chromatography. *Journal of Chromatography A*, *736*, 341–350. http://doi.org/10.1016/0021-9673(95)01319-9

Scott, M. J., & Morgan, J. J. (1995). Reactions at oxide surfaces. 1. Oxidation of As(III) by synthetic Birnessite. *Environmental Science & Technology*, *29*(8), 1898–1905. http://doi.org/10.1021/es00008a006

Servin, J. A., Herbold, C. W., Skophammer, R. G., & Lake, J. A. (2008). Evidence excluding the root of the tree of life from the Actinobacteria. *Molecular Biology and Evolution*, *25*(1), 1–4. http://doi.org/10.1093/molbev/msm249

Shankar, S., Shanker, U., & Shikha. (2014). Arsenic Contamination of Groundwater : A Review of Sources, Prevalence, Health Risks, and Strategies for Mitigation. *The Scientific World Journal*, 1–18.

Shinkai, Y., Truc, D. Van, Sumi, D., Canh, D., & Kumagai, Y. (2007). Arsenic and Other Metal Contamination of Groundwater in the Mekong River Delta, Vietnam. *Journal of Health Science*, *53*(3), 344–346. http://doi.org/10.1248/jhs.53.344

Shraim, A., Sekaran, N. C., Anuradha, C. D., & Hirano, S. (2002). Speciation of arsenic in tube-well water samples collected from West Bengal, India, by high-performance liquid chromatography-inductively coupled plasma mass spectrometry. *Applied Organometallic Chemistry*, *16*, 202–209. http://doi.org/10.1002/aoc.279

Shumlas, S. L., Singireddy, S., Thenuwara, A. C., Attanayake, N. H., Reeder, R. J., & Strongin, D. R. (2016). Oxidation of arsenite to arsenate on birnessite in the presence of light. *Geochemical Transactions*, *17*(1), 5. http://doi.org/10.1186/s12932-016-0037-5

Singer, P. C., & Stumm, W. (1970). Acidic Mine Drainage: The rate-determining step. *Science*, *167*, 1121–1123.

Smedley, P. L., & Kinniburgh, D. G. (2002). A review of the source, behaviour and distribution of

arsenic in natural waters. *Applied Geochemistry*, *17*(5), 517–568. http://doi.org/10.1016/S0883-2927(02)00018-5

Smith, A. H., Ercumen, A., Yuan, Y., & Steinmaus, C. M. (2009). Increased lung cancer risks are similar whether arsenic is ingested or inhaled. *J Expo Sci Environ Epidemiol*, *19*(4), 343–348. http://doi.org/10.1038/jes.2008.73

Smith, A. H., Hopenhayn-Rich, C., Bates, M. N., Goeden, H. M., Hertz-Picciotto, I., Duggan, H. M., … Smith, M. T. (1992). Cancer risks from arsenic in drinking water. *Environmental Health Perspectives*, *97*(6), 259–267. http://doi.org/10.1289/ehp.9297259

Snoeyenbos-West, O. L., Nevin, K. P., Anderson, R. T., & Lovley, D. R. (2000). Enrichment of Geobacter species in response to stimulation of Fe(III) reduction in sandy aquifer sediments. *Microbial Ecology*, *39*(2), 153–167. http://doi.org/10.1007/s002480000018

SØ, H. U., Postma, D., Jakobsen, R., & Larsen, F. (2008). Sorption and desorption of arsenate and arsenite on calcite. *Geochimica et Cosmochimica Acta*, *72*(24), 5871–5884. http://doi.org/10.1016/j.gca.2008.09.023

Stanger, G., Truong, T. Van, Ngoc, K. S. L. T. M., Luyen, T. V, & Thanh, T. T. (2005). Arsenic in groundwaters of the Lower Mekong. *Environmental Geochemistry and Health*, *27*(4), 341–57. http://doi.org/10.1007/s10653-005-3991-x

Stempvoort, D. R. Van, & Krouse, H. R. (1994). *Chapter 29: Controls of δ18O in Sulfate: Review of Experimental data and application to specific environments*. American Chemical Society.

Steudel, R. (1989). *Chapter 16On the nature of the elemental sulfur produced by sulfur oxidising bacteria - a model for S(0) globules*. (H. G. S. and B. Bowien, Ed.). Science Technology Publication, Madison, USA. http://doi.org/10.1142/S0217751X11052062

Steudel, R. (1996). Mechanism for the Formation of Elemental Sulfur from Aqueous Sulfide in Chemical and Microbiological Desulfurization Processes. *Industrial & Engineering Chemistry Research*, *35*(4), 1417–1423. http://doi.org/10.1021/ie950558t

Stookey, L. L. (1970). Ferrozine-a new spectrophotometric reagent for iron. *Analytical Chemistry*, *42*(7), 779–781. http://doi.org/10.1021/ac60289a016

Stuckey, J. W., Schaefer, M. V, Benner, S. G., & Fendorf, S. (2015). Reactivity and speciation of mineral-associated arsenic in seasonal and permanent wetlands of the Mekong Delta. *Geochimica et Cosmochimica Acta*, *171*, 143–155. http://doi.org/10.1016/j.gca.2015.09.002

Stuckey, J. W., Schaefer, M. V, Kocar, B. D., Benner, S. G., & Fendorf, S. (2015). Arsenic release metabolically limited to permanently water-saturated soil in Mekong Delta. *Nature Geoscience*, *8*, 1–9. http://doi.org/10.1038/NGEO2589

Stuckey, J. W., Schaefer, M. V, Kocar, B. D., Dittmar, J., Lezama, J., Benner, S. G., & Fendorf, S. (2015). Peat formation concentrates arsenic within sediment deposits of the Mekong Delta. *Geochimica et Cosmochimica Acta*, *149*, 190–205. http://doi.org/10.1016/j.gca.2014.10.021

Suess, E., Scheinost, A. C., Bostick, B. C., Merkel, B. J., Wallschlaeger, D., & Planer-Friedrich, B. (2009). Discrimination of thioarsenites and thioarsenates by X-ray absorption spectroscopy. *Analytical Chemistry*, *81*(20), 8318–26. http://doi.org/10.1021/ac901094b

Suess, E., Wallschläger, D., & Planer-Friedrich, B. (2011). Stabilization of thioarsenates in iron-rich waters. *Chemosphere*, *83*(11), 1524–31. http://doi.org/10.1016/j.chemosphere.2011.01.045

Tabbagh, A., & Panissod, C. (2002). Numerical modeling of the role of water and clay content in soils' and rocks' bulk electrical conductivity. *Journal of Geophysical Research*, *107*, 1–9. http://doi.org/10.1029/2000JB000025

Takeshita, T., Tanaka, K., Ishizaki, A., & Stanbury, P. F. (1993). Development of a dissolved hydrogen sensor and its application to evaluation of hydrogen mass transfer. *Journal of Fermentation and Bioengineering*, *76*(2), 148–150. http://doi.org/10.1016/0922-

338X(93)90073-H

Tamura, T., Saito, Y., Sieng, S., Ben, B., Kong, M., Choup, S., & Tsukawaki, S. (2007). Depositional facies and radiocarbon ages of a drill core from the Mekong River lowland near Phnom Penh, Cambodia: Evidence for tidal sedimentation at the time of Holocene maximum flooding. *Journal of Asian Earth Sciences*, *29*, 585–592. http://doi.org/10.1016/j.jseaes.2006.03.009

Taylor, B. E., Wheeler, M. C., & Nordstrom, D. K. (1984). Stable isotope geochemistry of acid mine drainage: Experimental oxidation of pyrite. *Geochimica et Cosmochimica Acta*, *48*(12), 2669–2678. http://doi.org/10.1016/0016-7037(84)90315-6

Thompson, A., Chadwick, O. A., Rancourt, D. G., & Chorover, J. (2006). Iron-oxide crystallinity increases during soil redox oscillations. *Geochimica et Cosmochimica Acta*, *70*(7), 1710–1727. http://doi.org/10.1016/j.gca.2005.12.005

Thurston, R. S., Mandernack, K. W., & Shanks, W. C. (2010). Laboratory chalcopyrite oxidation by Acidithiobacillus ferrooxidans: Oxygen and sulfur isotope fractionation. *Chemical Geology*, *269*, 252–261. http://doi.org/10.1016/j.chemgeo.2009.10.001

Tisserand, D., Pili, E., Hellmann, R., Boullier, A., & Charlet, L. (2014). Geogenic arsenic in groundwaters in the western Alps. *Journal of Hydrology*, *518*, 317–325. http://doi.org/10.1016/j.jhydrol.2013.06.023

Tran, A. T., Tran, K. T., & Vo, Q. M. (2011). Investigating sources of arsenic contamination in groundwater in An Phu district, An Giang province. *Journal of Science (Can Tho University, Vietnam)*, *17a*, 118–123.

Tseng, W. P. (1977). Effects and dose response relationships of skin cancer and blackfoot disease with arsenic. *Environmental Health Perspectives*, *19*, 109–119. http://doi.org/10.1289/ehp.7719109

Van Geen, A., Ahsan, H., Horneman, A. H., Dhar, R. K., Zheng, Y., Hussain, I., … Graziano, J. H. (2002). Promotion of well-switching to mitigate the current arsenic crisis in Bangladesh. *Bulletin of the World Health Organization*, *80*(9), 732–7.

van Geen, A., Aziz, Z., Horneman, A., Weinman, B., Dhar, R. K., Zheng, Y., … Ahmed, K. . (2006). Preliminary evidence of a link between surface soil properties and the arsenic content of shallow groundwater in Bangladesh. *Journal of Geochemical Exploration*, *88*, 157–161. http://doi.org/10.1016/j.gexplo.2005.08.106

van Geen, A., Bostick, B. C., Pham, T. K. T., Vi, M. L., Nguyen-Ngoc, M., Phu, D. M., … Berg, M. (2013). Retardation of arsenic transport through a Pleistocene aquifer. *Nature*, *501*(7466), 204–7. http://doi.org/10.1038/nature12444

van Geen, A., Radloff, K., Aziz, Z., Cheng, Z., Huq, M. R., Ahmed, K. M., … Upreti, B. N. (2008). Comparison of arsenic concentrations in simultaneously-collected groundwater and aquifer particles from Bangladesh, India, Vietnam, and Nepal. *Applied Geochemistry*, *23*(11), 3019–3028. http://doi.org/10.1016/j.apgeochem.2008.07.005

van Geen, A., Zheng, Y., Stute, M., & Ahmed, K. M. (2003). Comment on "Arsenic Mobility and Groundwater Extraction in Bangladesh" (II). *Science*, *300*, 584. http://doi.org/10.1126/science.1081057

Vaningelgem, F., Zamfir, M., Adriany, T., & De Vuyst, L. (2004). Fermentation conditions affecting the bacterial growth and exopolysaccharide production by Streptococcus thermophilus ST 111 in milk-based medium. *Journal of Applied Microbiology*, *97*(6), 1257–1273. http://doi.org/10.1111/j.1365-2672.2004.02418.x

Vega, L., Styblo, M., Patterson, R., Cullen, W., Wang, C., & Germolec, D. (2001). Differential effects of trivalent and pentavalent arsenicals on cell proliferation and cytokine secretion in normal human epidermal keratinocytes. *Toxicology and Applied Pharmacology*, *172*(3), 225–232. http://doi.org/10.1006/taap.2001.9152

Villa-Bellosta, R., & Sorribas, V. (2008). Role of rat sodium/phosphate cotransporters in the cell membrane transport of arsenate. *Toxicology and Applied Pharmacology*, *232*, 125–134. http://doi.org/10.1016/j.taap.2008.05.026

Violante, A., Ricciardella, M., Gaudio, S. D., & Pigna, M. (2006). Coprecipitation of Arsenate with Metal Oxides: Nature, Mineralogy, and Reactivity Aluminum Precipitates. *Environmental Science and Technology*, *40*, 4961–4967.

Viollier, E., Inglett, P. W., Hunter, K., Roychoudhury, A. N., & Van Cappellen, P. (2000). The ferrozine method revisited: Fe(II)/Fe(III) determination in natural waters. *Applied Geochemistry*, *15*(6), 785–790. http://doi.org/10.1016/S0883-2927(99)00097-9

Wan, M., Shchukarev, A., Lohmayer, R., Planer-friedrich, B., & Pei, S. (2014). Occurrence of surface polysulfides during the interacrion betwwen Ferric (hydr)Oxides and Aqueous Sulfide. *Environmental Science & Technology*, *48*(9), 5076–5084.

Wang, Y., Morin, G., Ona-Nguema, G., Juillot, F., Calas, G., & Brown, G. E. (2011). Distinctive arsenic(V) trapping modes by magnetite nanoparticles induced by different sorption processes. *Environmental Science and Technology*, *45*(17), 7258–7266. http://doi.org/10.1021/es200299f

Wang, Y., Morin, G., Ona-Nguema, G., Menguy, N., Juillot, F., Aubry, E., … Brown, G. E. (2008). Arsenite sorption at the magnetite-water interface during aqueous precipitation of magnetite: EXAFS evidence for a new arsenite surface complex. *Geochimica et Cosmochimica Acta*, *72*(11), 2573–2586. http://doi.org/10.1016/j.gca.2008.03.011

Wang, Y., Pape, P. Le, Morin, G., Suvorova, E., Bártová, B., Asta, M. P., … Bernier-Latmani, R. (n.d.). A carbon nanotube-associated arsenic phosphate in Mekong Delta sediments. *Nature Geonature*.

Welch, A. H., & Lico, M. S. (1998). Factors controlling As and U in shallow ground water, southern Carson Desert, Nevada. *Applied Geochemistry*, *13*(4), 521–539. http://doi.org/10.1016/S0883-2927(97)00083-8

Welch, A. H., & Stollenwerk, K. G. (2003). *Arsenic thermodynamic data and environmental geochemistry*. *Kluwer Academic Publishers*. Kluwer Academic. http://doi.org/10.1007/b101867

Weller, U., Zipprich, M., Sommer, M., Castell, W. Z., & Wehrhan, M. (2007). Mapping Clay Content across Boundaries at the Landscape Scale with Electromagnetic Induction. *Soil Science Society of America Journal*, *71*(6), 1740. http://doi.org/10.2136/sssaj2006.0177

WHO. (2004). *Some Drinking-water disinfectants and Contaminants, including Arsenic* (Vol. 83).

Wigley, T. M. L. (1973). Chemical Evolution of the System Calcite–Gypsum–Water. *Canadian Journal of Earth Sciences*, *10*, 306–315. http://doi.org/10.1139/e73-027

Wilkin, R. T., Wallschla, D., & Ford, R. G. (2003). Speciation of arsenic in sulfidic waters. *Geochemical Transactions*, *4*(1), 1–7. http://doi.org/10.1039/b211188h

Willems, A., Busse, J., Goor, M., Pot, B., Falsen, E., Jantzen, E., … Gillis, M. (1989). Hydrogenophaga, a New Genus of Hydrogen-Oxidizing Bacteria that Includes Hydrogenophaga flava comb. nov. (Formerly Pseudomonas flava), Hydrogenophaga palleronii (Formerly Pseudomonas palleronii), Hydrogenophaga pseudoflava (Formerly Pseudomonas pseudofla . *Systematic Bacteriology*, *39*(3), 319–333.

Winkel, L. H. E., Trang, P., Vi, L., Stengel, C., Amini, M., Nguyen, H., … Berg, M. (2010). Arsenic pollution of groundwater in Vietnam exacerbated by deep aquifer exploitation for more than a century. *PNAS*, *108*(4), 1246–1251. http://doi.org/10.1073/pnas.1011915108/-/DCSupplemental.www.pnas.org/cgi/doi/10.1073/pnas.1011915108

Wirsen, C. O., Sievert, S. M., Cavanaugh, C. M., Molyneaux, S. J., Ahmad, A., Taylor, L. T., … Taylor, C. D. (2002). Characterization of an Autotrophic Sulfide-Oxidizing Marine Arcobacter sp . That Produces Filamentous Sulfur. *Applied and Environmental Microbiology*,

68(1), 316–325. http://doi.org/10.1128/AEM.68.1.316

Wolf, J. B. W. (2013). Principles of transcriptome analysis and gene expression quantification: An RNA-seq tutorial. *Molecular Ecology Resources*, *13*(4), 559–572. http://doi.org/10.1111/1755-0998.12109

Wolthers, M., Charlet, L., van Der Linde, P. R., Rickard, D., & van Der Weijden, C. H. (2005). Surface chemistry of disordered mackinawite (FeS). *Geochimica et Cosmochimica Acta*, *69*(14), 3469–3481. http://doi.org/10.1016/j.gca.2005.01.027

Wolthers, M., Charlet, L., van Der Weijden, C. H., van der Linde, P. R., & Rickard, D. (2005). Arsenic mobility in the ambient sulfidic environment: Sorption of arsenic(V) and arsenic(III) onto disordered mackinawite. *Geochimica et Cosmochimica Acta*, *69*(14), 3483–3492. http://doi.org/10.1016/j.gca.2005.03.003

Xu, H., Allard, B., & Grimvall, A. (1988). Influence of pH and organic substance on the adsorption on As(V) on geologic materials. *Water Air Soil Pollution*, *40*, 293–305.

Xu, Y., Itzek, A., & Kreth, J. (2014). Comparison of genes required for H2O2 resistance in Streptococcus gordonii and Streptococcus sanguinis. *Microbiology*, *160*(12), 2627–2638. http://doi.org/10.1099/mic.0.082156-0

Yacob, T., Pandey, S., Silverstein, J., & Rajaram, H. (2013). Soluble microbial products decrease pyrite oxidation by ferric iron at pH < 2. *Environmental Science and Technology*, *47*(15), 8658–8665. http://doi.org/10.1021/es400828g

Yadav, V. K., & Archer, D. B. (1989). Sodium molybdate inhibits sulphate reduction in the anaerobic treatment of high-sulphate molasses wastewater. *Applied Microbiology and Biotechnology*, *31*(1), 103–106. http://doi.org/10.1007/BF00252537

Yaginuma, H., Kawai, S., Tabata, K. V, Tomiyama, K., Kakizuka, A., Komatsuzaki, T., … Imamura, H. (2014). Diversity in ATP concentrations in a single bacterial cell population revealed by quantitative single-cell imaging. *Science Report*, *4*(6522). http://doi.org/10.1038/srep06522

Ying, S. C., Damashek, J., Fendorf, S., & Francis, C. A. (2015). Indigenous arsenic (V) -reducing microbial communities in redox-fluctuating near-surface sediments of the Mekong Delta. *Geobiology*. http://doi.org/10.1111/gbi.12152

Zhang, G., Sun, M., Liu, Y., Lang, X., Liu, L., Liu, H., … Li, J. (2015). Visible-light induced photocatalytic activity of electrospun-TiO2 in arsenic(III) oxidation. *Applied Materials and Interfaces*, *7*(1), 511–518. http://doi.org/10.1021/am506640k

Zhang, H., & Selim, H. M. (2008). *Reaction and transport of arsenic in soils: Equilibrium and kinetic modeling*. *Advances in Agronomy*. http://doi.org/10.1016/S0065-2113(08)00202-2

Zheng, Y., Stute, M., Geen, A. Van, Gavrieli, I., & Dhar, R. (2004). Redox control of arsenic mobilization in Bangladesh groundwater. *Applied Geochemistry*, *19*, 201–214. http://doi.org/10.1016/j.apgeochem.2003.09.007

Zhu, J., Pigna, M., Cozzolino, V., Caporale, A. G., & Violante, A. (2011). Sorption of arsenite and arsenate on ferrihydrite: Effect of organic and inorganic ligands. *Journal of Hazardous Materials*, *189*, 564–571. http://doi.org/10.1016/j.jhazmat.2011.02.071

Zhu, Y.-G., Yoshinaga, M., Zhao, F.-J., & Rosen, B. P. (2014). Earth Abides Arsenic Biotransformations. *Annual Review of Earth and Planetary Sciences*, *42*(1), 443–467. http://doi.org/10.1146/annurev-earth-060313-054942

Zhu, Y., Yoshinaga, M., Zhao, F., & Rosen, B. P. (2014). Earth Abides Arsenic Biotransformations. *Annual Reviews*. http://doi.org/10.1146/annurev-earth-060313-054942

List of Figures

List of Tables

Curriculum vitae

Thi Hai Van PHAN

Institute of Earth Science (ISTerre)
University of Grenoble-Alpes, Grenoble
BP 53, 38041 Grenoble Cedex 9, France
Email: phanhaivan@gmail.com; thi-hai-van.phan@univ-grenoble-alpes.fr
Tel: +33 7 81 56 66 52

CIVIL STATUS

Family status	: Married (1 child)
Nationality	: Vietnamese
Date of birth	: 25 January 1984
Place of birth	: Buon Ma Thuot, Vietnam

EDUCATION

2013 – 2017 **PhD in Geochemistry**- Institute of Earth Science**,** University of Grenoble-Alpes (UGA), France
Advisors: Prof. Laurent Charlet and Prof. Rizlan Bernier-Latmani
Dissertation title: Mechanism of Arsenic release in the Southeast Asia: Mekong Delta Vietnam

2007 – 2009 **Master in Environmental Technology -** Faculty of Environment and Natural Resources**,** Ho Chi Minh City University of Technology, Vietnam
Advisor: Dr. Nguyen Phuoc Dan
Dissertation title: Removal of organic in raw water using advanced oxidation processes (AOPs) and biological activated carbon (BAC).

2002 – 2007 **Bachelor in Environmental Engineering -** Faculty of Environment and Natural Resources**,** Ho Chi Minh City University of Technology, Vietnam
Dissertation title: Removal of Arsenic in groundwater using sand filters and iron(III) phosphate

PROFESSIONAL EXPERIENCE

2013 - 2017 **PhD Researcher** - Institute of Earth Science (ISTerre)**,** University of Grenoble-Alpes (UGA), France

- Biogeochemistry of As, Fe and S to investigate mechanism of As him/mobilization during redox oscillations induced microbial sulfate reduction
- Focusing on aqueous analysis (ICP-AES, IC, HPLC-UV (Grenoble), solid phase analysis (XRD, XAS) (Grenoble, Trieste), and genomic analysis (16S

rRNA) (Lausanne, Switzerland)

2008 – 2013 **Lecturer -** Faculty of Environment and Natural Resources - Ho Chi Minh University of Technology, Vietnam

- Focusing on advanced oxidation technologies on water, wastewater treatment processes
- Working on wetlands roof project collaborated with Korean Environment Corporation (KECO)
- Joining into a research for application of wetlands roof for domestic wastewater treatment: A solution for climate change mitigation
- Working on a project for market survey on Ceramic Membrane Water Treatment System in Mekong Delta and Southeast Region in Vietnam

2007 - 2008 **Environmental Engineer -** TRACODI Ltd. – Ho Chi Minh City, Vietnam
Work on the wastewater treatment plant for paper factory

PUBLICATIONS

1. T.H.V. Phan, R. Bernier-Latmani, D. Tisserand, F. Bardelli, M. Frutschi, A. Gain, R-M, Couture, L. Charlet. Arsenic release during redox oscillations in Mekong upper delta aquifers in Vietnam: a mechanistic study (submitted). Target Journal: Science of the Total Environment.
2. T.H.V. Phan, L. Charlet, A. Fernandez-Martinez, D. Tisserand, R. Bernier-Latmani. Immobilization and mobilization of Arsenic in the Mekong Delta sediments induced by mineralogical changes during redox condition. In preparation. Target Journal: Hazardous Materials.
3. T.H.V. Phan, T. Bonnet, S. Garambois, D. Tisserand, R. Bernier-Latmani, L. Charlet. Arsenic release in shallow Mekong Delta aquifers linked to the electromagnetic ground conductivity. In preparation. Target Journal: Geoscience Research
4. Van, P.T.H., Tin, N.T., Hien, V.T.D., Quan, T.M., Hang, VT, Tuc, D.Q., Khoa, L.V., Phu, V.L., Kwon, E., Park, C., Jung, J., Yoon, I., Lee, S., Dan, N.P., Thanh, B.X. (2014). Nutrient removal of different plants in wetland roof systems treating domestic wastewater, *Desalination and Water Treatment*, *54*(4-5), 1344-1352.
5. Thanh, B.X., Tin, N.T., Van, P.T.H., Hien, V.T.D., Dan, N.P., Koottatep, T. (2013). Performance of wetlands roof with *Melampodium paludosum* treating septic tank effluent, *Desalination and Water Treatment*, *53*(4-6), 1070 - 1076.
6. Thanh, B.X., Hien, V.T.D., Dan, N.P., Van, P.T.H., Tin, N.T. (2012). Performance of wetland roof treating domestic wastewater in the tropic urban area, *Journal of Water Sustainability*, 2(1), 79-86.

ORAL PRESENTATIONS

1. Van Phan, Laurent Charlet (2016). L'arsenic dans les ecosystems de deltas du sud-est asiatique. Journée thématique Santé-Environnement/Santé des ecosystems, 6th July 2016 Grenoble, France.
2. T.H.V. Phan, D. Tisserand, F. Bardelli, L. Charlet, M. Frutschi, and R. Bernier-Latmani. (2016) Mechanism of arsenic release in sulfate rich sediment during microbial sulfate reduction. The 6th international congress on arsenic in the environment, Stockholm, Sweden, 19 – 23 June 2016.
3. Phan, V., Tisserand, D., Frutschi, M., Charlet, L., and Bernier-Latmani, R. (2015) Mechanism of Arsenic release from deltaic sediment during microbial sulfate reduction. Goldschmidt Conference, 16th -21 August 2015, Prague, Czech Republic.
4. Thanh, B.X & Van, P.T.H (2013). Influence of plant types on organic and nutrient removal in wetland roof systems for urban cities. The six annual conference on the Challenges in Environmental Science and Engineering 2013 (CESE 2013), pp. 98-99, 29th October – 2nd November, Daegu, Korea
5. Thanh, B.X., Hien, V.T.D., Van, P.T.H., Dan, N.P., Koottatep, T. (2012). Wetland roof with *Melampodium Paludosum* for domestic wastewater treatment. The fifth annual conference on the Challenges in Environmental Science and Engineering 2012 (CESE 2012), p. 46, 9th-13th September, RACV, Melbourne, Australia
6. Hien, V.T.D., Thu, T.N.T., Mai, T.T.T., Tin, N.T., Van, P.T.H., Thanh, B.X. (2011). Application of Wetland Roof for Domestic Wastewater Treatment: Evaluation of Wastewater

LANGUAGES AND SKILLS

Languages	• Vietnamese: mother tongue
	• English: fluent
	• French: A2
Computer skills	• Photoshop, AutoCAD, PhreeqC, PhreePlot, Datagraph, MEGA
Analytical skills	• ICP – AES, TOC/DOC/DIC, UV vis, HPLC – AFS (UV-detector)
	• DNA Extraction, PCR (Polymerase chain reaction)
	• Sequential extraction for Acid Volatile Sulfide

Annex: Impact of organic matter on arsenic release during redox oscillations

Introduction

Many processes related to the mobilization of as are directly or indirectly linked to microbial activity. These microbial transformations require some kind of degradable organic matter (OM) as electron donors (Charlet & Polya, 2006). Peat layers are common in delta environments, resulting from the development of mangrove flats (Kocar et al., 2008). Some authors highlighted the possible role of OC leaching from peat layers in the release of. As from sediments and affected to microbial sulfate reduction (Burton et al., 2013). In particular, some organic matters such as humic acids can form stable complexes with iron (oxyhydr)oxides surface and as a result may compete with as for sorption sites (Bauer & Blodau, 2006; Grafe et al., 2001). Moreover, thiols(C-SH) present in OM-rich wetlands and peaty soils can efficiently bind As(III) (Langner et al., 2011; Couture et al., 2013 a; Wang et al., in review). Therefore, the objective was to examine the influence of organic matter using cellobiose, which is a kind of mono cellulose on subsurface as mobility. To achieve this objective, we carried out a series of bioreactors experiments with initial sediment comprising As(III) and sulfate (SO_4^{2-}). The effect of organic matter (cellobiose) (the monomer of cellulose) will be evaluated by comparing reactors including to (i) the first reactor with 2.5 mM of cellobiose addition, and (ii) the second one with 30 mM of cellobiose. As, S and Fe behavior in the reactors will be investigated by chemical and spectra analysis to calculate thermodynamic reaction progress. Changes in the chemical speciation of these elements were used to explain the geochemical behavior of arsenic change between oxidized and reduced and to identify conditions that maximize dissolved arsenic concentration in groundwater.

Methods and Materials

Sediment, which previously was used in chapter 4, was suspended in 18 MΩ cm^{-1} water at the concentration approximately 100 g/L (dry weight). A set of experiments was performed with 2 reactors containing 50 µM of dissolved arsenite ($NaAsO_2$ – Sigma-Aldrich), 1 mM of Na_2SO_4. In the beginning of reducing cycle, reactor R1 and R2 were supplied with 2.5 mM and 30 mM of cellobiose, respectively ($C_{12}H_{22}O_{11}$ – Sigma-Aldrich) at the beginning

of each reducing cycle (Fig. A-1). Design of bioreactor and sampling procedures is same to chapter 3 and chapter 4.

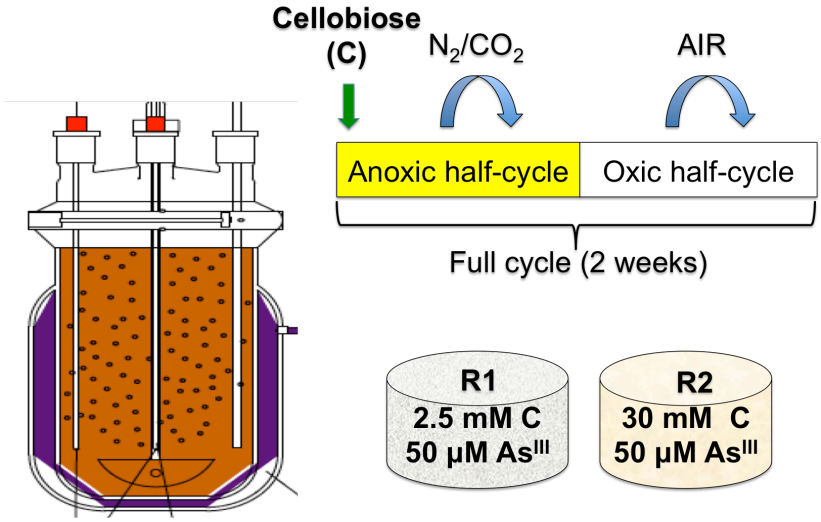

Figure A-1. Experimental set-up of the redox-cycling bioreactors and the inputs of R1 and R2

Aqueous total elemental concentration: To measure the concentration of major and trace elements (Na, Ca, Mn, Fe, As and S) in solution, an Agilent 720ES inductively coupled plasma atomic emission spectrometer (ICP – OES) was used. DOC concentration was determined using a Shimazu VCSN analyzer (TOC-5000, Shimadzu, France) with a detection limit of 0.3 mg/L and a precision better than 2.5%. All glassware was heated at 400°C for 3 hours avoiding DOC contamination. Major anions were analyzed by ion chromatography using a Metrohm 761 compact ion chromatography with a detection limit of 0.1 mg/L and a precision better than 5%. [Fe^{2+}] and [$\Sigma S^{-2}_{(aq)}$] was determined photometrically on the sample filtered by the method modified by (Lovley & Phillips, 1986; Viollier et al., 2000) of the ferrozine assay (Stookey, 1970) and Cline method (Cline, 1969).

Results and Discussion

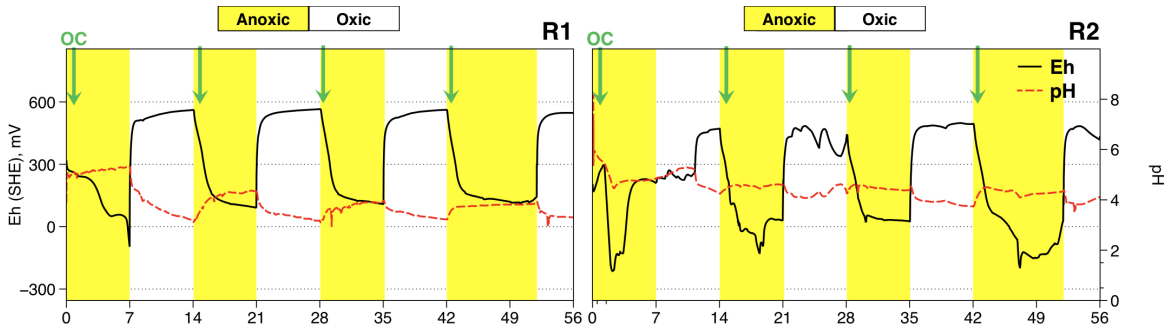

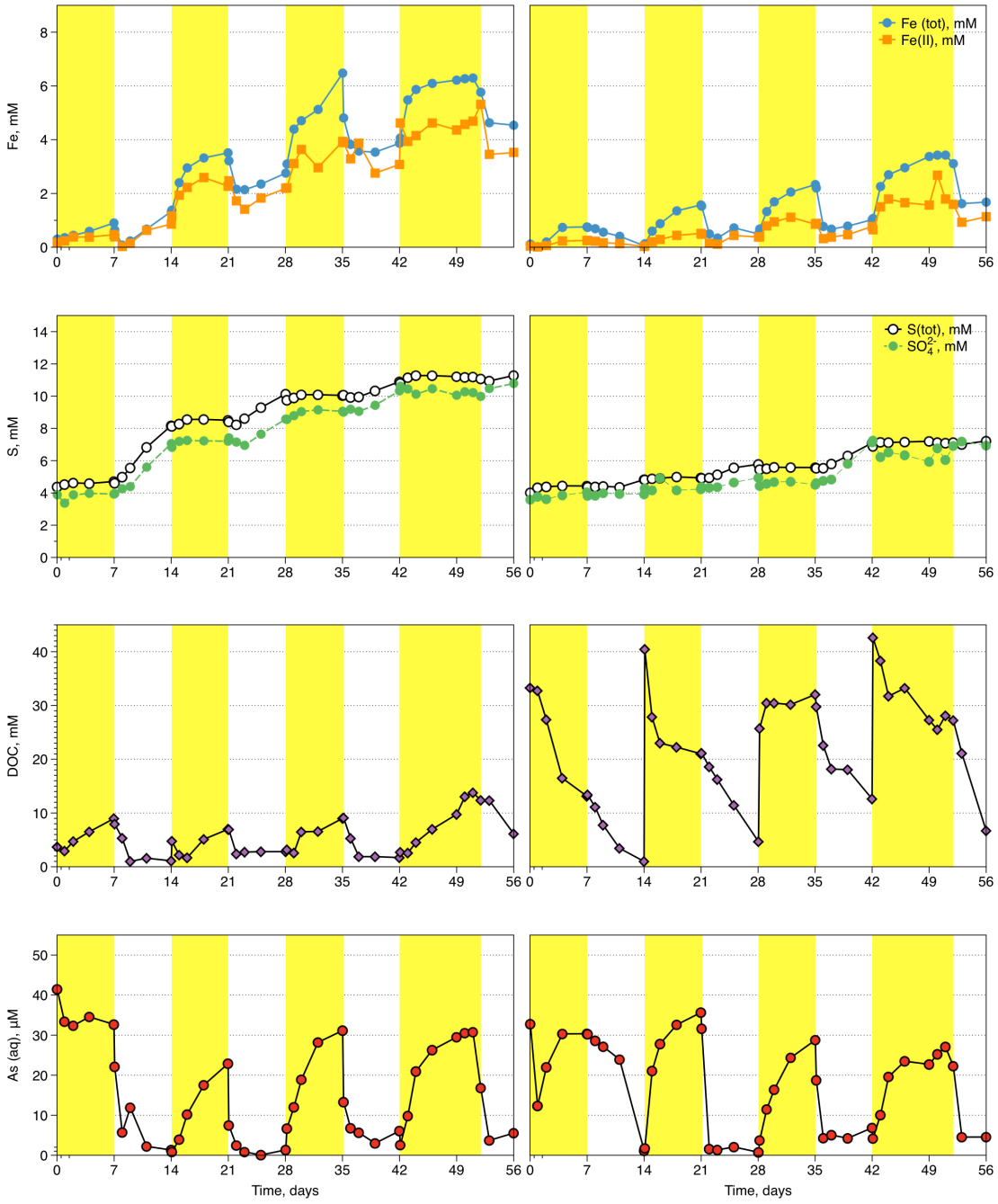

Figure A-2. Aqueous phase chemistry measured e_h, pH, Fe(tot), Fe^{2+}, S(tot), SO_4^{2-} and as(tot) data with time in R1 (2.5 mM) and R2 (30 mM) of cellobiose.

Reducing and oxidizing cycles were identified clearly by e_h and pH values. E_h was 550 mV in toxic half-cycle and 100 mV during the anoxic half-cycle in R1. While a change of e_h was from 500 mV (exec half-cycle) and -200 mV (anoxic half-cycle) was recorded in R2 lower than R1 in the anoxic half-cycle. In the first of anoxic cycle, pH drops quickly from 8 to 5.5. After this, the pH stays within 3 – 4, with an increase during the anoxic half cycles and a decrease in the toxic half cycle (4 to 3) in the repeating manner at R1. While

at R2 reactor, the solution displays a smaller variation that remains within the average range 3.8 – 4.5.

Evidence for reduction of Fe was clear with the high Fe^{2+} concentration indicates the dominant role of iron reduction in the sediment during the anoxic condition. In the exit half cycles, concentration of total Fe and Fe^{2+} decrease in the start of changing from N_2/CO_2 to AIR but increase slowly. This means pyrite was oxidized to form Fe^{2+} (Lipfert et al., 2007; Yacob et al., 2013), depending strongly on reactive minerals, oxygen and water:

$FeS_2 + 7/2\ O_2 + H_2O \rightarrow Fe^{2+} + 2SO_4^{2-} + 2H^+$

$4Fe^{2+} + O_2 + 4H^+ \rightarrow 4Fe^{3+} + 2\ H_2O$

Pyrite was oxidized to make a drop of pH 3.5 and presumably allow an acidophilic pyrite oxidizing community to develop. That obviously explains the high initial sulfate and the low pH. This seems to have prevented the development of sulfur reducing conditions during the anaerobic phases of the redox oscillation experiment. Total S and SO_4^{2-} increase dramatically in the toxic half cycles and stay stable in the anoxic half-cycle. During the reactor experiments sulfate reduction appears to have been limited even thought concentration of sulfate from sediment in the beginning was quite high (4 mM: 3 mM from natural sediment and 1 mM from addition). Moreover, S^{2-} was analyzed during the experiment but the concentration was lower than the detection limit. This means that sulfate reduction was inhibited during the anoxic half-cycles. At low pH < 5, metal sulfide precipitation and competition with other bacteria, namely iron-reducing bacteria, can inhibit sulfate reduction (Koschorreck, 2008).

DOC increases during each reducing half cycle indicating that rates of microbial mediated solubilization of particulate organic matter (POM) exceeded rates of DOC consumption by heterotrophic metabolism. DOC decreases during each oxidation cycle because of respiration, oxidation of Fe^{2+}, S and As. Addition of organic substrates to acidic system usually initiates or stimulates sulfate reduction. This effect was observed in a variety of systems with different substrates (for example acetate, lactate, ethanol and various complex organic matter sources (Koschorreck, 2008). In some cases, substrate addition had no effect or even inhibited sulfate reduction (Gore et al., 1990). In R2, sulfate concentration still kept stable during the anoxic half-cycle. However, pyrite oxidation was inhibited. When organic matter increases, the pyrite oxidation is limited, and further retarded by low oxygen availability and competition for oxygen by organic matter and bacteriological activity (Rigby et al., 2006; Yacob et al., 2013). The inhibition of pyrite

oxidation results from the complication of Fe^{3+} by soluble microbial products from cell growth and decay (Yacob et al., 2013). Therefore, DOC concentration at R2 decreases in both exit and anoxic half cycles via respiration and fermentation.

Total as concentration shows that as is released from the sediment in the anoxic half cycles and is re-immobilized during oxidizing half cycle. Pyrite oxidation generates a lot of precipitated ferric (oxyhydr)oxides, favoring iron reduction once anaerobic conditions are established (Ferna et al., 2003; Lynch et al., 2014). Under the present redox conditions, bacteria reduction of ferric (oxyhydr)oxides release arsenic (Lipfert et al., 2007; Molinari et al., 2013; Parsons et al., 2013).

Conclusions

The redox oscillating experiments containing pyrite rich sediment shows that microbial sulfate reduction was not occurred in both reactors. It seems that the low pH value accompanying to the presence of sulfate and iron release in both anoxic and toxic half-cycles. Additionally, an increase of cellobiose concentration, the pyrite oxidation was decreased, and further retarded by low oxygen availability and competition for oxygen by organic matter and bacteriological activity. Although pH drop was higher than the one of low organic matter, microbial sulfate reduction was not produced during the anoxic half-cycles. Therefore, it is likely that As mobility mechanism is potentially associated with microbial reduction of as-bearing iron oxides during the anoxic half-cycles. On the contrary, As(V) was served on the surface of iron oxides when oxidizing environment was prevailed.

Abstract: Aquifer arsenic (As) contamination is occurring throughout deltaic areas of Southeast Asia, including the Mekong Delta, and affects the health of millions of people. As is highly sensitive to fluctuations of redox conditions which are generated by the alternating wet-dry cycles during the monsoonal seasons. A survey of geophysical and chemical characteristics of soil and groundwater in the An Phu district, located in the vicinity of the Mekong Delta in Vietnam, shows the occurrence high As aqueous concentration in this region. Chemical and geophysical data indicate a strong positive correlation between As concentrations in the anoxic groundwater and conductivity of soils. In addition, mechanisms of As release are shown to be associated with colloidal and iron (oxyhydr)oxides which undergo microbial mediated reductive dissolution under redox oscillatting conditions. The presence of sulfate microbial reduction potentially stabilizes As in the solid phase and diminish As in the aqueous phase through the adsorption/desorption of As onto iron (oxyhydr)oxides and/ or sulfides with formation of thiols complexes in solid phase. Because of the high pyrite content in sediment, pyrite oxidation may drop in pH values, leads to inhibition of sulfate reducing bacteria and reduces sequestration of dissolved As. Although the biogeochemical cycling of redox sensitive species such as As in dynamic systems is challenging, it has been possible to strengthen our collective understanding of such system.
Key words: Mekong Delta, arsenic, redox oscillation, pyrite oxidation, microbial sulfate reduction, thiols As complexes

Résumé: On retrouve des contaminations d'aquifère à l'arsenic dans tous les deltasde l'Asie du Sud-Est, y compris dans le delta du Mékong, ce qui affecte la santé de millions de personnes. L'arsenic est très sensible aux fluctuations des conditions redox qui sont générées par les cycles alternés humides/secs pendant la saison de mousson. Une étude sur les caractéristiques géophysiques et chimiques du sol et des eaux souterraines dans le district de An Phu, dans le haut du delta du Mékong au Vietnam, suggère une forte contamination à l'As dans cette région. Les données chimiques et géophysiques indiquent une forte corrélation entre la concentrations dans les eaux souterraines anoxiques et la conductivité des sols. La libération de l'arsenic est associée à la dissolution réductrice, induite par des microorganismes des colloïdes et (oxyhydr)oxydes de fer dans des conditions d'oxydo-réduction oscillantes. La présence de bactéries sulforéductrices a le potentiel de stabiliser l'arsenic dans la phase solide et de l'atténuer dans la phase aqueuse par adsorption / désorption de l'arsenic sur les (oxyhydr)oxydes, et / ou sulfures de fer via la formation de complexes thiols. En raison de la teneur en pyrite élevée dans les sédiments, l'oxydation de la pyrite peut abaisser le pH et conduire à l'inhibition de la réduction microbienne du sulfate et ainsi empêcher la séquestration de l'arsenic dissous. Bien que le cycle biogéochimique de l'arsenic dans un système dynamique d'oxydoréduction soit un problème complexe, il a été possible de renforcer notre compréhension de ce système.
Mots clés: Mékong Delta, arsenic, oscillation redox, oxydation de la pyrite, sulforéduction microbienne, complexes thiols d'arsenic.